Sensory molecularly imprinted polymer (MIP) coatings for nanoparticle- and fiber optic-based assays

DISSERTATION

zur Erlangung des akademischen Grades
doctor rerum naturalium
(Dr. rer. nat.)
im Fach Chemie
Spezialisierung: Analytische Chemie

eingereicht an der
Mathematisch-Naturwissenschaftlichen Fakultät
der Humboldt-Universität zu Berlin

von
M. Sc. Sabine Wagner

Präsidentin der Humboldt-Universität zu Berlin:
Prof. Dr.-Ing. Dr. Sabine Kunst

Dekan der Mathematisch-Naturwissenschaftlichen Fakultät:
Prof. Dr. Elmar Kulke

Gutachter/innen: 1. Prof. Dr. Ulrich Panne
2. Prof. Dr. Kannan Balasubramanian
3. S-Jun.-Prof. Dr. Annabelle Bertin

Tag der mündlichen Prüfung: 16. November 2018

Die vorliegende Arbeit wurde in der Zeit von April 2014 bis Juli 2017 am Institut für Chemie der Humboldt-Universität zu Berlin und an der Bundesanstalt für Materialforschung und –prüfung (BAM) im Fachbereich 1.9 Chemische und Optische Sensorik unter der Leitung von Prof. Dr. rer. nat. Ulrich Panne und Dr. rer. nat. Knut Rurack angefertigt.

Acknowledgments

It is a pleasure to express my sincere gratitude to my supervisor Dr. Knut Rurack for his kind supervision, continuous encouragement, valuable enthusiastic discussion and unfailing advice throughout the present work. He assisted in all matters and provided solutions to different problems. I want to thank my "Doktorvater" Prof. Ulrich Panne as well, for taking responsibility for my Ph.D. study and serving as my university supervisor. I am very lucky being one of his students.

I gratefully acknowledge Prof. Ulrich Panne, Prof. Kannan Balasubramanian and S-Jun.-Prof. Annabelle Bertin for giving me the honor to review my thesis and Prof. Pinna and Prof. Ray for being the examiners of this work.

I would not have been able to carry out this work without the help and collaboration of many people. First of all I would like to thank the current and former members of Dr. Rurack´s research group for generating a pleasant and enjoyable working atmosphere which has helped me to finish this research and let me come to work with a big smile. I would like to express my deep thanks to Dr. Wei Wan and Dr. Mustafa Biyikal who introduced, helped and advised me in the fields of fluorescent dyes and molecular imprinting and for the intensive discussions. I especially thank Dr. Jérémy Bell for providing me with great guidance throughout the field of microfluidic devices.

As for our external collaborations, I am very thankful to Prof. Maria C. Moreno-Bondi and Dr. Elena Benito-Peña, for friendly welcoming me to Complutense University of Madrid and giving me the opportunity to work together and to introduce me in the field of optical fibers.

Things would have been completely different if during the second year of my PhD Dr. Kornelia Gawlitza had not come to BAM. I would like to express my profound thanks to her for helpful and hilarious discussions on scientific and private level. Work is completely different and much more fun when you can share and discuss ideas. I feel lucky to have spent this part of the journey with her. I will miss her laugh resounds the 5^{th} floor.

I thank Dr. Kornelia Gawlitza and Dr. Sören Selve for TEM measurements, Holger Hoffmann for HPLC validation, Dr. Md Asad Asadujjaman for TGA measurements, Sigrid Benemman for T-SEM measurements and Dr. Katherine Chulvi Iborra for crystal structure measurements.

I am extremely grateful to my mother, my sister and my grandparents, who did all the best to help me in my education and for their love and support. Without them I would not be that person who I am. There are no words to express how I feel about what they have done for me all my life in every situation. Absolutely none of it would be possible without them.

Thank you to all my friends for standing by me through tough times and for understanding the lack of time. A special thanks to my office mates and friends Benita Schmidt and Benedikt Heller for all the help and short talks in between. Their presences in the office gave a very nice company.

Abstract

Nowadays society is highly sensitive towards contaminants in water and foodstuff due to their harmful properties to humans and animals. For the detection of these contaminants in low concentration ranges fast and sensitive analytical tools are required especially in environmental and food analysis. Molecularly imprinted polymers (MIPs) have been used as synthetic materials mimicking molecular recognition by natural receptors e.g. antibodies due to their ability to recognize selectively a wide range of analytes, their stability and ease of synthesis. They have been used already as separation material in chromatography for a long time, however, have gained more and more attention in chemical sensing as receptor material for the detection of suitable groups of analytes at low concentrations especially in combination with fluorescence due to the latter's high sensitivity.

This work aimed the development of optical sensor materials using MIPs as recognition elements connected with fluorescence for the sensitive detection of herbicides and antibiotics in water and food samples. More generally, the combination of a MIP-based sensing platform with various device formats for the future detection of a wide range of analytes of interest was aspired. Such systems are applicable for fast and sensitive on-site analysis in the areas of food control and environmental monitoring, that is, portable and robust against chemical and thermal influences. Fluorescent indicator dyes were incorporated into a thin MIP shell on supporting silica particles which lights up upon binding of the analyte of interest in an organic solvent. Detailed investigation of the receptor materials' optical response, sensitivity and selectivity led to a combination with a droplet-based 3D microfluidic system and integration into fiber optic bead-based arrays, which allows the determination of oxoanionic analytes of interest at sufficiently low concentrations directly in a sample.

Zusammenfassung

Heutzutage ist die Gesellschaft gegenüber Verunreinigungen im Wasser und in Lebensmitteln sehr aufmerksam aufgrund ihrer schädlichen Eigenschaften für Mensch und Tier. Für den Nachweis dieser Schadstoffe in niedrigen Konzentrationsbereichen sind insbesondere in der Umwelt- und Lebensmittelanalytik schnelle und empfindliche Analysemethoden erforderlich. Molekular geprägte Polymere (MIPs) wurden als synthetische Materialien entwickelt, um die molekulare Erkennung von natürlichen Rezeptoren, z.B. Antikörper, nachzuahmen, aufgrund ihrer Fähigkeit, selektiv eine Vielzahl von Analyten zu erkennen, ihre Stabilität und ihrer einfachen Herstellung. Sie wurden bereits als Trennmaterial in der Chromatographie verwendet, sind jedoch zunehmend in der chemischen Sensorik als Rezeptormaterial für den Nachweis bestimmter Analyten bei niedrigen Konzentrationen zu finden, insbesondere in Kombination mit Fluoreszenz aufgrund dessen hoher Empfindlichkeit.

Ziel dieser Arbeit war die Entwicklung von optischen Sensormaterialien unter Verwendung von MIPs als Erkennungselemente im Zusammenhang mit Fluoreszenz zum sensitiven Nachweis von Herbiziden und Antibiotika in Wasser- und Lebensmittelproben. Allgemeiner wurde die Kombination einer MIP-basierten Sensorplattform mit verschiedenen Vorrichtungsformaten für die zukünftige Detektion einer breiten Palette von wichtigen Analyten angestrebt. Solche Systeme sind für schnelle und sensible Analysen vor Ort in den Bereichen Lebensmittel- und Umweltüberwachung anwendbar, und sollten tragbar und robust gegenüber chemischen und thermischen Einflüssen sein. Fluoreszierende Indikatorfarbstoffe wurden in eine dünne MIP-Schale auf Silikatpartikel eingearbeitet, die bei der Bindung des Analyten in einem organischen Lösungsmittel aufleuchten. Die detaillierte Untersuchung der optischen Reaktion, der Empfindlichkeit und der Selektivität der Rezeptormaterialien führte zu einer Kombination mit einem tröpfchenbasierten 3D-Mikrofluidiksystem und der Integration in faseroptische Bead-basierte Plattform, was die Bestimmung von oxoanionischen Analyten bei ausreichend niedrigen Konzentrationen ermöglicht.

Table of Contents

List of Figures

List of Tables

List of Abbreviations

ABDV	azo-bis-dimethylvaleronitrile
AIBN	azo-bis-isobutyronitrile
AM	acrylamide
AMPI	ampicillin
AMOX	amoxicillin
APTES	Aminopropyl triethoxysilane
Ar	argon
ATRP	atom transfer radical polymerization
BHT	2,6-di-tert-butyl-4-methylphenol
BMA	benzylmethacrylate
BPA	bisphenol A
CHCl3	chloroform
CLRP	controlled/living free radical polymerization
CMMC	7-carboxymethoxy-4-methylcoumarin
CPDB	4-cyano-4-(thiobenzoylthio)pentanoic acid
CS	core/shell
CSP	chiral stationary phases
dansyl-L-Phe	dansyl-L-phenylalanine
DF	discrimination factor
DMAP	4-,4-(dimethylamino)-pyridine
DVB	divinylbenzene
EGDMA	ethylene glycol dimethacrylate
EF	enantioselectivity factor

Eq.	equation
ELISA	enzyme-linked immunosorbent assay
ENOX	enoxacin
ENRO	enrofloxacin
EPA	Environmental Protection Agency
EtOH	ethanol
FLRLP	fluorophore-linker-receptor-linker probe
FLRP	fluorophore-linker-receptor probe
fMIP	fluorescent molecularly imprinted polymer
H-bonds	Hydrogen bonds
HEMA	2-hydroxyethyl methacrylate
HEPES	2-[4-(2-hydroxyethyl)piperazin-1-yl]ethanesulfonic acid
HOMO	highest occupied molecular orbital
HPLC	high-performance liquid chromatography
HSA	human serum albumin
IF	imprinting factor
ICT	intramolecular charge transfer
LC	liquid chromatography
LED	light emitting diode
LOD	limit of detection
LOQ	limit of quantification
LUMO	lowest unoccupied molecular orbital
λ-cy	λ-cyhalothrin
MAA	methacrylic acid
MAC	maximum acceptable concentration

MAAm	methacryl amide
MeCN	acetonitrile
MeOH	methanol
MIP	molecularly imprinted polymer
MISPE	molecularly imprinted solid-phase extraction
MISPE	molecularly imprinted solid-phase extraction
MICSP	molecularly imprinted chiral stationary phases
MMA	methyl methacrylate
MPS	3-methacryloxypropyl trimethoxysilane
MS	mass spectrometry
MSN	mesoporous silica nanoparticles
NBD	nitrobenzoxadiazole
NIP	non-imprinted polymer
NMP	nitroxide-mediated polymerization
NMR	nuclear magnetic resonance
PET	photoinduced electron transfer
PETRA	pentaerythritoltriacrylate
PFA	perfluoroalkoxy alkanes
PMP	1,2,2,6,6-pentamethylpiperidine
PTFE	polytetrafluoroethylene
RAFT	reversible addition fragmentation chain transfer
RT	room temperature
SEM	scanning electron microscopy
SPE	solid phase extraction
SPR	surface plasmon resonance

TBA	tetrabutylammonium
TEA	tetraethylammonium
TEOS	tetraethylorthosilicate
TEM	transmission electron microscopy
TGA	thermogravimetric analysis
THA	tetrahexylammonium
THF	tetrahydrofuran
TMA	tetramehtylammonium
TOA	tetraocylammonium
TrEA	triethylamine
TRIM	trimethylolpropane trimethacrylate
TSA	transition state analogue
UV	ultra-violet
WHO	World health organisation
Z-D-Glu	*N*-(carbobenzyloxy)-D-glutamic acid
Z-D-Phe	*N*-(carbobenzyloxy)-D-phenylalanine
Z-D-Tyr	*N*-(carbobenzyloxy)-D-tyrosin
Z-L-Phe	*N*-(carbobenzyloxy)-L-phenylalanine
ZnPP	zinc(II) protoporphyrin
2,4-D	2,4-dichlorophenoxyacetic acid
2-Vyp	2-vinyl pyridine
4-Vyp	4-vinyl pyridine
2,4-DB	4-(2,4-dichlorophenoxy)butanoic
2,4-DP	2-(2,4-dichlorophenoxy)propionic acid

1 General Introduction

Sensors are used in almost all areas of our daily life and their progress has fundamentally changed our professional and private life with breathtaking speed. At work and at home, even in our free time, sensors make our life easier, safer and more comfortable. Exemplarily, sensors can initiate the switch-on of light, music and heater. Even the refrigerator can recognize finished food and directly order fresh products online. Some time ago, such ideas of a smart home were already developed by the film industry, however, they were ahead of their time. In many movies, technical progress has been shown to make life more comfortable. The design of such scripted innovations was not always convincing, but some examples have been overtaken already partially by the reality. The movie "The fifth element" showed flexible flat furniture to create more space which is important especially in big metropolitan areas with limited space. In "Back to the future 2" from 1989, Marty McFly travels to the future and jumps into self-closing shoes. Almost 30 years later, a big US American sporting goods manufacturer brought such shoes to the market. A sensor recognizes the heels and closes the shoes automatically by a mechanism. Even in 1966, in "Star Trek", a small gadget to record and analyze data as well as for sensing was presented. Today, everyone is using smartphones with hundreds of apps which can do many of those things as well. "Minority report" in 2002 and "Iron Man" in 2008 demonstrated already the world of touchscreens including sensor technology which is common today in many areas of our life.

It is obvious that the development of sensor technology dreamt up by writers and directors of the "dream factory" became to some extent reality. With the help of these sensors, it is possible to increase the functionality and thereby the worth of many products, without significantly raising the production costs. For instance, also modern cars have been developed by integrating various physical sensors. An end to this development trend is not seen yet.[1,2]

Sensors have also very high importance in chemical, food, health, and, pharmaceutical industries, as well as environmental, clinical, and indoor monitoring applications.[3] Despite today's advancements in technology, the simple

and on-site detection of environmental pollutants like antibiotics, pesticides, insecticides, and herbicides remains a challenge. Current analytical techniques for such pollutants generally have high sensitivity, but are complex, expensive and require skilled technicians and large laboratory based instrumentation. Additionally, most of these techniques need sophisticated and time-consuming extraction procedures prior to the indication step. Extrapolating the urge illustrated above with the example of scripted sensor reality, there is a strong trend since more than a decade to bring the "lab to the sample rather than the sample to the lab".[4] One of the current focus in analytical chemistry thus is the development of rather simple, miniaturized, and robust chemical sensors that could detect such species with the necessary sensitivity and selectivity on-site or in the field.

The main element of such a sensor is the detection element (receptor), which is directly coupled to the chemical signal converter (transducer). The recognition element is responsible for the specific binding of a target molecule from a complex sample. This binding event is converted by the transducer to a readable chemical signal (Fig. 1).

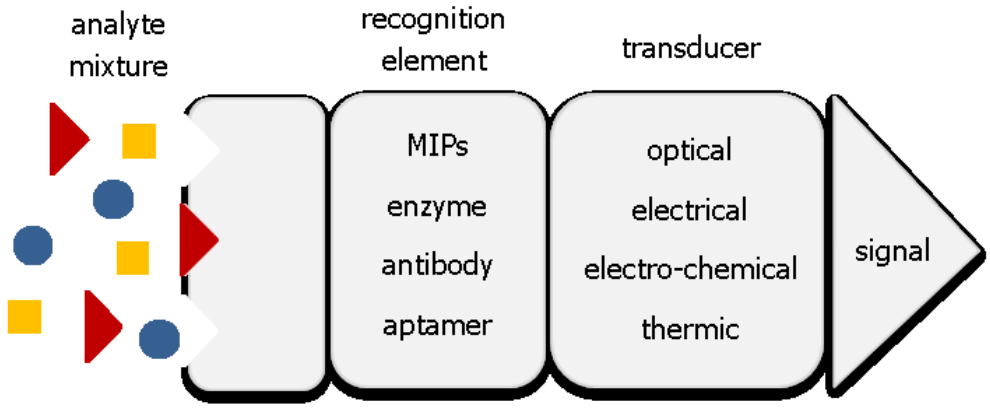

Fig.1: Illustration of a chemical sensor.

Chemical sensors can be divided into solid, liquid and gas sensors based on the phases of the analyte. An overview regarding this possible classification of chemical sensors and the corresponding operating principles are shown in Tab. 1.

Tab. 1: The chemical sensors classification proposed in 1991 by IUPAC Analytical chemistry division.[5]

Class of Sensors	Operating Principle
Optical devices	Absorbance Reflectance Luminescence Fluorescence Light scattering
Electrochemical devices	Voltammetry and amperometry Potentiometry Chemically sensitized field effect transistor Potentiometry with solid electrolytes for gas sensing
Electrical devices	Metal oxide semi-conductivity Organic semi-conductivity Electrolytic conductivity
Mass sensitive devices	Piezoelectric Surface acoustic wave propagation
Magnetic devices	Changes of paramagnetic gas properties
Thermometric devices	Heat effects of a specific chemical reaction

However, compared with the development of physical sensors, the development of chemical sensors for actual (bio)chemical substances is relatively slow. This is mainly because such sensors commonly do not only have to recognize a compound (or a class of compounds) specifically, but that this encounter has to be transformed into a measurable signal. Furthermore, since sensing is usually a continuous process of acquiring information, the molecular chemical interaction has to be reversible.[6] In addition, the recognition sites have to be at best embedded into a matrix that can be interfaced with the physical detection system. Further important requirements pertain to robustness, format adaptability and modularity with regard to targeting various compounds with a single technology, the major areas of application certainly stretching.

There are already many biosensors using antibodies and enzymes as recognition elements. However, numerous drawbacks like instability in changing physical and chemical conditions, expensive preparation, low yield, and the use of animals make them inconvenient for the use in sensor materials.

An elegant way to overcome this problem is molecular imprinting. The imprinting of a template molecule with functional monomers into a polymer matrix leads to a material with comparable function as biological receptors found in nature.[7] With such stable and tailor-made materials for the specific recognition of analytes, the possibility to change properties to adapt to their environment depending on their future uses is ensured.[8] Even though they can have applications in many fields of chemistry, biology and medicine compared to natural receptors, however, there are some limitations. For instance non-interaction, slow kinetic as well as poor recognition in water.[9] Nevertheless, due to the spatial fixation of the functional groups good selectivity for small molecules could be obtained.

The history of molecularly imprinted polymers (MIPs) can be traced back to the earlier 1930s. Polyakov and Dickey observed preferential adsorption of small molecules in a silica matrix and set the stage for the molecular imprinting approach.[10,11] However, the pioneer works of Wulff, Mosbach, and Shea made the method more popular. In the earlier 1970s, Wulff used organic polymers as backbone for imprinting and renewed the interest in MIPs.[12] Not quite a decade later, Mosbach propelled the field significantly when introducing the concept of non-covalent imprinting which is up until now the most popular and versatile approach to polymer-based artificial receptors.[13] Shea and a constantly growing number of scientists worldwide devoted their attention to this field and made MIPs an attractive material for a broad range of applications, including separation, solid phase extraction, catalysis, and chemical sensing.[14-17]

Despite the enormous potential of MIPs for various technical applications, they are just limited to a few special applications with very manageable economic effect.[18] To establish more promising systems, the development of new synthesis methods and more accurate characterizations of the MIPs are required closely tied to the needs of the application technologies.

2 Theoretical Background

2.1 Molecularly imprinted polymers (MIPs)

The molecularly imprinted polymers are prepared by polymerization of various functional monomers and cross-linkers that are complementary to the functional groups on the target species in the presence of the latter, i.e., the so-called template (Fig. 2). Following this strategy, the self-assembled complexes of functional monomers and template molecules are copolymerized in the presence of a cross-linker and suitable solvent leading to an imprinting of the shape of the complexes into a cross-linked and durable matrix. After preparation, the template is removed by extraction, leaving imprinted cavities in the matrix, which can specifically rebind the target analyte in the analytical process.[19] Free radical polymerization is typically the method of choice for the MIP synthesis. The polymerization can be initiate photochemically or thermochemically. The reaction is usually performed under mild conditions (low temperature and atmospheric pressure) in bulk or solution which favours a better stability of the monomer/template complex.[20] With this imprinting process, functions of biological receptors are imitated by synthetic polymers. This is the reason why MIPs are often referred to as "artificial antibodies".[7] In comparison to biological receptors, MIPs are more stable and robust combined with the possibility to imprint small molecules as well as larger molecular structures, ultimately proteins or viruses, which leads to their ability to recognize a wide range of target analytes. [21]

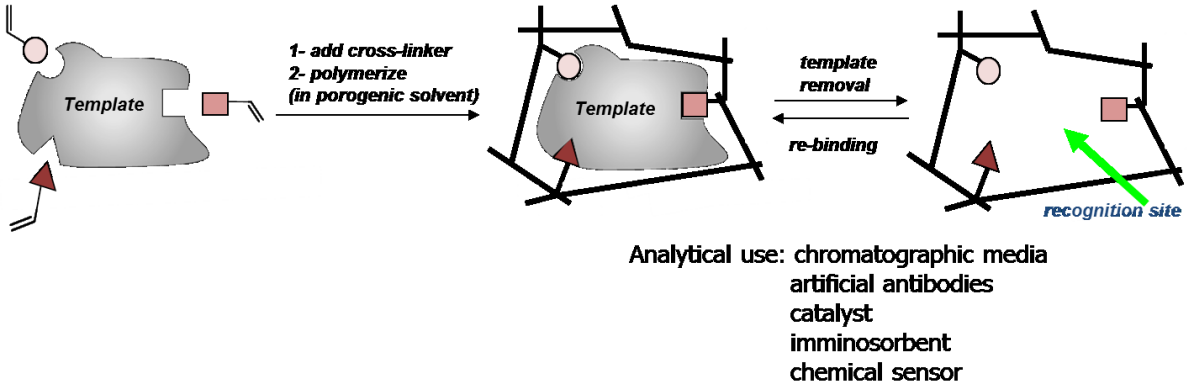

Fig. 2: Illustration of the steps in the synthesis of MIPs.

2.1.1 Different binding site interaction in MIPs

Depending on the future application of the MIP, the interaction between the template molecule and the functional monomer must be considered. Wulff et al. were the first to report on the **covalent** strategy (Fig. 3) where the template molecule is covalently bound to polymerizable functional groups, forming highly specific and selective binding sites in the network.[7, 22-24] After cleavage of these labile bonds by e.g. hydrolysis to remove the analyte, it can covalently rebind to the cavity in case of new contact. For this purpose, only a few systems like boron-diols, Schiff bases and amides have been proven to be effective.[25] However, the strong binding often worsen the kinetic (slow elution, as well as the rebinding process).[26-27]

In **semi-covalent** imprinting (Fig. 3), a template molecule is covalently bound to polymerizable groups. This ensures that the binding functionalities, responsible for selective binding, are only in the cavities. After the polymerization and removal of the template, it can rebind to the cavity *via* non-covalent interactions.[28] This strategy offers a good stability between template and functional monomer as well as a fast rebinding step.[29-30] Whitcombe et al. used a 4-vinylphenyl carbonate ester of the target analyte which functions as a covalently bound template monomer which can be removed easily with the loss of CO_2 (Fig 3 C).[31] The remaining non-covalent recognition site, bearing a phenolic residue, can interact with the cholesterol through hydrogen bonding. Often such a spacer is used, which connects the template molecule and functional monomer and extends the binding between these components to improve the rebinding step in the cavity.[32-35] This spacer is removed during the cleavage step. Like the covalent imprinting, this strategy is limited to a number of analytes.

Non-covalent imprinting is by far the most widespread strategy in MIP synthesis firstly described by Mosbach and his group (Fig 3). During the pre-polymerization and imprinting step as well as during the later rebinding, only non-covalent interactions are dominating e.g. van der Waals forces, electrostatic interaction, π stacking, and hydrogen bonding.[36-37] The preparation is simple because only mixing of the chemicals is necessary without any chemical

modification. In addition to that, a higher number of functional monomer types can be used. However, the formed interactions between the template molecule and the functional monomer are often weak, thus a larger amount of functional monomer has to be added to the reaction mixture in order to shift the binding equilibrium to the side of the complex which can, however, lead to larger heterogeneity of binding sites.[24, 38] Also monomers could be developed with more binding possibilities and higher binding affinities to the analyte of interest which also offers fast extraction.[24]

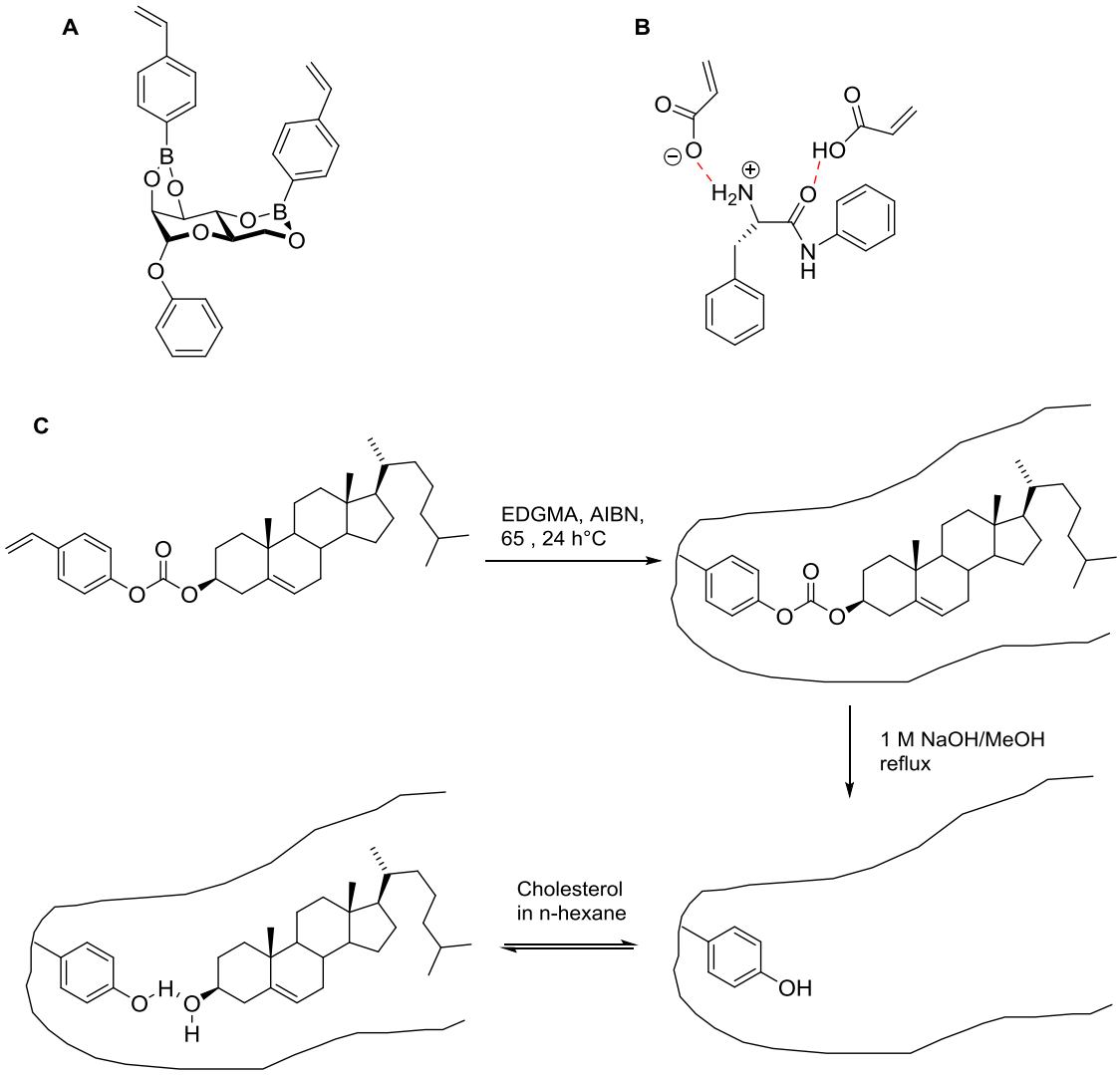

Fig. 3: A) covalent interaction; B) non-covalent interaction ; C) semi-covalent interaction.[23, 39,31, 40]

2.1.2 Components for MIP synthesis

Functional monomer

For molecular imprinting processes the functional monomer as the main component has to be chosen based on its interaction with the template in order to give a high stability of the polymer. The functional monomer contains at least two functional groups. One reacts with the template through covalent or non-covalent interactions and the other one is polymerized with the cross-linker.[20, 41] For a stable complex the monomers should have functional groups that are complementary to those of the template. The combination of two or more functional monomers leads to higher recognition properties of the MIP. After the polymerization, the template should be completely removed and binding sites complimentary to the analyte should remain for a reversible rebinding step. However, an excess of functional monomer leads to an increase of the number of non-selective binding sites, which reduces the selectivity of MIPs.[42,43]

For non-covalent imprinting polymerization, vinyl and acrylate monomers are normally used, which can be divided into basic, acidic and neutral ones. Most of them shown in Fig. 4 are commercial available.[44]

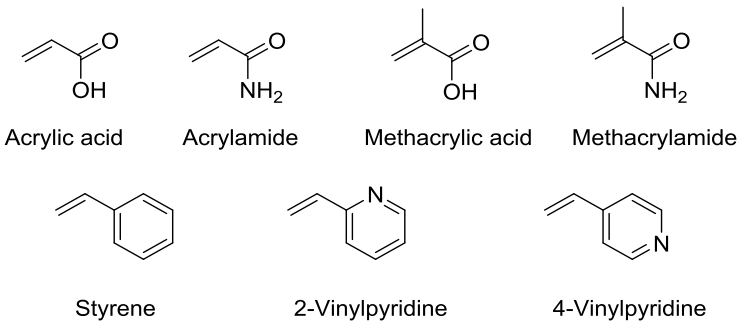

Fig. 4: Functional monomers.[44]

In the case of the presented work, the commercially available monomers were only employed as co-monomers to a functional monomer. Furthermore, small amounts of functional indicator monomer compare to the co-monomer were used to avoid self-aggregation.

Template

Many templates have been used for imprinting, including amino acids, proteins, nucleotide derivatives, pollutants, pesticides and drugs.[45-47] It is important to choose the template molecule based on the size, the interaction with the monomers and the solubility in the preparation solvent. The molecule must contain functional groups which can interact with the functional monomer leading to a stable complex. Naturally, the template should not offer any polymerizable group which would trap it irreversibly in the network and make extraction impossible.

Large molecules such as longer peptides and proteins cannot diffuse very well through the highly cross-linked polymer matrix to reach the binding sites which make the corresponding MIP synthesis very difficult, often including additional preparation steps or restricting the strategy to surface imprinting.[48-50] This is the reason why most systems are employed for small organic molecules, ions or short peptides.

The interaction between the template molecule and the functional monomer must be stable during the entire polymerization process. Normally, hydrogen bonds are used for the interaction, however, electrostatic interactions become more important. The combination of several different interactions can lead to better binding sites and increases the affinity to the monomer and the recognition properties of the MIP, exemplifying multivalent imprinting.[7]

Cross-linker

The cross-linker has a high influence on the chemical and physical properties of the polymer. It controls the morphology of the polymer matrix, provides mechanical stability and stabilizes the molecularly imprinted binding sites.[20, 41] In addition, the type and amount (typically 60-90 %) is crucial for the selectivity of the MIP.[43, 51] Furthermore, the cross-linker ensures that the imprinted polymer is insoluble in different solvents which facilitate practical application.

These cross-linkers contain minimum two polymerizable groups like ethyleneglycol dimethacrylate (EGDMA) and divinylbenzene (DVB) (Fig 5). EGDMA is often used

for non-covalent and methacrylate-based approaches providing a good stability, wettability in most rebinding solvents and fast mass transfer with good selectivity.[52]

However, a smaller amount leads to an increase of the recognition of the analyte.[53] Other multifunctional cross-linkers like trimethylolpropane trimethacrylate (TRIM) and pentaerythritoltriacrylate (PETRA) were also successfully exploited in the MIP field. The higher number of polymerizable groups often improves the sample load capacity and the efficiency of the MIP due to its better anchoring in the MIP network.[52]

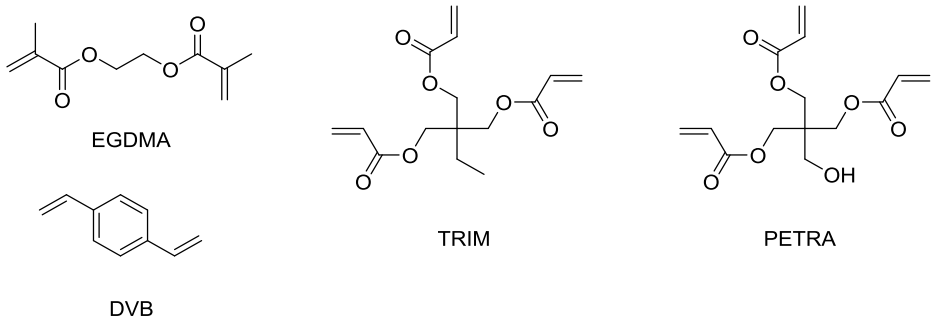

Fig. 5: Most common used cross-linkers for MIP synthesis.

The reactivity of the cross-linker and the functional monomer must be similar to ensure an efficient imprinting and a homogeneous polymer network. Sellergren showed that the ratio of both molecules is crucial for the selectivity.[39] The selectivity of an EGDMA/methacrylic acid system with L-phenylalanine (L-phe) as a template molecule[39] increased up to 30 mol.-% of functional monomer. Above 50 mol.-%, the selectivity was reduced because no stable polymer network was formed.

Initiator

Azo initiators such as azobisisobutyronitrile (AIBN) and 2,2'-azobis(2,4-dimethyl)valeronitrile (ABDV) (Fig. 6) are primarily used for the initiation of the free radical polymerization because the resulting radicals show a low reactivity against hydrogen bonds.[20, 53] The ability of the photochemical decomposition of those initiators allows the production of polymers at low temperatures, and thus, with an increased specificity due to a thermal stabilization of the template-

monomer complex.[54] The decomposition of AIBN and ABDV starts at 60 °C and 40 °C, respectively. Due to the lower temperature needed, ABDV was used in this study.

Benzoyl peroxide and lauroyl peroxide are examples for thermal initiators whereas benzophenone and 2,2'-dimethoxy-2-phenylacetophenone are used as photo initiators for the preparation of MIPs.[55-57]

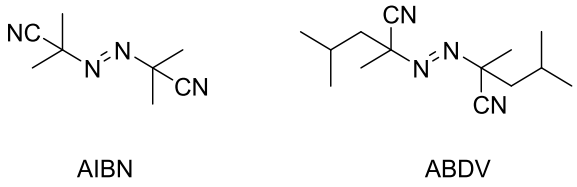

AIBN ABDV

Fig. 6: Most commonly used initiators in MIP synthesis.

Solvent

The choice of the right solvent is crucial for the MIP synthesis showing influence on the polymerization procedure and the structure of the whole polymer network. The main task of the solvent is, to combine and dissolve all the components that are used for the MIP preparation. The most used solvents are typically chloroform, acetonitrile (MeCN), toluene, and dichloromethane.[58]

In MIP studies, the solvent is usually called *porogen* because it generates the porous structure in the imprinted polymer, and thus, influences the formation of the imprints.[59] During the polymerization the solvent molecules are incorporated in the polymer matrix being removed from their position in the network during the post treatment step, and pores remain in the polymer. If the *porogen* volume is lower than the monomer volume, only a polymer with poor porosity can be obtained which leads to slow template extraction and recognition properties.[53]

The *porogen* can influence the functional monomer-template complex as well. MIPs are often compared to natural antibodies, but there is a big difference. Most imprinted polymers can only be prepared and used in organic solvents, however, antibodies bind only in aqueous medium. Current studies focus on water-compatible MIP systems but there are still significant challenges. In non-covalent imprinting polymerization, more protic solvents can interfere with

hydrogen bonds in the complex. In addition, the selective binding ability decreases with increasing polarity of the solvent, because hydrophobic interactions are too weak. In contrast, less polar solvents do not form competing bonds and promote non-covalent interactions between the monomer and the template.[60-62] However, with either stronger non-covalent monomer-template interaction with for example electrostatic attraction or with multivalent imprinting, the step to work in more polar solvents can become possible.[63-65]

2.2 MIP formats

2.2.1 Bulk MIPs

In the field of MIPs, various formats have been established. Bulk polymers are the most commonly used type due to their facile preparation by mixing all components of the MIP reaction (functional monomer, template of interest, cross-linker and initiator) in the solvent or *porogen* without using expensive instrumentation or additional chemicals. The free radical reaction can be initiated by temperature or UV light.[54, 66] However, after the preparation, the monoliths are grounded and sieved which is time-consuming and leaves particles with different shapes and sizes.[67] Moreover, binding sites can also be destroyed during processing and often a significant number of them is difficult to access for the analyte when buried deeply in the bulk. However, for high-performance sensing MIPs, a homogeneity of material shape, size and binding cavities is mandatory. In addition, inaccessible cavities shall be avoided since they contribute to a non-specific background signal.

In many cases the diffusion time of the analytes to the recognition sites of the rather compact particle monolith is quite slow. In addition, quantitative extraction of template after the preparation is also often tedious. When the incorporation of dyes into MIP bulk particles is concerned, the use of high concentrations of fluorescent dye can further initiate reabsorption or self-quenching effects which are detrimental to straight-forward analyte quantification.

2.2.2 MIP films

As an alternative, MIP films and MIP membranes can be used. Their planar structure is often obtained by synthesis in a casting mold or on the plane surface of a supporting medium.[68-69] The opportunity to prepare them on a surface by e.g. spin-coating or surface polymerization allows to directly integrate these films into chemical sensors. Sergeyeva et al. demonstrated thin, stable and flexible MIP membranes for the detection of atrazine. They were integrated as the recognition element and showed good selectivity and sensitivity.[68]

Ton et al. also studied an integration of a thin polymer layer into an optical sensor for the herbicide 2,4-dichlorophenoxyacetic acid (2,4-D).[70] For the detection as well as for the polymerization of the MIP onto an optical fiber, evanescent wave spectroscopy was used yielding a thin homogeneous MIP layer. The entire ensemble is compatible with commercial instruments. Unfortunately, the thickness control during the synthesis is still a challenge. It is complicated to obtain a reproducible uniform thickness and to prevent irregularities. The fragility of such films makes them quite unstable against external influences such as mechanical impact.

2.2.3 MIPs-containing micro- and nanoparticles

Since organic polymer, magnetic and especially silica micro- and nanoparticles became very important in sensor techniques, MIP-based sensor research shifted the focus on grafting the MIP as a thin layer onto the surface of such supporting materials.[17, 71-72] The core defines the shape and size, with often good and precise control over these parameters. The usually very thin MIP film largely avoids influences through mechanical damage which is advantageous for many applications. In addition, the use of porous support materials can enable the grafting of thin films onto the inner pore walls and thus a higher mass transfer. Compared to the other formats discussed before, thin MIP shells on carrier micro- or nanoparticles or on the walls of porous particles generally guarantee a faster response. Additionally, the extraction of the template molecule after MIP preparation is usually completed in much shorter time and in quantitative fashion.

The surface of silica particles can be modified with polymerizable vinyl groups as well as with initiators to ensure the covalent grafting of the MIP layer. The group of Zhang grafted a MIP layer onto the surface of spherical silica particles which were previously modified with 3-methacryloxypropyl trimethoxysilane (MPS) to introduce the vinyl groups.[73] In that study, vinyl-substituted zinc(II) protoporphyrin (ZnPP) was presented as fluorescent reporter and functional monomer at the same time. The template molecule atrazine can coordinate to the Zn^{2+} ion forming a complex during the MIP synthesis. Upon binding the fluorescence properties of ZnPP are changed leading to a detectable fluorescence signal. Furthermore, Gao et al. prepared silica core-MIP shell particles for the detection of λ-cyhalothrin (λ-cy).[74] In order to synthesize the MIP shell, acrylamide (AM) was copolymerized with allyl fluorescein using λ-cy as template. MIP showed a stronger fluorescence enhancement upon addition of λ-cy then the control non-imprinted polymer (NIP) particles. However, the control of the polymerization process, chain length and MIP layer thickness in this 'grafting to' method is difficult, because MIP formation can also take place in solution due to remaining initiator in the solvent. In addition, the anchoring of new chains on the surface is hampered by previously formed chains.

Therefore, the "grafting from" technique was established to prevent these problems and prepare a dense MIP layer onto a material's surface. In the beginning, azo initiators were immobilized which on one hand could improve the mass transfer but on the other hand did not inhibit the polymerization in solution. Sulitzky et al. demonstrated MIP layer preparation using the radical initiator 4,4´-azobis(4-cyanopentanoic acid) which is covalently bound to amino-functionalized silica particles.[75] The same group introduced benzyl-*N,N*-diethyldithiocarbamate as initiator for the polymerization which decreased the propagation of the polymer chains in solution.[76-77]

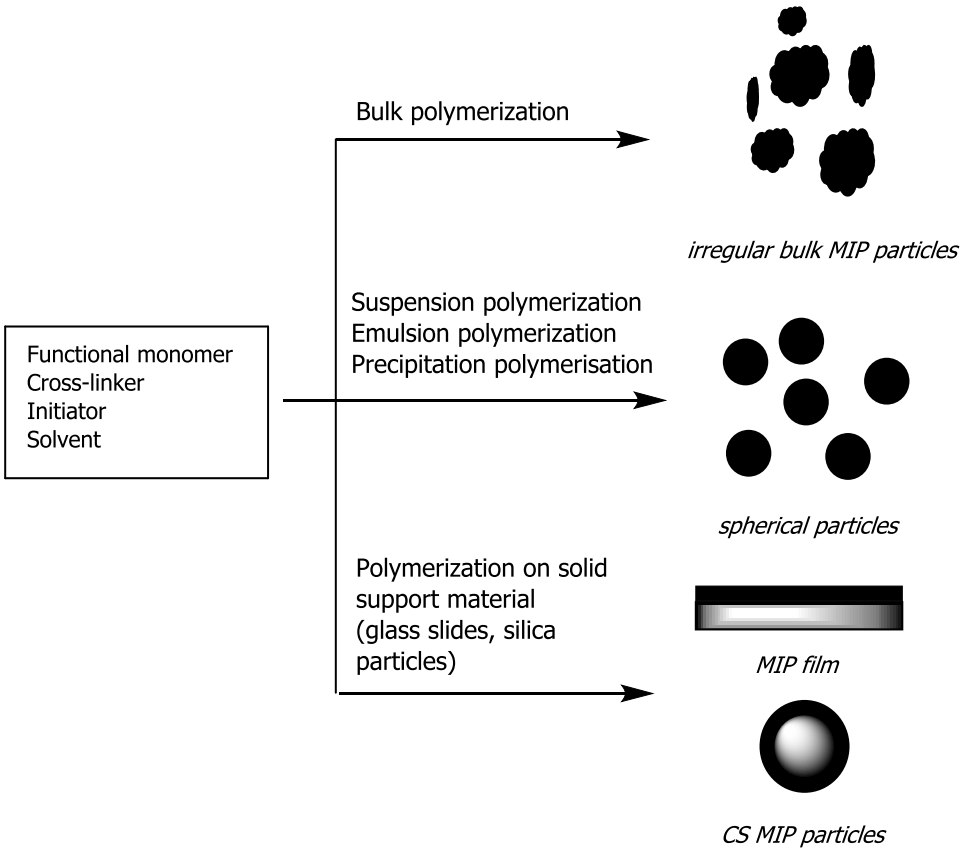

Fig. 7: Schematic illustration of the different MIP formats.

In recent years, the focus shifted more to the controlled/living free radical polymerization (CLRP), including reversible addition-fragmentation chain transfer (RAFT) polymerization, metal-catalyzed atom transfer radical polymerization (ATRP) and nitroxide-mediated polymerization (NMP).[78-82] These methods lead to more homogenous polymer layers on the surface and a better control over molecular weight, composition and network structure.[83]

The RAFT polymerization is by far the most commonly used method of CLRP. In comparison to traditional azoinitiators, dithiocarbonyl compounds define the reversible chain transfer group. During the polymerization process, the radical is formed through thermal or photo dissociation of the initiator in the bulk solvent. The formed radical is deposited on the C=S double bond of the RAFT reagent to form a stabilized radical intermediate. The add-on rearrangement leads to a release of the other growing chain whereby the polymer chains can grow from the surface with similar lengths. With the recombination of two radicals the growth of the chain is terminated.[84,85] The process is schematically shown in Fig. 8.

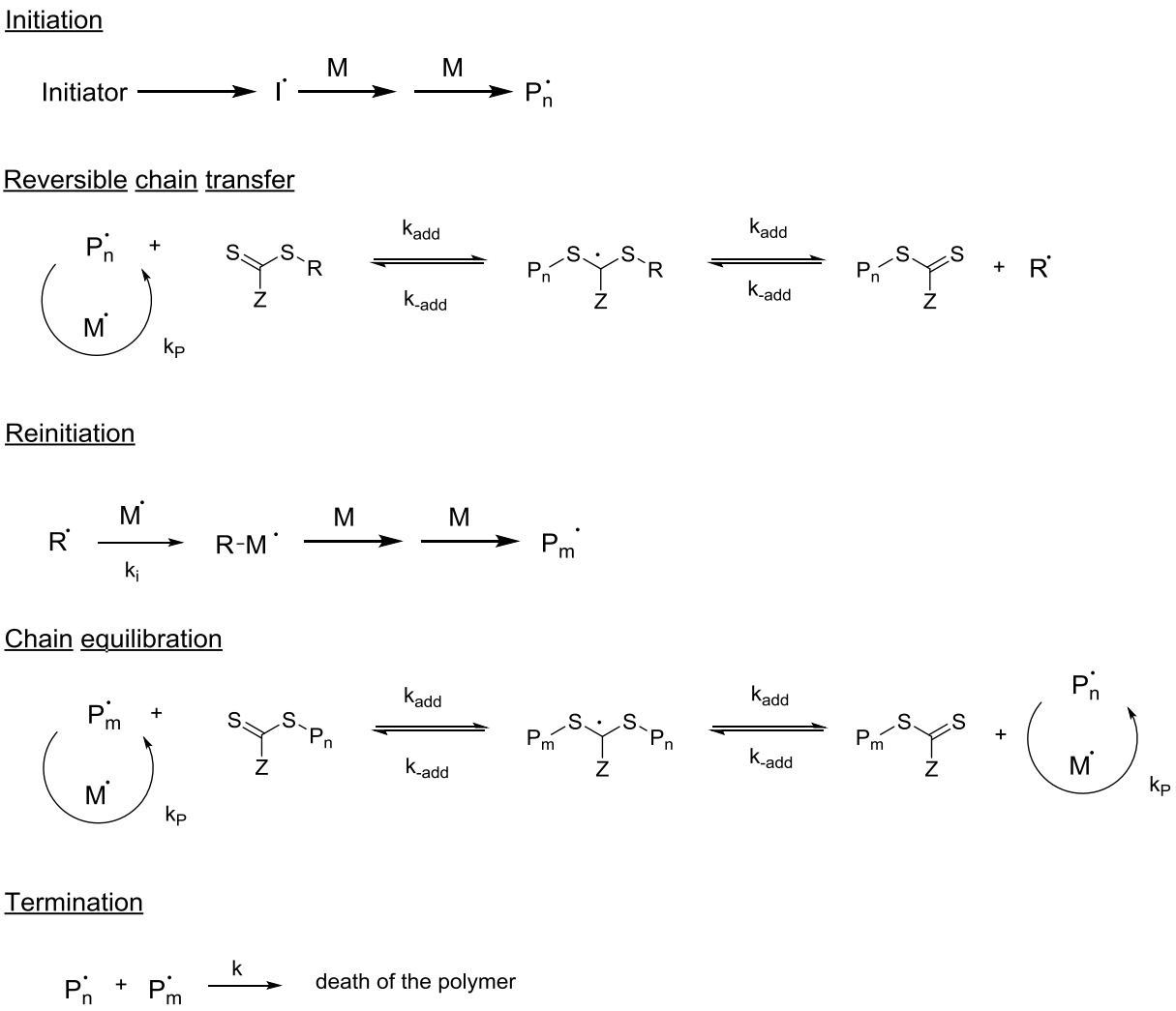

Fig. 8: Mechanism of RAFT polymerization.

This process can be applied to a wide diversity of monomers under mild reaction conditions.[86] Exclusively, the RAFT technique gives the possibility to control the polymerization of reactive monomers such as vinyl compounds. Pan et al. demonstrated water-compatible MIP microspheres with good recognition properties by using RAFT polymerization for synthesis.[87]

Except for the use of these sulfur-containing compounds that can lead to undesirable odors, this technique offers great control over molecular weight and reduction of the heterogeneity in the polymers and thus, the possibility to create a homogeneous MIP layer on silica particles.[88,17]

However, the used RAFT agents have to be adapted to the monomers. These transfer agents are not commercially available and must be prepared in

often demanding laboratory work. Dithioesters are perhaps used most widely because they are suitable for a large number of monomers.[89] Due to the intense color of the RAFT agent, usually a red polymer is formed which indicates the preservation of the active sites on the substrate.

Lu et. al. used RAFT polymerization to coat a thin homogeneous MIP layer onto the surface of silica particles obtaining a fast and selective response to sulfadiazine.[72] The integration of these core-shell MIP particles into (micro)fluidic assays or fibre optics can produce suitable sensors for monitoring the analyte in real time and on-site.

2.3 Applications of MIPs

The detection of contaminants in air, water and food is crucial to ensure human health. In addition, health authorities and industries are interested in fast, simple and accurate methods for contaminants such as herbicides, pesticides and heavy metals. Therefore, various applications based on MIPs to separate and purify, detect and determine the contaminants have been developed in recent years.

2.3.1 Separation

Especially separation techniques came to the fore. In 1994, MIPs were used as sorbent solid-phase extraction (SPE) for the first time by Sellergren.[90] With molecularly imprinted solid-phase extraction (MISPE), the analyte is extracted from a mixture by the imprinted polymer. The sample is cleaned up and pre-concentrated since the analyte may exist in low concentration.[15, 91] Theodoridis et al. demonstrated a MIP for caffeine as the target molecule which is used as a selective sorbent for solid-phase extraction (SPE), within an automated on-line sample preparation method.[92]

The use of molecular imprinted chiral stationary phases (MICSPs) offers an efficient way to produce binding sites for a specific enantiomer which binds to the stationary phase while the other one is eluted earlier. This method is used for the separation of various species of drugs, peptides, amino acids and other chiral compounds and often shows higher selectivity than those obtained with

conventional CSPs.[93] Furthermore, the high mechanical stability due to the high crosslinking degree of MIPs und thus, stability against high pressure and wide pH range makes them applicable under extreme conditions. Compare to conventional adsorption methods, these MISPs do not lose their performance over long time.

However, problems associated with leakage of remaining imprinted molecules during sample pre-concentration can occur.[94] Even after an intensive extraction step, template molecules can still remain in the polymer network. This leads to an adverse effect particularly when the MIPs are used in trace and ultra-trace analysis. To solve that problem, a close structural analogue of the analyte can be used as the imprinted species.[94]

2.3.2 Binding assay

With immunoassays analytes in liquid phase can be detected by the binding of an antigen to an antibody. However, the preparation of these systems are time-consuming and expensive.[95] Therefore, MIPs are increasingly considered as an alternative to bio-macromolecular recognition units such as antibodies or enzymes due to their facilely tailorable selectivity towards certain analytes or a group of structurally related species, low production costs, stability and robustness.[96] In addition, no time-consuming conjugation step with larger carrier molecule for the antibody production is necessary. In first experiments, dealing with bronchodilator theophylline and the tranquilizer diazepam, antibodies in radio- and enzyme immunoassays have been successfully replaced by MIPs. For theophylline, the analyte was detected in blood in linear range of 14 –224 µM. Serums from 32 patients were tested and showed excellent accordance with enzyme-multiplied immunoassay technique (EMIT) as well as cross-reactivity against other compounds.[97] However, this method is more complex than EMIT. Prior the analysis, an extra extraction step of analyte from the biological sample was necessary because MIPs give the best binding results und thus, selectivity in organic solvents. MIPs as plastic antibody for in-vivo applications was performed by Hoshino et. al., who used imprinted nanoparticles to capture the cytotoxic peptide melittin in the blood of living mice and thus, mortality and peripheral toxic

symptoms of melittin were significantly decreased.[98] Meanwhile, there are immunoassays with MIPs for other drugs and herbicides.[99,100]

2.3.3 Catalysis

MIPs can also be used as catalysts where catalytic groups, which are similar to the active site of an enzyme, are integrated to the binding sites of the MIPs.[101] Such enzyme-mimics for hydrolysis of p-nitrophenyl acetate was firstly shown by Robinson et al..[102] Here, an imprinted polymer was prepared which is specific for a transition state analogue (TSA) p-nitrophenyl methyl phosphonate. Due to this imprinting, the rates of hydrolysis of p-nitrophenol acetate is increased and can be inhibited by addition of the p-nitrophenol methyl phosphonate. An catalytical effect of $k_{imp}/_{knon\text{-}imp}$=1.6 (k, rate of hydrolysis of p-nitrophenol acetate) could be reached. Further TSA approaches were used for aldolase reactions, transamination and diels-alder-reaction.[103-105]

2.3.4 Sensors

Compared to the other presented application fields, the use of MIPs as artificial receptors in sensing applications develops more slowly due to the challenging preparation of MIP-based chemical sensors. The sensing response has to be governed by the interaction of the MIP and the template in one step and the MIP has to be coupled to a suitable transducer obtaining the chemical response. Meanwhile, there are many different areas for MIP sensor applications. Especially in chemical industry normally harsh conditions are used, for instance strong acidic and basic solvents as well as high temperature. Due to their high stability, MIPs can stand these extreme environments and thus are suitable for being immobilized on sensor surfaces. In addition to this, investigations of molecularly imprinted sensors are increasing year by year, which is shown in Fig. 9.

Furthermore, the low material cost, facile preparation process and high selectivity of MIPs make them suitable as artificial recognition element in biomimetic sensor materials in medical and therapeutic areas to bind bioactive molecules under specific conditions. Like antibodies, MIPs can exhibit selective

binding for an analyte. Recently, many MIP-based biosensors have been developed for different small molecules.

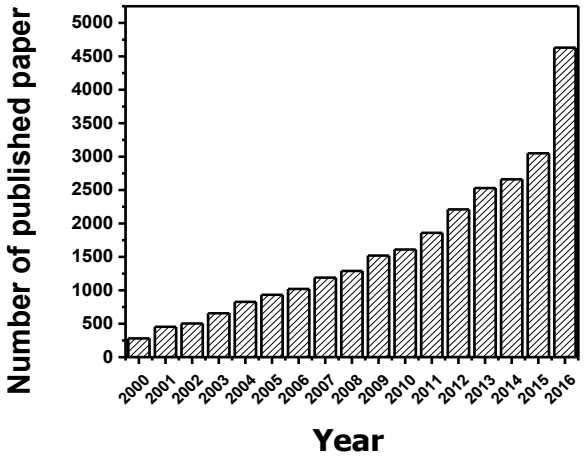

Fig. 9: The number of published papers about "molecularly imprinted sensors" in the last 16 years (Google Scholar).

In recent years, more and more researchers have started to investigate the combination of the advantages of MIPs and optical sensors. Such an optical MIP sensor can measure the changes of the optical properties e.g. surface plasmon resonances (SPR) or fluorescence. Due to the high sensitivity and the feature to assess the MIP's structural and binding properties, especially fluorescence spectroscopy is often used in optical MIP sensor technology.[106-109]

2.4 Fluorescence

2.4.1 Background

In the last two decades, an growth in the use of fluorescence probes for fluorescence sensing and reporting in various fields of science has been observed. It is a powerful and essential method for clinical diagnostics, biotechnology, molecular biology and biochemistry, materials and environmental sciences.[110] Compared for example with electrochemical detection or NMR (nuclear magnetic resonance), fluorescence offers a more powerful detection mechanism to report chemical recognition events especially at low concentrations and with rather moderate instrumental effort. Using fluorescence with its high sensitivity and

specificity single molecules can be detected.[111] Thus, fluorescence is one of the most important methods for future miniaturized detection and sensing technology. Mechanistically in the absorption/fluorescence cycle, the incoming light raises the energy of an electron in the fluorophore molecule to the excited state (absorption). The electron then loses some energy due to relaxation of the Franck-Condon excited state into the lowest vibrational state of the excited molecule, eventually returning to the ground state accompanied by emission of a photon. The emitted light has less energy than the absorbed light due to the loss of energy between the absorption of the photon and its emission, termed the Stokes shift. Furthermore, the direct proportionality of the fluorescence intensity to the absorbed excitation light allows to a certain extent to reduce detection limits by increasing the excitation power (yet photobleaching has to be avoided). There are already hundreds of commercially available fluorophores for many different applications in the field of chemical sensing due to their absorption and emission at characteristic wavelengths. However, in fluorescent sensors an excitation wavelength in the green to red wavelength region of the visible spectrum is preferred because of the availability of economical light sources and the suppression of matrix autofluorescence. This background fluorescence often stemming from fluorescent groups on bioorganic material is commonly reduced beyond 350 nm.

2.4.2 Design principles of common fluorescent probes

Fluorescent probes or indicators commonly consist of a fluorophore and a receptor unit that are either directly linked by a covalent bond or through a linker unit. The photophysical communication of the two subunits that is important for the spectroscopic response is commonly achieved by excited state mechanisms. The receptor recognizes the analyte with its binding sites, while the fluorophore as the fluorescent reporter moiety translates the binding event between the analyte and the receptor into a fluorescent signal. The linker or spacer insulates the fluorophore and the receptor but is able to allow for long-range photophysical process to happen.[112] The sensing response of the fluorescent probe can be

measured through changes in absorption and emission spectra, fluorescence intensities (or quantum yields) and lifetimes.

Photoinduced electron transfer (PET) is a widely used process to implement fluorescence intensity changes into a fluorescent probe. Such a PET system usually contains an electron-deficient fluorophore, an electron-rich receptor (often an aliphatic amine) and an alkyl chain as the insulating linker between both units. The receptor acts as the electron donor and commonly quenches the fluorophore's fluorescence in the unbound state of the probe. However, as soon as an electron-poor analyte binds to the receptor unit, the PET process becomes energetically less favored and is blocked, reviving fluorescence. The mechanism can be explained using frontier orbital theory (Fig. 10). In order to reach a PET, the $HOMO^{\dagger}$ (highest occupied molecular orbital) of the electron donor (receptor) has to be energetically higher-lying than the HOMO of the electron acceptor (fluorophore). If the HOMO of the fluorophore is then again fully occupied after electron transfer, the excited electron cannot relax back from the fluorophore's LUMO into its HOMO, meanwhile emitting a photon, but has to sidestep into the half-emptied $HOMO^{\dagger}$ of the receptor, which commonly is a "dark" process. No fluorescence can be observed.[113] If the $HOMO^{\dagger}$ of the receptor is energetically decreased, e.g. by the binding of an analyte, no electron can be transferred from the $HOMO^{\dagger}$ into the HOMO of the fluorophore, and fluorescence is restored (Fig 10). Of course, the architecture can also be reversed for electron-rich analytes. In such a case, the receptor's $HOMO^{\dagger}$ can only donate an electron into the half-emptied HOMO of the excited fluorophore when an electron-rich analyte is bound.[114] Such a system would indicate the analyte through ON–OFF fluorescence switching. Leung et al. demonstrated a fluorescent organosilane in which the sensing was based on PET quenching suppression upon protonation of the tertiary amine as soon as the analyte binds to the MIP. As the result of this effect, the fluorescence is enhanced. That system was applied for a sol-gel 2,4-D-imprinted polymer which showed a 2,4-D concentrations dependent fluorescence enhancement with a LOD of 45 µM.[115]

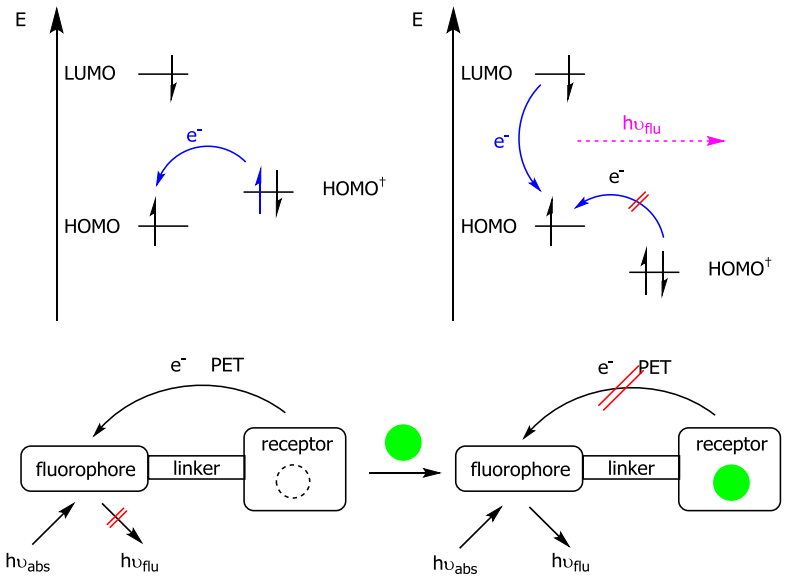

Fig. 10: Quenching of fluorescence by PET (left) and obtained fluorescence after binding of the analyte • (right).[112]

The other widely employed photophysical signaling principle is based on an *intramolecular charge transfer* (ICT), which is often considered in push-pull-π-systems linking an electron donating and an electron withdrawing (acceptor) group (without a spacer).[116] Here, HOMO and LUMO are commonly localized on different fragments of a fully π-conjugated molecule. As soon as the light excitation takes place, an ICT proceeds from the electron-rich (HOMO) to the electron-poor (LUMO) fragment of the probe which changes the dipole moment significantly. Normally, such mechanism is noticeable in spectral shifts of both absorption and emission, also changing the Stoke shifts. As shown in Fig 11., the position of the receptor defines whether a red or blue shift can be observed in the spectra.[112] The former is obtained when the analyte interacts with the electron-accepting group. On the other hand, the connection of the receptor group to the electron-donating group leads to a reduction of the donating character and thus to a blue shift in the emission as well as absorption spectra.[117]

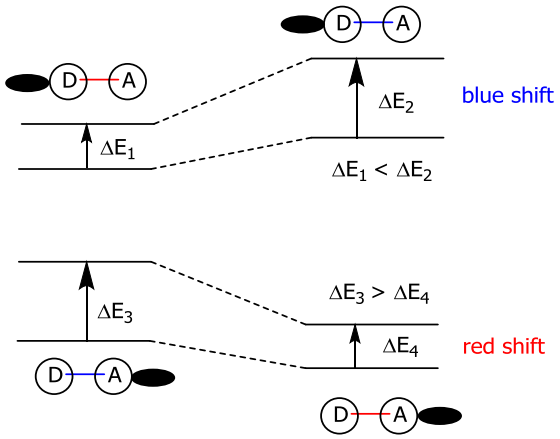

Fig. 11: ICT system: the analyte interacts with the donor group (top) and acceptor group (bottom).[117]

The design and development of novel probes with suitable fluorescence properties guaranteeing high sensitivities in combination with recognition elements with high selectivity are highly desired, especially to detect molecules in a simple manner at low concentrations in the environment.

2.5 Fluorescent MIP (fMIP) sensor

Chemical sensing using fluorescence to report the molecular recognition by MIPs was firstly demonstrated by Mosbachs group during the 1990´s.[118] They developed a MIP based fiber-optic sensing device for the detection of an amino acid derivatized with a fluorescent labeling group dansyl-L-phenylalanine **1** with good enantiospecific discrimination by using MAA and 2-vinylpyridine (2-VPy) as the functional monomers and EGDMA as the cross-linker. Fiber optics were used to assess the fluorescence of the MIP upon analyte binding in MeCN. It could be shown that the fluorescence enhancement upon addition of the analyte is a function of the concentration of the fluorescence-labeled derivative. Subsequently, various fluorescent or chromogenic molecules have been incorporated into sensing MIPs.

A fluorescent sensor has to be developed in a way, that the target binding generates a fluorescence signal. One way to signal the target binding in the MIP is the direct measurement of a fluorescent analyte. Rachkov et al. combined fluorescence sensing and high-performance liquid chromatography (HPLC)

separation. The fluorescence method was used for the detection of the steroid hormone β-estradiol.[119] For the preparation MAA and EGDMA in the presence of the target molecule were used.

However, because fluorescent analytes are in general very rare, a tailor-made fluorescent template analog as a probe can be used in a competitive assay like in competitive immunoassays. Such an assay has been established for 2,4-D using 4-vinylpyridine (4-VPy) as the functional monomer and EGDMA as the cross-linker.[96] A 7-carboxymethoxy-4-methylcoumarin (CMMC) **2** was used as the non-related fluorescent probe. With this assay a good limit of detection (LOD) of about 100 nM were reached but with a bad cross-reactivity against other analogs.[96] The MIP functioned as selective recognition element for analyte binding in such pseudo-immunosensors, however, the polymer itself is non-fluorescent. The fluorescent signal has to be produced by something external to the sensor. The right choice of the labeled analog and the synthesis of such tailor-made fluorescent analyte analog can be complicated.

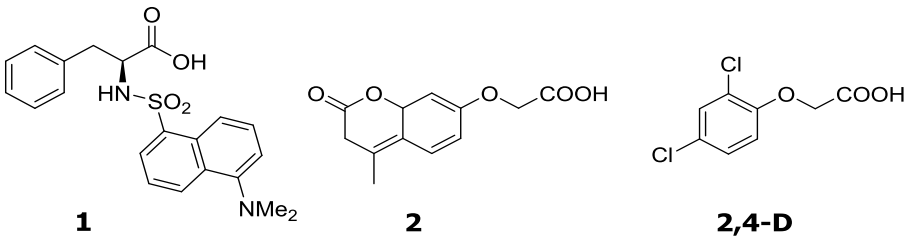

1 **2** **2,4-D**

Fig. 12: Chemical structures of **1**, **2 and 2,4-D**.

To circumvent these extra time-consuming steps, a fluorescent reporter (fluorophore) sensitive to the interaction with an analyte can be used. Here, the interaction or the binding event with the analyte is converted into an output signal which is related to the analyte concentration. The fluorophore is incorporated into the polymer matrix by a polymerizable linker and offers to use the response to the binding of the target molecule directly for identification and quantification. This approach leads to many possibilities of integrating different fluorescent dye or probe monomers.

2.5.1 Fluorescent dyes as monomer and their interaction with analytes

Wu et al. have reported the synthesis of a polymerizable dansyl-based monomer **3** through coupling of 3,3-dimethylacrylic acid and dansylchloride. **3** was used to prepare fluorescent MIP nanoparticles by precipitation polymerization to finally detect bisphenol A (BPA) in tap and river water.[120] Upon binding of BPA *via* its phenolic groups, a significant fluorescence quenching was shown. In contrast to that, the NIP as well as analytes with similar structure showed less response. The LOD and the limit of quantification (LOQ) were 3 and 10 µg L^{-1}, respectively.

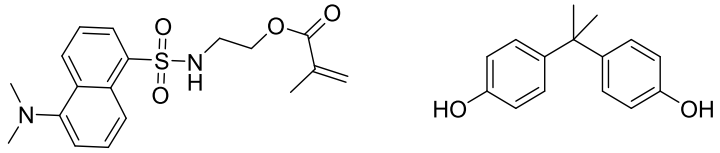

3 **Bisphenol A**

Fig. 13: Chemical structure of **3** and respective template.

Analysis like gas chromatography-mass spectrometry (GC–MS), liquid chromatography-tandem mass spectrometry (LC–MS/MS) or high-performance liquid chromatography (HPLC)-UV detection were applied to determine BPA in aqueous samples at ng/L to µg/L levels.[121,122,123] Thus, the fluorescent MIP nanoparticles can match with these other techniques.

Nguyen et al. used cocaine as the template and acrylamidofluorescein **4** as fluorescent monomer with a polymerizable group for integration into the MIP matrix.[124] The fMIP film was grafted onto an optical fiber. When the fMIP-coated optical fiber was dipped into a water–acetonitrile mixture containing cocaine, a fluorescence enhancement was observed with 0.5 mM template.

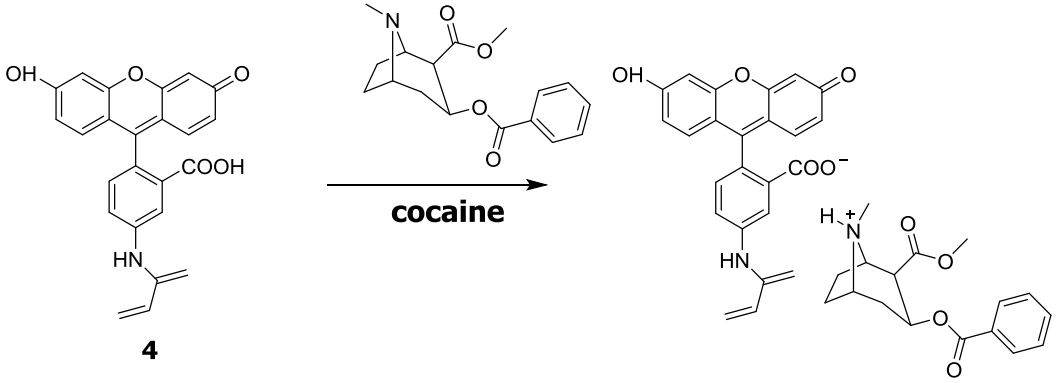

4

Fig. 14: The anticipated interaction of **4** with cocaine.

Furthermore, Lavignac et al. prepared a fluorescent monomer **5** by coupling of 4-chloro-7-nitrobenzofurazan (NBD-Cl) with allylamine.[125] The monomer was then copolymerized with MAA and EGDMA into bulk fMIPs for atrazine. Although a high dissociation constant of $\log K_D$ = 4.75 ± 1.98 was determined by batch rebinding, the fluorescence response was not reported, suggesting that the interaction between both partners is too weak to overcome the absence of designated binding modes.

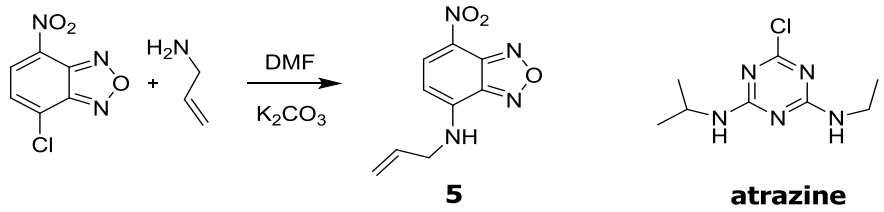

Fig. 15: Synthetic scheme for **5** and respective template.

Additionally, coumarin was introduced by the groups of Nguyen and Ansell for the preparation of fluorescent monomers **6 and 7** for sensing the target molecule (−)-ephedrine.[126] **6** and **7** (Fig. 16), differing in both electronic nature and the length of linker, have been investigated for their fluorescence response toward chiral amines. When studied in solution, both fluorescent monomers show blue-shifted fluorescence and quenching (**7**) as well as enhancement (**6**) on interaction with the analyte. If the carboxylic acid group of the coumarin moiety interacts with the amino and hydroxyl groups of (−)-ephedrine as proposed by the authors, the charge transfer character in the chromophore is diminished, leading to the blue shift. Moreover, such interactions are expected to entail a reduction of the twisting angle between the chromophore (here coumarin) and an appended phenyl ring (here the vinylphenyl group only in **6**), thus leading to higher fluorescence of **6** compared to **7**. However, once incorporated into the fMIPs, both **6** and **7** show fluorescence quenching after binding to (−)-ephedrine, with binding constants of 10^5 M^{-1}. Such a strong binding constant demonstrates a high affinity of the analyte to the MIP. Apparently, the rotational freedom is reduced in the polymer matrix and the overall environment is less polar than the bulk solvent. Nguyen and Ansell suggested that the addition of a co-monomer such as MAA or methyl methacrylate (MMA) can amend the recognition ability, yet the

experimental results point against this supposition. The fMIP prepared from **7** exhibit the highest imprinting effect and quenching efficiency of up to 59% with 1 mM (−)-ephedrine. The poorer performance of **6**–fMIP compared with **7**–fMIP is not fully understood. A disadvantage is the poor fluorescence response of both fMIPs in aqueous buffer.

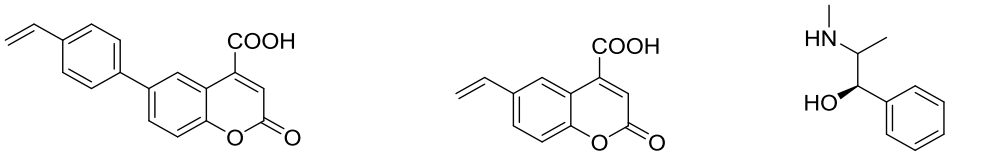

6 **7** **(-)-ephedrine**

Fig. 16: Chemical structure of **6** and **7** and respective template.

In addition, Kubo et al. have prepared a 2-acrylamidoquinoline monomer **8** for imprinting cyclobarbital. This barbiturate belongs to anticonvulsant drugs and has sedative and hypnotic properties.[127] The monomer forms two directional hydrogen bonds (H-bonds) with the target molecule cyclobarbital for a stable complex which also reduces the rotation in the MIP cavity (Fig. 17).[128] After binding of the target molecule, a 3-fold increase in fluorescence intensity was observed. The NIPs showed less fluorescence enhancement. They have also found that the fluorescence response is in good correlation to the batch rebinding results. This indicates that the fluorescent probe molecule is mostly located in binding cavities.

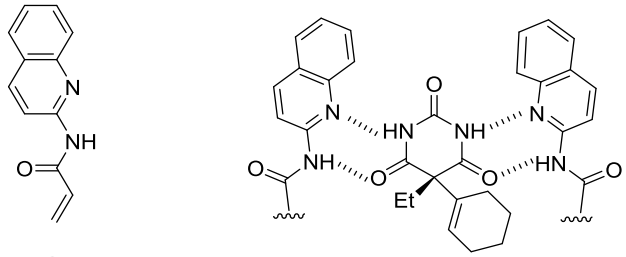

8

Fig. 17: Chemical structure of **8** and binding mode of **8** and cyclobarbital.

The group of Rathbone prepared a fMIP using benzylidine 3-acrylamidorhodanine **9**, TRIM as cross-linker and (*Z*)-*N*′-cyclododecylidenepicolinohy-drazonamide as the template (Fig. 18). The binding of the target molecule *via* H-bonds can be detected through a 2-fold decrease of the fluorescence signal.[129]

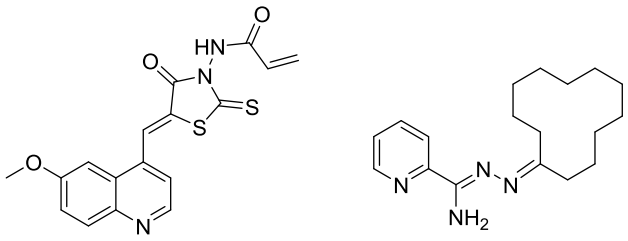

9 **template**

Fig. 18: Chemical structure of **9** and template.

However, often H-bonds are not optimal for the detection in aqueous solution. To prevent the competition of the water molecules with the analyte for the fluorescent monomer, electrostatic interactions are better suited. Turkewitsch et al. have prepared a fluorescent monomer trans-4-[p-(N,N-dimethylamino) styryl]-N-vinylbenzylpyridinium chloride **10** for the recognition of cyclic monophosphate neucleotide.[130] Due to electrostatic interactions between these compounds a location of probe molecules inside the cavity is preferred for better signaling in water samples. Upon addition of the analyte, the fluorescence is quenched by 20% while it remains unchanged upon addition of the structurally similar molecule as well as for the fNIP samples.

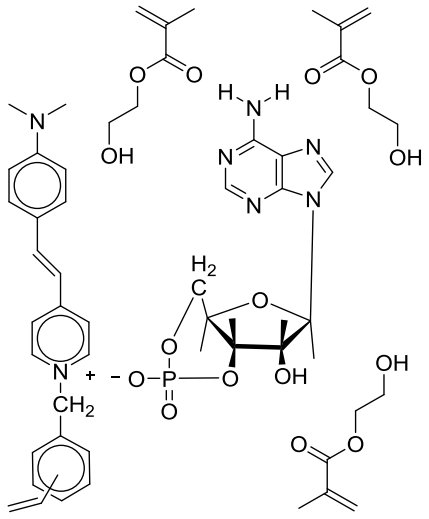

10

Fig. 19: Chemical structure of **10** and components of corresponding MIP system.

Another study was performed by Chen et al., whereby dianionic pyrene-based monomer **11** and the herbicides paraquat and diquat as templates were used for

imprinting in water.[131] Again, fluorescence decrease could be observed after binding of the analytes.

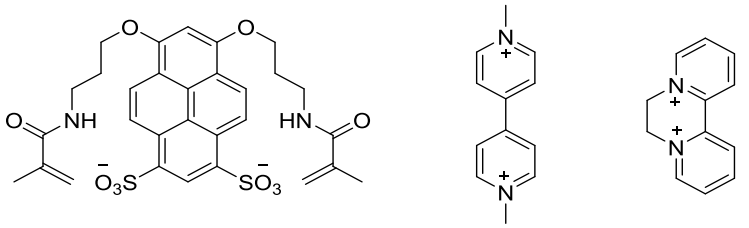

11 **paraquat** **diquat**

Fig. 20: Chemical structure of **11** and respective templates.

2.5.2 Fluorescent probes as fluorescent monomers

As described in the previous section, polymerization of fluorescent dyes into the MIP matrix is a promising option to obtain an optical signal upon binding of the analyte. However, up to this point no designated binding site able to change the signal intensity has been directly integrated. To solve this problem, fluorescent probe monomers with four (or more) subunits, e.g., fluorophore-linker-receptor-linker polymerizable (FLRLP) unit can be used instead of the regular fluorophore–linker–polymerizable unit architecture.[114]

Inoue et al. prepared the functional monomer **12**, *O*-acryloyl L-hydroxyproline conjugated with dansyl ethylenediamine. The pyrrolidine moiety responsible for binding proteins *via* H-bonds is separated from the dansyl moiety by a spacer to place it precisely at the hydrophobic regions of human serum albumin (HSA).[132] The fMIP films show fluorescence quenching upon binding HSA which was used as template molecule. The study revealed significant cross-sensitivity only for bovine serum albumin and that the fluorescence method is more selective than a surface plasmon resonance method.

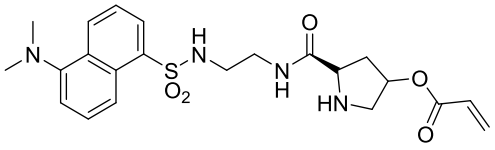

12

Fig. 21: Chemical structure of **12**.

However, more popular than this FLRLP unit approach, is the usage of fluorophore-linker-receptor-polymerizable (FLRP) units due to their smaller sizes

as well as the direct coupling of receptor and fluorophore which leads to an immediate signal. In the literature, the use of a urea moiety as a suitable receptor has been proven. The two NH groups are able to form two direct H-bonds with anionic species.

Wagner et al. presented a naphthalimide-based fluorescent monomer **13** for the integration into a MIP network.[133] The deprotonated *N*-carbobenzyloxy-L-phenylalanine (Z-L-Phe) template molecule can bind to the urea binding site of the monomer in MeCN via non-covalent H-bonds, resulting in a bathochromic shift in absorption and fluorescence quenching.

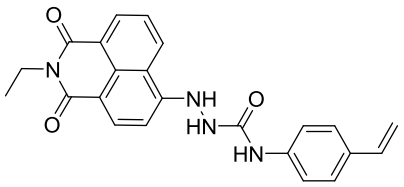

13

Fig. 22: Chemical structure of **13**.

In previous work by Wei et al. suitable fluorescent units for the detection of small organic molecules *via* MIP technique were synthesized. In addition, a fluorogenic NBD-based monomer **14** with an urea group was designed as recognition element for oxoanions e.g. tetrabutylammonium (TBA) salt of Z-L-Phe.[17] Upon the analyte binding to the functional monomer *via* H-bonds, a prominent fluorescence enhancement can be observed. An imprinting factor of 3.6 could be obtained as well as the fMIP showing a higher response for the TBA salt of Z-L-Phe than for the corresponding enantiomer *N*-carbobenzyloxy-D-phenylalanine (Z-D-Phe) and *N*-(carbobenzyloxy)-L-glutamic acid (Z-L-Glu) as conformationally closely related compounds. With this method, it is possible to detect small organic molecules with LODs down to 60 nM. The 10 nm thin MIP film on the RAFT agent coated silica particles offers high diffusion rates of the analyte in the cavity and signal saturation in about 20 seconds.

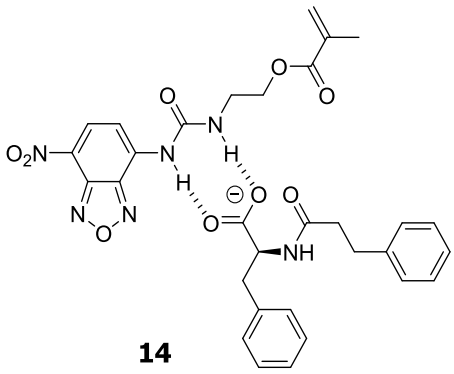

14

Fig. 23: Chemical structure of **14** and its binding mode with Z-L-Phe.

2.5.3 Excited-state proton transfer (ESPT)

Compared to the previous systems, another signal transduction mechanism is invoked in this Chapter, excited-state proton transfer (ESPT). Proton transfer reactions are very important in chemistry and biology.[134-137] Especially, increasing attention has been paid to ESPT in recent years. Due to the straightforward initiation by photoexcitation, this mechanism has become more and more important in fluorescence sensing and imaging applications.[136, 138-140] Various multi proton-transfer reactions have been investigated, however, excited state double proton transfer (ESDPT) in a complex bound through two hydrogen bonds is one of the most fascinating processes.[141-146] In ESDPT, both partners carry a proton donating and a proton accepting site that are usually tightly bound in a double Y-shaped motif..

There are three possible theories about the movement of the two protons (Fig. 24. It can happen concerted or stepwise. In the first ESDPT process (**A**), both protons are transferred coincidentally along the intermolecular hydrogen bonding paths and the tautomer is immediately formed after excitation. The stepwise mechanism proceeds in two cycles. In the first step (**B**), one proton moves from the hydroxy group of the acid to the ring nitrogen of the 2-aminopyridine to create an ion-pair intermediate. After this transfer, the second proton from the amino moiety starts to move to the acid, forming an imino tautomer. The second cycle (**C**) proceeds in the opposite order of proton transfers. Previous works of Ishikawa et al. and Chai et al. already reported the ESDPT reaction of an intermolecular hydrogen-bonded 2-aminopyridine/acid

system in hexane.[147] The stepwise mechanism of the ESDPT for 2-aminopyridines in acids was confirmed by experimental and theoretical methods. It was demonstrated that the proton transfer along the intermolecular hydrogen bond O–H···N takes place first. Subsequently, after the first proton transfer was completed, the second proton moved along the intermolecular hydrogen bond N–H···O.

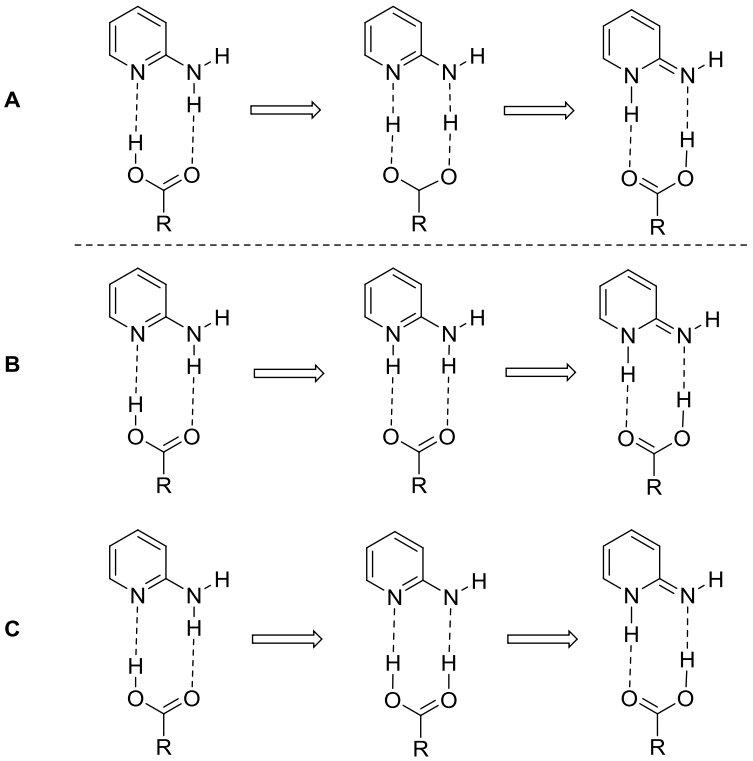

Fig. 24: Concerted (A) and stepwise (B, C) ESDPT reaction mechanism.[147]

3 Objectives

The aim of this thesis was to develop fluorescence-based optical sensors based on MIPs as the recognition element for the detection of small analytes.

In the first step, new fluorescent functional monomers/ cross-linker were designed and synthesized containing a polymerizable group to incorporate these dyes into a MIP matrix and offer a sensitive and selective recognition towards small target analytes of environmental interest. These fluorescent MIPs were transferred as a thin shell to silica particles to obtain a high surface area and thus, a fast sensing response.

By combining the MIP shell/ silica core particles with the field of microfluidic systems and optical fibers in the second step, the sensing and selective determination of small analytes in low concentration ranges for real-life applications were obtained and thus, showed a new way to extend the MIP applicability towards a new generation of optical sensing.

4 Material and Methods

4.1 Reagents and materials

Chloroform, acetonitrile, methanol, ethanol, dimethyl sulfoxide (DMSO) tetrahydrofuran (THF), dichloromethane, cyclohexane, toluene, pyridine, acetone, hexane, ethylchloroformate, ethyl ether, acetic acid, 4-cyano-4-(thiobenzoylthio)pentanoic acid (CPDB), aminopropyltriethoxysilane (APTES), ampicillin (AMPI), amoxicillin (AMOX), benzylmethacrylate (BMA), 3,5-dihydroxybenzyl alcohol, enoxacin (ENOX), enrofloxacin (ENRO), ethylene glycol dimethacrylate (EGDMA), (1E,4E)-N,N'-Dichloro-2,5-cyclohexadiene-1,4-diimine, 2-amino-4-bromopyridine, 4-ethynyl-*N,N,*-dimethylanilin, 2-[4-(2-hydroxyethyl)-1-piperazinyl]-ethanesulfonic acid (HEPES, >99.5%), 2-hydroxyethyl methacrylate (HEMA), 2-isocyanatoethyl methacrylate, methacryl amide (MAAm), triethylamine (TrEA), tetrabutylammonium hydroxide (TBA-OH), tetraethylammonium hydroxide (TEA-OH), tetramethylammonium hydroxide (TMA-OH), tetrahexylammonium hydroxide (THA-OH), tetraocylammonium hydroxide (TOA-OH) and Z-D-glutamic acid (Z-D-Glu), 2,4-dichlorophenoxyacetic acid (2,4-D) and 2-(2,4-dichlorophenoxy)propionic acid (2,4-DP), copper(I) iodide (CuI) were purchased from Sigma Aldrich, tetraethylorthosilicat (TEOS) from Merck, methanol (MeOH) with HPLC gradient grade from J.T.Baker, ethylchloroformate, 2,6-di-tert-butyl-4-methylphenol and 4-(2,4-dichlorophenoxy)-butanoic acid (2,4-DB) from Fluka, ammonium acetate (NH_4Ac), hydrochloric acid (HCl) and glacial acetic acid (AcOH) from Fisher Chemicals and ammonia (32%) from Applichem. 1,2,2,6,6-Pentamethylpiperidine (PMP) and 4-vinylpyridine (4-Vy) were purchased from Alfa Aesar. *N*-Carbobenzyloxy-D/L-phenylalanine (Z-D/L-Phe) and Z-D-tyrosin (Z-D-Tyr) were obtained from ABCR, 4-,4-(dimethylamino)-pyridine (DMAP) from Janssen Chimica, bis(triphenylphosphine)palladium(II) dichloride ($(Pd(PPh_3)_2Cl_2$) from Chempur and pyridine from Lancaster. Milli-Q water was drawn from a Milli-Q® ultrapure water purification system (Millipore Synthesis A10). 2,2'-Azobis(2,4-

dimethyl)valeronitrile (ABDV) was used from Wako Chemicals. **14** was received from Dr. Wei Wan[17] and **16**, **19** and **22** from modified in-house procedure.

4.2 Preparation of phenoxazinone-based monomer 16

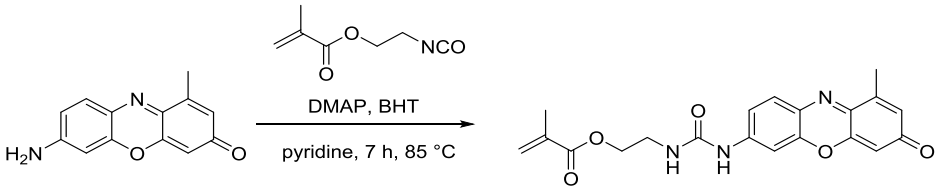

15 **16**

Fig. 25: Synthesis of **16.**

754 mg of 7-amino-1-methyl-3H-phenoxazin-3-one **15** (3.3 mmol) (prepared following the procedure of Descalzo et. al.)[148] and 8 mL methylacrylic acid-2-isocyanato-ethyl-ester (56.6 mmol) were dissolved in 18 mL pyridine, 470 mg DMAP (3.8 mmol) was added into the solution and the mixture was stirred at 85°C for 7 h. After cooling to room temperature (RT), 50 mL hexane were added into the solution and a black solid as raw product precipitated. The raw product was purified by column chromatography on Alox (neutral Al_2O_3) with CH_2Cl_2: ethanol (5:0.05) to obtain 500 mg (39%) as black powder.

^{1}H-NMR (500 MHz, DMSO-d_6) δ: 1.90 (s, 3H), 2.34 (s, 3H), 3.43 (q, J = 9 Hz, 2H), 4.15 (t, J = 4,5 Hz, 2H), 5.71 (t, J = 2.5 Hz, 1H), 6.09 (m, 1H), 6.17 (d, J = 3.5 Hz, 1H), 6.63 (m, 2H), 7.28 (dd, J1 = 4 Hz, J2 = 18.5 Hz, 1H), 7.688 (s, 1H), 7.73 (t, J = 3.5 Hz, 1H), 9.47 (s, 1H).

^{13}C-NMR (DMSO-d_6) δ: 16.80, 18.47, 64.14, 94.38, 103.10, 105.39, 115.62, 126.49, 127.86, 131.33, 131.83, 136.25, 143.31, 145.32, 145.72, 150.65, 155.07, 167.00, 185.31, 215.68.

4.3 Preparation of phenoxazinone–based crosslinker 19

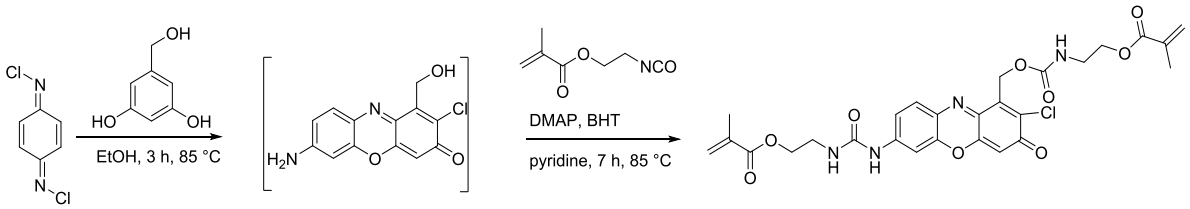

17 **18** **19**

Fig. 26: Synthesis of **19**.

71.6 mg of (1E,4E)-N,N'-Dichloro-2,5-cyclohexadiene-1,4-diimine **17** (0.41 mmol) and 51.0 mg of 3,5-dihydroxybenzyl alcohol (0.36 mmol) were heated in ethanol (5 mL) at 85 °C for 3 h.[149] After solvent concentration and drying under vacuum, the crude product **18** was re-dissolved in 2.4 mL dry pyridine with 68.0 mg DMAP (0.56 mmol) and 50.0 mg 3,5-dihydroxybenzyl alcohol (0.23 mmol). 2-Isocyanatoethyl methacrylate (200 µL, 1.42 mmol) was added to the solution under argon (Ar) atmosphere and the mixture was heated at 85°C for 7 h. Subsequently, the crude product **19** was precipitated in cyclohexane (50 mL), washed with cyclohexane (2 x 50 mL) and toluene (3 x 50 mL). The black solid was dissolved in CH_2Cl_2/methanol (25:1) and poured into water. The organic layer was dried with anhydrous Na_2SO_4, filtered and the solvent was evaporated under reduced pressure. The crude product was purified by column chromatography on silica gel with CH_2Cl_2/ethanol (25:1) as eluent. After concentration and drying under vacuum **19** was obtained as a dark purple solid with a yield of 28 %.

19 (R = Cl) HRMS m/e (MH^+) 587.1530 (calculated 587.1539)

NMR characterization was not possible because **19** is insoluble in apolar solvents and at the concentrations required for NMR. The molecules underwent π-π-staking even in DMSO, which made unequivocal signal assignment impossible. Beside the main molecular peak of the chlorinated compound **19**, mass spectrometric analyses also showed the presence of a minor co-product 2H (H instead of Cl, ca. 5%) HRMS m/e (MH^+) 553.1921 (calculated 553.1929), which could not be separated despite multiple column runs. However, this minor species

did not impinge any problems on MIP synthesis or performance and further, more elaborate purification steps were not considered.

4.4 Preparation of 2-aminopyridine–based monomer 22

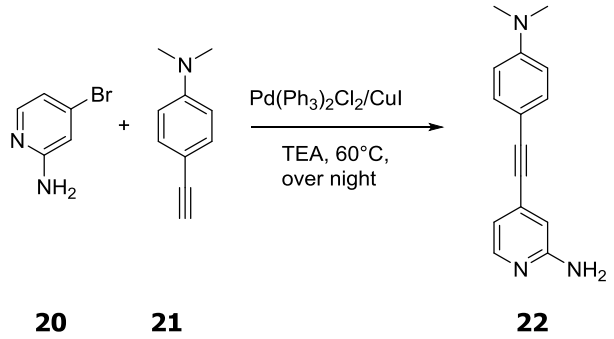

20 **21** **22**

Fig. 27: Synthesis of **22**

161.2 mg of 2-amino-4-bromopyridine **20** (0.91 mmol), 148.7 mg 4-ethynyl-*N,N,*-dimethylanilin **21** (1.02 mmol), 30.5 mg $(PPh_3)_2Cl_2$ (0.04 mmol) and 16.8 mg CuI (0.09 mmol) were heated at 60°C overnight in 8 mL TrEA. Subsequently, the crude product **22** was extracted in diethylether/water. The crude product was purified by column chromatography on silica gel with CH_2Cl_2/methanol (5:0.1) as eluent. After concentration and drying under vacuum **22** was obtained as a green-yellow solid with a yield of 83 %.

^{1}H-NMR (500 MHz, $CDCl_3$) δ: 3.01 (s, 6H), 4.52 (s, 2H), 6.67 (d, J = 7.0 Hz, 2H), 6,78 (m, 2H), 7.42 (d, J = 7.0 Hz, 2H), 8.12 (m, 1H).

^{13}C-NMR ($CDCl_3$) δ: 40.13, 85.06, 85.68, 94.49, 108.81, 111.71, 133.11, 133.66, 147.74, 150.52, 158.37.

4.5 Preparation of CPDB-coated SiO_2 particles with various sizes

Firstly, monodisperse and spherical SiO_2 particles with a diameter of 0.35 µm were prepared by the Stöber method, involving the hydrolysis and condensation of TEOS in the presence of water and ammonia as a catalyst. The preparation route was adopted from Wan et al. by mixing 32% ammonia solution (9 mL) and 99.9% pure ethanol (16.25 mL) in the presence of Milli-Q water (24.75 mL) and stirring at 1000 rpm, followed by the addition of a mixture of TEOS (4.5 mL) and ethanol

(45.5 mL) and further stirring at 500 rpm for 2 h. The particles were washed with Milli-Q water and ethanol and dried in a vacuum overnight.[150,17]

The activation procedure of the core particles was also adapted from Wan et al. by adding 3 g silica particles and 12 mL APTES into 140 mL anhydrous toluene.[17] The mixture was refluxed for 12 h under dry Ar atmosphere. The resulting APTES-modified silica particles were separated by centrifugation, washed with toluene, and dried in a vacuum.[17]

During the last years, controlled radical polymerization methods, e.g., reversible addition-fragmentation chain transfer (RAFT) polymerization, have been widely used to graft polymeric chains onto solid supports. Hence, we used this method to synthesize a homogeneous MIP layer onto silica particles. These RAFT agent-functionalized particles were prepared according to the protocol reported by Wan et al. by mixing CPDB as RAFT agent, ethylchloroformate and 60 mL anhydrous THF.[17] The silica particles are varying in size so that the amount of the components during the synthesis were adjusted as can be seen in Tab. 2. The mixture was purged with Ar and cooled to –78°C for 40 min. Subsequently, 3.5 g APTES-modified SiO_2 particles were added at –10 °C and the mixture was stirred at room temperature overnight. The particles were precipitated in 200 mL hexane, washed with acetone and THF and dried in a vacuum overnight.[17]

Tab. 2: Modification of SiO_2 particles with various sizes.

size SiO_2 core	**APTES-SiO_2**	**CPDB**	**Ethylchloro-formate**	**TrEA**	**THF**
[µm]	**[g]**	**[mg]**	**[µL]**	**[µL]**	**[mL]**
0.35	3.50	822.0	282	411	60.0
0.60	0.35	75.0	26.0	39.0	5.70
0.90	0.35	73.0	24.0	37.0	5.50
2.06	0.18	35.0	11.0	16.0	2.70

4.6 Preparation of core/shell (CS) particles

4.6.1 MIP(14)-Z-D-Phe/TXA@SiO_2 particles (0.35 µm size) with 14

To synthesize MIP-Z-D-Phe@SiO_2 particles, the following protocol was used:[17] For template preparation, Z-D-Phe (2.9 mg) and tetraalkylammonium hydroxide (TXA-OH) were combined in 100 µL acetonitrile (MeCN) and dried in a vacuum for 20 h. For the synthesis of the core/shell MIP-Z-D-Phe/TXA@SiO_2 particles, 50 mg of RAFT-agent functionalized SiO_2 particles and 4.5 mg ABDV were stirred in 5 mL anhydrous chloroform ($CHCl_3$) for 30 min at 50°C. BMA (18.6 µL), EGDMA (104.0 µL), the template and NBD-based monomer **14** (2.23 mg) (prepared following the procedure of Wan et. al.)[17] were added and further stirred for 18 h at 50°C and then for 2 h at 70°C for polymerization. After adding 10 mL of hexane, the synthesized particles were washed once with chloroform and three times with MeCN. For the removal of the template, a methanol/acetic acid (99/1) mixture was used. Subsequently, the particles were washed again with MeCN. The NIP control particles were synthesized under simultaneous conditions but without using the template.

4.6.2 MIP(16)-2,4-D@SiO_2 and MIP(19)-2,4-D@SiO_2 particles (0.35 µm size) with 16 and 19

The TBA salt of 2,4-D as template was prepared for the synthesis of silica core/shell MIP-2,4-D@SiO_2 particles. 30 mg of RAFT-agent functionalized SiO_2 particles and ABDV (2.5 mg) were stirred in anhydrous $CHCl_3$ (3.5 mL) for 30 min at 50°C. 4.78 µL MAAm, 57.6 µL EGDMA, the template and 5.8 mg of monomer **16** (for MIP(**16**)-2,4-D@SiO_2) or 8.9 mg cross-linker **19** (for MIP(**19**)-2,4-D@SiO_2) were added and further stirred for 18 h at 50°C and then for 2 h at 70°C for polymerization. After adding 10 mL of hexane, the synthesized particles were washed once with chloroform and three times with MeCN. For the removal of template, methanol/acetic acid (99/1) mixture was used. Subsequently, particles were washed with MeCN again. The SiO_2@NIP control particles were synthesized under same conditions but without using the template.

4.6.3 MIP(19)-AMPI@SiO_2(n) particles

In this part different MIP shell/silica core particles were synthesized with the same template AMPI/TBA but in different solvents and with different sizes. To differentiate the sensor particles better, we introduced (**n**) into the nomenclature (Tab. 3). The TBA salt of AMPI as template was prepared for the synthesis of silica core/shell MIP(**19**)-AMPI@SiO_2(**n**) particles with different sizes (**n**) (Tab. 3). RAFT-agent functionalized SiO_2 particles and ABDV were stirred in anhydrous solvent for 30 min at 50°C. MAAm, EGDMA, the template and cross-linker **19** were added and further stirred for 18 h at 50 °C and then for 2 h at 70°C for polymerization. After adding 10 mL of hexane, the synthesized particles were washed once with chloroform and three times with MeCN. For the removal of template, methanol/acetic acid (99/1) mixture was used. Subsequently, particles were washed with MeCN again. The NIP(**n**)@SiO_2 control particles were synthesized under similar conditions but without using the template.

Tab. 3: Modification of **19**-based MIP particle with different sizes, AMPI/TBA was used as template in all cases.

n	size SiO_2 core	RAFT-agent functionalized SiO_2	ABDV	Solvent/ Volume	MAAm	EGDMA	Cross-linker	template
	[µm]	[mg]	[mg]	[mL]	[µL]	[µL]	[mg]	[mg]
1	0.35	30.0	2.50	$CHCl_3$/ 3.5	5.70	68.4	9.80	6.40
2	0.35	30.0	2.50	MeCN/ 3.5	5.70	68.4	9.80	6.40
3	2.06	30.0	2.50	MeCN/3.5	4.06	48.9	7.60	7.89

4.6.4 MIP(22)-2,4-D@SiO_2 particles

For the synthesis of the core/shell MIP(**22**)-2,4-D@SiO_2 particles, 30 mg of RAFT-agent functionalized SiO_2 particles and 2.8 mg ABDV were stirred in 3 mL anhydrous chloroform ($CHCl_3$) for 30 min at 50°C. BMA (13.24 µL), EGDMA (74.31 µL), the 2,4-D (1.5 mg) and the monomer **22** (2.3 mg) were added and further

stirred for 18 h at 50°C and then for 2 h at 70°C for polymerization. After adding 10 mL of hexane, the synthesized particles were washed once with chloroform and three times with MeCN. For the removal of the template, a methanol/acetic acid (99/1) mixture was used. Subsequently, the particles were washed again with MeCN. The non-imprinted polymer (NIP) control particles were synthesized under simultaneous conditions but without using template. Subsequently, Soxhlet extraction with CH_2Cl_2 for 4 h was performed.

4.7 Spectroscopic studies

Absorption spectra and UV/vis-spectrophotometric titrations were carried out with a Specord 210 Plus absorption spectrometer (Analytik Jena), using dilute solutions with an absorbance of less than 0.1 at the absorption maximum. In case of spectra normalization, the maximum absorption was normalized to 1. The binding constant was assessed using HyperSpec software from Protonic software (Leeds).[151] For the measurement of the pre-polymerization mixture with much higher concentration a very thin micro-cell with a path length below 100 µm was used.

Fluorescence spectra and titrations were carried out with a FluoroMax 4 spectrofluorometer (Horiba Jobin Yvon) using standard 10 mm path length quartz cuvettes. The slit widths of the excitation and emission monochromators were 2 nm.

4.8 Fluorescence measurements of MIP sensor particles in $CHCl_3$

The binding properties of the MIP and NIP particles were investigated by fluorescence measurements. Typically, 2 mg core/shell particles were suspended in 2 mL solvent in a 10 mm quartz cell. The suspension was titrated with 1 mM TBA salt of the template and structurally similar compounds. After each step of addition, the suspension was allowed to equilibrate for 2 min by stirring before measuring the fluorescence spectra.

Plotting the reduced fluorescence change dF/F_0 (F_0 = fluorescence in absence of analyte; dF = fluorescence enhancement at the various titration steps)

of the MIP and NIP particles against the concentration of the analyte allows assessment of the sensing performance. This normalization is important to avoid experimental influences related to slight polydispersity of the microparticles or minimize errors arising from different shell thicknesses.

4.9 Two phase extraction assay

Typically, 3 mg particles were suspended in 2 mL $CHCl_3$ and 1 mL Milli-Q water was added in a 10 mm quartz cell creating a two-phase assay. 5 mM 2,4-D salt was added into the aqueous phase steadily. The suspension was stirred for 5 minutes to reach the equilibrium before each fluorescence measurement. The remaining 2,4-D/TBA in the aqueous phase was quantified by HPLC for validation.

4.10 Droplet-based modular microfluidic system

4.10.1 Set-up design and fabrication

The microfluidic device is based on our previously described set-up for mercury detection in water samples (Fig. 28).[152] The system was designed and set up using commercially available low pressure fittings and polytetrafluoroethylene (PTFE)– perfluoroalkoxy alkanes (PFA) tubes (OD, 1.6 mm, ID 500 µm). Two inlet tubes (PTFE) for introducing the water sample containing the analyte (2,4-D) and the MIP sensory particles (1 mg mL^{-1} in $CHCl_3$) were connected to syringes placed on standard syringe pumps (Chemyx Fusion 100 Touch). The pump for the MIP containing syringe stood in vertical position to avoid sedimentation. Via these two inlet tubes, both solutions were injected into a T-shaped micro-droplet generator (IDEX P-890 MicroTee) to produce homogeneous and stable droplets (110 nL, 1.4 Hz) as a result of shear forces and interfacial tension at the fluid-fluid interface. The droplets went through a reactor tube (transparent PFA) which was wrapped around a metallic bar to ensure droplets mixing by chaotic advection as well as the phase transfer of 2,4-D in the organic phase.

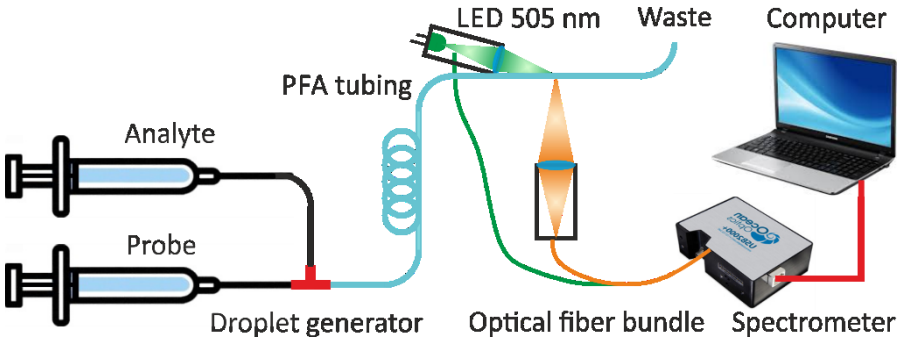

Fig. 28: Modular microfluidic platform for extraction and detection of 2,4-D in water samples using the MIP(**19**)-2,4-D@SiO_2 particles.

Fluorescence intensity changes were read out with a modular set up based on a standard opto-mechanical filter cube crossed by the microfluidic tube. Excitation of the fluorescent particles was achieved with a light emitting diode (LED, Everlight Opto 264-7SUGC/S400-A4) powered with 3.5 V DC. A band pass interferential filter (Semrock FF01 510/42) centered at 510 nm was positioned between the LED and the lens used to focus the beam into the microfluidic tube. In 90° to excitation, the fluorescence light was focused through a bundle of six optical fibers (core diameter 400 µm, external diameter 440 µm) and collected through a band pass filter (Semrock FF01 590/104) into an Ocean Optics spectrometer USB2000+ (tint = 5 ms, background, linearity, dark current and residual light corrections).

Treatment of the fluorescence signal was achieved in two steps. First, like for conventional fluorometers, fluctuations of the light source, here the LED and its power supply, were accounted for by collecting directly the excitation light as a reference into the seventh fiber of the optical fiber bundle through a short-pass filter (Semrock FF01 440/SP). Secondly, fluorescence signal from the organic phase was extracted by applying a logic formula (see below). When solely water or chloroform were circulating through the tube, there was no detectable fluorescence.

4.10.2 Signal treatment

MIP particles fluorescence signal (organic phase) was extracted from the recorded raw signal using the following logic equation (Eq. 1) and conditions:

$$I_F = I_0 \times (A \wedge B \wedge C)$$

Eq. 1: Extraction of the MIP particles' fluorescence signal in the organic phase from the recorded raw signal (see Tab. Tab. 4 for the detailed mathematical conditions)

Tab. 4: Conditions for validation of the signal treatment logic equation

Formula	Operation
$\mathrm{A}: \mathrm{I}_0 > \sum_{\mathrm{i}=1}^{100} \mathrm{I}_0$	Separation in two samples (organic phase/aqueous phase), above and below signal averaged at least over 100 s.
$B: \frac{120-\tau}{\sum_{i=1}^{100} \mathrm{A}} > I_0 > \frac{125+\tau}{\sum_{i=1}^{100} \mathrm{A}}$	Cleaning of the two samples using empiric bounds and a variable rate τ, fixed at 2 for these experiments. Removal of outliers coming from gas bubbles, dust or aggregates.
C: E{Bn, . . , Bn+12} = 12	Second cleaning, value kept only when 12 successive values were found. Removal of artefacts as a droplet correspond to 15-20 points.

Calculation of uncertainties[153]

$$u_{rel}{}^2 = n \times u_{rel}^w{}^2 + p \times u_{rel}^s{}^2 + q \times u_{rel}^d{}^2 + u_{rel}^a{}^2 + u_{rel}^r{}^2$$

Eq. 2: Total relative errors for each sample taking in account the errors coming from the different steps.[153]

with

- n x weighting of the products: $u_{rel}^w = 0.02\%$
- p x dissolving of the products: $u_{rel}^s = 0.5\%$
- q x dilution of mother solution: $u_{rel}^d = 0.5\%$
- Fluorescence analysis and numerical treatment: $u_{rel}^a = 0.7 - 0.8\%$
- Repetition of the experiment (N = 3): $u_{rel}^r = 0.4 - 5.6\%$

Tab. 5: Total relative errors calculated (Eq. 2) for ground water samples: A. Santa Fe River, Florida, USA; B. Mississippi, Minneapolis, USA; C. Hàn River, Da Nang, Vietnam; D. Lake Nghệ An, Vietnam; E. Teltow Canal, Berlin, Germany; F. Teltow Canal, spiked with 0.2 µM of 2,4-D; G. Rio Paranapanema, Salto Grande, Brazil.

Water sample	Preparation error %	Analysis error %	Repetition error %	Total relative error %
A	0.9	0.7	2.2	2.5
B	0.9	0.8	1.7	2.1
C	0.9	0.8	0.4	1.3
D	0.9	0.8	1.2	1.7
E	0.9	0.8	5.4	5.5
F	0.9	0.7	5.6	5.7
G	0.9	0.7	4.0	4.2

4.10.3 Titration of water samples collected worldwide

Traces of 2,4-D were investigated in samples collected around the world following a standard spiking method with aliquots of 20 to 60 nM of the analyte. No further preparation of the samples was required.

4.11 HPLC measurement

An Agilent 1200 Series LC system with a quaternary pump, degasser, autosampler, column heater and UV-detector was used with a Kinetex XB C18, 2.6 µm, 150 mm x 3 mm (Phenomenex, Aschaffenburg, Germany) analytical LC column with a UHPLC C18, 3 mm (Phenomenex) column guard. The software OpenLAB (CDS) ChemStation Edition for LC & LC/MS systems was used for operation and evaluation. The injection volume was 20 µL. The mobile phases were ultrapure water with 10 mM NH_4Ac and 0.1% (v/v) acetic acid (A) and MeOH with 10 mM NH_4Ac and 0.1% (v/v) acetic acid (B). The flow rate was 350 µL min^{-1} and the column heater temperature was 50°C. An elution gradient was applied, starting with 80% A, held for 3 min. Afterwards A was decreased to 5% within 5

min and held constant for the next 4 min, increased back to 80% A within 2 min and held for the next 8 min to re equilibrate the column.

4.12 ELISA Test

For method validation with regard to the quantitative determination of 2,4-D in water samples a commercial ELISA test for 2,4-D (Abraxis 2,4-D ELISA–Microtiter Plate) was used.

4.13 Fiber-optic array

4.13.1 Fiber-optic microarray fabrication

Microarray fabrication was adapted from references Nie et al. and Carrasco et al..[40, 154] The two ends of optical fibers were polished with diamond lapping films with varying abrasive sites (30, 15, 9, 6, 3, 1, 0.5, 0.1 and 0.05 µm, Allied High Tech) using a fiber polisher (Allied High Tech, Ranch Dominguez).

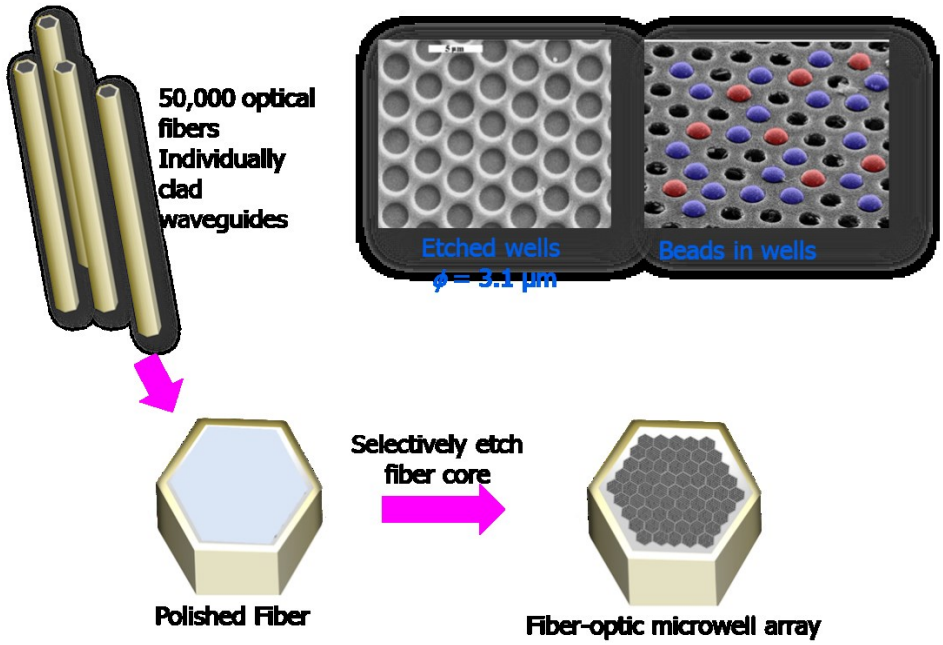

Fig. 29: Bead-based microarrays using fiber optic bundles; MIP/NIP sensor particles randomly loaded into the etched wells of an optical fiber bundle.[155-156]

The distal end was sonicated 20 s in DMSO as well as in EtOH and subsequently etched by immersing it into a 0.025 M HCl solution for 1 min 20 s to create microwells of 3.1 µm in depth. After sonication in distilled water for 5 s, the fiber was washed and immediately dried in an Ar stream. 1 µL of a 0.25 mg mL^{-1} MIP or NIP particle solution in MeCN was placed on the etched end of the fiber and left for the solvent to completely evaporate. This process was repeated 10 times to ensure an efficient loading into the microwells. To remove the excess of particles, the distal end was wiped with a cotton swap.

4.13.2 Assay protocol

The distal end of the fiber containing the MIP or NIP sensor particles was incubated in 1.5 mL of abs. MeCN or (25:75, v/v) MeCN:HEPES 25 mM, pH 7.5, (incubation solvent) while shaking for 15 min at 80 rpm several times to ensure the removal of monomer residues obtaining similar background signal for all fibers before incubating with the analyte. The fiber was placed vertically in a home-built fiber holder in the epi-fluorescence microscope (Olympus BX51) and the background signal images were recorded. Subsequently, the fibers were incubated in 1.0 mL solutions containing different concentrations of AMPI (0–25 nM) while shaking for 15 min at 80 rpm. After incubation, the fiber was washed with 1.5 mL of MeCN or working buffer ((25:75, v/v) MeCN:HEPES 25 mM, pH 7.5)) for 15 min at 80 rpm and then dried.

4.13.3 Image Capturing and Data analysis

The optical fibers were placed in a home-build fiber holder in the vertical direction whereby the microarray side (distal end) was opposite to the microscope objective. The proximal end was cleaned again with ethanol using a cotton swap to remove impurities which can decrease the image quality. Subsequently, six images of each fiber, containing the respective magnified views (insets), were recorded using an epi-fluorescence microscope (Olympus BX51). The microscope was equipped with a 16-bit charge-coupled device (CCD) camera (Infinity 3, Lumenera Corporation) and a 100 W halogen lamp (operating at 6 V to acquire bright field images and 12 V for fluorescence images). Both fluorescence and

bright field micrographs (1392 × 1040 pixels) were acquired using a 16 bit output format. The interference filter used was set at 470 nm, dichroic mirror was set at 490 nm and a 500 nm cut-off was selected, exposing the sample to light during 3 s.

For data analysis, fluorescence micrographs were set as RGB images and deconvoluted in their respective channels. Green and blue channels were discarded and the analysis was performed in the red channel. A threshold for intensities (15–255 a.u.) was applied and the microspheres were analyzed by displaying the measurements inside their size range of 30–130 pixel with a circularity of 0.7–1.0. The tri-mean criterion (see section 4.4.3) was employed instead of conventional mean statistics to avoid outliers, which gives more importance to the center of the population than to extreme points and thus provides a more robust analysis. The mathematical model is based on the weighted average of the distribution median distributing the population into quartiles: Q1, Q2, and Q3 are the 25%, 50% and 75% points in the distribution.[154] The experimental signals were normalized by the same mathematical procedure as described in 3.8.

4.14 TGA measurement

TGA measurements were performed on an instrument from Mettler-Toledo, equipped with a single-arm balance TGA/SDTA 851 and an autosampler. The implementation was based on the standard DIN EN ISO 11358:1997 standard instrument. For each case, around 10 mg of sample was heated from 25°C to 700°C with 10°C min^{-1} in a nitrogen flow of 30 mL min^{-1}.

4.15 ATR-FTIR spectroscopy

ATR-FTIR spectra were measured on a Nicolet 8700 Thermo Scientific spectrometer with smart orbit diamond cryo 2012 equipped with an IR light source, a MCT/A detector in the range of 650 to 3800 cm^{-1}. The measurements were performed using Omnic version 7.3 software (Thermo Electron Corporation).

Each spectrum is the average of 32 scans with a measurement time of 32 s and a resolution of 3800 cm^{-1} using auto baseline correction.

4.16 TEM and SEM measurement

High-resolution scanning electron microscopy (SEM) was performed on a Zeiss Supra 40 equipped with a high-resolution cathode (Schottky field emitter), an In-Lens SE secondary electron detector used in the high-resolution mode, and single unit transmission set-up. Transmission electron microscopy (TEM) was conducted with a FEI Tecnai G2 20 S-TWIN or Philips CM200 microscope operating at 200 kV.

Samples for the measurement were prepared on carbon thin film-modified copper grids (200 mesh) by drying 2 µL of a 0.1% (w/v) dispersion in ethanol. ImageJ software (National Institute of Health, US) was used for calculating the diameters of the particles. The diameters of the cores were subtracted from those of the core-shell hybrids.

4.17 Crystal structure

Crystal structure ORTEP plots were generated with ORTEP-III (Oak Ridge National Laboratory, Tennessee, USA) by Werner Kraus (BAM Federal Institute for Materials Research and Testing, Berlin, Germany) and generated by Katherine Chulvi Iborra (BAM Federal Institute for Materials Research and Testing, Berlin, Germany) using Mercury Software.

5 Results and Discussion

5.1 On the Role of Counterions in Molecularly Imprinted Polymers for Anionic Species

5.1.1 Introduction

Anion sensing has received strongly increasing attention over the past three decades, because anions are of paramount importance in all biological systems, most of all in the form of nucleotides and amino acids.[157-159] Furthermore, important ingredients of industrial products such as pesticides and fertilizers are also often potentially anionic in nature.[160] The detection and quantification of anionic species is thus an essential task in many areas ranging from medical diagnostics to environmental monitoring.[161-162] However, the detection of anions is comparatively difficult, because of their significantly lower charge density compared to isoelectronic cations and their rather complex shapes, often precluding strong electrostatic interactions.[163] The structural variety of anions also greatly increases the difficulty in receptor design. Especially for synthetic molecular receptors, advanced synthesis knowledge and skills are often required to obtain binders with appropriate selectivity. Biological receptors such as antibodies on the other hand generally possess a high affinity to the respective anionic species, yet the high costs and chemical/thermal instabilities of these materials limit their application range.[21, 164] As we could already see in the introduction, MIPs can be used as artificial receptors due to their outstanding properties.

The abundance of commercially available and custom-designed monomers enables the preparation of a vast number of MIPs for targeting a wide range of species. For example, functional urea-based monomers are promising candidates for MIPs targeting oxoanionic species.[17, 133, 165-166] Their high selectivity stems from the fact that urea can provide two directional H-bonds through its NH groups toward the two oxygen atoms of the carboxylate group. Ghosh and Boiocchi recently reported that the binding affinity between a urea and an oxoanion

depends on the charge density on the oxygen of the anion and its basicity as well as the acidity of the urea NHs.[167-168] However, MIPs are often prepared in organic solvents in which ionic species are not well solvated. This in turn means that also the type, electronic and chemical nature of the counterion might become decisive for successful receptor preparation. Surprisingly, very little research has been undertaken to elucidate the role of counterions in the preparation of MIPs toward anions. Here, we will explore the effects of counterions in MIP synthesis by both, experimental and theoretical means, and correlate these findings to the results obtained from analytical rebinding studies.

Fig. 30 gives an overview of the key components and synthetic steps of the system studied here.

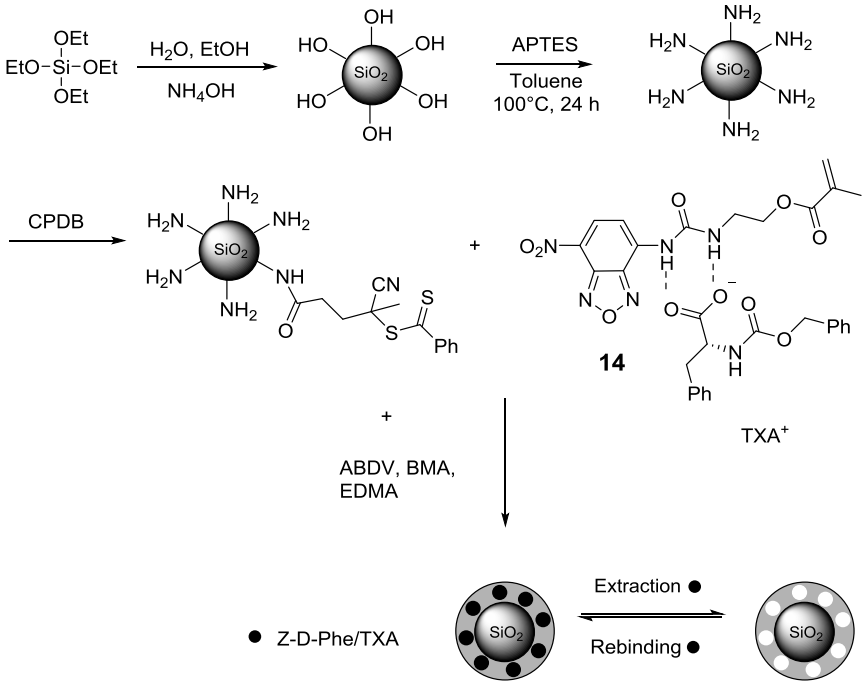

Fig. 30: Synthesis of RAFT agent-coated SiO_2 particles (0.35 µm) and silica core/MIP shell nanoparticles using TMA, TEA, TBA, THA and TOA as counterions (TXA).

First, we opted for MIPs that contain a fluorescent probe monomer as the designated binding partner, because besides the fact that fluorescent MIPs are very attractive sensor materials, such a functional monomer is able to report on its status (bound or not bound, microenvironmental polarity as well as acidity/basicity) at any time during the pre-polymerization, polymerization and

rebinding steps simply through the band maxima in absorption and/or fluorescence and its fluorescence yield.[169-170] Second, we investigated a format that recently proved to possess superior sensing performance in the enantioselective recognition of amino acids, that is, a few-nanometer thin MIP layer grown by RAFT polymerization of a fluorescent monomer (NBD-functionalized urea **14**), a skeletal comonomer BMA and a cross-linker EGDMA from the surface of aminopropyltriethoxysilane (APTES)- and RAFT agent-functionalized silica microparticles.[17] Z-D-Phenylalanine (Z-D-Phe) was chosen as the template/analyte here because it is a suitable model amino acid and because these investigations allowed to countercheck previous results obtained for the L-analogue.[17, 171-172] The cations investigated in this study were tetramethyl- (TMA), tetraethyl- (TEA), tetrabutyl- (TBA), tetrahexyl- (THA) and tetraoctylammonium (TOA; the latter three as linear *n*-alkyl variants) as permanent cations and pentamethylpiperidine (PMP) as protonatable cation. These cations are by far the most frequently used counterions when MIPs are developed for carboxylate-containing small-molecule analytes.

5.1.2 Binding studies with Z-D-Phe with different counterions

When carefully screening the literature, the use of counterions during the characterization of the (isolated) host-guest pairs, as well as during the stages of choosing components for a MIP, MIP preparation and rebinding studies, is not always consistent. For instance, PMP was used frequently for the *in situ* deprotonation of acidic templates to imprint the corresponding anions, yet the host-guest features, that is, the binding constant of template and functional urea monomer, were reported for the TBA salt, respectively.[173-174] Memory effects for the counterion have also been observed accordingly.[174] Thus, the counterion seems to have a more important role than simply acting as a cation that guarantees solubility of the carboxylate salt and maintains charge neutrality during polymer preparation. Moreover, when developing MIPs for optical sensing applications one has to rely on as strong as possible interactions between template and functional monomer, not only for efficient binding but also for

achieving the best possible spectroscopic response. The detailed study reported here thus lay the focus on both, the influence of the counterion on the formation of the preassembled complex in the pre-polymerization mixture, and the rebinding performance of the resulting crosslinked polymer matrix.

Monomer **14** was synthesized as described previously.[17] The urea moiety endows the monomer with a considerably high affinity for carboxylates. In addition, the directly fused NBD chromophore is sensitive to the change of the electron density on the urea's NH group and can thus respond to the binding of a carboxylate through two directional H-bonds by a modulation of the NBD's absorption and fluorescence. The methacrylate group helps to embed the complex covalently into the polymer matrix. UV-Vis absorption and fluorescence titrations were used to assess the binding affinity between anionic guest and fluorescent host in dilute solution. Due to the rather acidic character of the NBD urea, anions with a high charge density or high partial charges on the oxygens can deprotonate the monomer, especially in organic solvents. Usually, only weak bases form H-bonds with the urea group of **14** and induce a bathochromic shift in absorption and an increase in fluorescence as a result of the reinforcement of an intramolecular charge transfer (ICT) process that is operative with the chromophore upon optical excitation. The influence of the different counterions on these features is discussed in the following. The use of PMP to deprotonate Z-D-Phe, and hence $HPMP^+$ to act as the counterion, led to a red-shift of the absorption spectra of **14** by ca. 20 nm in $CHCl_3$ (Fig. 31).

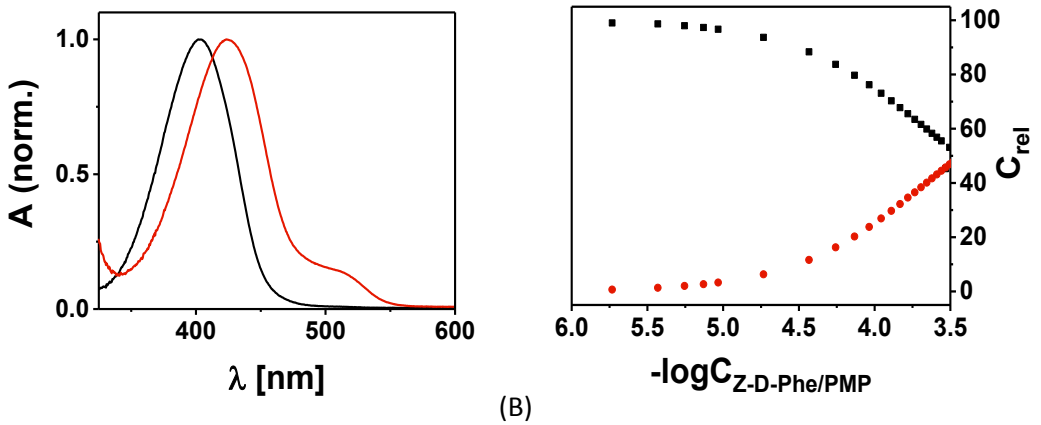

(A) (B)

Fig. 31: Normalized absorption spectra (A) and the species distribution during the titration of **14** (5 µM) with Z-D-Phe/HPMP in $CHCl_3$ (B, free **14,** back square and H-bonded complex, red circle).

The fluorescence increased accordingly, as expected for NBD dyes with reinforced ICT character.[175] Since PMP itself does not have an influence on the spectroscopic properties of **14**, the spectral changes are attributed to the formation of the **14**:Z-D-Phe/HPMP ternary complex or ensemble. A binding constant of $\log K = 2.55 \pm 0.01$ was determined through fitting the titration results with the software HyperSpec. For the calculation the maximum absorption at defined wavelength are used. Only two UV/vis-spectroscopically active species were found to be involved in the whole titration process, free **14** and **14**:Z-D-Phe/HPMP). Fig. 31 B illustrates that the relative concentration of **14** decrease as soon as Z-D-Phe/HPMP start binding to **14**, while the relative concentration of this H-bonded complex is increased.

In a second step, monomer **14** was titrated with the different tetraalkylammonium (TXA) salts of Z-D-Phe, varying from TMA to TOA. Also for these counterions, strong fluorescence enhancement was observed upon addition of the templates as shown exemplarily in Fig. 32. Fig. 32 further reveals that addition of Z-D-Phe/TXA leads to a bathochromic shift of the absorption maximum of **14** from 405 to ca. 440 nm with a concomitant appearance of a new, red-shifted band at 510 nm. Based on work from others and ours, the latter species is ascribed to the deprotonated form $\mathbf{14}^{-}$.[17, 167-168, 176]

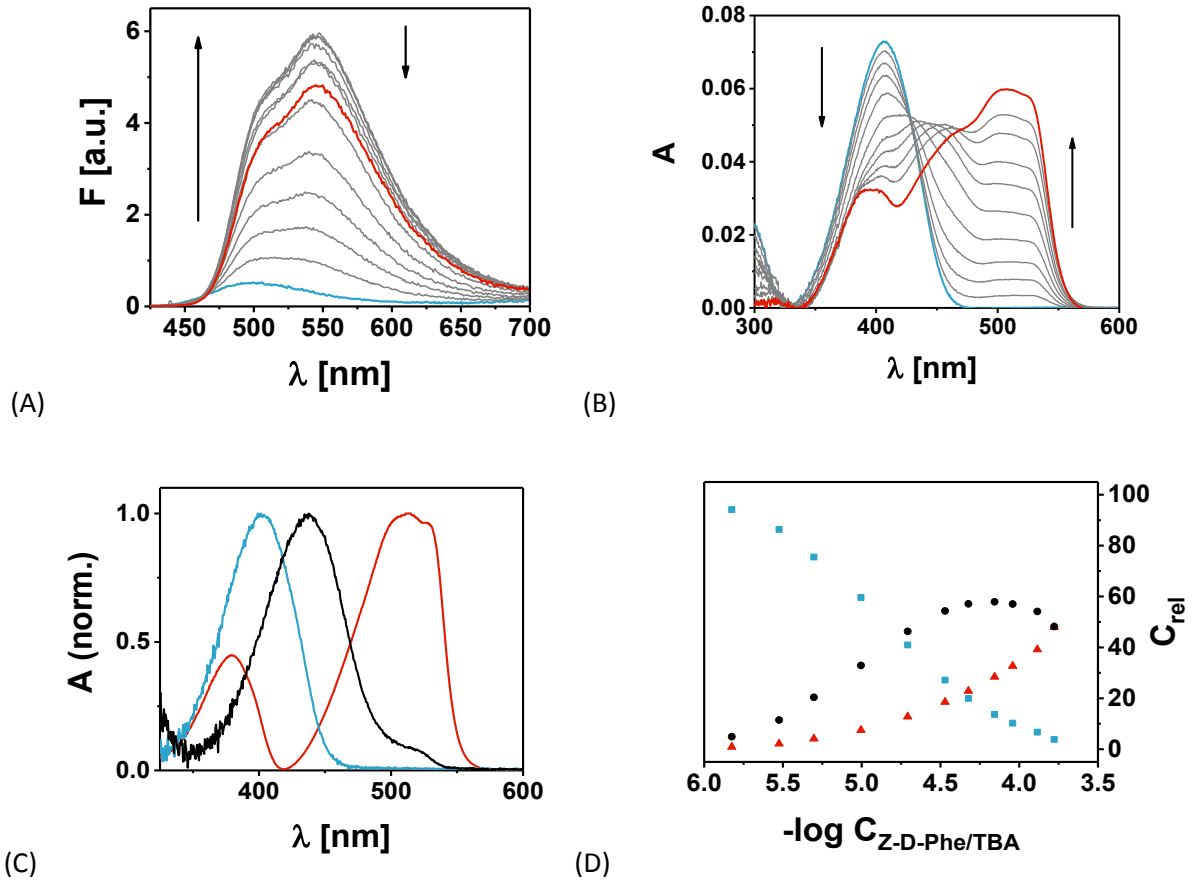

Fig. 32. Fluorescence (A) and absorption (B) spectra of **14** (5 µM) in $CHCl_3$ in the absence and presence of 0–250 µM Z-D-Phe/TBA (increasing concentrations in grey, start point spectrum in blue and end point spectrum in red, steps of 0, 1.0, 5.0, 9.9, 19.6, 33.8, 47.6, 69.8, 90.9, 130.4, 250 µM are shown). Species spectra (C) and the species distribution (D) during the titration calculated by HyperSpec (free **14** in blue; H-bonded complex in black and $\mathbf{14}^-$ in red).

Since the urea unit is electronically conjugated to the NBD chromophore and forms the electron donating part of a donor–acceptor π system, an increase of the electron richness at the urea by deprotonation of one NH leads to an increase in donor strength and hence to a strong bathochromic shift. The absence of well-defined isosbestic points on the other hand, suggests that not only a single acid-base reaction is taking place but that most likely two competing reactions are involved, presumably hydrogen bond-mediated complexation and deprotonation. Comparing all the different TXA counterions, the deprotonation tendency increases from Z-D-Phe/TMA to Z-D-Phe/TOA. Especially in case of Z-D-Phe/THA and Z-D-

Phe/TOA, deprotonation starts already at very low analyte concentrations. Data analysis with the HyperSpec software supports our phenomenological interpretation, that is, three species are required to obtain a good fit. Thus, during titration of **14** with the various salts, the free monomer is first converted into the H-bonded complex with an absorption maximum at 440 nm and then into the anion $\mathbf{14}^-$. The log*K* data derived from the fit for **14**:Z-D-Phe complex formation are given in Tab. 6.

Tab. 6: Binding constant of **14**:Z-D-Phe complexes with $HPMP^+$ and different TXA^+ counterions in $CHCl_3$ as derived from HyperSpec fits.

Counterion	**log*K*** [a]	$(\Delta\lambda^{abs}_{14:Phe-1})_d$ **/nm** [b]	$(\Delta\lambda^{abs}_{14:Phe-1})_{pp}$ **/nm** [b]
$HPMP^+$	2.55 ± 0.01	21	–
TMA^+	4.32 ± 0.03	29	12
TEA^+	4.43 ± 0.04	34	14
TBA^+	4.75 ± 0.02	35	16
THA^+	4.92 ± 0.01	38	18
TOA^+	5.06 ± 0.03	40	20

a: Obtained at diluted concentrations. *b*: Difference between absorption maxima of **14**:Z-D-Phe and **14**, at dilute (d) and prepolymerization (pp) concentrations.

Comparison of these data with those of PMP/Z-D-Phe mentioned above suggests that in contrast to several published works, PMP is not as effective as the TXAs counterions for Z-D-Phe imprinting because of the lower affinity (that is, smaller log*K*) of the salt Z-D-Phe/HPMP to **14** in $CHCl_3$. This is also reflected by the distinctly smaller template-induced absorption shift in the case of PMP. Apparently, $HPMP^+$ resides in closer vicinity to the anion center, possibly due to stronger electrostatic interactions. Such behavior would result in competition between the two H-bonds pointing from the urea NH to the carboxylate oxygens and the single H-bond that can be formed between the proton on the PMP and the

carboxylate, leading to an overall decreased basicity and a weaker fluorescence response.

For successful imprinting, high affinity between the functional monomer and the template is necessary. In addition, binding constants log*K* higher than 3 are preferred to reach stoichiometric and noncovalent imprinting whereby over 95% of template is complexed in the pre-polymerization mixture.[17,24,177] Stronger ion-pairing and enhanced ternary complex formation in the pre-polymerization mixture might in turn have an adverse effect on designated cavity formation during the polymerization step. Moreover, since the features reported for dilute concentrations in Tab. 6 are retained at higher concentrations under pre-polymerization conditions (Fig. 33), though to a lesser extent, we set out to prepare a series of MIPs and studied in detail their rebinding behavior as a function of the chain length on the ammonium-N of the TXA cations. It should be kept in mind that pre-polymerization conditions do not only mean higher concentrations but also the presence of an excess of co-monomer and cross-linker. In our case, the latter are more polar than $CHCl_3$ and can thus also influence the interaction between fluorescent monomer and template and hence the shift in absorption. With respect to optimum imprinting it is additionally important to avoid any non-directional electrostatic interactions due to species' deprotonation, because non-directional interactions can lead to a higher heterogeneity of the cavities. Fig. 32 demonstrates as well that with increasing size of the counter ion, the deprotonation tendency increase under pre-polymerization condition with can be observed by the second band at higher wavelengths.

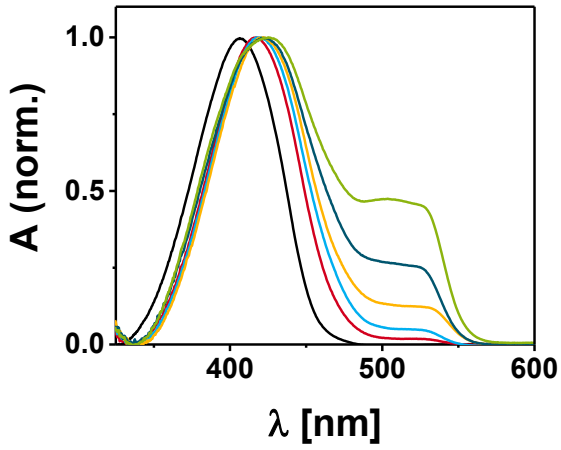

Fig. 33: Normalized absorption spectra of **14** (1 mM) in $CHCl_3$ (black), **14** with various Z-D-Phe/TXA in $CHCl_3$ and in the presence of BMA and EGDMA at pre-polymerization conditions; with TXA = TMA (red), TEA (blue), TBA (yellow), THA (dark blue) and TOA (green).

5.1.3 Preparation and performance of the MIP particles

MIP shells on silica particles were prepared by RAFT polymerization employing the pre-polymerization mixtures containing **14** and the various Z-D-Phe/TXA salts as mentioned above. The coating of the surface with the RAFT agent ensures the formation of a ca. 5 ± 2 nm thin and homogeneous MIP film on the core particles (Fig. 34). Non-covalent complex imprinting is mediated by EGDMA as the cross-linker. Finally, Z-D-Phe/TXA is removed from the MIP network by washing with acidic methanol, leaving specific cavities with binding sites in the shell that are complementary to the template molecule.

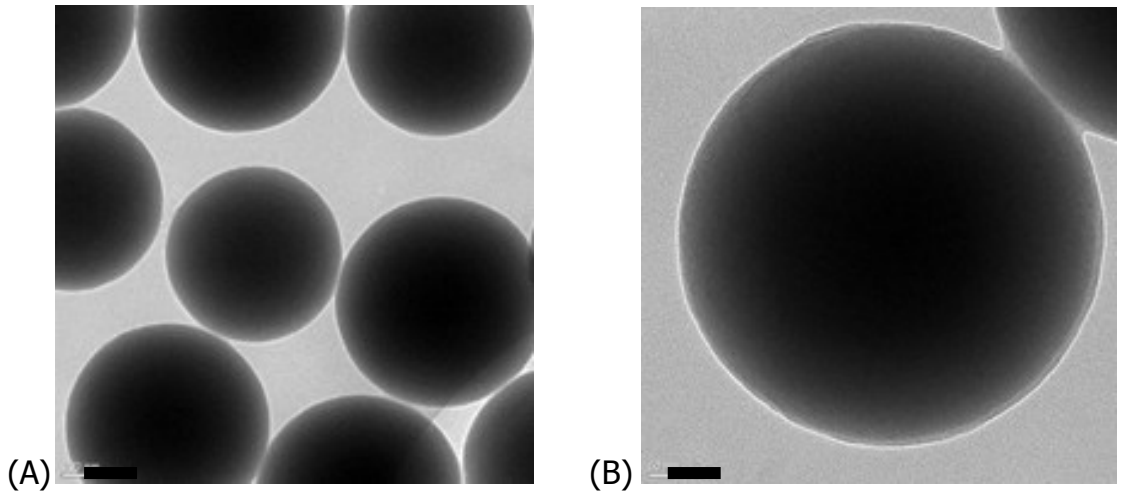

Fig. 34: Representative TEM images of core-shell particles prepared with Z-D-Phe/TEA.

Before analyzing the effect of the different TXA counterions in detail, it is important to assess the overall performance of the system. In the present case of imprinting amino acids, the most important figures of merit are the (enantio)selectivity, that is, the discrimination of the core-shell (CS) sensor particles MIP(**14**)-Z-D-Phe/TXA@SiO_2 between Z-D-Phe and its enantiomer Z-L-Phe, and the selectivity with regards to chemically competing amino acids such as Z-D-Glu, possessing two carboxylate moieties, or Z-D-Tyr, able to undergo π-stacking interactions with the co-monomer BMA. Rebinding titrations were thus performed with Z-D-Phe/TXA, Z-L-Phe/TXA, Z-D-Glu/TXA and Z-D-Tyr/TXA. Here, we show a representative binding behavior of Z-D-Phe to MIP(**14**)-Z-D-Phe/TBA@SiO_2 and NIP@SiO_2 nanoparticles using TBA as counterion, and the corresponding cross-sensitivity studies with Z-L-Phe/TBA, Z-D-Glu/TBA and Z-D-Tyr/TBA.

According to Fig. 35, MIP(**14**)-Z-D-Phe/TBA@SiO_2 nanoparticles obviously show a better sensing response to Z-D-Phe/TBA compared to the enantiomer and the other amino acids. This high selectivity is attributed to the formation of rather well-matching cavities during the imprinting process and the retention of the directed H-bonding between the carboxylate group of the analyte and the NH groups of the urea. Thus, the enantioselectivity factor EF = $dF_{Z\text{-}D\text{-}Phe}/dF_{Z\text{-}L\text{-}Phe}$ was determined to 5.6. Apparently, Z-L-Phe does not fit well into the specific cavity due to its different stereoisomeric structure compared to Z-D-Phe. The MIP

showed also a good discrimination against Z-D-Glu/TBA and Z-D-Tyr/TBA with a discrimination factor DF = $dF_{Z\text{-}D\text{-}Phe}/dF_{analogues}$) of 3.7 for both analytes. The NIP@SiO_2 particles show only a very weak effect, stressing the fact that non-specific binding is negligible in this case. The difference in selectivity between MIPs and NIPs results in a high imprinting factor IF = dF_{MIP}/dF_{NIP} of 9.6. Compared to previous study with these systems, the imprinting effect could be further enhanced due to the thinner MIP shell and a presumable reduction of heterogeneity among the cavities.[17]

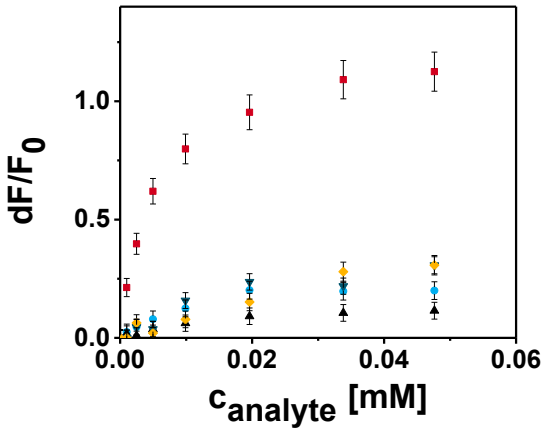

Fig. 35: Sensing response of MIP(**14**)-Z-D-Phe/TBA@SiO_2 (1 mg mL^{-1}) in $CHCl_3$, toward template (red squares), corresponding enantiomer Z-L-Phe (blue circles) and two other selected amino acids Z-D-Tyr (dark blue down-triangle) and Z-D-Glu (yellow diamonds) and response of NIP(**14**)@SiO_2 (1 mg mL^{-1}) toward template (black up-triangles).

5.1.4 Influence of the counter-ion during imprinting

Having established the favorable performance and repeatability of our approach, we proceeded to investigate whether the counterion effect seen in the pre-polymerization mixture can also influence the imprinting process during the MIP synthesis. We studied the impact of the counterion on carboxylate imprinting, and if the use of the different TXA salts governs the MIP's selectivity in the analytical reaction.

Fig. 36 reveals that the MIPs which were prepared with smaller counterions like TMA showed lower sensing responses after titration with the corresponding Z-

D-Phe/TXA stock solutions.[1] The sensing response increases from TMA to TOA, reflecting well the order of log*K* values in Tab. 6. The weaker fluorescence enhancement found in the presence of TMA suggests that also in the MIP TMA approaches closer to the carboxylate center, leading to weaker interaction with the NBD's urea binding site as was discussed before. In contrast, the larger counterions seem to stay farther away from the **14**:Z-D-Phe complexes also in the cavities, entailing a more pronounced spectroscopic response due to stronger H-bonding between **14** and Z-D-Phe (Fig. 34). Analysis of the curves in Fig. 36 yielded binding constants (by non-linear fitting) for the MIP particles as collected in Tab. 7. The data show that the log*K* of the MIP particles increases from TMA to TOA, consistent with the trend of the log*K* in Tab. 6.

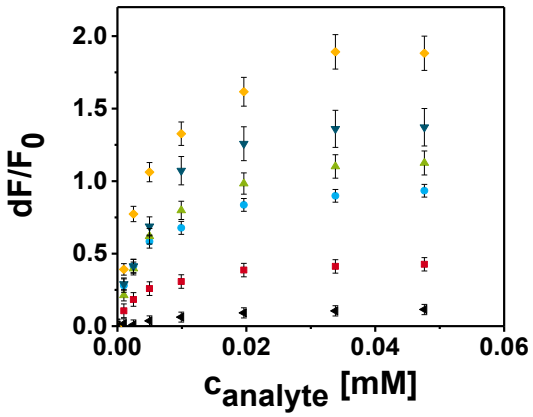

Fig. 36: Sensing response of the various MIP(**14**)-Z-D-Phe/TXA@SiO_2 CS particles (1 mg mL^{-1}) in $CHCl_3$ with X = M (red square), E (blue circle), B (green up triangle), H (dark blue down triangle) and O (yellow diamond) toward the respective template Z-D-Phe/TXA used for imprinting and NIP(**14**)@SiO_2 (black left triangle); the response of NIP(**14**)@SiO_2 to all species is identical within uncertainty.

The results in Fig. 36 immediately trigger the question whether only the TXA-modulated interaction between carboxylate and urea is decisive or whether the cavities as such have a major influence, that is, whether in all cases Z-D-Phe/TXA is imprinted or whether for instance for the larger counterions only Z-D-Phe is

[1] To avoid confusion, MIP-Z-D-Phe/TMA@SiO_2 were titrated with Z-D-Phe/TMA, MIP-Z-D-Phe/TEA@SiO_2 were titrated with Z-D-Phe/TEA, etc.

imprinted and the lipophilic TXA is sitting close in the polymer network (for electroneutrality), yet not necessarily directly in the cavity.

Tab. 7: Binding constants for MIP(**1**4)-Z-D-Phe/TXA@SiO_2 and corresponding Z-D-Phe/TXA in $CHCl_3$; the counterion used in imprinting and for rebinding was always identical.

Counteriona	**log*K***
TMA^+	4.10 ± 0.01
TEA^+	4.98 ± 0.02
TBA^+	5.16 ± 0.02
THA^+	5.39 ± 0.01
TOA^+	5.71 ± 0.01

We thus performed another series of experiments by titrating each MIP(**14**)-Z-D-Phe/TX_iA@SiO_2 CS particle solution with the different tetraalkylammonium salts TX_rA of Z-D-Phe to screen for possible recognition patterns among the MIP sensor particles. The results of these titration experiments are collected in Fig. 37. The different subscripts of TX_iA and TX_rA refer to the use of the different counterions during the imprinting (TX_iA) and the rebinding titration (TX_rA).

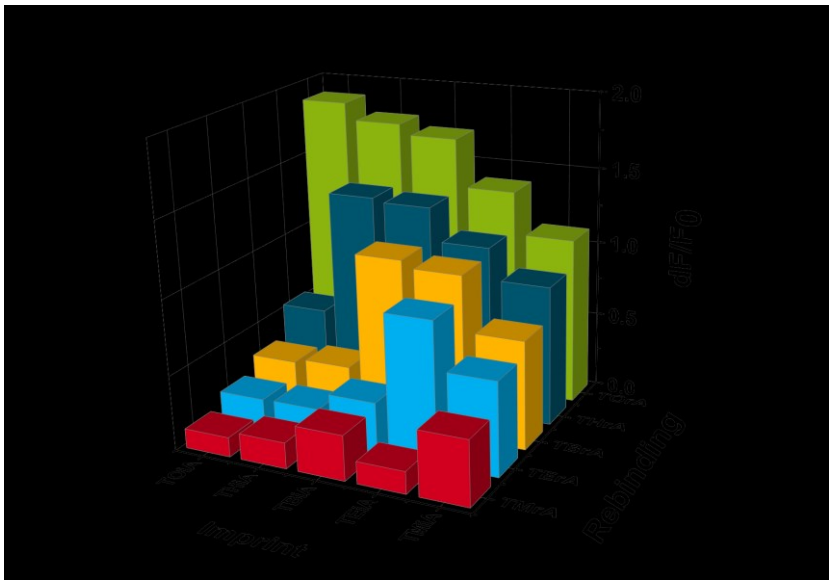

Fig. 37: Sensing response of each MIP(**14**)-Z-D-Phe/TXA@SiO_2 (1 mg mL^{-1}) in $CHCl_3$ titrated with each tetraalkylammonium salt of Z-D-Phe/TXA (at 0.048 mM).

Fig. 37 allows to draw the following conclusions.

- The nature of the counterion of the analyte X_r is least decisive when the smallest X_i = M is used.
- The nature of the counterion of the analyte X_r is most decisive when the largest X_i = O is used.
- In all cases of TX_iA, the best response is found when TOA salts are used as TX_rA.
- Counterion selectivity is only found for the pair MIP-Z-D-Phe/TO_iA@SiO_2 and Z-D-Phe/TO_rA.
- In all cases, a good response is found for all TX_rA with a size that is larger than or equal to that of the TX_iA used.

Considering the system of moderately polar template/analyte, fairly polar fluorescent monomer, slightly polar polymer matrix and counterions ranging from polar (TMA) to largely non-polar (TOA), the following two embedding scenarios are principally possible (Fig. 38). First, regardless of the polarity of the counterion and because of electrostatic attraction, the cavity is always formed around both,

template and counterion (scenario A). Second, due to the fact that TBA, THA and especially TOA are rather lipophilic and possess a low charge density, these counterions are not necessarily co-embedded into the cavity but can reside in the porous polymer network close by (scenario B). In case A, the size of the cavity should increase monotonically as X_i is changed from M over E, B and H to O. For scenario B, the cavity size first increases for the more tightly bound and polar M and E but then levels off for the fairly non-polar counterions when these are located in the network nearby; for B, H and O, the size of the cavity should then match rather closely that of Z-D-Phe alone. In the next section we will discuss in detail the responses to be expected in these two cases.

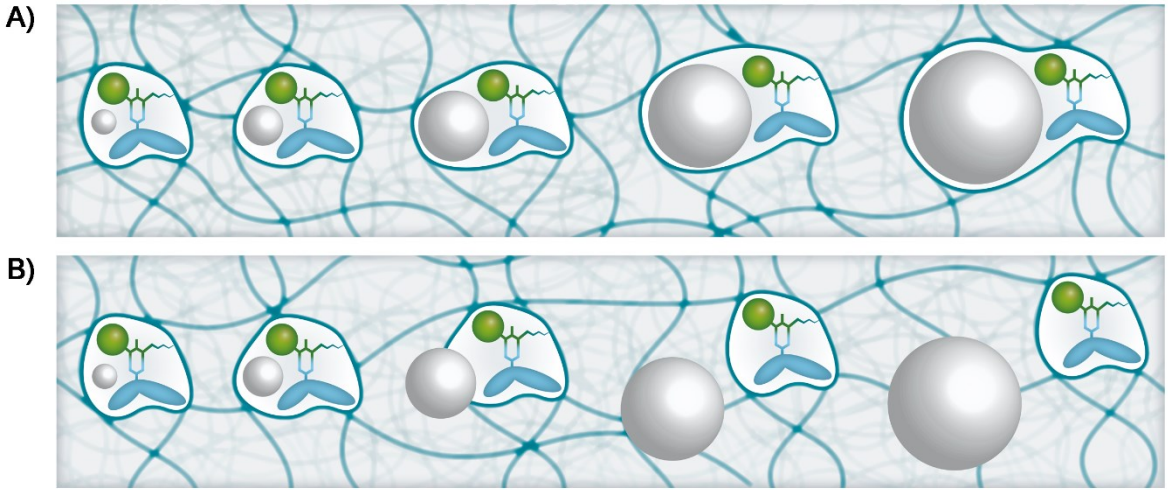

Fig. 38: Graphical representation of the two imprinting scenarios A (top) and B (bottom) described in the text with increasing size of counterion from left (TMA) to right (TOA). The size of all the relevant partners is roughly proportional, the greyish ball denoting the TXA counterions.

Response expected for scenario A. For Z-D-Phe/$TM_iA@SiO_2$, Z-D-Phe/TM_rA should reoccupy the cavity best. All the other Z-D-Phe/TX_rA should bind to a (progressively) lesser extent or not at all. For Z-D-Phe/$TE_iA@SiO_2$, Z-D-Phe/TE_rA should bind best, Z-D-Phe/TM_rA to a lesser degree and Z-D-Phe/TB_rA,Z-D-Phe/TH_rA and Z-D-Phe/TO_rA even less or not at all, etc. A response pattern such as in Fig. 38 would be expected.

Response expected for scenario B. In this scenario, the cavity size would only increase from TMA to TEA because these counter-ions bind tightly enough to

14:Z-D-Phe so that the ternary complexes are only fully imprinted for X_i = M, E. For TX_iA with X_i = B, H and O, these more lipophilic counterions retreat into the porous polymer network already during MIP formation and the cavities formed in all these cases reflect the size of Z-D-Phe alone. Upon rebinding to Z-D-Phe/$TM_iA@SiO_2$ and Z-D-Phe/$TE_iA@SiO_2$, largely similar results as in scenario A would be expected. For the larger TX_iA, however, the influence of the counterion should be much less prominent once the ability of X_r for ternary complex formation is low; a response as in Fig. 40 would be expected.

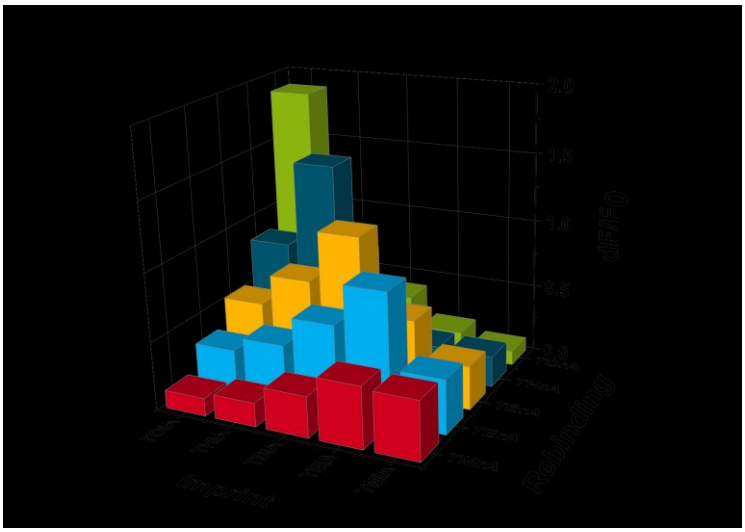

Fig. 39: Hypothetical sensing response according to scenario A sketched in the main text for MIP(**14**)-Z-D-Phe/$TX_iA@SiO_2$ assuming the formation of progressively increasing, rigid cavities with increasing X_i and rebinding studies with the various tetraalkylammonium salts of Z-D-Phe/TX_rA. Values on Y axis arbitrarily chosen.

Expected vs observed responses. According to Fig. 37, all the data on the right side of the diagonal described by the data points TX_iA = TX_rA indicate progressively stronger binding when $X_r > X_i$. A pure size effect of a (considerably rigid) cavity as expected for scenario A thus does not seem to be the key decisive factor. This part of Fig. 37 suggests that scenario B might be effective, that is, that the larger TX_rA could penetrate into the network and responses would be generally high. However, scenario B does not account for the left side of the line TX_iA = TX_rA in Fig. 37, the weak response for essentially all cases of $X_r < X_i$ (cf. Fig. 39).

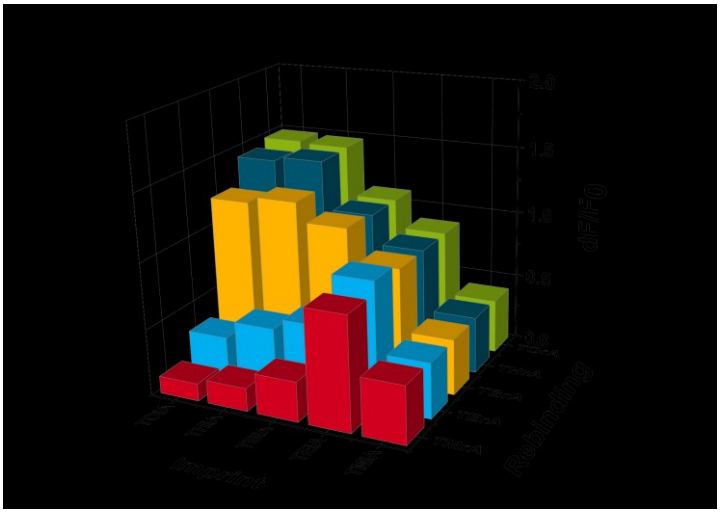

Fig. 40: Hypothetical sensing response according to scenario B sketched in the main text for MIP(**14**)-Z-D-Phe/TX_iA@SiO_2 assuming the progressive retraction of the counterions into the polymer network as the alkyl chains on the ammonium ion become increasingly lipophilic and rebinding studies with the various tetraalkylammonium salts of Z-D-Phe/TX_rA. Values on Y axis arbitrarily chosen.

Ternary complex imprinting into a flexible cavity in a porous network (scenario C). If we assume that the cavity is not as rigid as it might intuitively seem from the point of view of imprinting, enantioselectivity or discrimination factors, but rather flexible, the right side of Fig. 41 can be understood by analogy with a very well-known biological behavior, the induced fit of enzyme–substrate complementarity.[178] If we assume that cavities in MIPs are embedded into a porous network—like here, guaranteeing macroscopic equilibration and response times on the order of seconds—and are flexible, the slightly increasing size of the counterion might progressively be accommodated by an adaptive cavity. Since the counterion's increase in size correlates with an increase in spectroscopic response, the gradually and moderately increasing data bars on the right side of the diagonal in Fig. 39 seem to match well with this model. However, the distinctly weaker response on the left side can still not fully be explained by fit-induced cavities because an adaptive cavity should also accommodate ternary complexes with smaller counterions (at least in a progressive manner, see left side of Fig. 38). However, if we take into account that Fig. 37 shows the spectroscopic

response of the system, that is, the fit into the cavity plus the designated hydrogen bonded interaction between monomer and template, a weak signal in case of a smaller counterion can either mean that the ternary complex (or the template) is not significantly bound or that the ternary complex resides in the cavity, although its rather large size and flexibility still allows for more efficient ion pair formation than interaction between template and monomer (Fig. 41). Uptake would thus happen in all cases, yet would largely escape spectroscopic detection for $TX_rA < TX_iA$. This scenario would also be stressed by the previously determined binding constants of the MIP particles.

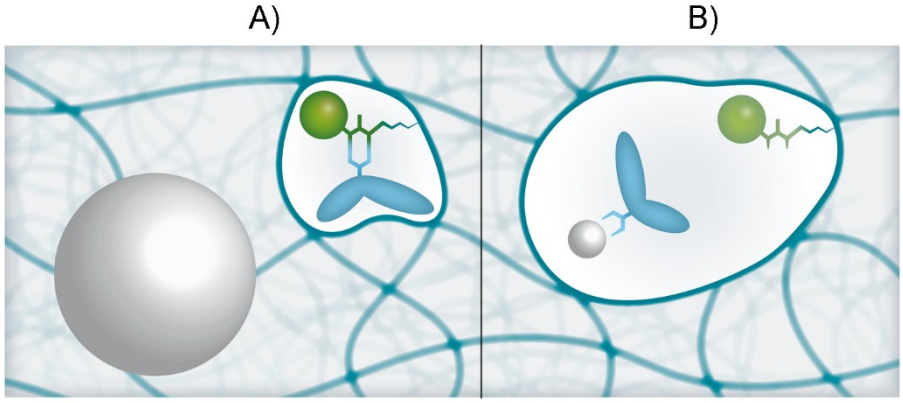

Fig. 41: **1**. A) Case of only Z-D-Phe fitting tightly into a cavity with counterion residing in the network. B) Case of cavity being too large for Z-D-Phe/counterion pair so that the attractive forces exerted on Z-D-Phe/TXrA are not strong enough to dissociate the ion pair; Z-D-Phe is thus largely unable to H-bond to the urea moiety.

5.1.5 Control experiments by HPLC

To further probe the afore mentioned considerations, the binding capacity of the cavities was determined by HPLC. If uptake happens also for ternary complexes with $TX_rA < TX_iA$ but remains spectroscopically silent, this should be seen in the HPLC experiments. Applying the same conditions as for the spectroscopic titration experiments, a solution of 1 mg mL^{-1} MIP sensor particles containing 0.048 mM of Z-D-Phe/TX_rA was prepared and equilibrated for 14 min. After centrifugation, the concentration of Z-D-Phe/TX_rA in the supernatant was quantified by HPLC measurements. Back calculation allowed the determination of the adsorbed amount of analyte independent of the analyte's influence on the spectroscopic properties. The calculated concentrations for the MIPs prepared with TM_iA, TB_iA and TO_iA are presented in a 3D diagram (Fig. 42). It can be seen, that for Z-D-Phe/$TM_iA@SiO_2$ a somewhat higher amount of Z-D-Phe/TB_rA is bound to the MIP and even a slightly higher amount of Z-D-Phe/TO_rA is retained. Apparently, the mechanism of fit-induced cavity formation allows the ternary complex with TB_rA to be efficiently retained, and even the much bigger TO_rA does not aggravate retention when the smallest counterion is used during imprinting. In addition, considering the magnitude of the spectroscopic responses (e.g., Fig. 36 for all the optimal pairs), less retained Z-D-Phe/TO_rA can induce a higher spectroscopic response than better retained Z-D-Phe/TB_rA, and especially than strongly interacting TM_rA, arriving at an order as in Fig. 37. For Z-D-Phe/$TB_iA@SiO_2$, the HPLC data show that Z-D-Phe/TO_rA can also be accommodated to a sizeable degree, though Z-D-Phe/TM_rA in particular is efficiently retained. Comparison with the fluorescence response in Fig. 8 then immediately suggests that indeed the binding scenario B in Fig. 39 sketched in Fig. 41 seems very plausible. Finally, the data shown for Z-D-Phe/$TO_iA@SiO_2$ in Fig. 42 nicely complement this mechanistic explanation.

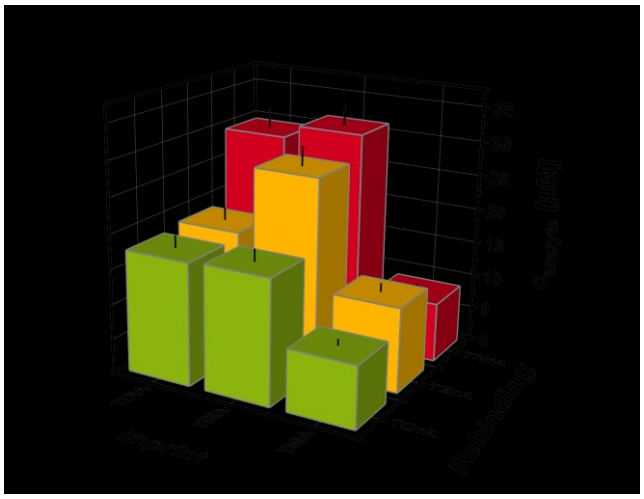

Fig. 42: Quantitative analysis of Z-D-Phe/TX_rA adsorption into MIP(**14**)-Z-D-Phe/$TX_iA@SiO_2$ sensor particles (1 mg mL^{-1}) in $CHCl_3$ by HPLC. For better illustration, the Z axis (rebinding) was reversed, as compared to Fig. 37.

5.1.6 Enantioselectivity control studies

Fit-induced cavity formation is also supported by the enantioselectivity patterns of the MIP sensor particles as determined from titrations with the TX_rA salts of Z-D-Phe and the corresponding L-isomer as the enantiomeric twin. Tab. 8 shows representative enantioselectivity factors of MIP(**14**)-Z-D-Phe/$TE_iA@SiO_2$, MIP-Z-D-Phe/$TH_iA@SiO_2$ as well as MIP(**14**)-Z-D-Phe/$TO_iA@SiO_2$, which were calculated according to $EF = dF_{Z\text{-}D\text{-}Phe/TXA}/dF_{Z\text{-}L\text{-}Phe/TXA}$.

Tab. 8: Enantioselectivity factors of MIP(**14**)-Z-D-Phe/$TX_iA@SiO_2$ with X = E, H and O.

Salt used for rebinding	**$EF_{MIP\text{-}Z\text{-}D\text{-}Phe/TEiA@SiO2}$**	**$EF_{MIP\text{-}Z\text{-}D\text{-}Phe/THiA@SiO2}$**	**$EF_{MIP\text{-}Z\text{-}D\text{-}Phe/TOiA@SiO2}$**
Z-D-Phe/TM_rA	1.1	1.4	1.1
Z-D-Phe/TE_rA	2.3	1.5	1.2
Z-D-Phe/TB_rA	2.4	1.7	1.3
Z-D-Phe/TH_rA	2.8	5.8	1.7
Z-D-Phe/TO_rA	2.5	5.4	5.6

If a considerably small cavity is imprinted like in case of MIP(**14**)-Z-D-Phe/$TE_iA@SiO_2$, the enantiomeric selectivity is largely similar regardless of TX_rA when $X_r \geq E$. On the contrary, in presence of the smaller TM_rA, no enantioselectivity is found; the ternary complex is obviously too mobile and TM_rA interacting too strongly with Z-D/L-Phe so that no preference is found for Z-D-Phe compared to Z-L-Phe. On the other hand, MIP(**14**)-Z-D-Phe/$TH_iA@SiO_2$ as well as MIP(**14**)-Z-D-Phe/$TO_iA@SiO_2$ can receive all the Z-L-Phe/TX_rA ($TX_rA < TH_iA$ or TO_iA) into their considerably large cavities, revealing absence of enantioselectivity. Enantioselectivity is only found when the counterions are big enough to closely fill the space in the adaptive cavity. In addition, this enantioselectivity is distinctly higher than the one found for the smaller counterions, suggesting that although the cavity is adaptive, it is still sufficiently small to prevent accommodation of species that have a stereoisomerically different preferential orientation.

5.1.7 Control studies with NIP(14)@SiO_2

Until now, we have only discussed the various scenarios pertaining to MIPs and TX_iA/TX_rA pairs. Tab. 9 collects the IFs for all TX_rA, that is, their responses when bound by the corresponding MIP(**14**)-Z-D-Phe/$TX_iA@SiO_2$ compared to the responses found by binding to NIP(**14**)@SiO_2 (see also Fig. 35 above). It should be mentioned that because the application-oriented background is sensing, we only considered here spectroscopic imprinting effects.

Tab. 9: Imprinting factors for Z-D-Phe/TX_rA and MIP(**14**)-Z-D-Phe/TX_iA@SiO_2 (X_r = X_i) referenced against NIP(14)@SiO_2.

$TX_{i/r}A$	**IF**
TMA	4.1
TEA	4.8
TBA	9.6
THA	8.9
TOA	6.2

The imprinting effect has been already introduced and discussed above for MIP(**14**)-Z-D-Phe/TB_iA@SiO_2 (Fig. 35), which showed a favorable IF = 9.6. Tab. 9 reveals that MIPs imprinted with smaller TX_iA gave lower IF values, most likely due to the stronger interaction with the anion and the consequent reduced response. The decrease of the imprinting effect when considering the more lipophilic counterions from TB_iA to TO_iAis then tentatively attributed to a higher non-specific binding in the moderately low-polar organic NIP network or on its surface.

5.1.8 Molecular dynamics simulations

To go more in detail and to prove the spectroscopic studies of the counterion effect, molecular dynamic simulations of the pre-polymerization have been carried our as well. The calculations were performed by Carlos Zapata and Marcus Weber from the Zuse Institute Berlin (ZIB). This analysis should offer quantitative information about the binding stability, the molecular interactions as well as chemical affinity between different components in the pre-polymerization mixture when it is supposed that the fluorescent monomer–template complex still moves freely. However, it was figured out that the molecular effects derived from the changes in counterion size are not strong enough to change the stability of the

complex but the size tuning can definitively improve the template binding with the consequent improvement of the MIP sensing response.

5.1.9 Conclusion

The binding between the functional monomer **14** and the target molecule is an impotent factor in MIP syntheses. In the current work, the high affinity of the deprotonated analyte Z-D-Phe to the urea-containing fluorescent monomer increased by decreasing its basicity using counter-ions ranging from TMA^+ to TOA^+ with different chain length. For the first time, we could show that the deliberate use of counter-ions offers control over selectivity features through their influence on the cavity size and thus the recognition behavior of MIP shells on particles. Larger counter-ions employed in the preparation step of the MIP-based sensor materials lead to larger cavities, but still show excellent discrimination features for instance against enantiomers. For broad-band sensing features, i.e., for sensing a specific anionic species in a sample of unknown (counter-ion) composition, however, the use of tetraalkylammonium ions with chain length of four and longer are not advantageous. In such cases, either lower responses have to be accepted or a phase-transfer (ion-exchange) step has to be implemented.

5.2 Integrating fluorescent molecularly imprinted polymer (MIP) sensor particles with a modular microfluidic platform for nanomolar small-molecule detection directly in aqueous samples

5.2.1 Introduction

In many parts of the world, most prominently in South Asia, North and South America and Australia, the herbicide 2,4-dichlorophenoxyacetic acid (2,4-D) is used extensively in agriculture for the control of weeds, preventing crop production from potential losses.[179-182] Following the recent development of new herbicide-resistant crops, it is further expected that the use of 2,4-D will increase dramatically in the nearer future.[183] Unfortunately, this kind of herbicide can infiltrate into ground and surface water, potentially contaminating drinking water.[184-185] If treated plants are used as animal feed, residues can also end up in meat, milk or eggs. To prevent water and food from contamination, potentially entailing various adverse health effects, health and environmental agencies such as the WHO and the EPA set maximum acceptable concentrations in drinking water to 30 µg L^{-1} (136 nM) or 70 µg L^{-1} (317 nM) (U.S. EPA, 2008).[186-188] For optimum prevention, the monitoring of 2,4-D levels in aqueous environments would thus be desirable, especially during and after pesticide application periods. Consequently, rapid, sensitive and selective analytical tools for herbicide residue monitoring in aqueous environments at best in a miniaturized format for in-the-field use are urgently required. Lab-based methods involving chromatography and mass spectrometry or requiring rather controlled conditions as for immunoassays largely disqualify for such purposes. An alternative would be microfluidic devices in combination with suitable recognition matrices. As the latter, molecularly imprinted polymers (MIPs) are very attractive. Accordingly with 2,4-D being a prominent analyte of global environmental concern, MIPs for extraction, separation and detection of 2,4-D have already been developed.[189-195] The latter examples constitute few reports on electrochemical as well as optical approaches,

all of them showing one or the other drawback when aiming at fast, potentially on-site sensing of the analyte without sample pre-treatment or conditioning in the relevant concentration range.[196-203] An overview of reported MIP sensors for 2,4-D are shown in Tab. S1.

Particularly interesting for such purposes are optical sensing technologies, because they are ideally suited for the design of powerful miniaturized detection devices.[204] Until today, MIPs have only considerably scarcely been used in combination with microfluidic devices. Moreover, although microfluidic chips have been frequently employed for the synthesis of MIP particles, thin films have almost exclusively been used in MIP-based microfluidic sensory devices for instance with a quartz crystal microbalance, as conducting MIP films or for detection via surface plasmon resonance colour reactions or of fluorescently labelled analytes.[205-213] Only very recently, two examples of luminescent quantum dots coated with a molecularly imprinted silica shell have been reported for MIP-based sensing in a microfluidic device.[214-215]

In this chapter, the development of a new fluorescent probe cross-linker that is incorporated into a thin MIP layer grafted from the surface of few hundred nanometre-sized silica particles is reported. These core-shell particles should be combined with a droplet-based 3D microfluidic system that allows the determination of the analyte at low concentrations directly in water samples without pre-treatment or clean-up.

5.2.2 Binding studies with 2,4-D

The first step in the sensor development was the design and synthesis of a fluorescent molecular probe that can translate the target binding event into an optical signal. Besides binding to the analyte, the probe should ideally give a response in the visible spectral range, to avoid interference by scattering and allow for the use of cost-effective equipment. Moreover, an essential requirement pertains to the fact that the signalling mechanism upon binding the target 2,4-D in a non-covalent fashion should not involve any molecular motions or electronic processes that require large spatial volumes, which a polymeric sensor matrix can simply not offer; nonetheless, the aspired response shall be pronounced to

guarantee high sensitivity.[169-170] Based on our previous experience in confining indicator dyes in mesopores of silica host materials, we chose the merocyanine-type phenoxazinone skeleton for our present purpose.[148] Phenoxazinones are not only promising with respect to signal generation in rigid matrices, but possess sufficient synthetic flexibility to not only prepare probe monomers but also a probe cross-linker and assess the latter's performance in view of improving a MIP's response. Two phenoxazinone derivatives were thus synthetized, fluorescent monomer **16** and cross-linker **19**, both carrying a urea group as binding motif for the carboxylate group of 2,4-D (Fig. 43).

While monomer **16** was obtained directly from a commercial phenoxazinone by reaction with isocyanate, the cross-linker **19** was obtained from a home-made phenoxazinone with an additional primary alcohol, which could then react a second time with an isocyanate. The second methacrylate group of cross-linker **19** was added to embed the complex into the polymer matrix more efficiently, leading to a better stability by reducing the possibility for a free dye rotor attached only through one anchor point into the matrix to create a distinctly larger cavity.

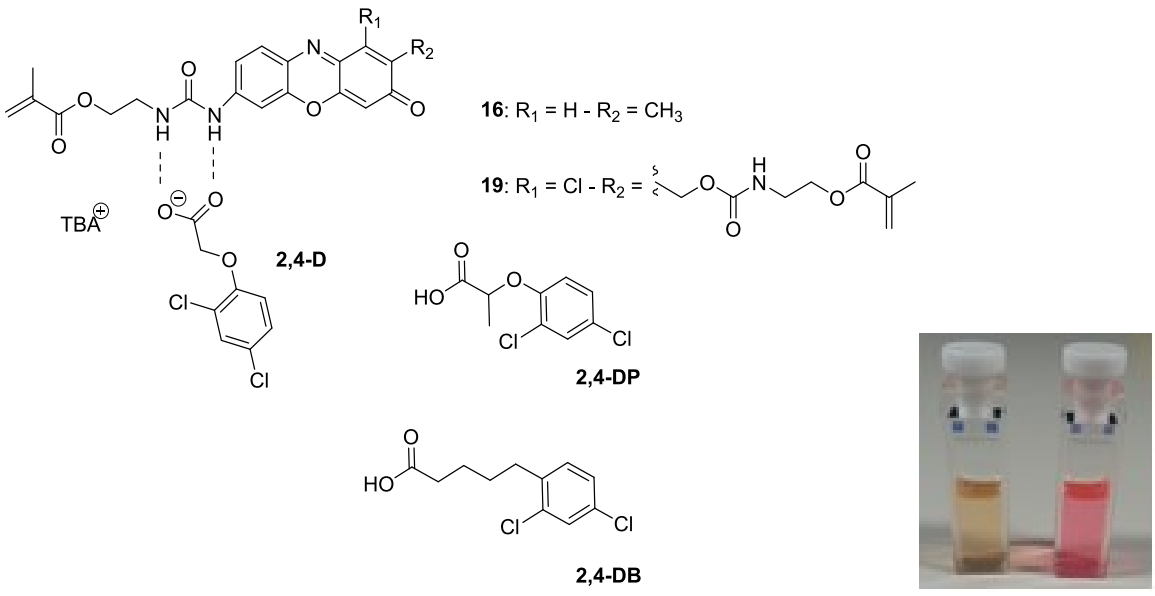

Fig. 43: Molecular architectures of the phenoxazinone derivatives monomer **16** and cross-linker **19** as well as structures of 2,4-D and closely related compounds 2,4-DP and 2,4-DB.

The complexing urea moiety with good affinity towards carboxylate was positioned at one terminus of the phenoxazinone's π system. Thus, any electron density changes at the urea upon H-bonding interactions with a carboxylate-expressing analyte like 2,4-D should influence the chromophore's properties.

Indeed, upon addition of 2,4-D in $CHCl_3$ the broad and non-structured absorption bands with maxima at 472 and 485 nm for **16** and **19**, respectively, were shifted to 479 and 516 nm accompanied by an increase of the molar absorption coefficient (Fig. 44). These red shifts of the absorption bands were in accordance with the formation of H-bonded complexes.[148]

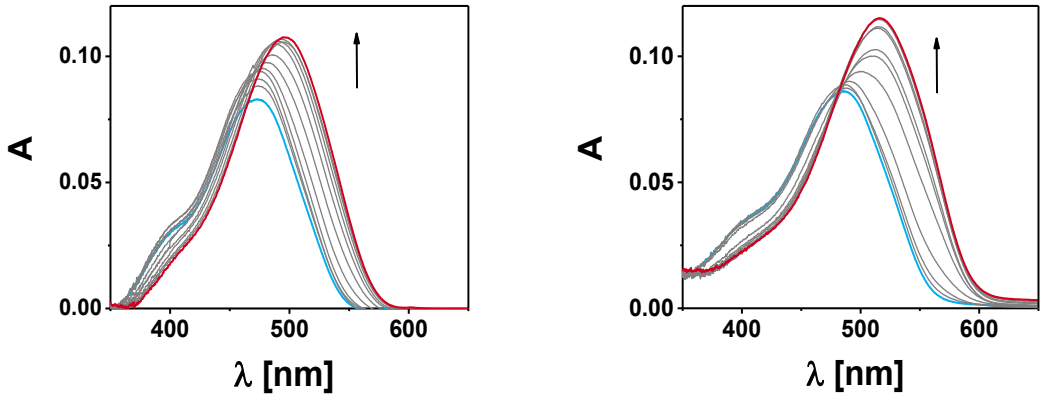

(A) (B)

Fig. 44: Absorption titration spectra of 5 µM **16** (A) and **19** (B) in the absence and in the presence of 0–250 µM 2,4 D/TBA in $CHCl_3$ (increasing concentrations in grey, start point spectrum in blue and end point spectrum in red, steps of 0, 1.0, 5.0, 9.9, 19.6, 33.8, 47.6, 69.8, 90.9, 130.4, 250 µM are shown).

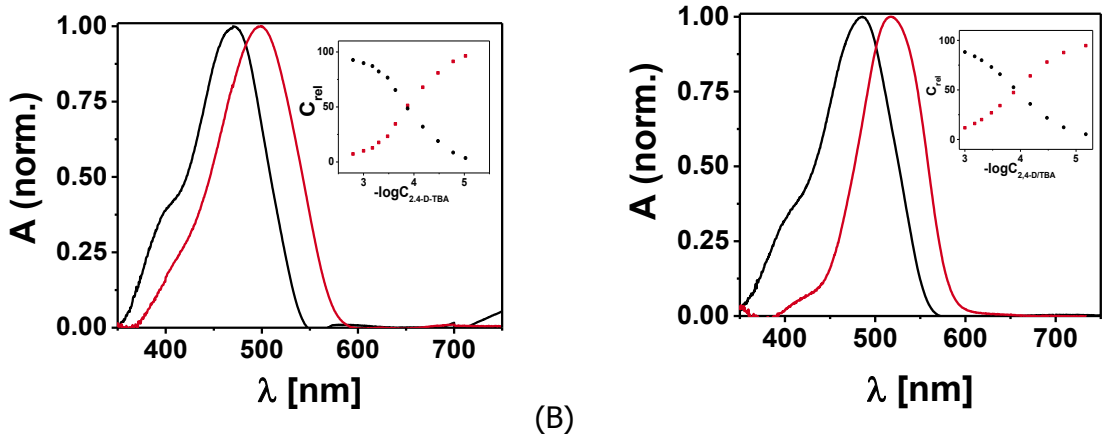

(A) (B)

Fig. 45: Species normalized spectra and the species distribution during the titration of **16** (A) and **19** (B) with 2,4-D/TBA in $CHCl_3$ calculated by HyperSpec (free **16** and **19** in black; complex in red).

Clear isosbestic points at 474 and 486 nm were observed from the species spectra and numerical treatment of the data allowed us to verify a distinct 1:1 stoichiometry and calculate binding constants for [**16**⊂2,4-D]$^-$ and [**19**⊂2,4-D]$^-$ of log$K$ = 3.88 ± 0.02 and log$K$ = 3.92 ± 0.03 (Fig. 45), which is ideal for stoichiometric imprinting whereby over 95 % of the template molecules are complexed under typical pre-polymerization conditions.[24, 177]

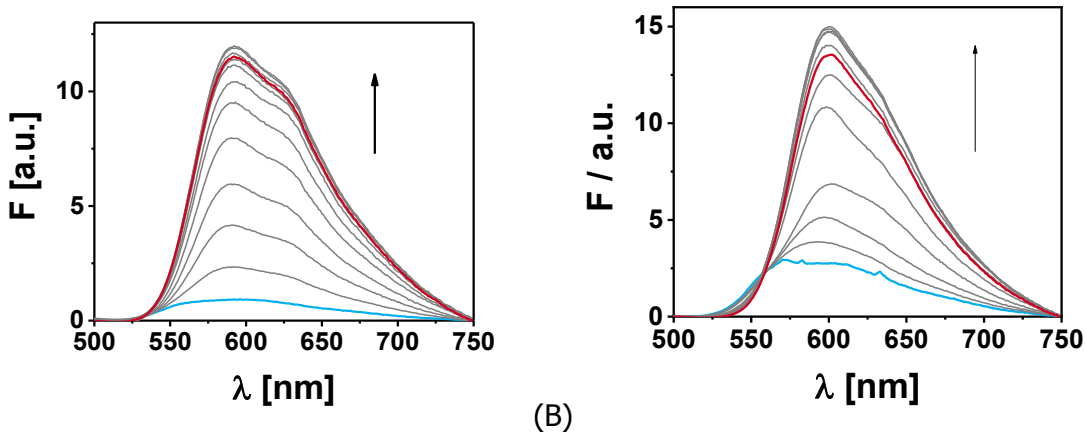

(A) (B)

Fig. 46: Fluorescence (A) and (B) titration spectra of **16** and **19** (5 µM) in the absence and in the presence of 0–250 µM 2,4-D/TBA in $CHCl_3$ (increasing concentrations in grey, start point spectrum in blue and end point spectrum in red, steps of 0, 1.0, 2.5, 5.0, 9.9, 19.6, 33.8, 47.6, 69.8, 90.9, 130.4, 250 µM are shown).

Furthermore, as was expected from our earlier works, the emission of phenoxazinones **16** and **19** was strongly enhanced after excitation at the isosbestic points and red-shifted by ca. 15 nm in the presence of 2,4-D, stressing the suitability of such molecular probe architectures for optical detection of a non-fluorescent analyte like 2,4-D (Fig. 46).

5.2.3 Preparation and performance of the MIP particles

Following recent success in devising thin MIP layers as potent sensing matrices, silica core-MIP shell microparticles were prepared (Fig. 48). Few-nanometre thin MIP phases excel over more traditional formats especially in terms of quantitative extraction of template, reducing unwanted background signals, and fast diffusion of the analyte to the binding pockets, accelerating response times.[17] For control purposes, NIP CS particles were also prepared, following the same synthesis procedure but without the template. For spectroscopically signalling MIPs it is important to guarantee that the complex between indicator monomer (or cross-linker) and template is stable under pre-polymerization conditions (Fig. 47). Here, transfer of the dilute system to pre-polymerization conditions had to include some optimization steps before polymerization. In neat solvent ($CHCl_3$), both absorption bands of free probes and complexes at 1 mM remained almost identical (472 and 499 nm in case of **16** and 487 and 513 nm for **19**), confirming the formation of complexes via hydrogen bonding. However, the addition of EGDMA as (co-)cross-linker and various co-monomers to the mixture seemed to influence the probe–analyte interactions. Lower band shifts were observed after addition of HEMA, BMA or 4-VPy, yielding absorption maxima at 487, 496, 498 nm for **16** and 496, 503 and 505 nm for **19**, respectively, indicating weaker binding in the presence of these components (Fig. 47). These species were thus unsuitable for the current MIP preparation. On the other hand, MAAm as co-monomer led to a band centred at 499 nm and 513 nm, rendering it an ideal candidate for the synthesis of MIP layers in both cases (Fig. 47).

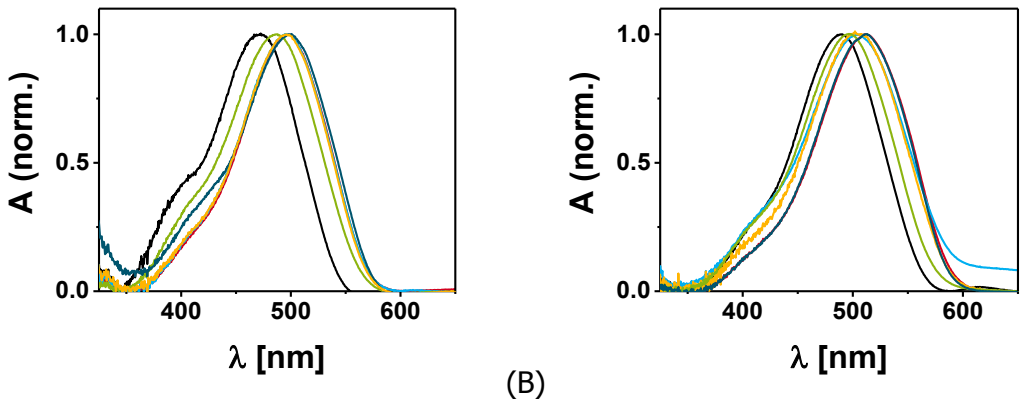

(A) (B)

Fig. 47: Normalized absorption spectra of **16** (A) and **19** (B) in $CHCl_3$ (black) with 1 mM 2,4-D/TBA in $CHCl_3$ (red) and in the presence of various co-monomers at pre-polymerization conditions, HEMA/EDGMA (green), 4-Vy/EDGMA (blue), BMA/EDGMA (yellow) and MAAm/EDGMA (dark-blue).

As supporting core material, we used 0.35 µm silica particles prepared according to the Stöber method.[17,150] Since RAFT polymerization is a suitable method to coat thin MIP layers onto SiO_2 particles, the surface was first functionalized with amino groups before a RAFT agent was covalently bound to it and finally thin homogenous polymer shells of approximately 7±1 nm were grown from the surface (Fig. 48 and Fig. 49).

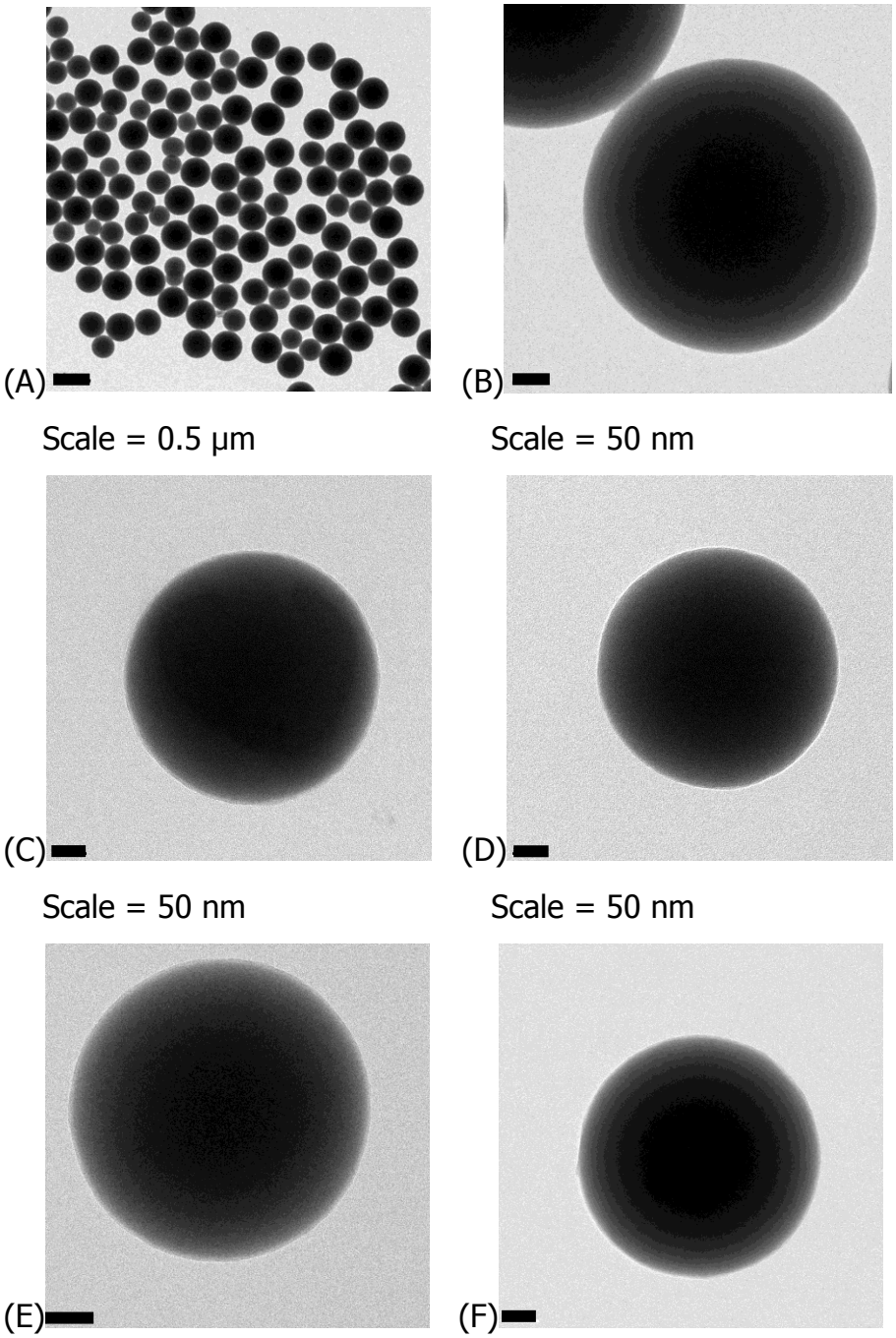

Fig. 48: TEM images of the SiO_2 (A,B), MIP(**16**)-2,4-D@SiO_2 (C) and NIP(**16**)@SiO_2 (D) and MIP(**19**)-2,4-D@SiO_2 (E) and NIP(**19**)@SiO_2 (F).

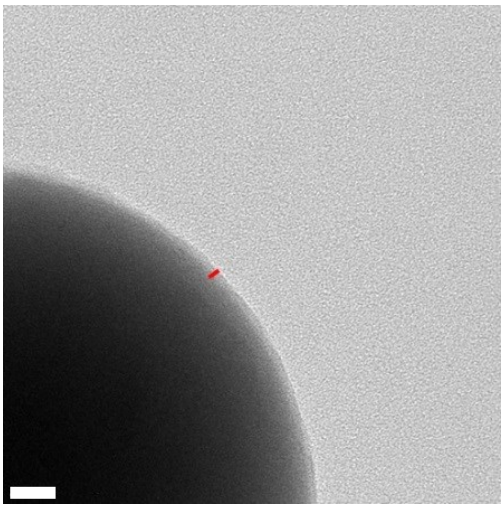

Scale = 20 nm

Fig. 49: TEM image zoom of shell region or a representative NIP(19)@SiO_2 particle

Thermogravimetric analyses (Fig. 50) of the APTES-SiO_2, RAFT agent coated APTES-SiO_2, MIP(**19**)-2,4-D@SiO_2 and NIP(**19**)@SiO_2 particles showed first a weight loss of ca. 3-4 % at 200 °C caused by the evaporation of remaining water or organic solvent. For APTES-SiO_2 particles, higher temperatures led to a degradation of the APTES layer and a weight loss of 9 % in total, while for the MIP(**19**)-2,4-D@SiO_2 and NIP(**19**)@SiO_2 particles weight losses of ca. 11–12% were found, respectively, corresponding to the polymer shells' degradation. These similar weight losses confirmed the comparable shell thicknesses of MIP and NIP particles already observed by TEM (Fig. 48, 49). Also, the FTIR measurement (Fig. 50) shows that the silica particles were successfully functionalized. After RAFT agent coupling two new bands are formed at 2499 and 2605 cm^{-1}. After polymerization, both bands disappeared which is in good agreement with our previously reported study. Finally, the 2,4-D/TBA imprinted particles were washed to remove any non-covalently bound template from the polymer network, leaving specific cavities with binding sites complementary to the desired analyte.

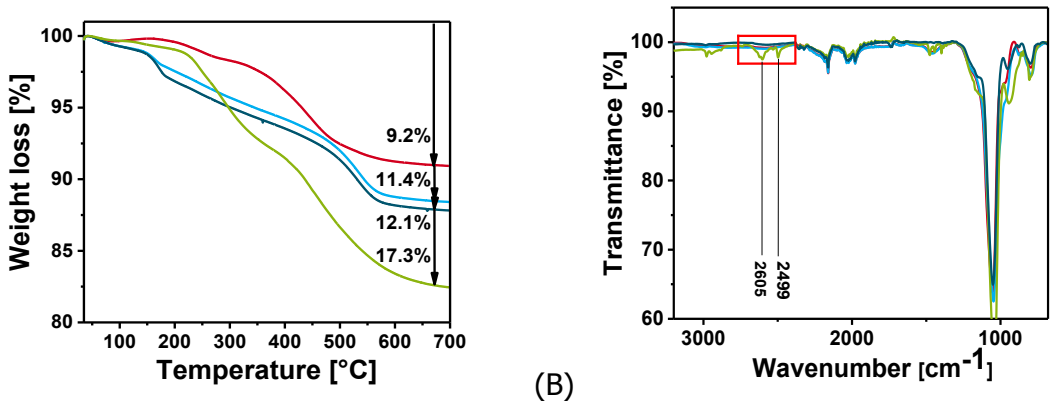

(A) (B)

Fig. 50: TGA curves (A) and ATR-FTIR (B) of APTES-functionalized silica (red), RAFT agent coated silica (green) and MIP(**19**)-2,4-D@SiO_2 (blue) and NIP(**19**)@SiO_2 (dark blue). In (B) red, blue and dark blue bands are overlapping significantly. Relevant bands of APTES-functionalized silica (green spectrum) are distinctly recognizable. The two steps found for CPDB-functionalized silica indicate that the RAFT agent is bound in two different ways, presumably physically adsorbed as well as chemically conjugated (in a ratio of ca. 1.3:1), leading to an apparent overall highest weight loss.[17]

Assessment of the sensing performance of the prepared particles was conducted in the solvent used for imprinting, i.e., $CHCl_3$, titrating with 2,4-D/TBA (Fig. 51). In the absence of template/analyte, the fluorescence emission of MIP and NIP CS particles prepared from monomer **16** and cross-linker **19** exhibited maxima at 600 nm upon excitation at 475 nm. Upon addition of 2,4-D/TBA, the fluorescence maxima were not dramatically altered, yet an intensity enhancement much higher than that for NIP CS particles was observed for MIP CS particles from both, **16** and **19**. Kinetically, this enhancement reached a plateau already after 15 s upon addition of 20 µM of 2,4-D/TBA, confirming the fast diffusion of the analyte to the binding sites in the thin MIP shell (Fig. 51).

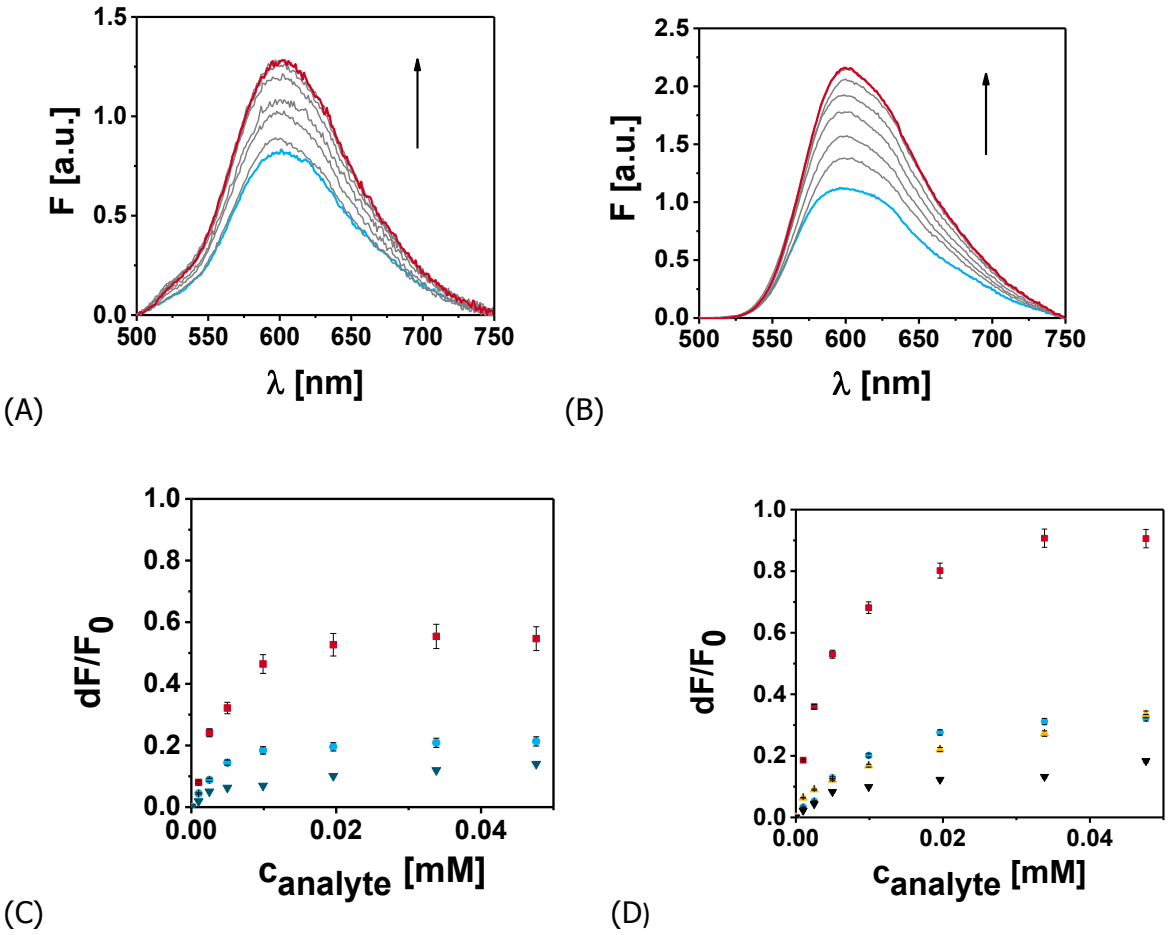

Fig. 51: Fluorescence spectra of 1 mg mL^{-1} MIP(**16**)-2,4-D@SiO_2 particles (A) and MIP(**19**)-2,4-D@SiO_2 particles (B) in $CHCl_3$ in the presence of 1 mM 2,4-D/TBA (increasing concentrations in grey, start point spectrum in blue and end point spectrum in red, steps of 0, 1.0, 2.5, 5.0, 9.9, 19.6, 33.8, 47.6 µM are shown). Sensing response of MIP(**16**)-2,4-D@SiO_2 (C) (1 mg mL^{-1}) in $CHCl_3$ toward template (red squares) and to the closely related compound 2,4-DP (blue circle), NIP(**16**)@SiO_2 toward template (dark blue down triangles); Sensing response of MIP(**19**)-2,4-D@SiO_2 (D) (1 mg mL^{-1}) in $CHCl_3$ toward template (red squares) and to the closely related compounds 2,4-DB (yellow up triangle) and 2,4-DP (blue circle), NIP(**19**)@SiO_2 toward template (dark blue down triangles).

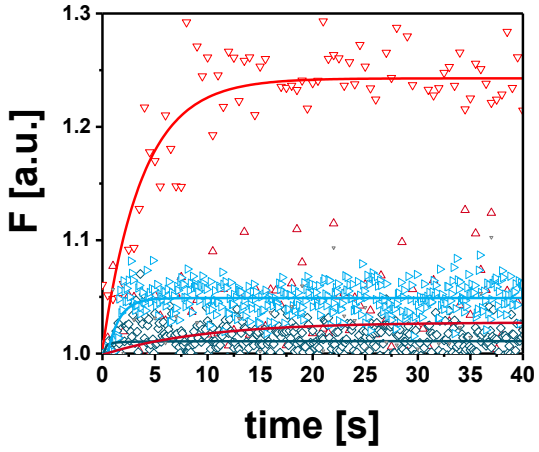

Fig. 52: Time course of the rebinding kinetics of 1 mg mL^{-1} MIP(**19**)-2,4-D@SiO2 (red) and NIP(**19**)@SiO_2 (blue) without (dark) and with 2,4-D/TBA (bright) (20 µM) in $CHCl_3$.

The favourably high imprinting factors of 3.9 and 4.8, respectively, calculated from the ratio of the sensing responses for **16**- and **19**-containing MIP(**n**)-2,4-D@SiO_2 relative to the respective NIP(**n**)@SiO_2, indicated the presence of specific molecular recognition sites. In presence of two close competitors, 2,4-DP and 2,4-DB (as TBA salts), whose structures are very similar to the targeted analyte (Fig. 43), only weak changes were noticed, the minor structural differences of these species already leading to an important mismatch and distinctly less favourable binding in the cavities (Fig. 51). Discrimination factors DF ($dF_{2,4\text{-}D}/dF_{analogues}$) of 2.7 and 2.8 against 2,4-DB and 2,4-DP were calculated, respectively. As expected the better anchoring of cross-linker **19** in the polymer matrix, and thus the higher stability of the imprinted cavities, led to a two-fold stronger response. This improved sensing behaviour and outstanding sensitivity in the organic solvent with a limit of detection (LOD, calculated again as three times the standard deviation 3σ) of 6.2 µg L^{-1} (28 nM) let us choose MIP(**19**)-2,4-D@SiO_2 for the next steps of the sensor development.

5.2.4 Phase transfer assay and droplet-based modular microfluidic platform

The development of water compatible MIPs dedicatedly binding through non-covalent forces such as hydrogen bonds is still a tremendous challenge. This impediment is even higher when the signalling response relies on the H bonding of a dye with another small organic molecule. Moreover, besides water as a prominent H bond competitor for the monomer–template complex as such, especially the fact that, when MIP synthesis has to be conducted in organic solvents, rebinding experiments in water often lead to dramatically different swelling effects are a major obstacle on the way to capture phases operating in aqueous systems.[216] As recently shown by authors, a first approach to overcome such problems is the use a phase-transfer assay in conventional quartz cells (Fig. 53).[17]

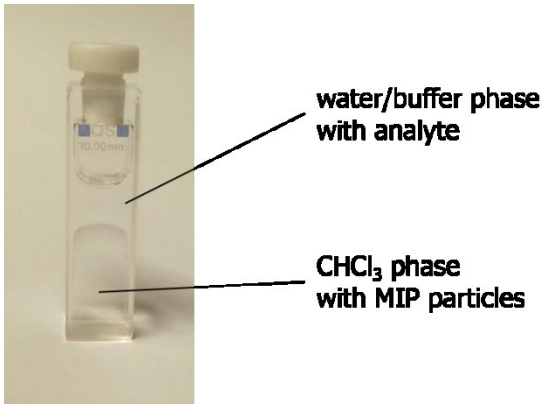

Fig. 53: Sensing design of phase-transfer assay in conventional quartz cells.

Accordingly, sensor particles (3 mg) were firstly suspended in 2 mL $CHCl_3$ before 1 mL of Milli-Q® water was added, followed by the addition of an aqueous stock solution of 2,4-D/TBA into the water phase. Then, the fluorescence intensities of the organic phases were measured 5 min after addition of the analyte and continuous stirring. In agreement with the monophasic results discussed above, the fluorescence intensity of the organic phase containing MIP(**19**)-2,4-D@SiO_2 increased as a function of the amount of 2,4-D/TBA added into the water phase, confirming the extraction of the analyte from the aqueous phase. In addition, the aqueous phases containing residual 2,4-D/TBA not transferred into the organic

phase were analysed by HPLC for validation. These results indeed indicated a partition coefficient higher than 2.5 (Tab. 10) and, therefore, a favourable transfer of the analyte from the aqueous to the organic phase.

Tab. 10: Partition coefficient (P) of 2,4-D in aqueous (1 mL) and organic phases (2 mL) determined by HPLC analyses.

$n_{2,4\text{-D}}$ added mmol	$n_{2,4\text{-D}}$ H_2O mmol	$C_{2,4\text{-D}}$ H_2O mol L^{-1}	$n_{2,4\text{-D}}$ $CHCl_3$ mmol	$C_{2,4\text{-D}}$ $CHCl_3$ mol L^{-1}	$P_{CHCl3/H2O}$
0.12	0.01	0.01	0.11	0.05	4.4
0.29	0.05	0.04	0.24	0.12	2.4
0.55	0.09	0.07	0.46	0.23	2.6
0.78	0.13	0.1	0.66	0.33	2.6
1.00	0.18	0.15	0.82	0.41	2.3
				$\overline{P_{CHCl_3/H_2O}}$ =	**2.5***

*not taking into account the 1st concentration

The NIP control particles did not show any fluorescence enhancement in this assay configuration, indicating a dramatic reduction of non-specific binding.

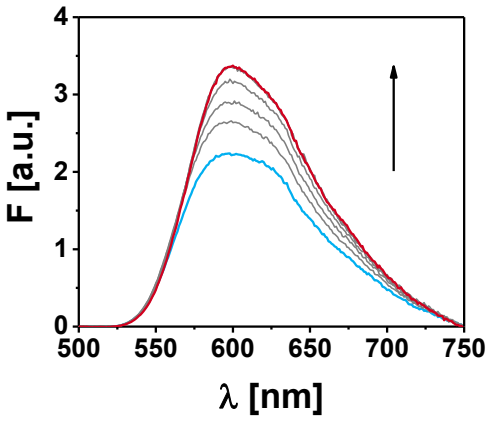

(A)

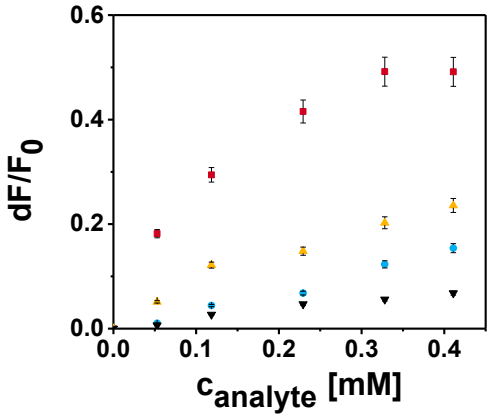

(B)

Fig. 54: Fluorescence spectrum (A) from the organic phase ($CHCl_3$) containing 1 mg mL^{-1} MIP(**19**)-2,4-D@SiO_2 particles upon addition of 2,4-D in the upper water phase (increasing concentrations in grey, start point spectrum in blue and end point spectrum in red, steps of 0, 50, 120, 230, 330, 411 µM are shown). Biphasic sensing response (B) of MIP(**19**)-2,4-D@SiO_2 particles towards 2,4-D (red square) to the closely related compounds 2,4-DB (yellow up triangle) and 2,4-DP (blue circle) as well as NIP(**19**)@SiO_2 particles towards 2,4-D (black down triangle).

An imprinting factor of 6.9 was calculated for this protocol, being much higher than for the monophasic assay. The discrimination against 2,4-DB and 2,4-DP remained largely unchanged with comparable discrimination factors of 2.0 and 3.0 (Fig. 54). Unfortunately, for the biphasic assay in cuvettes, a much higher LOD of 884 µg L^{-1} (4 µM) (3σ) was calculated. Since such LOD hardly meets the requirement for trace analysis, it deemed essential to us to improve the extraction step dramatically while at the same time miniaturizing the entire assay.

Today, analytical tool integration and miniaturization has reached a certain level of maturity. However, with respect to exploitation of the synergisms that can be expected to emerge from a combination of the chemical sensing power of indicator particles with the processing opportunities that miniaturized analytical systems offer, a wealth of possibilities remains to be uncovered. Powerful microfluidic devices combined with fluorescent indicators have proven beneficial in the last years, not only because of their miniaturized size and low probe as well as sample volumes, but also because of their almost immediate response and the short measurement times without sample pre-treatment that can be realized.[217-218] Combining fluorescent MIP indicator particles with a prototype microfluidic system for the real-time measurement of aqueous samples without pre-treatment therefore seemed very appealing to us. We thus designed a robust and miniaturized microfluidic setup for use with our sensor particles in an in-line two-phase assay (Fig. 28). Relying on droplet-based extraction, the phase-transfer efficiency should be dramatically enhanced, lowering LODs for 2,4-D analysis directly in aqueous samples while guaranteeing fast assay times.[152] The 3D modular microfluidic system devised here utilizes direct injection of the aqueous sample and a suspension of MIP(**19**)-2,4-D@SiO_2 in $CHCl_3$ (1 g L^{-1}), the latter in vertical position to reduce the influence of sedimentation, into a commercially available micro T-cross via standard PTFE tubing. Homogenous water droplets were successfully generated and injected into PFA tubing rolled on a metallic bar, acting like a micro-extractor for droplet mixing and analyte extraction by chaotic advection.[219] The intrinsic modularity of the looped tubing extraction system greatly facilitated the matching of the requirements to ensure a high extraction

and detection efficiency.[220] Flow rates of 15 and 10 µL min^{-1} for the aqueous and organic phase, respectively, were found to be optimal to guarantee an efficient recognition process. The length of the tubing, i.e., the size of the extractor was then adapted for an extraction time of 30 s (2x equilibrium time). Highly transparent PFA tubing permitted direct fluorescence signal collection with a preferred 90° angle between exciting beam and emission collection optics (Fig. 28 and 55).

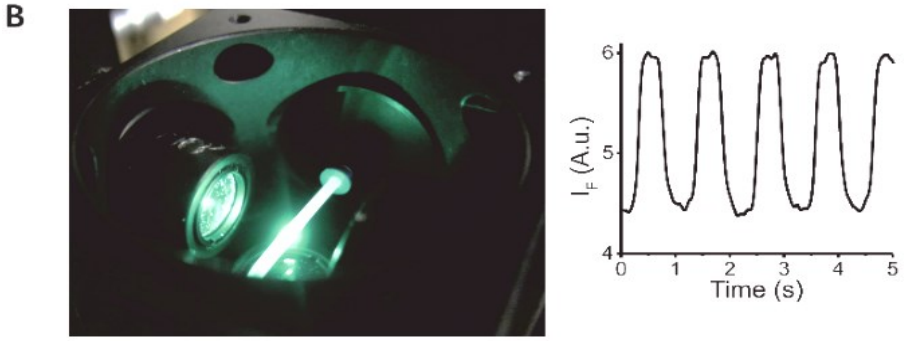

Fig. 55: Picture of the optomechanics cube with light excitation of the microfluidic tubing and perpendicular emission collection and (right) fluorescent droplets signals vs time.

This miniaturized optical setup was organised around a standard optomechanics cube with the microfluidic tube passing through, a mounted LED excitation source and, perpendicularly to it, an optical fibre bundle connected to a USB spectrometer to collect the emission. This optical fibre bundle was also used to measure back-scattered light of the LED, to account for LED fluctuations in the numerical data treatment. Such a setup allowed us to perform promising experiments in Milli-Q® water, detecting concentrations of 2,4-D down to 4.4 µg L^{-1} (20 nM) with a linearity range up to 5 µM, thus matching the WHO and EPA requirements (Fig. 56).

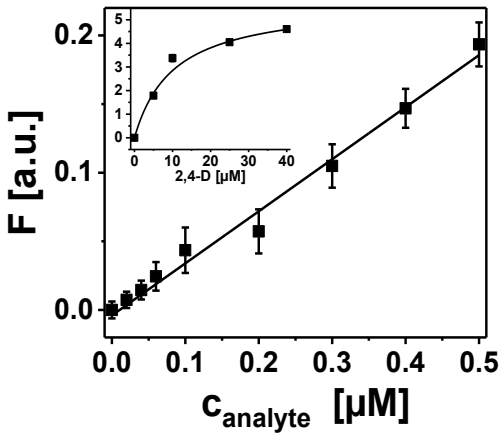

Fig. 56: Response of sensor towards 2,4-D ([particles] =1 mg mL^{-1}).

Because of the inert PTFE–PFA wall of the tubing used, highly reproducible experiments were obtained and no memory effects were found, even without any (regular rinsing of the fluidic system. Like for the cuvette assay, an increasing concentration of the analyte induced an enhancement of the fluorescence signal coming from the chloroform droplets containing the MIP particles. An acquisition of the signal over 100 s coupled with an integration time of 5 ms was sufficient to obtain a stable and acceptable standard deviation for the fluorescence measurement (0.5–1 %). This led to a total analysis time of 130 s, perfectly suitable for real-time monitoring, e.g., by replacing the syringe pump for the sample by a bypass from a drainage system or any other outlet of a potentially contaminated water body/system.

5.2.5 Analysis of water samples collected worldwide

To assess the possibilities for actual 2,4-D monitoring, various water samples from Asia, Europe and America were investigated, following a standard addition method (DIN 32633:2013-05). Aliquots of 2,4-D/TBA from 0 to 60 nM were directly added into the water samples, which were analysed without any further pre-treatment. Certain matrix effects were observed for the different samples, leading to somewhat enhanced background signals in some cases without any dramatic consequences on the ability of the MIP particles to detect the analyte. In all cases, signal intensities and titration plots from the analytes were similar and allowed us to detect 2,4-D containing samples (Tab. 11, Fig. 57).

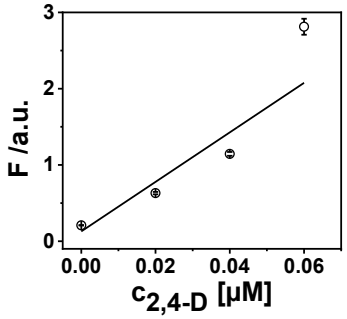

(A) Santa Fe River, Florida, USA

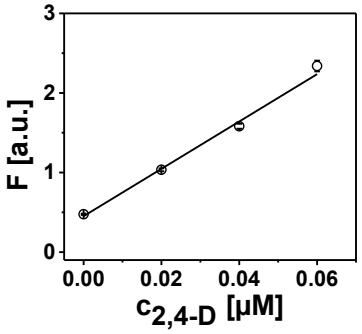

(B) Mississippi, Minneapolis, USA

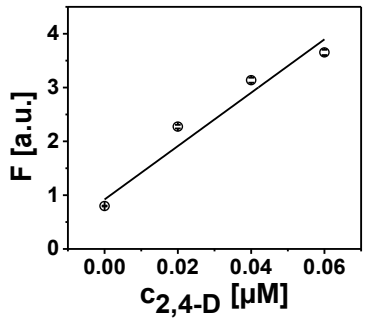

(C) Hàn River, Da Nang**,** Vietnam

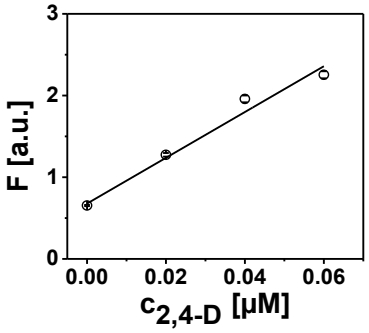

(D) Lake, Nghệ An, Vietnam

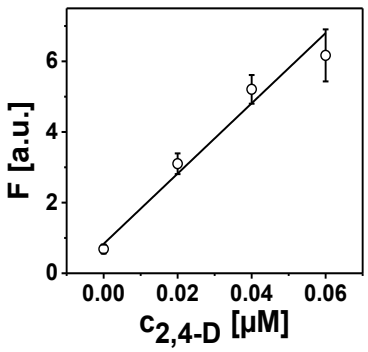

(E) Teltow Canal, Berlin, Germany

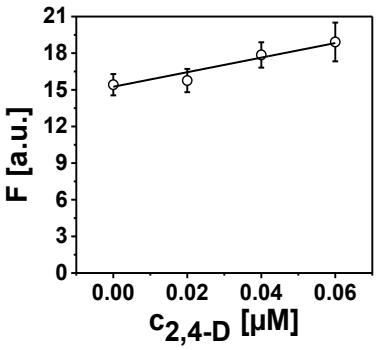

(F) Teltow Canal, Berlin, Germany (spiked 0.2 µM)

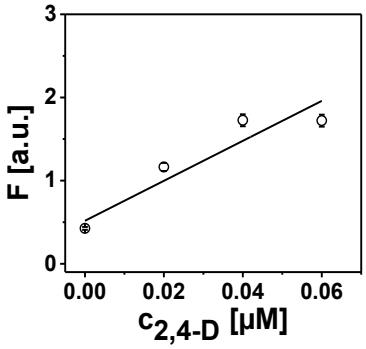

(G) Rio Paranapanema, Salto Grande, Brazil

Fig. 57: Analyses of real water samples from Florida (A), Minnesota (B), Vietnam (C) and (D), Germany ((E) and (F), while (F) was pre-spiked with 0.2 µM of 2,4-D) and Brazil (G), following a standard addition method. Aliquots of 2,4-D/TBA from 0 to 60 nM were directly added into the samples.

Tab. 11: Found 2,4-D concentrations in ground water samples: A. Santa Fe River, Florida, USA; B. Mississippi, Minneapolis, USA; C. Hàn River, Da Nang, Vietnam; D. Lake Nghệ An, Vietnam; E. Teltow Canal, Berlin, Germany; F. Teltow Canal, spiked with 0.2 µM of 2,4-D; G. Rio Paranapanema, Salto Grande, Brazil.

Water samples	Concentrations (nM)			
	Found	Corr. from NIP	Reported	ELISA
A	< 20	-	< 0.02	*n.d.*
B	< 20	-	0.14	*n.d.*
C	22.3 ± 0.3	-	-	*n.d.*
D	26.0 ± 0.4	-	-	13.7 ± 5.8
E	< 20		< 0.09	*n.d.*
F	239.4 ± 13.6	194 ± 11.6	-	*n.d.*
G	27.6 ± 0.1	17.8 ± 0.8	-	18.4 ± 2.3

In accordance with the reported values from various water quality control agencies for 2016, samples from North America (Florida Department of Environmental Protection and Minnesota Department of Health) and Europe (Berliner Wasserbetriebe) showed only slight responses which were below the LOD. In contrast, in samples taken rather soon after the common herbicide application season from lakes and rivers in Vietnam and Brazil, where 2,4-D was and/or is used regularly in agriculture, 2,4-D was detected, but still far below the (maximum acceptable concentration) MAC devised by the WHO. These positive samples were analysed in parallel with a commercial ELISA test for 2,4-D (Abraxis 2,4-D ELISA–Microtiter Plate) to confirm independently our results. The concentrations found by this procedure were in good agreement with those found with the microfluidic sensor system, the slightly lower values presumably resulting from the different cross-reactivities any metabolites or closely related substances have with either the "artificial antibody" (= MIP) or the real antibody of the ELISA. These results clearly stress the potential that the combination of fluorescent MIP particles with a microfluidic sensor setup harbours for the detection of herbicide in real water samples. Finally, to simulate a water sample distinctly exceeding the

WHO limit, 200 nM of 2,4-D/TBA were spiked to the European sample before being injected into the sensor. Also in this case, the analyte was easily detected, the certain overestimation most likely being related to the fact that the Teltow Canal sample showed the most pronounced matrix effects. Indeed, after subtraction of the signal coming from the non-specific interactions (obtained from titration with the NIP(**19**)-2,4-D@SiO2) the 2,4-D concentration was found to be 194 nM.

5.2.6 Conclusion

In this work, a fluorescent indicator monomer and a fluorescent indicator cross-linker were designed, synthetized and integrated into thin MIP shells on silica microparticles for the selective determination of 2,4-D. Both probes presented high affinity for the target analyte together with a favourable turn-on fluorescence response even when confined in a rigid matrix. After incorporation into a thin MIP polymer layer on a silica carrier particle, the cross-linker probe exhibited better imprinting effects, i.e. higher imprinting factors, presumably due to its more stable anchoring into the polymer matrix. Upon application of the sensory core-shell particles in a biphasic extraction assay, 2,4-D could be selectively determined in water. Integration of the MIP particles into a modular microfluidic platform allowed for efficient extraction of the analyte from untreated water samples and sensitive detection through analyte-induced fluorescence enhancement. The assay allows for the determination of 2,4-D between 20 nM and 5 µM, well complying with the WHO or EPA requirements for drinking water, and was successfully employed on actual river and lake water samples from various regions of the world. The work presented here shows for the first time that the step from a fluorescent probe monomer to a cross-linker can improve significantly the performance of fluorescent MIPs and that the combination of tailored core-MIP shell microparticles with a droplet-based microfluidic system can yield a simple yet very powerful miniaturized analytical tool for environmental analysis. Given the modularity of the particle platform, the MIP matrix and the microfluidic part, this toolbox harbours enormous potential for the development of integrated chemical sensors for the monitoring of a larger number of relevant, less hydrophilic

chemical parameters in liquid samples of not only environmental but also pharmaceutical, food chemical, biochemical or medical interest.

5.3 Fluorescent MIP Sensor Particles for the Detection of Antibiotics

5.3.1 Introduction

For a long time, antibiotics have been used in medicine and factory farming for treating diseases. The widespread administration of those drugs, especially in the latter, may lead to the presence of antibiotic residues in food products like e.g. milk, eggs and meat which causes a negative effect on human health, while increasing drug resistances and decreasing the disease treatment efficacy.[221] There are different groups of antibiotics, for instance, tetracycline, macrolide, aminoglykoside, fluoroquinolone and β-lactams.[222] The most common ones belong to the β-lactams, one of the most relevant being ampicillin (AMPI). This 'broad spectrum' penicillin is used in high amounts against many Gram-positive and Gram-negative microorganisms in human and veterinary medicine. In addition, maximum residue limits (MRLs) of AMPI have been set by the European Commission to 4 µg kg^{-1} in milk and in muscle, fat, liver and kidney to 50 µg kg^{-1}.[223]

Because of the low concentration level of AMPI, a fast, sensitive and selective recognition method and sensing device for the determination of AMPI in food products in a convenient functional format for daily use is urgently required. Several analytical screening tests have been developed for the detection of AMPI including tests based on enzyme assays, immunoassays or receptor binding assays.[224-226] There are already miniaturized and commercially available test kits used for milk samples e.g. the Beta-Star (Neogen Corporation), TwinSensor Milk &TwinExpress Milk (Unisensor s.a.) or Charm MRL Beta-Lactam/Tetracycline Combo Test & Charm MRLBLTET2 (Charm Sciences Inc.). However, such tests suffer from their high costs, preparation effort and limited application solvent.

Indeed, the last few decades in sensing science and the previous chapter 4.2 showed that miniaturizing of devices can improve their features, not only with regard to the response and measuring time but also in terms of a decrease of the probe and sample volume.[227] A promising alternative for a fast and rapid

recognition system for small-molecule analytes in food is the combination of functionalized particles as sensor platforms with optical detection. Thus, also in this chapter MIPs are used for targeting analytes. These "artificial antibodies" in combination with the integration of a specific tailor-made fluorescent indicator cross-linker in a thin polymer network coated on silica particles via RAFT polymerization are used again to proof the method before and show a promising detection method for AMPI.

5.3.2 Binding studies with AMPI/TBA in $CHCl_3$

As we could observe in the previous study (Chapter 4.2), **19** is the most successful fluorescent cross-linker that can be incorporated into a thin MIP layer grafted from the surface of silica particles for the detection of small analytes. In the next step, the procedure should be validated by exchanging the small carboxylate containing model analyte 2,4-D to AMPI for its detection in food products e.g. milk or cream (Fig. 58).

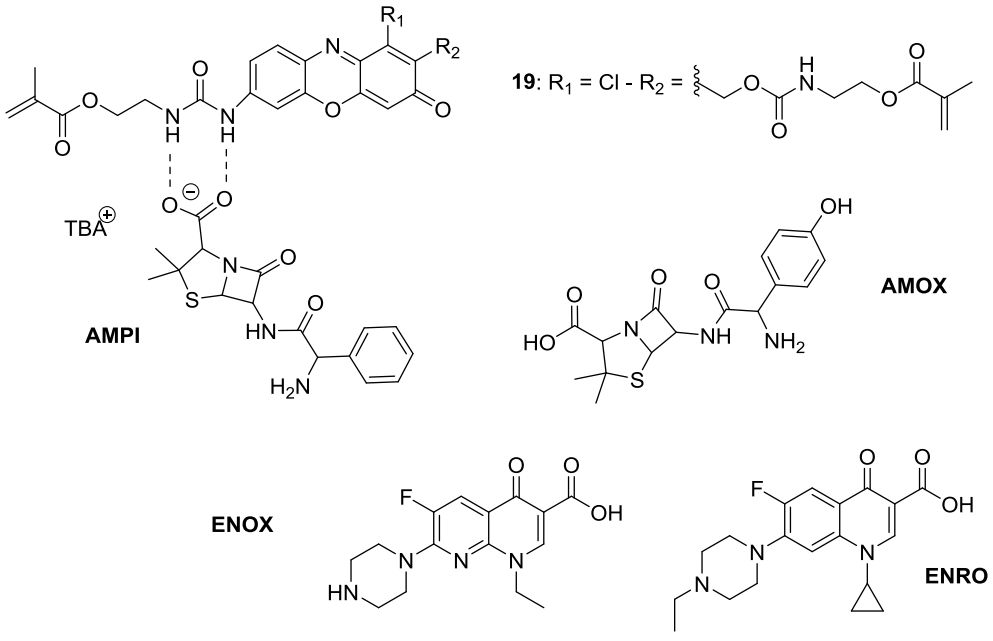

Fig. 58: Molecular architecture of the phenoxazinone cross-linker **19** as well as structures of AMPI and closely related compounds AMOX (amoxicillin), ENOX (enoxacin) and ENRO (enrofloxacin).

To investigate the behaviour in solution, first, the receptor cross-linker was titrated with 1 mM AMPI/TBA in $CHCl_3$. Fig. 59 illustrates the change in absorbance upon addition of the analyte. These results were used again to calculated the binding constant for [**19**⊂AMPI]$^-$ of log*K* = 3.83 ± 0.01 with HyperSpec. In agreement with the previously observed results (Chapter 4.2.2), the cross-linker formed a stable complex with AMPI/TBA like with 2,4-D/TBA. A red-shift of the absorption band from 486 nm to 521 nm could be observed as well as an isosbestic point at 495 nm, which was used as the excitation wavelength. The emission intensity (Fig. 60) is enhanced with a shift from 584 nm to 600 nm. These results show that the fluorescent cross-linker can be used for signalling a wide range of carboxylate containing analytes in organic solvents.

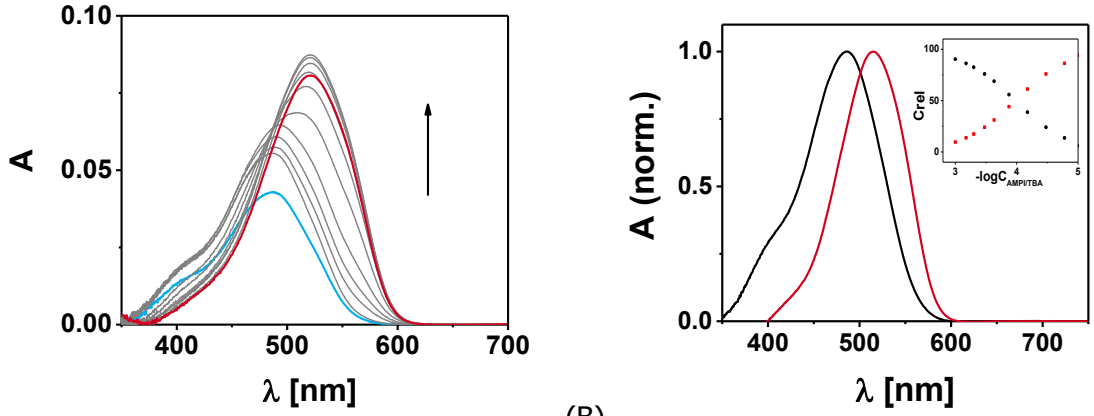

(A) (B)

Fig. 59: Absorption titration spectra of 5 µM **19** (A) in the absence and in the presence of 0–250 µM AMPI/TBA in $CHCl_3$ (increasing concentrations in grey, start point spectrum in blue and end point spectrum in red, steps of 0, 1.0, 2.5, 5.0, 9.9, 19.6, 33.8, 47.6, 69.8, 90.9, 130.4, 250 µM are shown). Species normalized spectra and the species distribution (B) during the titration of **19** with AMPI/TBA in $CHCl_3$ calculated by HyperSpec (free **19** in black; complex in red).

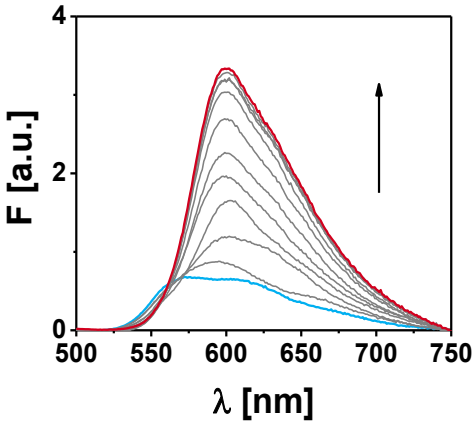

Fig. 60: Fluorescence titration spectrum of **19** (5 µM) in the absence and in the presence of 0–250 µM AMPI/TBA in $CHCl_3$ (increasing concentrations in grey, start point spectrum in blue and end point spectrum in red, steps of 0, 1.0, 2.5, 5.0, 9.9, 19.6, 33.8, 47.6, 69.8, 90.9, 130.4, 250 µM are shown).

5.3.3 Fluorescent core-shell MIP sensor microparticles in $CHCl_3$

Here, MIP(**19**)-AMPI@SiO_2(**1**) and NIP(**19**)@SiO_2(**1**) were prepared following a similar procedure like described in the chapter before, however, using AMIP/TBA as the template molecule. For better understanding and differentiation of the prepared MIP and NIP particles following different synthetic conditions (Tab. 3, chapter 3.6.3) we used MIP(**19**)-AMPI@SiO_2(**n**) and NIP(**19**)@SiO_2(**n**) as abbreviations. Again, 0.35 µm RAFT agent modified silica particles were used as the support material. As co-monomer and co-cross-linker, MAAm and EDGMA were used as well. Fig. 61 shows that a thin polymer shell of 10 ± 1 nm could be created on the surface according to the TEM images, which is, compared to the previous study, slightly thicker. Although the synthesis was performed under the same and best possible controlled conditions, the use of a different analyte for imprinting can influence the shell thickness.

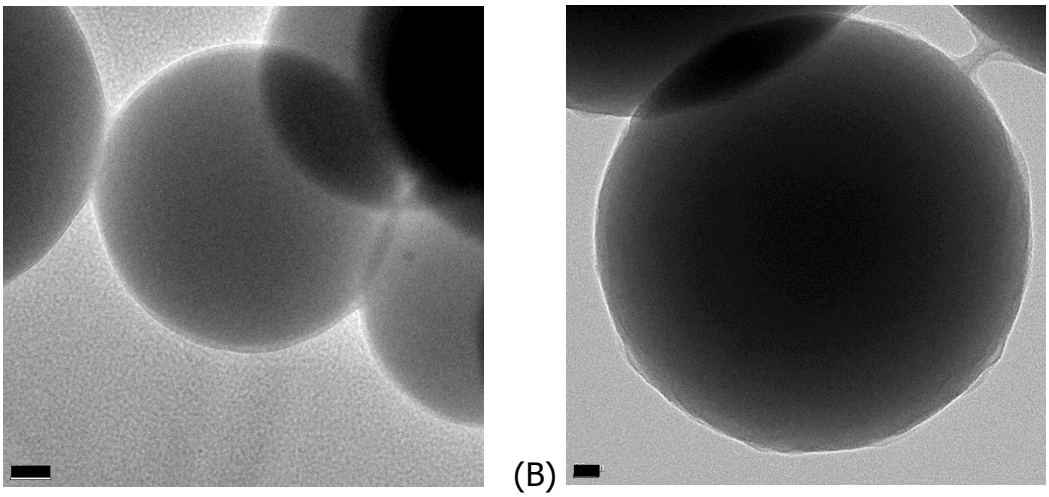

Fig. 61: TEM images of the MIP(**19**)-AMPI@SiO_2(**1**) (A) and NIP(**19**)@SiO_2(**1**) (B) prepared with **19** in $CHCl_3$.

Fluorescence spectroscopy was used to characterize the interaction between the analyte with the prepared receptor material. In the absence of the analyte AMPI/TBA the fluorescence of the MIP and NIP CS particles prepared with **19** show maxima at 600 nm upon excitation at 475 nm (Fig. 59). After addition of the analyte, the fluorescence maxima were not shifted strongly, however, the intensity increased much more for the MIPs than for NIPs until saturation was reached. The sensing response of the MIP and NIP sensor particles were not only investigated by the addition of the imprinted AMPI/TBA but also by the addition of the structurally similar compound AMOX/TBA, differing only in a single *p*-hydroxy group. It is obvious that the emission intensity of the MIP particles increased much stronger upon addition of the imprinted analyte than with AMOX/TBA. A LOD of 21 nM (3σ) was obtained. In contrast, the titration with AMOX/TBA resulted in a weaker sensing response of slightly mismatching AMOX/TBA with a cavity formed by AMPI/TBA resulting in a discrimination factor DF of 2.1. A good specificity of binding of the analyte to the polymer network can be seen by the lower analyte binding tendency to the NIP particles in Fig. 62; non-specific binding is not very pronounced. An IF of 3.5 was obtained.

However, compared to the previously studied system in chapter 4.2 (MIP(**19**)-2,4-D@SiO_2 and NIP(**19**)@SiO_2 in $CHCl_3$, IF=4.8) the lower value could

stem from two factors. First, the thicker shell can contain some deeper lying binding sites in the matrix that are not reachable for the analyte and second, the imprinting of the larger anion template leads to a larger cavity, potentially allowing for more unspecific binding in the polymer matrix. Chapter 4.1 demonstrated already that the affinity of the anion template to the urea group of the fluorescent monomer or cross-linker depends on the basicity of the anion. AMPI (pk_a = 2.5) is somewhat less basic than 2,4-D (pk_a = 2.7) which can also have an effect on the affinity to the binding site and reduce the sensing response.

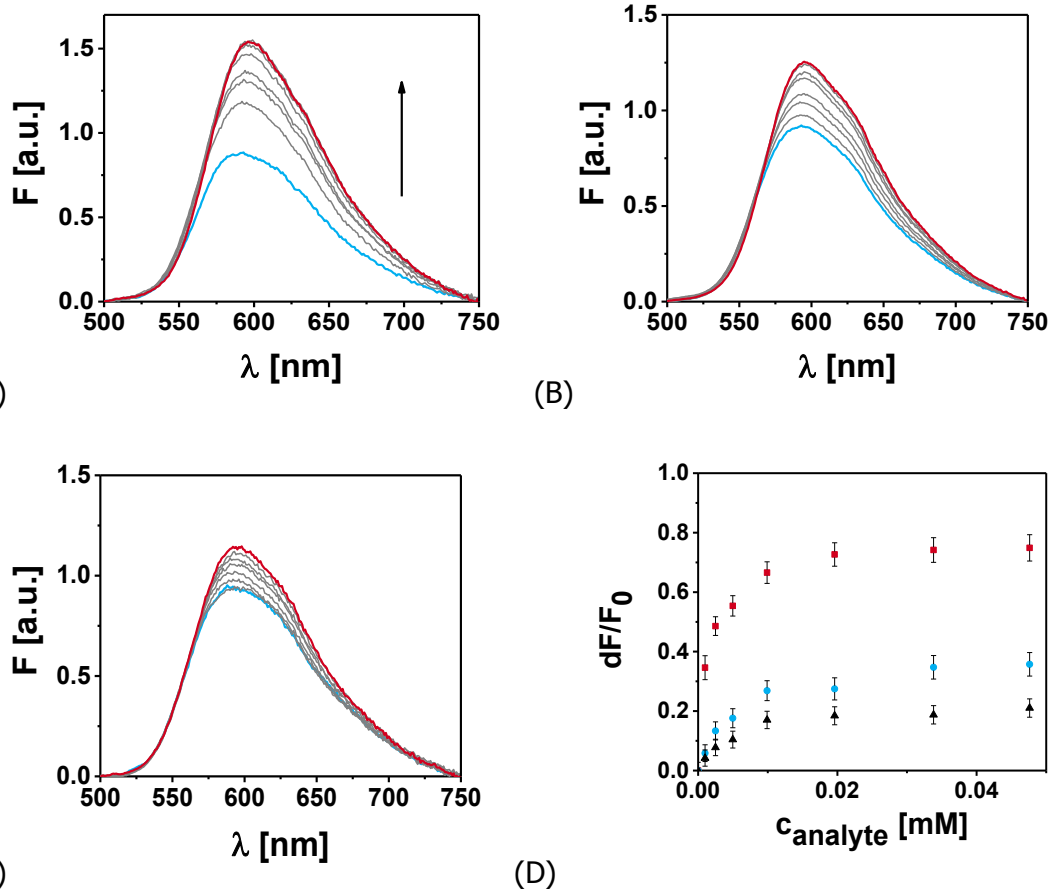

Fig. 62: Fluorescence spectra of 1 mg mL^{-1} MIP(**19**)-AMPI@SiO_2(**1**) particles in $CHCl_3$ in the presence of 1 mM AMPI/TBA (A) and to the closely related compound AMOX (B) as well as of 1 mg mL^{-1} NIP(**19**)@SiO_2(**1**) particles (C) in the presence of the template, (increasing concentrations in grey, start point spectrum in blue and end point spectrum in red, steps of 0, 1.0, 2.5, 5.0, 9.9, 19.6, 33.8, 47.6 µM are shown); Sensing response (D) of 1 mg mL^{-1} MIP(**19**)-AMPI@SiO_2(**1**) in $CHCl_3$ toward template (red squares) and to the closely related compound AMOX (blue circle) as well as of NIP(**19**)@SiO_2(**1**) toward template (dark-blue up triangles).

5.3.4 Phase transfer assay

It was already pointed out that the detection in water using MIPs reveals some problems due to swelling effects and competition of the water molecules to the urea binding moiety. Thus, a two-phase transfer assay seems to be a good method to overcome these problems (Chapter 4.2.4). To find out if this method is suitable for the prepared MIP system, the protocol was adapted from the previous study (Fig. 54). 3 mg Particles were suspended in 2 mL $CHCl_3$ and 1 mL buffer of pH 10 was added forming the second upper phase. Different concentrations of AMPI/TBA were added to the aqueous phase and after 5 min equilibration time the fluorescence was recorded. The remaining analyte concentration in buffer phase was determined with HPLC (Tab. 12). Obviously, the saturation was reached earlier compared to the 2,4-D study before. The hydrophilic character of AMPI makes it stay in the more aqueous phase and impede the transfer.

Tab. 12: Partition coefficient (P) of AMPI in aqueous (1 mL) and organic phases (2 mL) determined by HPLC analyses

n_{AMPI} added mmol	n_{AMPI} H_2O mmol	c_{AMPI} H_2O mol L^{-1}	n_{MPI} $CHCl_3$ mmol	C_{AMPI} $CHCl_3$ mol L^{-1}	$P_{CHCl3/H2O}$
0.06	0.01	0.01	0.05	0.03	3.0
0.12	0.01	0.04	0.11	0.06	6.0
0.29	0.05	0.17	0.24	0.12	2.4
0.55	0.2	0.18	0.35	0.17	0.9
0.78	0.28	0.24	0.5	0.25	0.9
1	0.39	0.33	0.61	0.30	0.8
				$\overline{P_{CHCl_3/H_2O}}$ =	**0.9**

*not taking in account the first three concentration due to the strong scattering

Fig. 62 shows the sensing response of the MIP and NIP particles against the analyte. dF/F_0 was used again to express the sensing response. This relative quantity reduces greatly uncertainties from weighting errors of the particles in the different assays. Indeed, the imprinting factor increased to 4.8, mainly by suppressing non-specific binding. However, it is still not as good as in the 2,4-D case before.

Unfortunately, the LOD of 78 µM (3σ) was worsened as well. Besides the thicker shell, the inferior transfer of the more hydrophilic AMPI to the organic phase due to its stronger affinity to the aqueous phase emerged as another problem. It is obvious that the biphasic assay works preferably for more hydrophobic analytes, moving easier into the organic phase and leading to a higher fluorescence enhancement.

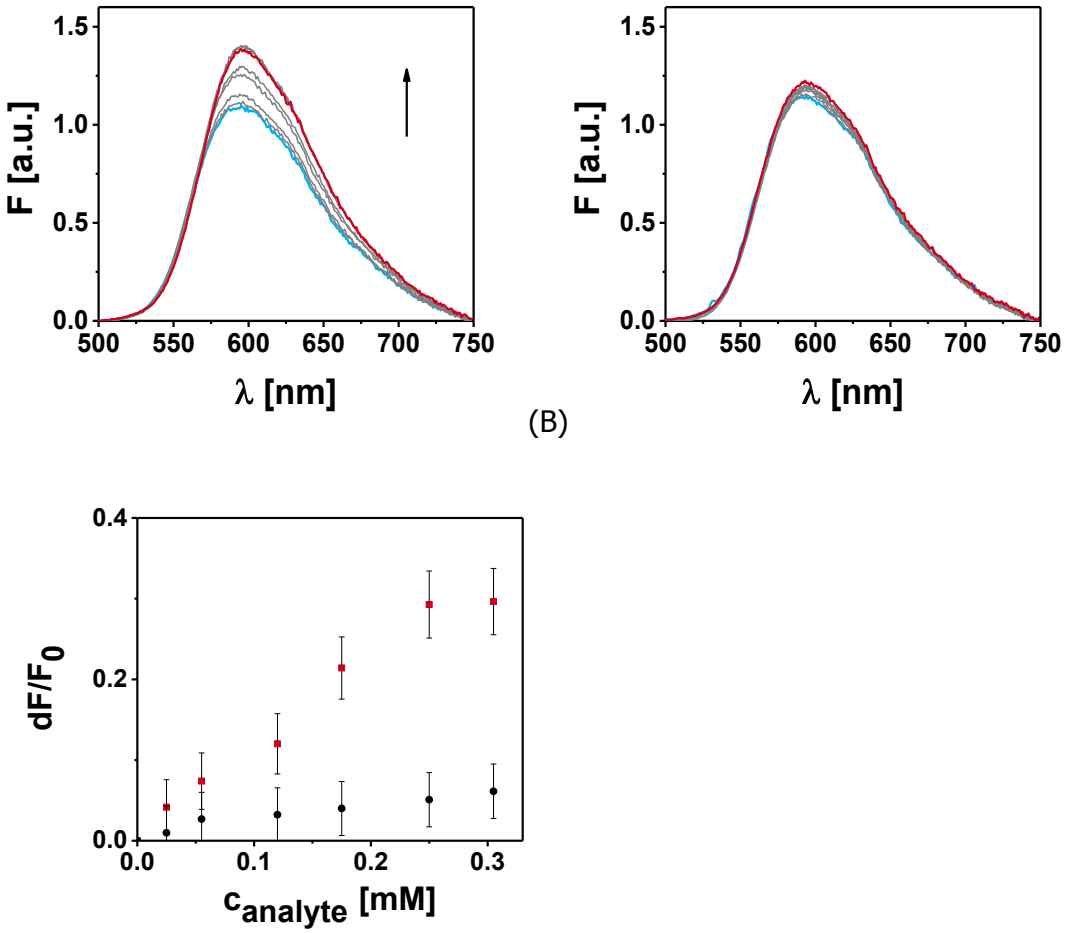

Fig. 63: Fluorescence spectrum from the organic phase ($CHCl_3$) containing 1 mg mL^{-1} MIP(**19**)-AMPI@SiO_2(**1**) (A) and NIP(**19**)@SiO_2(**1**) particles (B) upon addition of AMPI in the upper water phase (increasing concentrations in grey, start point spectrum in blue and end point spectrum in red, steps of 0, 30, 60, 120, 170, 250, 300 µM are shown). Biphasic sensing response (C) of MIP(**19**)-AMPI@SiO_2(**1**) (red square) and NIP(**19**)@SiO_2(**1**) particles (black circles) towards AMPI.

5.3.5 Binding studies with AMPI/TBA in MeCN

Because the phase transfer assay was not successful from the point of view of the final application, we repeated the experiments but used MeCN as a more polar solvent for preparation and the titration experiments. First, UV-Vis absorption and fluorescence titrations were used to assess the binding affinity between anionic guest and fluorescent host in pure MeCN. The fluorescence increased accordingly with a 15 nm shift, as expected for dye **19** (Fig. 63). A binding constant of log$K$ = 3.61 ± 0.03 was determined through fitting the absorption titration results with the software HyperSpec, and only two UV/vis-spectroscopically active species were found again to be involved in the whole titration process, free **19** and H-bonded complex (Fig. 65).

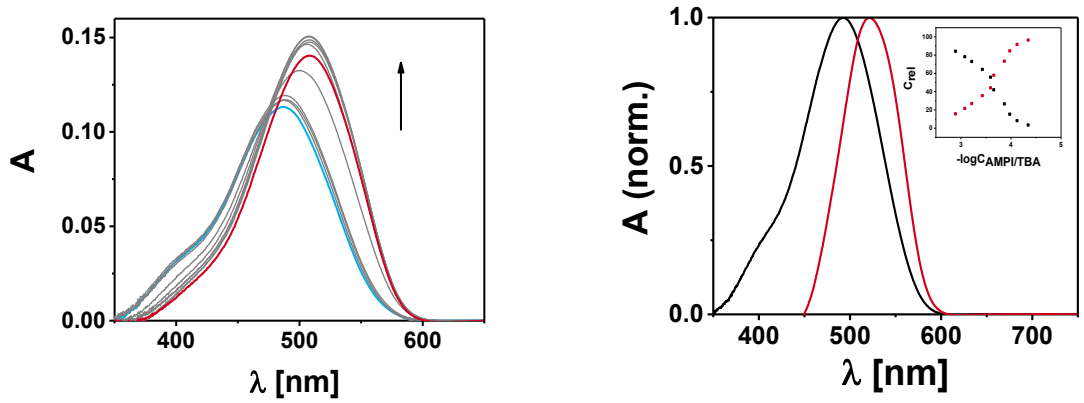

(A) (B)

Fig. 64: Absorption titration spectra of 5 µM **19** (A) in the absence and in the presence of 0–250 µM AMPI/TBA in MeCN (increasing concentrations in grey, start point spectrum in blue and end point spectrum in red, steps of 0, 5.0, 9.9, 19.6, 33.8, 47.6, 69.8, 90.9, 130.4, 250 µM are shown). Species normalized spectra and the species distribution (B) during the titration of **19** with AMPI/TBA in MeCN calculated by HyperSpec (free **19** in black; complex in red).

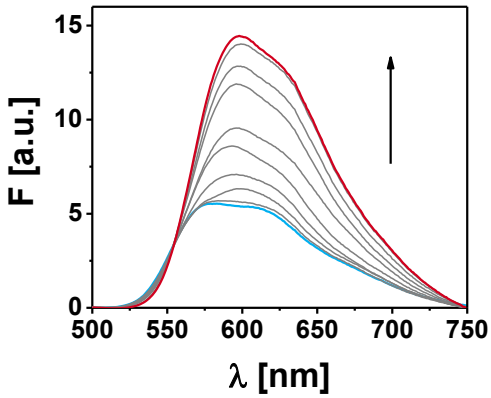

Fig. 65: Fluorescence titration spectrum of **19** (5 µM) in the absence and in the presence of 0–250 µM AMPI/TBA in MeCN (increasing concentrations in grey, start point spectrum in blue and end point spectrum in red, steps of 0, 5.0, 9.9, 19.6, 33.8, 47.6, 69.8, 90.9, 130.4, 250 µM are shown).

The MIP and NIP sensor particles were prepared again similarly to the protocol applied before but using MeCN as solvent. Subsequently, we examined the sensor particles' performance in the simple cuvette experiment in MeCN and mixtures of MeCN/MeOH and MeCN/H_2O in different ratios. In MeCN, the sensor particles fluoresce at 600 nm after excitation at the isosbestic point, and after adding increasing concentrations of AMPI/TBA, the fluorescence of the MIP particles increased much stronger compared to the NIP particles (Fig. 66). A LOD of 13 µM (3σ) was derived. In addition, a favorable DF (against AMOX/TBA) of 2.1 and an IF of 5.2 which is even higher than in case of the particle measurements in $CHCl_3$ were obtained.

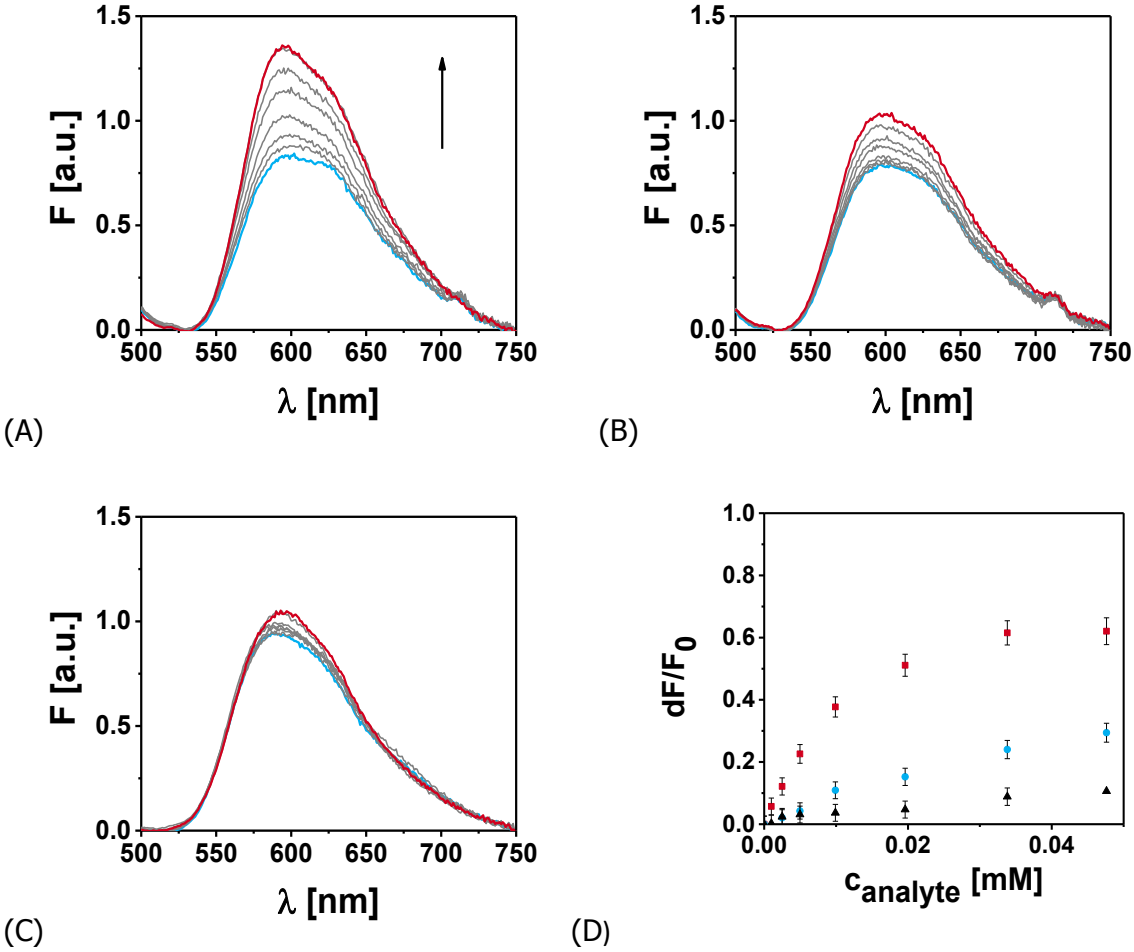

Fig. 66: Fluorescence spectra of 1 mg mL^{-1} MIP(**19**)-AMPI@SiO_2(**2**) particles in MeCN in the presence of 1 mM AMPI/TBA (A) and to the closely related compound AMOX (B) as well as of 1 mg mL^{-1} NIP(**19**)@SiO_2(**2**) particles in the presence of the template (C), (increasing concentrations in grey, start point spectrum in blue and end point spectrum in red, steps of 0, 1.0, 2.5, 5.0, 9.9, 19.6, 33.8, 47.6 µM are shown); Sensing response (D) of 1 mg mL^{-1} MIP(**19**)-AMPI@SiO_2(**2**) in MeCN toward template (red squares) and to the closely related compound AMOX (blue circle) as well as of NIP(**19**)@SiO_2(**2**) toward template (dark-blue up triangles).

From TEM measurements (Fig. 67) a thinner shell of around 5 ± 1 nm can be observed when particles are prepared in MeCN instead of $CHCl_3$. Apparently, a thinner shell results in a higher analyte-induced signal in general due to the better access of the analyte to the binding pockets.

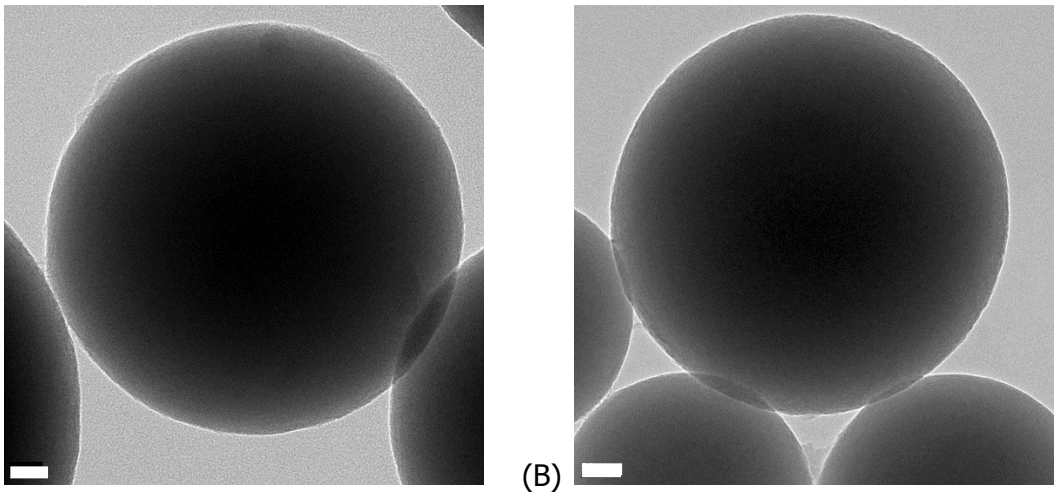

(A) Scale = 20 nm (B) Scale = 20 nm

Fig. 67: TEM images of the MIP(**19**)-AMPI@SiO_2(**2**) (A) and NIP(**19**)@SiO_2(**2**) (B) prepared with **19** in MeCN.

Unfortunately, as it can be seen in Fig. 68, less or no fluorescence response of the MIP sensor particles against AMPI/TBA could be observed when turning to mixtures of MeCN and hydrogen bonding solvents, i.e., the MeCN/MeOH and MeCN/H_2O mixtures also used above, due to the competition of methanol or water molecules with the urea and carboxylate groups as H bond partners.

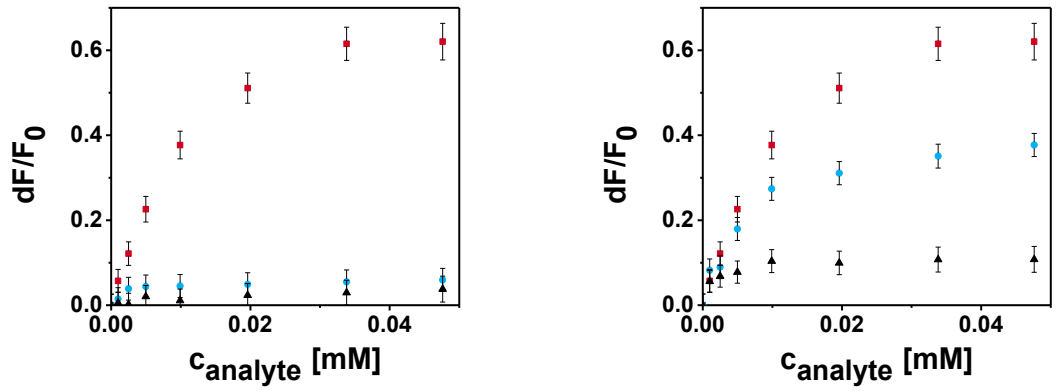

(A) (B)

Fig. 68: Sensing response of 1 mg mL^{-1} MIP(**19**)-AMPI@SiO_2(**2**) core/shell particles toward template in different mixtures of MeCN/H_2O (A) and MeCN/MeOH (B); 100/0 (red square), 99/1 (blue circle) and 90/10 (black up triangle).

5.3.6 Conclusion

MIP and NIP shell/silica core particles have been synthesized with the aim of detecting AMPI in aqueous solution and later on in food samples. The thin MIP shell on silica particles resulting from RAFT polymerization and the use of **19** as fluorescent cross-linker, MAAm as co-monomer and EGDMA as co-cross-linker in $CHCl_3$ demonstrated a high potential for the selective detection of the TBA salt of AMPI in the organic solvent with good imprinting effect. Application of the method developed in the previous chapter to transfer the analyte from an aqueous phase to an organic phase containing the MIP particles however has failed in the sense that analytically relevant sensitivities could not be reached. This can be mainly ascribed to the more hydrophilic character of AMPI compared with 2,4-D which precludes quantitative phase transfer and the induction of a correspondingly strong fluorescent signal. In conclusion, this phase transfer assay and thus the established microfluidic set-up cannot be used for such hydrophilic analytes. Even when the MIP and NIP particles were prepared in a more polar solvent such as MeCN, favorable results could only be obtained in the organic phase alone. The presence of MeOH and H_2O suppressed a response dramatically. These experiments showed the limits of the previously developed strategies.

5.4 Fluorescent Sensor Particles based on Molecularly Imprinted Polymers for the Detection of Antibiotics integrated in Fiber Optic Microarrays

5.4.1 Introduction

It was well-demonstrated that the fMIP-based sensor particles, prepared in previous sections, showed their best performance in $CHCl_3$ and similarly apolar solvents which were also used for their preparation. Apolar media are a suitable environment for the H-bonds between the analyte and the urea-based fluorescent monomer or cross-linker and reduce the swelling effect which can impede the binding strength. However, efficient binding in water-rich media is required to construct MIP-based sensors capable to analyse hydrophilic analytes in real samples, such as foodstuff or environmental samples. The previous chapters showed that integrating apolar-like MIP particles into a microfluidic platform is not sufficient to overcome the problem of measuring hydrophilic analytes, such as AMPI. In this context, the challenge for fMIP-based sensors is the detection of polar molecules under aqueous conditions while still benefitting from the strong H-bonding-induced fluorescence response and thus generating a suitable analytical signal.

Fiber optic (FO) sensors are perhaps the most exploited platform in the development of opto-chemical sensors due to their cheap preparation, ease of miniaturization and integration, minimal loss of light and the possibility to measure over long distances.[156] Fiber optic sensors have been extensively studied in the last decades, however, studies involving fiber optic sensors and MIPs as recognition elements are still rather scarce, especially in which the MIPs are integrated into the fiber.[70, 124, 154, 202, 228] The combination of fMIP microspheres with fiber optic arrays represents a potential solution to overcome the aforementioned problem. Indeed, the use of optical fiber bundles and arrays of microspheres, decorated with biorecogntion elements, has been a powerful tool for many practical fluorescent (bio)sensing applications (ref). The sensor described here combines the advantages of MIP sensor particles with optical fiber

bead-based microarrays for the detection of AMPI at low concentrations directly in milk samples.

5.4.2 Preparation and performance of the MIP particles

For the imprinting and detection of AMPI, the fluorescent cross-linker **19** based on phenoxazinone was used as well in this study due to its promising sensing ability against carboxylic acids.[229] **19** exhibits fluorescence which was shown by fluorescence titration experiments in MeCN in the chapter before. Fluorescence enhancement of **19** was observed with increasing concentration of AMPI/TBA in pure MeCN, confirming that **19** could be used as suitable fluorescent functional cross-linker to imprint the analyte in MeCN as well. The maximum excitation wavelength of **19** was found to be 485 nm and its emission wavelength 600 nm, which is perfectly suitable for optical sensing applications.

In respect of the further application of the MIP particles in combination with the fiber-optic microarray, our aim for this chapter is the preparation of MIP sensor particles which exhibit the correct size to be deposited in the microwells of the fiber-optic bundle as well as show a change in fluorescence properties in the presence of the target analyte.[40, 154, 230] This platform has been developed in collaboration with Prof. Moreno-Bondi's Group at Complutense University of Madrid who previously developed a fiber-optic array using molecularly imprinted microspheres for enrofloxacin analysis.[154]

The preparation of MIP(**19**)-AMPI@SiO_2(**2**) and NIP(**19**)@SiO_2(**2**) particles of 0.35 µm size in MeCN resulted in promising sensing response against the target analyte; however,. this particle size does not fit to the microwells created at the distal end of the FO bundle available that were 3.1 µm diameter. The synthesis strategy for the 0.35 µm particles was adapted to larger commercially available 2 µm silica particles. MIP(**19**)-AMPI@SiO_2(**3**) and NIP(**19**)@SiO_2(**3**) 2.0 µm (n=3) were thus prepared in MeCN. The MIP composition includes AMPI/TBA as template, **19** as fluorescent cross-linker, MAA as co-monomer and EGDMA as co-cross-linker. The effective coating of the MIP shell onto the silica particles was verified by SEM, TGA and ATR-FTIR. Fig. 69 shows SEM images of the blank commercially available silica particles and MIP silica particles. It is obvious, that a

nanometer-thin MIP shell is hardly discernible on the surface of the 2 µm particles because of the poor contrast emanating from the large size difference.

The FTIR measurement (Fig. 69) shows that the silica particles were successfully functionalized. After the RAFT agent coupling two new bands are formed at 2499 and 2605 cm^{-1}. After polymerization, these two bands disappeared which is in good agreement with our previously reported study. Fig. 69 collects the thermogravimetric analyses of the APTES-SiO_2, RAFT agent coated APTES-SiO_2, MIP(**19**)-2,4-D@SiO_2(**3**) and NIP(**19**)@SiO_2(**3**) particles.

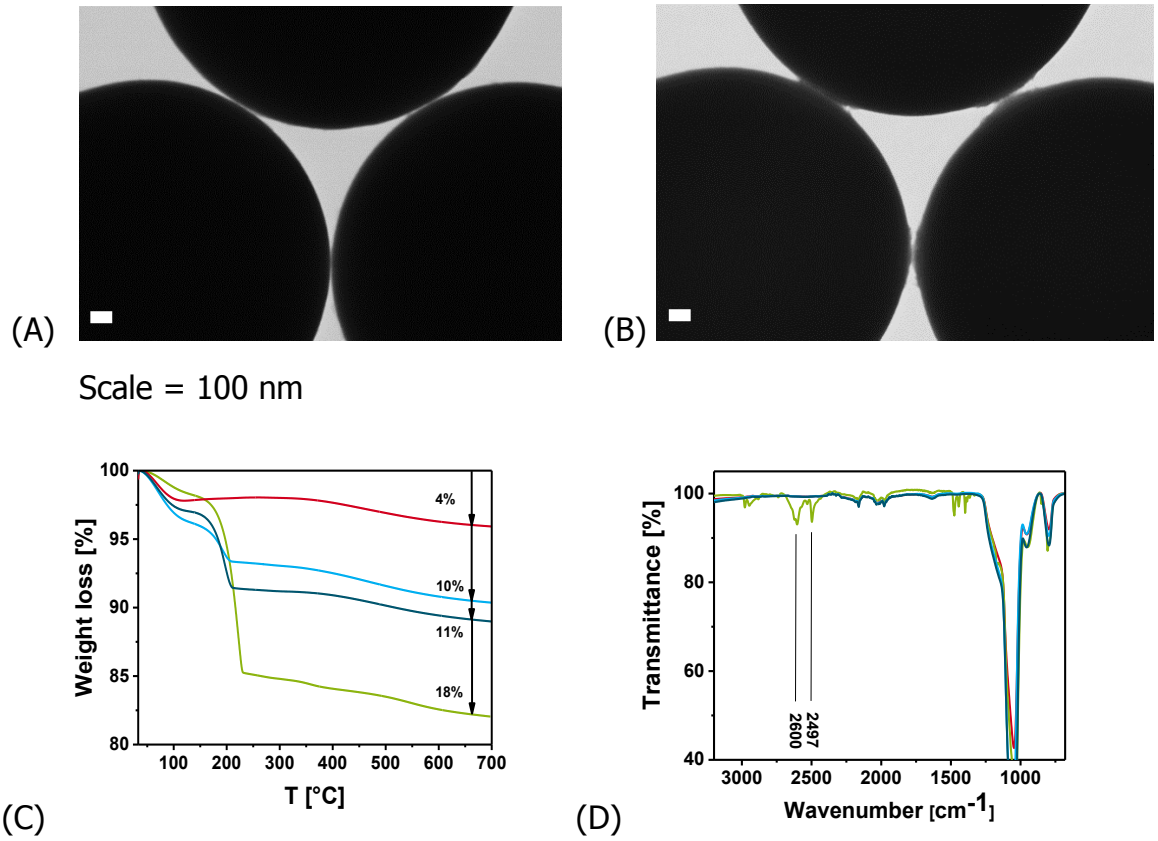

Fig. 69: SEM images (Scale = 100 nm) of blank SiO_2 particles (A) and MIP(**19**)-AMPI@SiO_2(**3**) (B). TGA curve (C) and ATR-FTIR (D) spectra of APTES-functionalized silica (red line), RAFT agent coated silica (green) and MIP(**19**)-2,4-D@SiO_2(**3**) (blue line) and NIP(**19**)@SiO_2(**3**) (dark blue line). In (D) red, blue and dark blue bands are overlapping significantly. Relevant bands of APTES-functionalized silica (green spectrum) are distinctly recognizable.

In all cases, a weight loss of ca. 2-3 % at 200 °C is obtained due to the evaporation of remaining water or organic solvent. For APTES-SiO_2 particles, higher temperatures led to a degradation of the APTES layer and a weight loss of 4 % in total, while for the MIP(**19**)-2,4-D@SiO_2(**3**) and NIP(**19**)@SiO_2(**3**) particles weight losses of ca. 10–11% were observed, respectively, corresponding to the polymer shells' degradation. Based on this data, a 30 nm polymer shell on the silica particles was estimated by calculation if a density of silica of 1.8 g cm^{-3} and a weight of 10 mg was assumed.[231]

The recognition properties and the selectivity of these MIP sensor particles were evaluated again by cuvette-based fluorescence titration experiments in pure MeCN which was also used for their synthesis. The MIP and NIP particles were titrated with AMPI/TBA. As illustrated in Fig. 70, MIP(**19**)-AMPI@SiO_2(**3**) show fluorescence enhancement upon addition of the imprinted analyte yielding a limit of detection (LOD) of 51 nM (3σ) in MeCN. For NIP(**19**)@SiO_2(3), the fluorescence enhancement upon analyte addition was significant lower, resulting in an IF of 2.4. In order to determine the selectivity of the MIPs, the particles were also titrated with the structurally similar compound AMOX/TBA. The measurement show that the MIP fluorescence enhancement is 1.6-times less than with AMPI, which demonstrated an acceptable selectivity of the sensor particles.

However, if we recall the results for MIP(**19**)-AMPI@SiO_2(**2**) and NIP(**19**)@SiO_2(**2**) (IF=5.8, DF=2.1), the smaller MIP(**19**)-AMPI@SiO_2(**2**) responded stronger to AMPI/TBA than the larger MIP(**19**)-AMPI@SiO_2(**3**) and a better imprinting effect was achieved. Due to the more planer surface of the larger silica particles, the polymer coating compared with 0.35 µm particles is challenging. It seem to be a thicker shell, however, the non-specific interaction in case of NIP particles could be attributed to larger cavities due to the larger porosity of the polymer network.

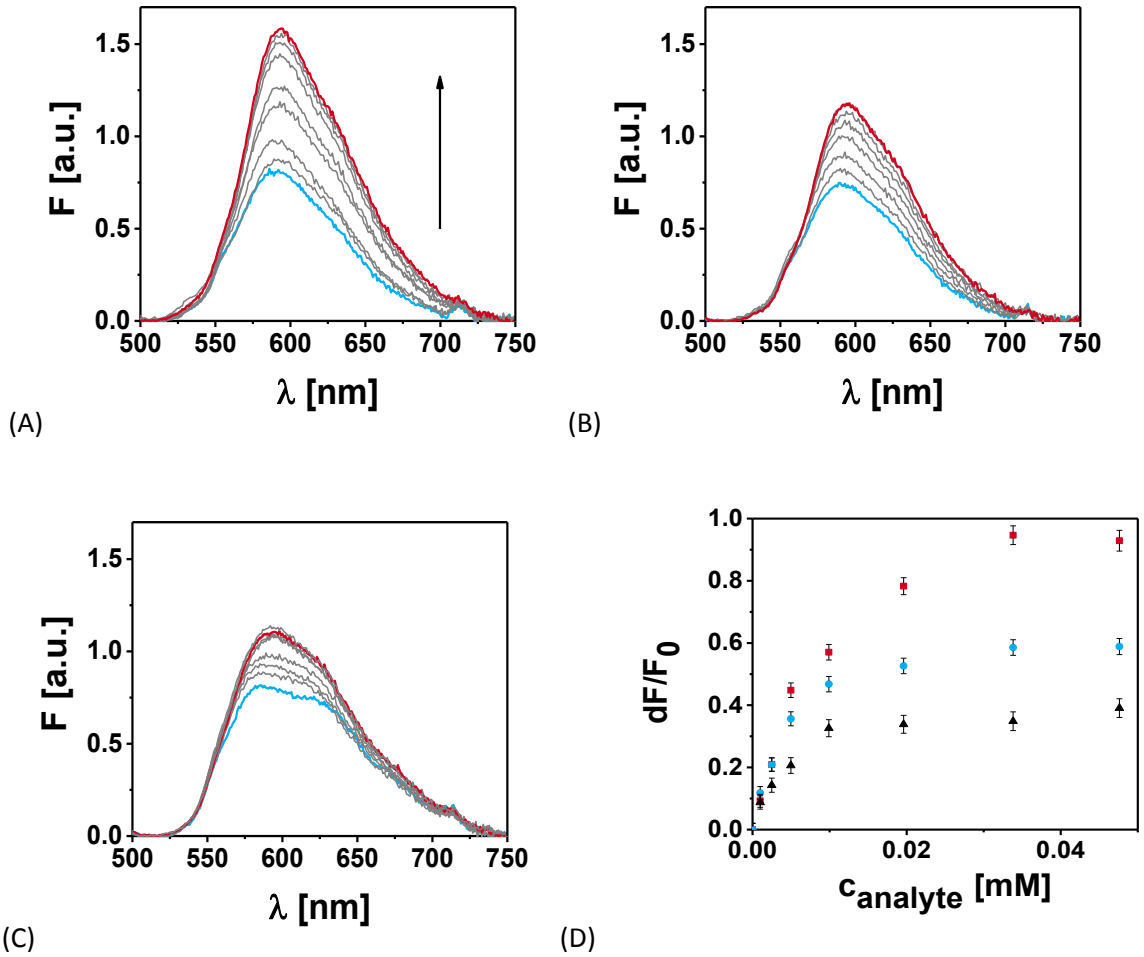

Fig. 70: Fluorescence spectra of 1 mg mL^{-1} MIP(**19**)-AMPI@SiO_2(**3**) particles in MeCN in the presence of 1 mM AMPI/TBA (A) and to the closely related compound AMOX (B) as well as of 1 mg mL^{-1} NIP(**19**)@SiO_2(**3**) particles in the presence of the template (C), (increasing concentrations in grey, start point spectrum in blue and end point spectrum in red, steps of 0, 1.0, 2.5, 5.0, 9.9, 19.6, 33.8, 47.6 µM are shown); Sensing response (D) of 1 mg mL^{-1} MIP(**19**)-AMPI@SiO_2(**3**) in MeCN toward template (red squares) and to the closely related compound AMOX (blue circle) as well as of NIP(**19**)@SiO_2(**3**) toward template (dark-blue up triangles).

The binding kinetics of AMPI/TBA to the sensor particles is depicted in Fig. 71. The signal response increased in the presence of 20 mM AMPI/TBA and leveled off after ca. 5 s. No signal variation was observed in the absence of analyte. The outstanding sensing kinetic is the result of the use MeCN as solvent and the more porous polymer network which greatly reduces the diffusion time of the analyte to the binding cavities.

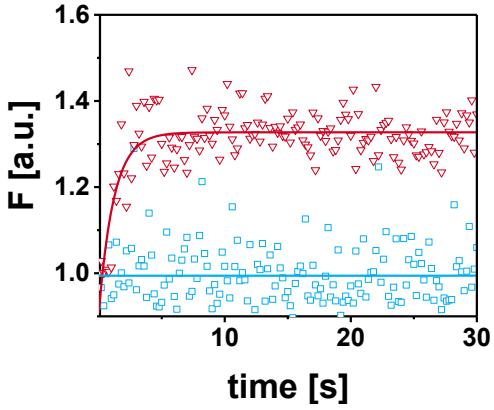

Fig. 71: Time course of the rebinding kinetics of MIP(**19**)-AMPI@SiO_2(**3**) with none (blue square) and 20 mM AMPI/TBA (red down triangle) in MeCN.

5.4.3 Fiber-optic microarray based on fluorescent MIP microparticles

A MIP-based sensing platform that combines the MIP(**19**)-AMPI@SiO_2(**3**) microparticles with bead-based microarrays was then fabricated, aspiring to improve the performance of the larger MIP-coated beads. This technology was available and applied at Prof. Moreno-Bondi Laboratory in Complutense University of Madrid as part of a research collaboration.

The 3 cm long optical fiber bundles, containing approximately 50 000 individual optical fibers (with diameters of 3.1 μm), are chemically etched with an acidic solution to create a two-dimensional array of microarrays. Then, the fluorescent MIP(**19**)-AMPI@SiO_2(**3**) are placed (1 μL of 0.25 mg mL^{-1} MIP particles solution) onto the etched distal end of the fiber to form a randomly and highly dense ordered array, addressable thanks to the intrinsic fluorescent properties of the particles. The fiber was kept in the dark until complete evaporation of the solvent and adequate incorporation of the particles into the wells. The process was repeated 10 times to increase loading efficiency and the excess of microspheres, those not loaded into the microwells, were removed using a cotton swab.[154]

Image capturing was performed in an epi-fluorescence microscope (Olympus BX51) by vertically placing the fiber-optic microarray in a home-built adaptor. The microscope was equipped with a 16-bit charge-coupled device (CCD) camera (Infinity 3, Lumenera Corporation) and a 100 W halogen lamp (operating

at 6 V to acquire bright field images and 12 V for fluorescence images). The fibers were imaged with 20x magnification the fluorescence filter set for monitoring fMIP microparticles includes an excitation interference filter 470/10, a dichroic mirror 490DCXR, and a cut-off emission filter of 500LP. Acquisition time was set at 3 s. Images of representative portions of the fiber bundles were analyzed using a home-made algorithm designed in ImageJ (v.1.44p, Wayne Rasband, National Institutes of Health, USA). The tri-mean criterion was employed instead of conventional mean statistics to avoid outliers. The mathematical model is based on the weighted average of the distribution median distributing the population into quartiles: Q1, Q2, and Q3 are the 25%, 50% and 75% points in the distribution, respectively.[154]

Before incubation with the analyte, the distal end of the fiber that holds the microspheres was washed several times with 100% MeCN. After solvent evaporation, background imaging acquisition was performed to confirm that the signal from the fiber-optic bundle was negligible.

For calibration purposes, the MIP(**19**)-AMPI@SiO_2(**3**) and the NIP(**19**)@SiO_2(**3**) were incubated in pure MeCN containing increasing concentrations of AMPI/TBA salt (0-25 nM). Fig. 72 shows that the recognition of the MIP microparticles is much larger than the corresponding NIP particles which is in good agreement with the previous cuvette experiments. The detection limit, estimated according to the IUPAC criteria as the AMPI concentration producing an analytical signal that is three times the standard deviation of the blank signal, was 0.72 nM (10 times for the quantification limit, LOQ=2.39 nM) which is much lower than in the cuvette titration experiment. Calibration curves were also obtained after incubating newly assembled MIP/NIP microarray in 1.5 mL of native AMPI standards without previous deprotonation, with concentrations ranging from 0 to 7.5 nM prepared in aqueous-rich media (25:75 (v/v) MeCN:HEPES (25 mM, pH 7.5)). As shown in Fig. 72, also under these conditions, the MIP sensor particles show the best response in comparison to the NIP particles resulting in a LOD and LOQ of 0.40 nM and 3.24 nM, respectively. The solvent evaporation avoids the disruption of the interaction between **19** and the analyte and enables a more

stable embedding of the analyte in the cavity. These results are promising for applying the developed platform for the analysis ampicillin residues in foodstuff, such as milk samples.

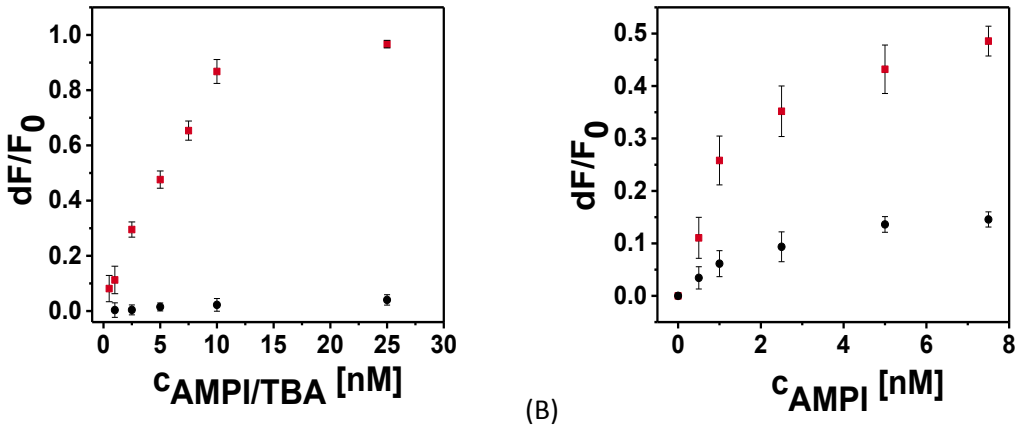

Fig. 72: Sensing response when MIP(**19**)-AMPI@SiO_2(**3**) (red square) and NIP(**19**)@SiO_2(**3**) (black circle) were deposited onto fiber microwell arrays and incubated with AMPI/TBA in MeCN (A) and AMPI in 25:75 MeCN:HEPES (25 mM pH 7.5) (B).

Furthermore, under the same conditions as described before, a cross-reactivity study was performed to investigate the selectivity of the sensor particles. Therefore, native AMOX and the fluoroquinolones ENOX and ENRO standards were incubated using concentrations ranging from 0 to 7.5 nM. Fig. 73 demonstrates the excellent selectivity of MIP(**19**)-AMPI@SiO_2(**3**) for the template molecule (50%, 7.5 nM) and AMOX (20%, 7.5 nM), structurally similar to AMPI. Responses of the other antimicrobial tested were negligible (<10%, 7.5 nM).

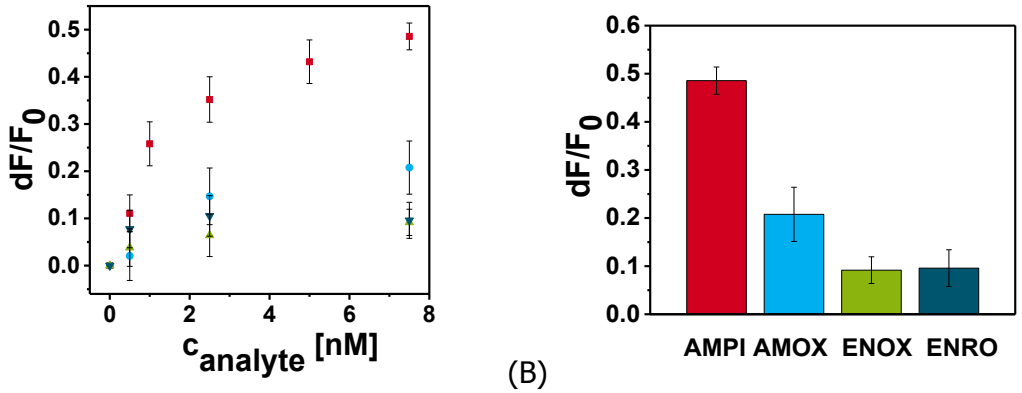

(A) (B)

Fig. 73: Cross-reactivity (A and B) with different antibiotics (AMPI (red square), AMOX (blue circle), ENOX (green up triangle) and ENRO (dark blue down triangle) in 25:75 MECN:HEPES (25 mM pH 7.5).

5.4.4 Conclusion

In this Chapter, we described a fiber-optic microarray platform using MIP particles for detecting AMPI in milk samples. For this study, larger MIP and NIP microparticles had to be synthesized fitting into the microwells of the optic fiber bundle. For that reason, the synthesis protocol of the 0.35 µm MIP and NIP particles was adapted to create a thin MIP layer onto 2.0 µm silica particles. These particles showed not only an outstanding fast response for AMPI and good selectivity in pure MeCN in the cuvette experiment but also using the optical fiber assay after optimization of image processing and data analysis.

This combination of a fiber-optic microarray and fluorescent MIP sensor particles as well as epi-fluorescence imaging detection, improved not only the imprinting effect but also the LOD compared to the cuvette titration experiment. These results are promising for applying the developed platform for the analysis of ampicillin residues in foodstuff, such as milk samples. Due to the flexible assay design, this application can be also transfer to further MIP particles, containing other fluorescent dyes, for the detection of an analyte of interest.

5.5. Detection of the herbicide 2,4-D through excited-state double proton transfer using thin MIP layer

5.5.1 Introduction

We have already discussed that still today, the on-site detection of environmental pollutants like herbicides remains a challenge. It was further elaborated that chemical sensors are a promising approach, especially when miniaturized. In addition, we have demonstrated that the robustness of MIPs combined with their ability to effectively recognize dedicated target analytes makes them very attractive in the context of chemical sensors, likewise, only few examples have shown promise for real sensing applications.[21]

The above works in this thesis were focused on the preparation and use of MIP-based sensor systems for the specific detection of carboxylate anions using designed functional fluorescent urea monomers based on phenoxazinone- and nitrobenzoxadiazole dye scaffolds.[17, 229] However, the synthesis of such polymerizable indicator molecules can be cumbersome and, quite frequently, the resulting compounds show rather limited solubility behaviour, also in many organic solvents. We were thus interested in elucidating the possibility of sterically imprinting a fluorescent probe–analyte complex into a polymer matrix without forming a single covalent bond between the polymer backbone and the indicator molecules. Besides the advantage of avoiding complicated synthesis, the combination of a rather simple dye with a single anion interaction site with a tailored pocket was envisioned to couple simplicity with synergism. Herein, we present for the first time a novel fluorescent probe, carrying a 2-aminopyridine unit as spectroscopically active binding site, as sterically imprinted signal transducer. Moreover, the dye was chosen in such a way that directional hydrogen bond-mediated binding of organic acids, respectively herbicides, is possible without previous deprotonation. Again, after incorporation into the polymer, the extent to which the analyte interacts with the chemical recognition phase determines the magnitude of the signal.

Beside this study, there are only few fluorophores in literature which show ESDPT. Herein, our fluorophore should fulfil the requirement. The 2-aminopyridine moiety was integrated into a chromophoric system that absorbs in the UV/visible range compatible with laser sources widely used in analytical instruments and that produces an enhanced fluorescence signal upon interaction with the guest molecule 2,4-D.

5.5.2 Binding studies with 2,4-D in different solvents

Fig 74. shows the absorption and emission spectra of **22** in various solvent as well as in presence of 2,4-D. The absorption spectra of **22** are similar in shape and position in solvents with different polarity and proticity. Due to the functionalization of 2-aminopyridine on the C3 position (see Fig. 75 below) and the additional conjugation, the absorption is more shifted to the visible range, which makes this dye more suitable for real applications.

Upon binding to the model analyte 2,4-D at lower concentrations, these maxima were slightly red-shifted. With further increasing the concentration of 2,4-D, a second absorption band at 400 nm was formed in all cases which is characteristic of the formation of intermolecular H-bonds between the aminopyridine moiety of the dye and the carboxyl group of the 2,4-D.[146-147] Isosbestic points were observed at 363, 365 and 366 nm in toluene, chloroform and MeCN. Based on these results the binding constants were evaluated by nonlinear regression fitting (Fig 74, Tab. 13). The affinity of 2,4-D to **22** is decreased in more polar solvents, which is again in good agreement with previous studies.[147] The small binding constant in MeCN suggest that the respective polar solvation of **22** and 2,4-D by MeCN disrupts the formation of intermolecular double hydrogen bonds between the components.

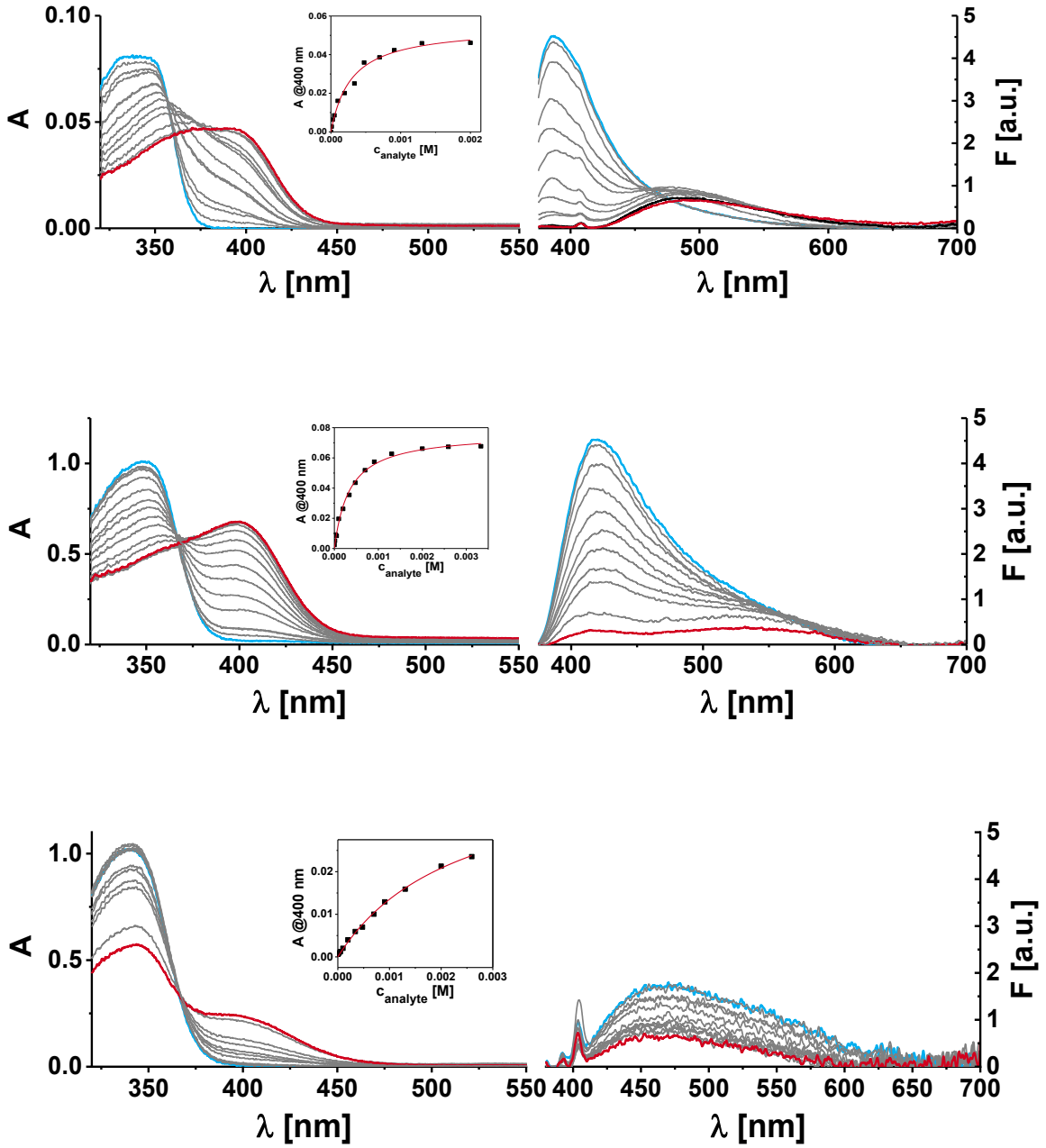

Fig. 74: Absorption (left) and fluorescence (right) spectra of **22** (2 µM) in toluene (top), $CHCl_3$ (middle) and MeCN (bottom) in the absence and presence of 0-2.5 mM 2,4-D (increasing concentrations in grey, start point spectrum in blue and end point spectrum in red, titration concentrations are shown in plot).

The fluorescence behavior of **22** depends on the solvent polarity (Fig. 74). The wavelengths of fluorescence maxima increase with the polarity of the solvent (Tab. 13).

Tab.13: Spectroscopic properties and binding constants of **22** in selected solvents.

solvents	λ_{abs} /nm	λ_{em} /nm	*log*K
Toluene	342	387	3.53±0.04
$CHCl_3$	348	418	3.46±0.06
MeCN	342	466	2.63±0.08

After complexation with the analyte *via* hydrogen bonds, the bands at lower wavelengths in toluene and $CHCl_3$ decrease strongly while new weaker fluorescence bands at 500 and 544 nm are formed indicating the ESDPT reaction.[146-147] However, only an isoemissive region can be observed at 470 nm in toluene. The corresponding fluorescence excitation spectra suggest that the two emission bands emerge from unbound **22** and the **22**/2,4-D complex. However, based on our observation and reported studies, the second band belongs to the double proton-transferred **22** imino tautomer, and not to a single proton-transferred **22** cation. Fig. 75 summarizes the ESDPT of the **22**/2,4-D system in $CHCl_3$ again for a better overview.[147] Before excitation, **22** and **22**/2,4-D are in an equilibrium. However, as soon as the **22**/2,4-D complex is excited with the wavelength at the isosbestic point, the proton moves from the hydroxyl group of 2,4-D to the ring nitrogen of **22**, forming an ion-pair intermediate with a protonated **22** cation and a 2,4-D anion, showing small fluorescence shift to 422 nm, which commonly decays on the order of a few ps. At the same time, the imino tautomer is formed while the second proton is transferred from the deprotonated 2,4-D to **22**. ESDPT here thus seems to proceed stepwise. The excited imino tautomer then relaxes under emission of green fluorescence.[146]

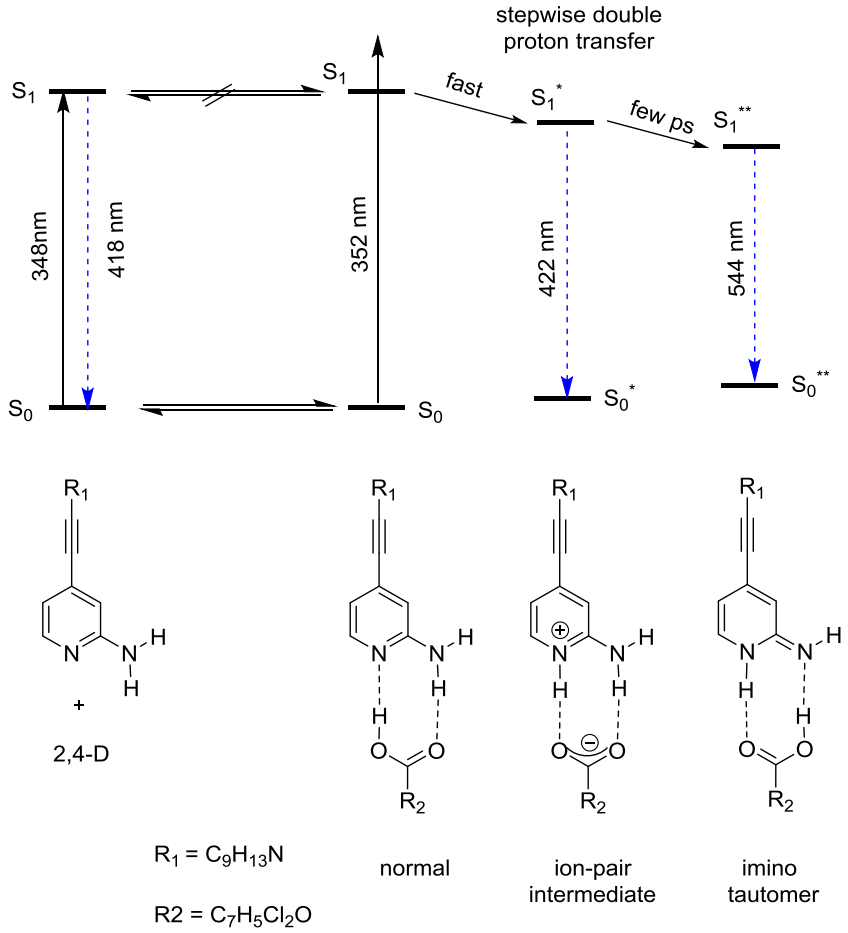

Fig. 75: Schematic energy diagram illustrates the dynamics of the excited-state double proton-transfer reaction of **22** and **22**/2,4-D complex in $CHCl_3$.[146]

In contrast, in the more polar solvent MeCN, this emission intensity is strongly suppressed. After increasing the concentration of the analyte, the fluorescence is slightly enhanced but at higher concentrations quenched again. The ESDPT imino tautomer band is presumably absent.

5.5.3 Crystal structure analysis

We successfully synthesized **22** in a moderate yield and obtained good-quality single crystals of **22** as well as the hydrogen-bonded **22**/2,4-D complex. The crystallographic data of these two crystals are summarized in Tab. S2 This X-ray analysis of **22** shows that the dye crystallized in triclinic space group P-1 with four molecules in the unit cell. In the asymmetric cell, two molecules of **22** and two molecules of solvent were obtained. The tree-dimensional structure of **22** is illustrated in Fig. 76 including the atomic labelling scheme. The two aromatic rings

are coplanar. In contrast, Fig. 77 shows the tree-dimensional structure of the hydrogen-bonded complex **22**/2,4-D. This crystal structure is monoclinic, in Pa 21/c space group. Again, there are four molecules in the unit cell and two molecules in the asymmetric unit. In this case, there are no disordered solvent molecules, consequently the R factor is much better than before in **22**. The structure of **22** is still planar in the complex, however, the analyte binds not in the same plane with **22** but with at a 20° angle to the plane due to the additional week interaction of halogen atoms of 2,4-D with the π-system of **22**.

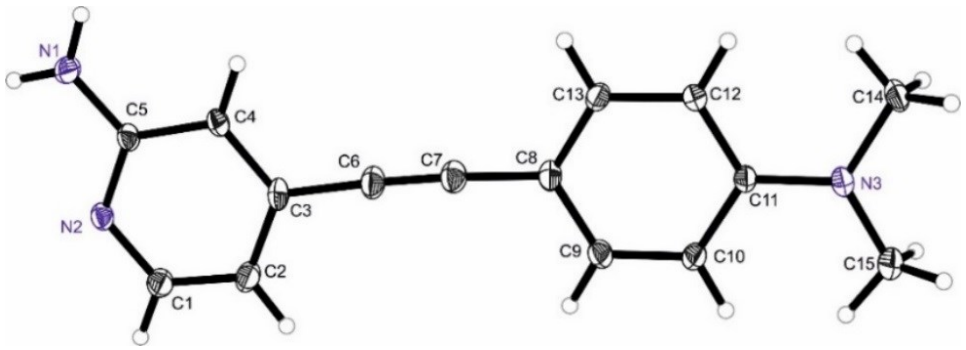

Fig. 76: Crystal structure of **22** as derived from X-ray analysis.

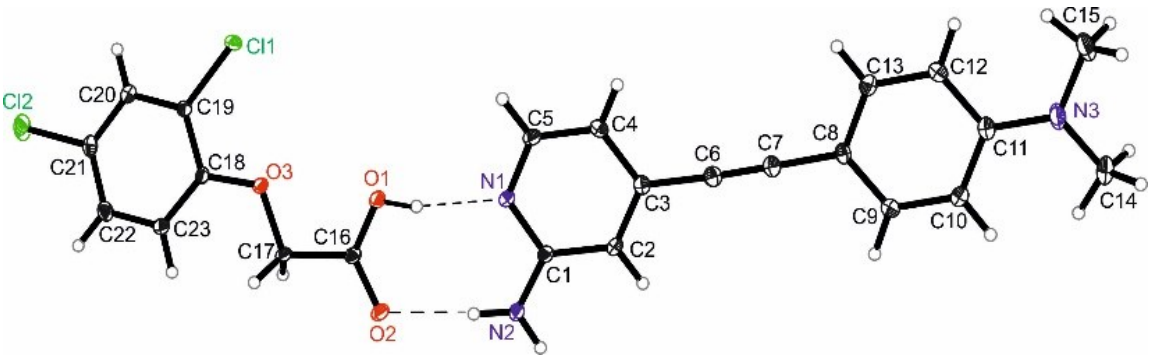

Fig. 77: Crystal structure of hydrogen bonded **22**/2,4-D as derived from X-ray analysis.

The formation of two intermolecular hydrogen bonds between the carboxyl group of 2,4-D and the 2-aminopyridine moiety determine the bond lengths which are summarized in Tab. 14. The O(1)-H(1)···N(1) hydrogen bond is formed by the OH group of 2,4-D and the pyridine hydrogen atom (2,69 Å). N(2)-H(2)···O shows a length of 2.821 Å between the amino NH group and the carbonyl oxygen of 2,4-D. As soon as the analyte binds to the dye, the length of the C(1)-N(2) bond in

22/2,4-D is reduced to 1.328 Å compared to **22** (C(4)-N(1)) with 1.348 Å while the length of the N(1)-C(1) bond in **22**/2,4-D is lengthened to 1.357 Å. The angle of N-C-N is increased from 116.5° to 118.24° after hydrogen bond formation which is as well in good agreement with comparable studies.[232]

Tab. 14: Hydrogen-Bond Geometries of Donor (D) and Acceptor (A) for **22**/2,4-D complex.

D-H····A	***d*(D-H)**	***d*(H···A)**	***d*(D···A)**	**< (DHA)**
O(1)-H(1)···N(1)	0.840 Å	1.871 Å	2.694 Å	165.91°
N(2)-H(2)···O(2)	0.880 Å	1.943 Å	2.821 Å	175.65°

The interatomic distances of 2,4-D before and after the formation of the two obviously moderate hydrogen bonds with **22** are changed as well (Tab. 15).[233] Smith et al. already reported the structure of 2,4-D and the respective bond lengths and angles.[234] Due to the double hydrogen bonds the covalent C(16)=O(2) double bond and the C(16)-O(1) are lengthened. Thus, by investigating the bond lengths, hydrogen bond formation between both components can be shown.

Tab. 15: Hydrogen-Bond Geometries of Donor (D) and Acceptor (A) for **22**/2,4-D complex.

compound	***d*(C=O)**	***d*(C-O)**
2,4-D	1.217 Å	1.304 Å
22/2,4-D complex	1.243 Å	1.259 Å

5.5.4 Preparation and performance of MIP particles

Before **22** was used for the synthesis of MIP(**22**)-2,4-D@SiO_2 and NIP(**22**)@SiO_2 sensor particles for the detection of 2,4-D, pre-polymerization studies were performed in $CHCl_3$. As shown above, 2,4-D forms a stable H-bonded complex with **22** in rather apolar solvents. Here, we investigated the influence of different

co-monomers and EGDMA as cross-linker in the pre-polymerization mixture (Fig. 78). The addition of only different co-monomers and cross-linkers to **22** under pre-polymerization conditions showed no or only minor changes of the absorption maximum of **22**. After addition of 2,4-D a stable H-bonded complex with **22** under these conditions is formed indicated by a red shift in the absorption spectra. The addition of both, a co-monomer and cross-linker EGDMA has different influences. The largest red shift is only observed in case of BMA and EGDMA. These conditions were thus used for the sensor particle preparation. Indeed, the band is formed in case of MAAm as well, but with a weaker red-shift of the absorption band and with still a small shoulder 360 nm. Compared to that, the use of 4-Vy and HEMA leads to almost no red-shift and H bonded complex.

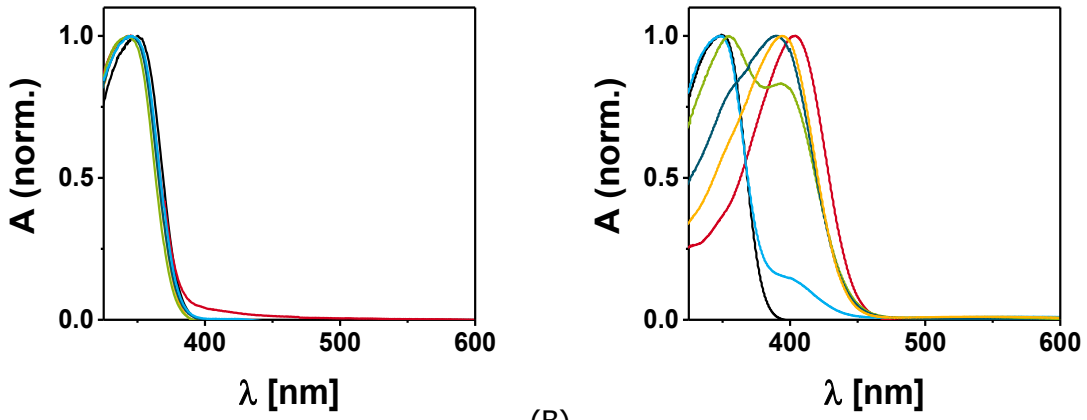

(A) (B)

Fig. 78: Normalized absorption spectra of **22** in $CHCl_3$ (black) before (A) and after addition (B) of 2,4-D (red) in the presence of various co-monomers at pre-polymerization conditions, HEMA/EGDMA (green), 4-Vy/EGDMA (blue), BMA/EGDMA (yellow) and MAAm/EGDMA (dark blue).

The preparation protocol for the synthesis of MIP(**22**)-2,4-D@SiO_2 and NIP(**22**)@SiO_2 sensor particles followed our previous works using the dye and template, co-monomers and cross-linkers for their incorporation into the polymer network. SiO_2 particles (0.35 µm) were used as support material. Their surfaces were functionalized with APTES and subsequently, a RAFT agent was again covalently coupled to the silica surface through an amide bond. The RAFT agent functionalized particles were mixed with the pre-polymerization mixture in $CHCl_3$

to create a 4 ± 1 nm thin, homogeneous MIP or NIP shell onto the core's surface (Fig. 79).

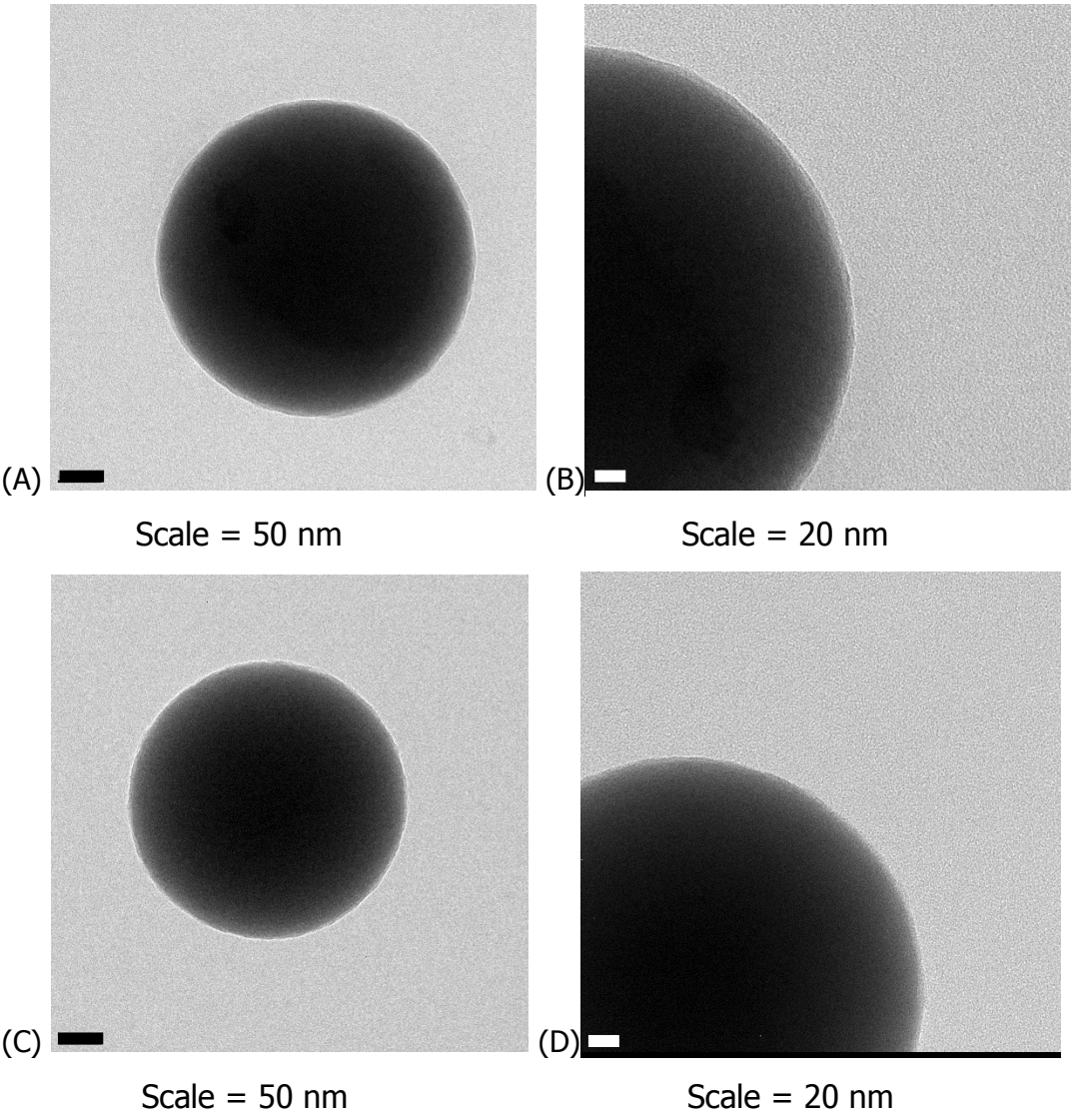

Fig. 79: TEM images of the MIP(**22**)-AMPI@SiO_2 (A, B) and NIP(**22**)@SiO_2 (C, D) prepared with **22** in $CHCl_3$.

In contrast to the previous studies, **22** or better the H-bonded complex was only sterically imprinted which means that the dye is not polymerized into the polymer matrix but only entrapped into it. To investigate the sensing performance of the MIP and NIP particles, fluorometric response tests were carried out following the same procedure like in the previous chapters and using $CHCl_3$ as solvent.

In the absence and after addition of the analyte, fluorescence emission of the MIPs exhibited maxima at 503 nm upon excitation at 365 nm (Fig. 80).

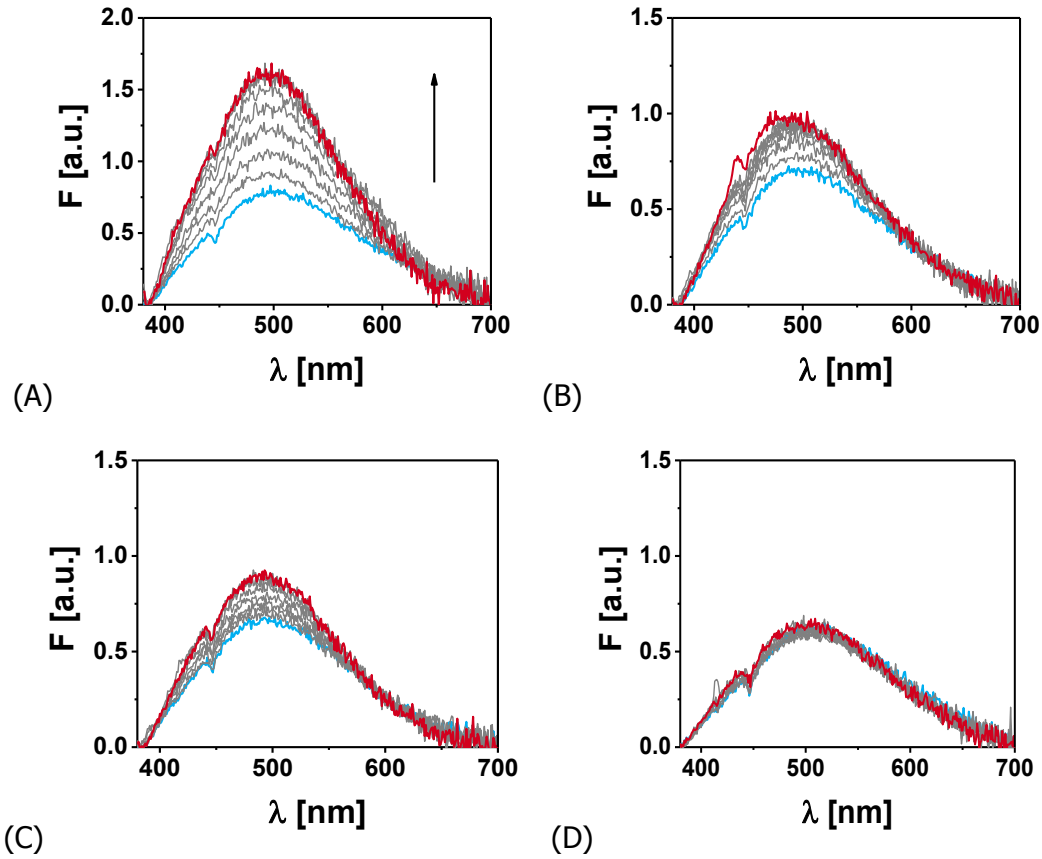

Fig. 80: Fluorescence spectra of 1 mg mL^{-1} MIP(**22**)-2,4-D@SiO_2 particles in $CHCl_3$ in the presence of 1 mM 2,4-D (A) and the closely related compound 2,4-DB (B) and 2,4-DP (C) as well as of 1 mg mL^{-1} NIP(**22**)@SiO_2 particles in the presence of the template (D), (increasing concentrations in grey, start point spectrum in blue and end point spectrum in red, steps of 0, 10, 25, 50, 100, 196, 338, 476, 698 µM are shown).

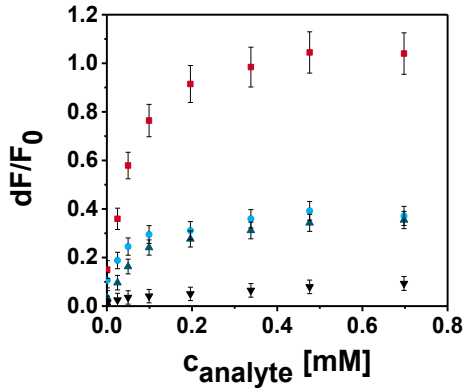

Fig. 81: Sensing response of 1 mg mL^{-1} MIP(**22**)-2,4-D@SiO_2 core/shell particles in $CHCl_3$ toward 10 mM template analyte 2,4-D (red square) and the closely related compounds 2,4-DB (blue circle) and 2,4-DP (dark blue up triangle) as well as of NIP(**22**)@SiO_2 toward template (black down triangles).

It is obviously that only one band at 503 nm is formed. It seems that both bands observed in titration study overlap in this sensing study due to the changing environment.

The polymer leads to a less polar environment which leads to an increase of the formation of the increasing second band at higher wavelength. Fig. 80 and Fig. 81 reveal that the MIPs showed the highest sensing response after titration with the corresponding analyte solution. The weaker fluorescence enhancement that was observed in the presence of the closely related compounds 2,4-DB and 2,4-DP suggests that these analytes do not fit into the cavity leading to weaker interactions with **22**. DFs ($dF_{2,4\text{-}D}/dF_{analogues}$) of 2.8 and 2.9 against 2,4-DB and 2,4-DP were calculated, respectively. The imprinting factor of 10.3 was determined as well again as the quotient of the fluorescence response (dF/dF_0) of the MIP and NIP. This value is obviously much higher compared to the studies using polymerizable fluorescent monomers or cross-linkers before. Compared to the previous chapters, there is no covalent incorporation of the dye into the polymer network due to the missing polymerizable methacrylate groups. In order to investigate the efficiency of the MIP particles prepared with such fluorescent dye, we introduced an additional washing step by Soxhlet extraction for 4 h in DCM and investigated the binding behavior again. As it can be observed in Fig. 82, the fluorescence intensity of the MIP particles in $CHCl_3$ without the analyte did not change after this washing step, which indicates that **22** was stably imprinted into the polymer network and is not washed out. However, upon titration with the analyte 2,4-D under the same conditions as before, the fluorescence did not reach the same endpoint, but the maximal enhancement was less. We tentatively assume that the binding environment for the analyte has changed due to the rugged treatment of the MIP shell during the washing procedure. Apparently, the number of intact cavities is lower so that less 2,4-D can bind resulting in a worse IF of 3.2. In order to determine the selectivity of the MIP particles, they were also titrated with 2,4-DB and 2,4-D. Fluorescence measurements showed that the MIP sensor particles are still selective against these structurally similar compounds, yet DFs were lower with 1.5 and 1.7.

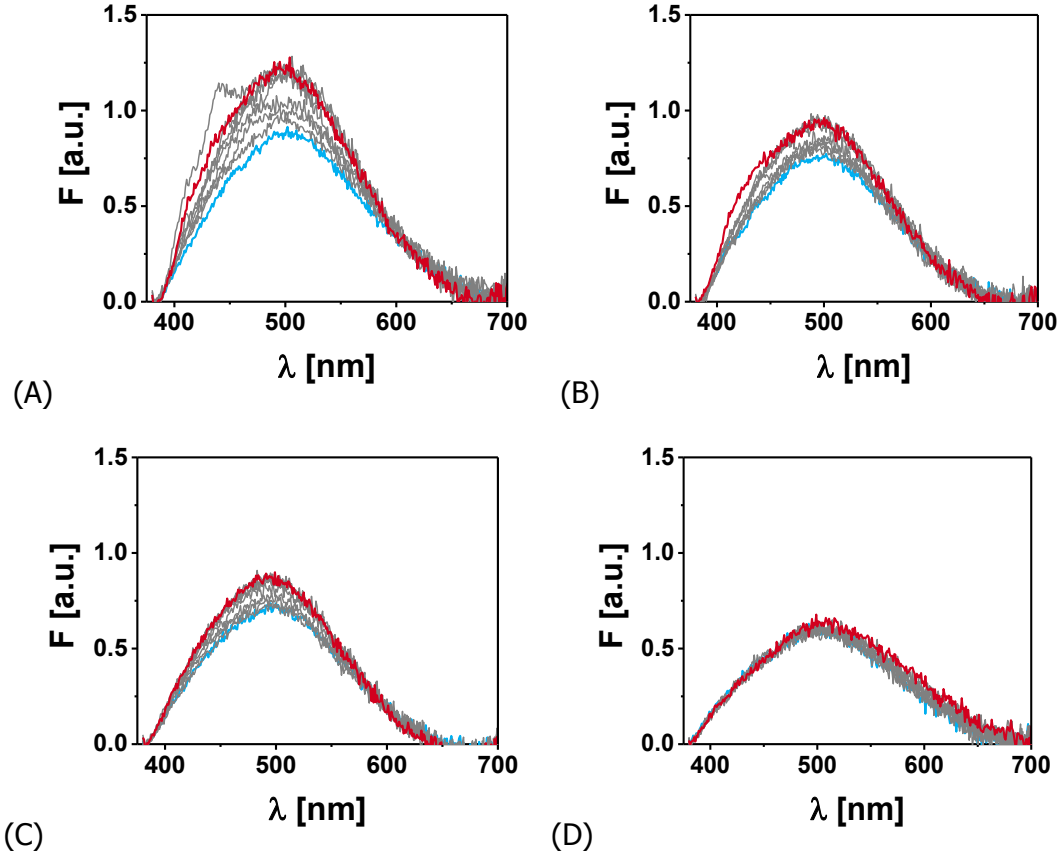

Fig. 82: Fluorescence spectra of 1 mg mL^{-1} MIP(**22**)-2,4-D@SiO_2 particles in $CHCl_3$ after 4 h Soxhlet washing in the presence of 1 mM 2,4-D (A) and the closely related compound 2,4-DB (B) and 2,4-DP (C) as well as of 1 mg mL^{-1} NIP(**22**)@SiO_2 particles in the presence of the template (D), (increasing concentrations in grey, start point spectrum in blue and end point spectrum in red, steps of 0, 10, 25, 50, 100, 196, 338, 476, 698 µM shown).

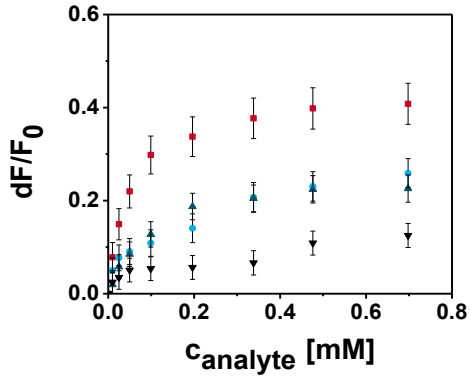

Fig. 83: Sensing response of 1 mg mL^{-1} MIP(**22**)-2,4-D@SiO_2 core/shell particles in $CHCl_3$ after 4 h Soxhlet washing toward 10 mM template analyte 2,4-D (red square) and the closely related compounds 2,4-DB (blue circle) and 2,4-DP (dark blue up triangle) as well as of NIP(**22**)@SiO_2 toward template (black down triangles).

5.5.5 Conclusion

The present work reports the design and synthesis of a new 2-aminopyridine-based fluorescent probe **22** that complexes the model analyte 2,4-D without previous deprotonation showing intermolecular ESDPT mechanism. The first part has proven the stepwise ESDPT in non-polar solvents with the ion-pair intermediate being identified using absorption and fluorescence titration experiments. Crystal structures of **22** and the hydrogen bonded complex are presented as well and clarified **22** as a favorable complementary module to carboxylic acids and as co-crystal agent forming O-H···N and N-H···O hydrogen bonds. A thin signaling MIP layer was coated on silica particles which could bind specifically and selectively 2,4-D in $CHCl_3$, indicating the good sensitivity of our sensor. This binding was monitored with strong fluorescence enhancement of the MIP. The use of an additional washing step did not remove the dye from the cavity, however, the binding environment for the analyte was changed and reduced the efficiency and selectivity of the sensor particles. Our results are very promising for further applications as such sterically imprinted dye-analyte complexes might show even better imprinting effects than covalent imprinted complexes and the wealth of fluorescent probes that can be used is potentially much higher.

6 General Conclusion and Outlook

In conclusion, several innovative optical sensing methods based on MIPs as recognition elements in combination with fluorescence for the detection of analytes, have been shown. To demonstrate the importance of the project by the relevance of the model analytes chosen, we were primarily targeting specific small organic molecule contaminants which play an important role in food safety and environmental monitoring such as antibiotics and pesticides. The development of new optical sensors, their miniaturization by the use of microfluidics, and the fabrication of sensor arrays have been demonstrated as well.

Fluorescent monomers and cross-linkers based on nitrobenzoxadiazole- and phenoxazinone-ureas as well as a 2-aminopyridine-based dye are the basis of this project for the preparation of MIP shell/silica core particles which show high affinity for the model acidic target compounds used for imprinting. Such chromophores satisfy the spectroscopic criteria of detection in the green-to-red visible range with changes in fluorescence. Optical spectroscopy was used for showing the binding behavior and binding constant in dilute and under pre-polymerization conditions. The latter directly indicated the analytical response to be expected from the materials. These dyes show different responses e.g. fluorescence enhancement and spectral shifts or ESDPT. These fluorescent monomers or cross-linkers were incorporated into thin MIP layers grafted from the surface of silica microparticles with various sizes following a RAFT polymerization protocol based on further studies in our group. The thin fluorescent MIP shell lights up upon binding of the analyte of interest in an organic solvent. The prepared thin MIP sensor particles were investigated for their optical response, sensitivity and selectivity. As well NIPs, which are prepared from the same polymerization mixture in the absence of the template, were used for control experiments.

The first chapter investigated the binding between the deprotonated target molecule Z-D-Phe to the urea-containing functional monomer **14** in an organic solvent and during MIP shell synthesis in the presence of different counter-ions ranging from TMA^+ to TOA^+ with different chain length. The use of the different

counter-ions influenced the selectivity of the MIPs due to the increasing deprotonation tendencies, their different influences on the cavity sizes and thus the recognition behavior.

The next chapter describes the synthesis, characterization and sensing properties of fluorescent monomer **16** and cross-linkers **19** in the presence of the TBA salt of 2,4-D. Due to the modification and introduction of a second polymerizable group in **19**, the sensing response could be enhanced dramatically which was shown by spectroscopic titration experiments. Obviously, direct measurements in water samples were not possible. Thus, the MIP sensor particles were combined with a miniaturized modular microfluidic platform based on a biphasic extraction assay which allowed the sensitive and selective detection of 2,4-D from untreated water samples from all over the world between 20 nM and 5 µM. Such a microfluidic system is a very promising sensing system for other analytes of biological and environmental interest for the future.

However, the subsequent chapter showed that this method is not applicable for hydrophilic analytes like AMPI due to their limited transfer ability to the organic, sensor particle containing phase. Thus, another approach based on a fiber-optic microarray was demonstrated in this thesis to solve this problem and offer a new way for its direct detection in food samples. 2 µm MIP shell/ silica core sensor particles composed of phenoxazinone-based fluorescent cross-linker were placed on a fiber-optic microarray which showed fluorescence enhancement upon binding with AMPI. The sensor detected AMPI with a LOD of 0.72 nM in MeCN and a LOD of 0.4 nM in 25:75 (v/v) MeCN:HEPES (25 mM, pH 7.5). Selectivity studies showed that the MIPs are highly selective for AMPI. The concept of this sensing method was well demonstrated, however, still need investigations regarding sensing medium (food samples). The assay design is flexible and should be applicable with other MIP sensor particles selective to other environmental and biological carboxyl-containing analytes. For a fiber-optic-based multiplexed microarray platform, MIP sensor particles based on different fluorescent monomer and cross-linkers showing emission at different wavelength selective to various analytes can be used as well. Another method would be also

the direct immobilization of a thin MIP layer onto the optical fiber to improve the performance of the fiber.

The last chapter presented a 2-aminopyridine-based fluorescent probe **22** that complexes 2,4-D via H-bonds without previous deprotonation in organic solvents showing a typical ESDPT emission band after guest binding. After imprinting **22**/2,4-D-compelx into the thin MIP shell fluorescence band caused by ESDPT could be observed at 503 nm in $CHCl_3$. Upon addition of 2,4-D to the particles this fluorescence increased. The particles showed good imprinting effect and selectivity. To further improve the imprinting effect and the discrimination against similar compounds the two-phase experiment can be used in future. Of course, there is also still space for the dye design. The previous sections demonstrated that sensor particles prepared with fluorescent monomers or cross-linkers in the MIP matrix showed promising sensing responses. The introduction of a polymerizable group and thus, the covalent integration into the network can increase the potential of the MIP sensor particles and would be an interesting study for the future.

A more sophisticated system based on mesoporous silica nanoparticles (MSNs) can be used as carrier material in future as well. Their ordered and one-dimensional pores would provide an even larger surface area for (bio)molecular recognition if a thin MIP layer is coated onto their inner pore walls and offer a higher sensing response.

A second protective and switchable layer can be grafted the MIP sensor particles or MIP@MSNs to allow the expose (active state) or the block (inactive state) of the binding sites. This layer should be controllable like for instance thermo-responsive polymers having either a lower or an upper critical solution temperature (LCST/UCST). Especially, MSNs would be a perfect platform for having such a protective shell on the outer surface. The switchable outer layer will be designed so that it can control the access to the pores.

7 References

1. Kaplan, R. M.; Stone, A. A., Bringing the laboratory and clinic to the community: mobile technologies for health promotion and disease prevention a. *Annual Review of Psychology* **2013,** *64*, 471-498.

2. Chan, M.; Estève, D.; Escriba, C.; Campo, E., A review of smart homes—Present state and future challenges. *Computer methods and programs in biomedicine* **2008,** *91* (1), 55-81.

3. Sekhar, P. K.; Brosha, E. L.; Mukundan, R.; Garzon, F. H., Chemical sensors for environmental monitoring and homeland security. *The Electrochemical Society Interface* **2010,** *19* (4), 35.

4. https://ec.europa.eu/digital-single-market/en/news/food-bringing-lab-sample.

5. Hulanicki, A.; Glab, S.; Ingman, F., Chemical sensors: definitions and classification. *Pure and Applied Chemistry* **1991,** *63* (9), 1247-1250.

6. Banica, F.-G., *Chemical sensors and biosensors: fundamentals and applications*. John Wiley & Sons: 2012.

7. Wulff, G., Molekulares Prägen (Imprinting) in vernetzten Materialien mit Hilfe von Matrizenmolekülen – auf dem Weg zu künstlichen Antikörpern. *Angewandte Chemie* **1995,** *107* (17), 1958-1979.

8. Sellergren, B., Polymer-and template-related factors influencing the efficiency in molecularly imprinted solid-phase extractions. *TrAC Trends in Analytical Chemistry* **1999,** *18* (3), 164-174.

9. Sellergren, B., *Molecularly Imprinted Polymers: Man-Made Mimics of Antibodies and their Application in Analytical Chemistry*. Elsevier Science: 2000.

10. Polyakov, M., Adsorption properties and structure of silica gel. *Zhurnal Fizicheskoi Khimii* **1931,** *2* (799), 799–805.

11. Dickey, F. H., The preparation of specific adsorbents. *Proceedings of the National Academy of Sciences. U.S.A.* **1949,** *35*, 227–229.

12. G. Wulff, A. S., Use of polymers with enzyme-analogous structures for the resolution of racemates. *Angewandte Chemie-International Edition Engl* **1972,** *11*, 341–344.

13. Arshady, R.; Mosbach, K., Synthesis of substrate-selective polymers by host-guest polymerization. *Macromolecular Chemistry and Physics* **1981,** *182* (2), 687-692.

14. Hoshino, Y.; Arata, Y.; Yonamine, Y.; Lee, S.-H.; Yamasaki, A.; Tsuhara, R.; Yano, K.; Shea, K. J.; Miura, Y., Preparation of nanogel-immobilized porous gel beads for affinity separation of proteins: fusion of nano and micro gel materials. *Polymer Journal* **2015,** *47* (2), 220-225.

15. Matsui, J.; Okada, M.; Tsuruoka, M.; Takeuchi, T., Solid-phase Extraction of a Triazine Herbicide Using a Molecularly Imprinted Synthetic Receptor. *Analytical Communications* **1997,** *34* (3), 85-87.

16. Bonomi, P.; Servant, A.; Resmini, M., Modulation of imprinting efficiency in nanogels with catalytic activity in the Kemp elimination. *Journal of Molecular Recognition* **2012,** *25* (6), 352-360.

17. Wan, W.; Biyikal, M.; Wagner, R.; Sellergren, B.; Rurack, K., Fluorescent Sensory Microparticles that "Light-up" Consisting of a Silica Core and a Molecularly Imprinted Polymer (MIP) Shell. *Angewandte Chemie-International Edition* **2013,** *52* (27), 7023-7027.

18. Hennion, M.-C., Solid-phase extraction: method development, sorbents, and coupling with liquid chromatography. *Journal of Chromatography A* **1999,** *856* (1–2), 3-54.

19. Haupt, K., Molecularly imprinted polymers in analytical chemistry. *Analyst* **2001,** *126* (6), 747-756.

20. Cormack, P. A. G.; Elorza, A. Z., Molecularly imprinted polymers: synthesis and characterisation. *Journal of Chromatography B-Analytical Technologies in the Biomedical and Life Sciences* **2004,** *804* (1), 173-182.

21. Haupt, K.; Mosbach, K., Molecularly imprinted polymers and their use in biomimetic sensors. *Chemical Reviews* **2000,** *100* (7), 2495-2504.

22. Wulff, G.; Schauhoff, S., Enzyme-analog-built polymers. 27. Racemic resolution of free sugars with macroporous polymers prepared by molecular imprinting. Selectivity dependence on the arrangement of functional groups versus spatial requirements. *The Journal of Organic Chemistry* **1991,** *56* (1), 395-400.

23. Wulff, G.; Vesper, W.; Grobe-Einsler, R.; Sarhan, A., Enzyme-analogue built polymers, 4. On the synthesis of polymers containing chiral cavities and their use for the resolution of racemates. *Die Makromolekulare Chemie* **1977,** *178* (10), 2799-2816.

24. Wulff, G.; Knorr, K., Stoichiometric noncovalent interaction in molecular imprinting. *Bioseparation* **2001,** *10* (6), 257-276.

25. Wulff, G., Enzyme-like catalysis by molecularly imprinted polymers. *Chemical Reviews* **2002,** *102* (1), 1-27.

26. Ye, L.; Mosbach, K., Molecular Imprinting: Synthetic Materials As Substitutes for Biological Antibodies and Receptors†. *Chemistry of Materials* **2008,** *20* (3), 859-868.

27. Shea, K. J.; Thompson, E. A., Template synthesis of macromolecules. Selective functionalization of an organic polymer. *Journal of Organic Chemistry* **1978,** *43* (21), 4253-4255.

28. Wulff, G.; Sarhan, A.; Zabrocki, K., Enzyme-analog built polymers and their use for resolution of racamates. *Tetrahedron Letters* **1973,** (44), 4329-4332.

29. Cheong, S. H.; McNiven, S.; Rachkov, K.; Levi, R.; Yano, K.; Karube, I., Testosterone receptor binding mimic constructed using molecular imprinting. *Macromolecules* **1997,** *30* (5), 1317-1322.

30. Caro, E.; Masqué, N.; Marcé, R. M.; Borrull, F.; Cormack, P. A. G.; Sherrington, D. C., Non-covalent and semi-covalent molecularly imprinted polymers for selective on-line solid-phase extraction of 4-nitrophenol from water samples. *Journal of Chromatography A* **2002,** *963* (1–2), 169-178.

31. Whitcombe, M. J.; Rodriguez, M. E.; Villar, P.; Vulfson, E. N., A new method for the introduction of recognition site functionality into polymers prepared by molecular imprinting-synthesis and characterization of polymeric receptors for cholesterol. *Journal of the American Chemical Society* **1995,** *117* (27), 7105-7111.

32. Mayes, A. G.; Whitcombe, M. J., Synthetic strategies for the generation of molecularly imprinted organic polymers. *Advanced Drug Delivery Reviews* **2005,** *57* (12), 1742-1778.

33. Sellergren, B.; Andersson, L., Molecular recognition in macroporous polymers prepared by a substrate analog imprinting strategy. *Journal of Organic Chemistry* **1990,** *55* (10), 3381-3383.

34. Whitcombe, M. J.; Rodriguez, M. E.; Villar, P.; Vulfson, E. N., A new method for the introduction of recognition site functionality into polymers prepared by molecular imprinting: synthesis and characterization of polymeric receptors for cholesterol. *Journal of the American Chemical Society* **1995,** *117* (27), 7105-7111.

35. Joshi, V. P.; Karmalkar, R. N.; Kulkarni, M. G.; Mashelkar, R. A., Effect of solvents on selectivity in separation using molecularly imprinted adsorbents: separation of phenol and bisphenol A. *Industrial & Engineering Chemistry Research* **1999,** *38* (11), 4417-4423.

36. Arshady, R.; Mosbach, K., SYNTHESIS OF SUBSTRATE-SELECTIVE POLYMERS BY HOST-GUEST POLYMERIZATION. *Macromolecular Chemistry and Physics-Makromolekulare Chemie* **1981,** *182* (2), 687-692.

37. Sellergren, B.; Lepisto, M.; Mosbach, K., Highly enantioselective and substrate-selective polymers obtained by molecular imprinting utilizing noncovalent interactions. NMR and chromatographic studies on the nature of recognition *Journal of the American Chemical Society* **1988,** *110* (17), 5853-5860.

38. Qi, P.; Wang, J.; Wang, L.; Li, Y.; Jin, J.; Su, F.; Tian, Y.; Chen, J., Molecularly imprinted polymers synthesized via semi-covalent imprinting with sacrificial spacer for imprinting phenols. *Polymer* **2010,** *51* (23), 5417-5423.

39. Sellergren, B., Molecular imprinting by noncovalent interactions. Enantioselectivity and binding capacity of polymers prepared under conditions favoring the formation of template complexes. *Die Makromolekulare Chemie* **1989,** *190* (11), 2703-2711.

40. Nie, S.; Benito-Peña, E.; Zhang, H.; Wu, Y.; Walt, D. R., Multiplexed salivary protein profiling for patients with respiratory diseases using fiber-optic bundles and fluorescent antibody-based microarrays. *Analytical Chemistry* **2013,** *85* (19), 9272-9280.

41. Martin-Esteban, A.; Turiel, E.; Stevenson, D., Effect of template size on the selectivity of molecularly imprinted polymers for phenylurea herbicides. *Chromatographia* **2001,** *53*, S434-S437.

42. Martin-Esteban, A., Molecularly imprinted polymers: new molecular recognition materials for selective solid-phase extraction of organic compounds. *Fresenius Journal of Analytical Chemistry* **2001,** *370* (7), 795-802.

43. Spivak, D. A., Optimization, evaluation, and characterization of molecularly imprinted polymers. *Advanced Drug Delivery Reviews* **2005,** *57* (12), 1779-1794.

44. Karim, K.; Breton, F.; Rouillon, R.; Piletska, E. V.; Guerreiro, A.; Chianella, I.; Piletsky, S. A., How to find effective functional monomers for effective molecularly imprinted polymers? *Advanced Drug Delivery Reviews* **2005,** *57* (12), 1795-1808.

45. Pichon, V.; Chapuis-Hugon, F., Role of molecularly imprinted polymers for selective determination of environmental pollutants—A review. *Analytica Chimica Acta* **2008,** *622* (1–2), 48-61.

46. Bossi, A.; Bonini, F.; Turner, A. P. F.; Piletsky, S. A., Molecularly imprinted polymers for the recognition of proteins: The state of the art. *Biosensors and Bioelectronics* **2007,** *22* (6), 1131-1137.

47. Puoci, F.; Cirillo, G.; Curcio, M.; Iemma, F.; Spizzirri, U. G.; Picci, N., Molecularly imprinted solid phase extraction for the selective HPLC determination of α-tocopherol in bay leaves. *Analytica Chimica Acta* **2007,** *593* (2), 164-170.

48. Ye, L.; Mosbach, K., The Technique of Molecular Imprinting – Principle, State of the Art, and Future Aspects. *Journal of Inclusion Phenomena* **2001,** *41* (1-4), 107-113.

49. Xing, R.; Wang, S.; Bie, Z.; He, H.; Liu, Z., Preparation of molecularly imprinted polymers specific to glycoproteins, glycans and monosaccharides via boronate affinity controllable–oriented surface imprinting. *Nature protocols* **2017,** *12* (5), 964.

50. Tan, C. J.; Tong, Y. W., Molecularly imprinted beads by surface imprinting. *Analytical and bioanalytical chemistry* **2007,** *389* (2), 369-376.

51. Sellergren, B.; Hall, A. J., Chapter 2 - Fundamental aspects on the synthesis and characterisation of imprinted network polymers. In *Techniques and Instrumentation in Analytical Chemistry*, Börje, S., Ed. Elsevier: 2001; Vol. Volume 23, pp 21-57.

52. Lanza, F.; Sellergren, B., Molecularly Imprinted Polymers via High-Throughput and Combinatorial Techniques. *Macromolecular Rapid Communications* **2004,** *25* (1), 59-68.

53. Sellergren, B., Imprinted chiral stationary phases in high-performance liquid chromatography. *Journal of Chromatography A* **2001,** *906* (1-2), 227-252.

54. O'Shannessy, D. J.; Ekberg, B.; Mosbach, K., Molecular imprinting of amino acid derivatives at low temperature (0°C) using photolytic homolysis of azobisnitriles. *Anal Biochem* **1989,** *177* (1), 144-149.

55. Haginaka, J.; Takehira, H.; Hosoya, K.; Tanaka, N., Molecularly imprinted uniform-sized polymer-based stationary phase for naproxen: Comparison of molecular recognition ability of the molecularly imprinted polymers prepared by thermal and redox polymerization techniques. *Journal of Chromatography A* **1998,** *816* (2), 113-121.

56. Hirayama, K.; Sakai, Y.; Kameoka, K.; Noda, K.; Naganawa, R., Preparation of a sensor device with specific recognition sites for acetaldehyde by molecular imprinting technique. *Sensors and Actuators B: Chemical* **2002,** *86* (1), 20-25.

57. Piletsky, S. A.; Matuschewski, H.; Schedler, U.; Wilpert, A.; Piletska, E. V.; Thiele, T. A.; Ulbricht, M., Surface Functionalization of Porous Polypropylene Membranes with Molecularly Imprinted Polymers by Photograft Copolymerization in Water. *Macromolecules* **2000,** *33* (8), 3092-3098.

58. Vasapollo, G.; Sole, R. D.; Mergola, L.; Lazzoi, M. R.; Scardino, A.; Scorrano, S.; Mele, G., Molecularly imprinted polymers: present and future prospective. *International Journal of Molecular Sciences* **2011,** *12* (9), 5908-5945.

59. Song, X.; Wang, J.; Zhu, J., Effect of porogenic solvent on selective performance of molecularly imprinted polymer for quercetin. *Materials Research* **2009,** *12* (3), 299-304.

60. Pap, T. m.; Horváth, V.; Tolokán, A.; Horvai, G.; Sellergren, B., Effect of solvents on the selectivity of terbutylazine imprinted polymer sorbents used in solid-phase extraction. *Journal of Chromatography A* **2002,** *973* (1–2), 1-12.

61. Rosengren, A. M.; Karlsson, J. G.; Andersson, P. O.; Nicholls, I. A., Chemometric Models of TemplateMolecularly Imprinted Polymer Binding. *Analytical Chemistry* **2005,** *77* (17), 5700-5705.

62. Yu, C.; Mosbach, K., Influence of mobile phase composition and cross-linking density on the enantiomeric recognition properties of molecularly imprinted polymers. *Journal of Chromatography A* **2000,** *888* (1–2), 63-72.

63. Scorrano, S.; Longo, L.; Vasapollo, G., Molecularly imprinted polymers for solid-phase extraction of 1-methyladenosine from human urine. *Analytica Chimica Acta* **2010,** *659* (1–2), 167-171.

64. Haupt, K., Biomaterials: Plastic antibodies. *Nat Mater* **2010,** *9* (8), 612-614.

65. Nestora, S.; Merlier, F.; Beyazit, S.; Prost, E.; Duma, L.; Baril, B.; Greaves, A.; Haupt, K.; Tse Sum Bui, B., Plastic Antibodies for Cosmetics: Molecularly Imprinted Polymers Scavenge Precursors of Malodors. *Angewandte Chemie* **2016,** *128* (21), 6360-6364.

66. Andersson, H. S.; Karlsson, J. G.; Piletsky, S. A.; Koch-Schmidt, A.-C.; Mosbach, K.; Nicholls, I. A., Study of the nature of recognition in molecularly imprinted polymers, II [1]: Influence of monomer–template ratio and sample load on retention and selectivity. *Journal of Chromatography A* **1999,** *848* (1–2), 39-49.

67. Strikovsky, A. G.; Kasper, D.; Grün, M.; Green, B. S.; Hradil, J.; Wulff, G., Catalytic molecularly imprinted polymers using conventional bulk polymerization or suspension polymerization: Selective hydrolysis of diphenyl carbonate and diphenyl carbamate. *Journal of the American Chemical Society* **2000,** *122* (26), 6295-6296.

68. Sergeyeva, T.; Piletsky, S.; Brovko, A.; Slinchenko, E.; Sergeeva, L.; El'Skaya, A., Selective recognition of atrazine by molecularly imprinted polymer membranes. Development of conductometric sensor for herbicides detection. *Analytica Chimica Acta* **1999,** *392* (2), 105-111.

69. Mathew-Krotz, J.; Shea, K., Imprinted polymer membranes for the selective transport of targeted neutral molecules. *Journal of the American Chemical Society* **1996,** *118* (34), 8154-8155.

70. Ton, X.-A.; Acha, V.; Bonomi, P.; Tse Sum Bui, B.; Haupt, K., A disposable evanescent wave fiber optic sensor coated with a molecularly imprinted polymer as a selective fluorescence probe. *Biosensors and Bioelectronics* **2015,** *64* (0), 359-366.

71. Guan, G.; Liu, R.; Mei, Q.; Zhang, Z., Molecularly imprinted shells from polymer and xerogel matrices on polystyrene colloidal spheres. *Chemistry-a European Journal* **2012,** *18* (15), 4692-4698.

72. Lu, F.; Li, H.; Sun, M.; Fan, L.; Qiu, H.; Li, X.; Luo, C., Flow injection chemiluminescence sensor based on core–shell magnetic molecularly imprinted nanoparticles for determination of sulfadiazine. *Analytica Chimica Acta* **2012,** *718*, 84-91.

73. Liu, R.; Guan, G.; Wang, S.; Zhang, Z., Core-shell nanostructured molecular imprinting fluorescent chemosensor for selective detection of atrazine herbicide. *Analyst* **2011,** *136* (1), 184-190.

74. Gao, L.; Han, W.; Li, X.; Wang, J.; Yan, Y.; Li, C.; Dai, J., Detection of λ-cyhalothrin by a core-shell spherical SiO2-based surface thin fluorescent molecularly imprinted polymer film. *Analytical and Bioanalytical Chemistry* **2015,** *407* (30), 9177-9184.

75. Sulitzky, C.; Rückert, B.; Hall, A. J.; Lanza, F.; Unger, K.; Sellergren, B., Grafting of molecularly imprinted polymer films on silica supports containing surface-bound free radical initiators. *Macromolecules* **2002,** *35*, 79.

76. Rückert, B.; Hall, A. J.; Sellergren, B., Molecularly imprinted composite materials via iniferter-modified supports. *Journal of Materials Chemistry* **2002,** *12* (8), 2275-2280.

77. Sellergren, B.; RüCKERT, B.; Hall, A. J., Layer-by-layer grafting of molecularly imprinted polymers via iniferter modified supports. *Advanced Materials* **2002,** *14* (17), 1204-1208.

78. Wei, X.; Li, X.; Husson, S. M., Surface Molecular Imprinting by Atom Transfer Radical Polymerization. *Biomacromolecules* **2005,** *6* (2), 1113-1121.

79. Lu, C. H.; Wang, Y.; Li, Y.; Yang, H. H.; Chen, X.; Wang, X. R., Bifunctional superparamagnetic surface molecularly imprinted polymer core-shell nanoparticles. *J. Mater. Chem.* **2009,** *19*, 1077.

80. Zu, B.; Pan, G.; Guo, X.; Zhang, Y.; Zhang, H., Preparation of molecularly imprinted polymer microspheres via atom transfer radical precipitation polymerization. *Journal of Polymer Science Part A: Polymer Chemistry* **2009,** *47* (13), 3257-3270.

81. Brinks, M. K.; Studer, A., Polymer Brushes by Nitroxide-Mediated Polymerization. *Macromolecular Rapid Communications* **2009,** *30* (13), 1043-1057.

82. Benoit, D.; Chaplinski, V.; Braslau, R.; Hawker, C. J., Development of a Universal Alkoxyamine for "Living" Free Radical Polymerizations. *Journal of the American Chemical Society* **1999,** *121* (16), 3904-3920.

83. An, Z.; Shi, Q.; Tang, W.; Tsung, C.-K.; Hawker, C. J.; Stucky, G. D., Facile RAFT Precipitation Polymerization for the Microwave-Assisted Synthesis of Well-Defined, Double Hydrophilic Block Copolymers and Nanostructured Hydrogels. *Journal of the American Chemical Society* **2007,** *129* (46), 14493-14499.

84. Barner-Kowollik, C., *Handbook of RAFT polymerization*. John Wiley & Sons: 2008.

85. Moad, G.; Rizzardo, E.; Thang, S. H., Living radical polymerization by the RAFT process. *Australian Journal of Chemistry* **2005,** *58* (6), 379-410.

86. Zhang, Y.; Ding, J.; Gong, S., Preparation of molecularly imprinted polymers for vanillin via reversible addition-fragmentation chain transfer suspension polymerization. *Journal of Applied Polymer Science* **2013,** *128* (5), 2927-2932.

87. Pan, G.; Zhang, Y.; Ma, Y.; Li, C.; Zhang, H., Efficient One-Pot synthesis of water-compatible molecularly imprinted polymer microspheres by facile RAFT precipitation polymerization. *Angewandte Chemie International Edition* **2011,** *50* (49), 11731-11734.

88. Moraes, J.; Ohno, K.; Gody, G.; Maschmeyer, T.; Perrier, S., The synthesis of well-defined poly(vinylbenzyl chloride)-grafted nanoparticles via RAFT polymerization. *Beilstein Journal of Organic Chemistry* **2013,** *9*, 1226-1234.

89. Chong, Y. K.; Krstina, J.; Le, T. P. T.; Moad, G.; Postma, A.; Rizzardo, E.; Thang, S. H., Thiocarbonylthio Compounds [SC(Ph)S−R] in Free Radical Polymerization with Reversible Addition-Fragmentation Chain Transfer (RAFT Polymerization). Role of the Free-Radical Leaving Group (R). *Macromolecules* **2003,** *36* (7), 2256-2272.

90. Sellergren, B., Direct Drug Determination by Selective Sample Enrichment on an Imprinted Polymer. *Analytical Chemistry* **1994,** *66* (9), 1578-1582.

91. Zhu, Q.-Z.; Degelmann, P.; Niessner, R.; Knopp, D., Selective Trace Analysis of Sulfonylurea Herbicides in Water and Soil Samples Based on Solid-Phase Extraction Using a Molecularly Imprinted Polymer. *Environmental Science & Technology* **2002,** *36* (24), 5411-5420.

92. Theodoridis, G.; Zacharis, C. K.; Tzanavaras, P. D.; Themelis, D. G.; Economou, A., Automated sample preparation based on the sequential injection principle: Solid-phase extraction on a molecularly imprinted polymer coupled on-line to high-performance liquid chromatography. *Journal of Chromatography A* **2004,** *1030* (1–2), 69-76.

93. Lasáková, M.; Jandera, P., Molecularly imprinted polymers and their application in solid phase extraction. *Journal of Separation Science* **2009,** *32* (5-6), 799-812.

94. Andersson, L. I.; Paprica, A.; Arvidsson, T., A highly selective solid phase extraction sorbent for pre-concentration of sameridine made by molecular imprinting. *Chromatographia* **1997,** *46* (1-2), 57-62.

95. Ye, L.; Haupt, K., Molecularly imprinted polymers as antibody and receptor mimics for assays, sensors and drug discovery. *Analytical and Bioanalytical Chemistry* **2004,** *378* (8), 1887-1897.

96. Haupt, K.; Mayes, A. G.; Mosbach, K., Herbicide Assay Using an Imprinted Polymer-Based System Analogous to Competitive Fluoroimmunoassays. *Analytical Chemistry* **1998,** *70* (18), 3936-3939.

97. Vlatakis, G.; Andersson, L. I.; Muller, R.; Mosbach, K., Drug assay using antibody mimics made by molecular imprinting. *Nature* **1993,** *361* (6413), 645-647.

98. Hoshino, Y.; Koide, H.; Urakami, T.; Kanazawa, H.; Kodama, T.; Oku, N.; Shea, K. J., Recognition, Neutralization, and Clearance of Target Peptides in the Bloodstream of Living Mice by Molecularly Imprinted Polymer Nanoparticles: A Plastic Antibody. *Journal of the American Chemical Society* **2010,** *132* (19), 6644-6645.

99. Andersson, L. I.; Muller, R.; Vlatakis, G.; Mosbach, K., MIMICS OF THE BINDING-SITES OF OPIOID RECEPTORS OBTAINED BY MOLECULAR IMPRINTING OF ENKEPHALIN AND MORPHINE. *Proceedings of the National Academy of Sciences of the United States of America* **1995,** *92* (11), 4788-4792.

100. Muldoon, M. T.; Stanker, L. H., Polymer Synthesis and Characterization of a Molecularly Imprinted Sorbent Assay for Atrazine. *Journal of Agricultural and Food Chemistry* **1995,** *43* (6), 1424-1427.

101. Alexander, C.; Davidson, L.; Hayes, W., Imprinted polymers: artificial molecular recognition materials with applications in synthesis and catalysis. *Tetrahedron* **2003,** *59* (12), 2025-2057.

102. Robinson, D. K.; Mosbach, K., Molecular imprinting of a transition state analogue leads to a polymer exhibiting esterolytic activity. *Journal of the Chemical Society, Chemical Communications* **1989,** (14), 969-970.

103. Carboni, D.; Flavin, K.; Servant, A.; Gouverneur, V.; Resmini, M., The first example of molecularly imprinted nanogels with aldolase type I activity. *Chemistry-a European Journal* **2008,** *14* (23), 7059-7065.

104. Svenson, J.; Zheng, N.; Nicholls, I. A., A molecularly imprinted polymer-based synthetic transaminase. *Journal of the American Chemical Society* **2004,** *126* (27), 8554-8560.

105. Kirsch, N.; Hedin-Dahlström, J.; Henschel, H.; Whitcombe, M. J.; Wikman, S.; Nicholls, I. A., Molecularly imprinted polymer catalysis of a Diels-Alder reaction. *Journal of Molecular Catalysis B: Enzymatic* **2009,** *58* (1–4), 110-117.

106. Henry, O. Y.; Cullen, D. C.; Piletsky, S. A., Optical interrogation of molecularly imprinted polymers and development of MIP sensors: a review. *Analytical and Bioanalytical Chemistry* **2005,** *382* (4), 947-956.

107. Sunayama, H.; Ooya, T.; Takeuchi, T., Fluorescent protein recognition polymer thin films capable of selective signal transduction of target binding events prepared by molecular imprinting with a post-imprinting treatment. *Biosensors and Bioelectronics 26* (2), 458-462.

108. Manju, S.; Hari, P.; Sreenivasan, K., Fluorescent molecularly imprinted polymer film binds glucose with a concomitant changes in fluorescence. *Biosensors and Bioelectronics* **2010,** *26* (2), 894-897.

109. Sunayama, H.; Ooya, T.; Takeuchi, T., Fluorescent protein recognition polymer thin films capable of selective signal transduction of target binding events prepared by molecular imprinting with a post-imprinting treatment. *Biosensors and Bioelectronics* **2010,** *26* (2), 458-462.

110. Udenfriend, S., Development of the spectrophotofluorometer and its commercialization. *Protein Science* **1995,** *4* (3), 542-551.

111. Lakowicz, J. R., *Principles of fluorescence spectroscopy*. Springer Science & Business Media: 2013.

112. de Silva, A. P.; Fox, D. B.; Moody, T. S.; Weir, S. M., The development of molecular fluorescent switches. *Trends in Biotechnology* **2001,** *19* (1), 29-34.

113. Bissell, R. A.; de Silva, A. P.; Gunaratne, H. N.; Lynch, P. M.; Maguire, G. E.; McCoy, C. P.; Sandanayake, K. S., Fluorescent PET (photoinduced electron transfer) sensors. In *Photoinduced Electron Transfer V*, Springer: 1993; pp 223-264.

114. Lakowicz, J. R., *Topics in Fluorescence Spectroscopy: Volume 4: Probe Design and Chemical Sensing*. Springer Science & Business Media: 1994; Vol. 4.

115. Leung, M. K. P.; Chow, C.-F.; Lam, M. H. W., A sol-gel derived molecular imprinted luminescent PET sensing material for 2,4-dichlorophenoxyacetic acid. *Journal of Materials Chemistry* **2001,** *11* (12), 2985-2991.

116. Kollmannsberger, M.; Rurack, K.; Resch-Genger, U.; Daub, J., Ultrafast charge transfer in amino-substituted boron dipyrromethene dyes and its inhibition

by cation complexation: a new design concept for highly sensitive fluorescent probes. *The Journal of Physical Chemistry A* **1998,** *102* (50), 10211-10220.

117. Kim, J. S.; Quang, D. T., Calixarene-derived fluorescent probes. *Chemical Reviews* **2007,** *107* (9), 3780-3799.

118. Kriz, D.; Ramstroem, O.; Svensson, A.; Mosbach, K., A biomimetic sensor based on a molecularly imprinted polymer as a recognition element combined with fiber-optic detection. *Analytical Chemistry* **1995,** *67* (13), 2142-2144.

119. Rachkov, A.; McNiven, S.; El'skaya, A.; Yano, K.; Karube, I., Fluorescence detection of β-estradiol using a molecularly imprinted polymer. *Analytica Chimica Acta* **2000,** *405* (1–2), 23-29.

120. Wu, Y.-t.; Liu, Y.-j.; Gao, X.; Gao, K.-c.; Xia, H.; Luo, M.-f.; Wang, X.-j.; Ye, L.; Shi, Y.; Lu, B., Monitoring bisphenol A and its biodegradation in water using a fluorescent molecularly imprinted chemosensor. *Chemosphere* **2015,** *119*, 515-523.

121. Selvaraj, K. K.; Shanmugam, G.; Sampath, S.; Larsson, D. J.; Ramaswamy, B. R., GC–MS determination of bisphenol A and alkylphenol ethoxylates in river water from India and their ecotoxicological risk assessment. *Ecotoxicology and environmental safety* **2014,** *99*, 13-20.

122. Zimmers, S. M.; Browne, E. P.; O'Keefe, P. W.; Anderton, D. L.; Kramer, L.; Reckhow, D. A.; Arcaro, K. F., Determination of free Bisphenol A (BPA) concentrations in breast milk of US women using a sensitive LC/MS/MS method. *Chemosphere* **2014,** *104*, 237-243.

123. Rezaee, M.; Yamini, Y.; Shariati, S.; Esrafili, A.; Shamsipur, M., Dispersive liquid–liquid microextraction combined with high-performance liquid chromatography-UV detection as a very simple, rapid and sensitive method for the determination of bisphenol A in water samples. *Journal of Chromatography A* **2009,** *1216* (9), 1511-1514.

124. Nguyen, T. H.; Hardwick, S. A.; Sun, T.; Grattan, K. T., Intrinsic fluorescence-based optical fiber sensor for cocaine using a molecularly imprinted polymer as the recognition element. *IEEE Sensors Journal* **2012,** *12* (1), 255-260.

125. Lavignac, N.; Allender, C. J.; Brain, K. R., 4-(3-Aminopropylene)-7-nitrobenzofurazan: a new polymerisable monomer for use in homogeneous molecularly imprinted sorbent fluoroassays. *Tetrahedron Letters* **2004,** *45* (18), 3625-3627.

126. Nguyen, T. H.; Ansell, R. J., Fluorescent imprinted polymer sensors for chiral amines. *Organic & Biomolecular Chemistry* **2009,** *7* (6), 1211-1220.

127. Kwan, P.; Brodie, M. J., Phenobarbital for the treatment of epilepsy in the 21st century: a critical review. *Epilepsia* **2004,** *45* (9), 1141-1149.

128. Kubo, H.; Yoshioka, N.; Takeuchi, T., Fluorescent Imprinted Polymers Prepared with 2-Acrylamidoquinoline as a Signaling Monomer. *Organic Letters* **2005,** *7* (3), 359-362.

129. Rathbone, D. L.; Su, D.; Wang, Y.; Billington, D. C., Molecular recognition by fluorescent imprinted polymers. *Tetrahedron Letters* **2000,** *41* (1), 123-126.

130. Turkewitsch, P.; Wandelt, B.; Darling, G. D.; Powell, W. S., Fluorescent Functional Recognition Sites through Molecular Imprinting. A Polymer-Based Fluorescent Chemosensor for Aqueous cAMP. *Analytical Chemistry* **1998,** *70* (10), 2025-2030.

131. Chen, Z.; Alvarez-Perez, M.; Navarro-Villoslada, F.; Moreno-Bondi, M. C.; Orellana, G., Fluorescent sensing of "quat" herbicides with a multifunctional pyrene-labeled monomer and molecular imprinting. *Sens. Actuator B-Chem.* **2014,** *191*, 137-142.

132. Inoue, Y.; Kuwahara, A.; Ohmori, K.; Sunayama, H.; Ooya, T.; Takeuchi, T., Fluorescent molecularly imprinted polymer thin films for specific protein detection prepared with dansyl ethylenediamine-conjugated O-acryloyl L-hydroxyproline. *Biosensors & Bioelectronics* **2013,** *48*, 113-119.

133. Wagner, R.; Wan, W.; Biyikal, M.; Benito-Pena, E.; Cruz Moreno-Bondi, M.; Lazraq, I.; Rurack, K.; Sellergren, B., Synthesis, Spectroscopic, and Analyte-Responsive Behavior of a Polymerizable Naphthalimide-Based Carboxylate Probe and Molecularly Imprinted Polymers Prepared Thereof. *Journal of Organic Chemistry* **2013,** *78* (4), 1377-1389.

134. Kosower, E. M.; Huppert, D., Excited state electron and proton transfers. *Annual Review of Physical Chemistry* **1986,** *37* (1), 127-156.

135. E. Caldin, V. G. E., *Proton Transfer Reactions*. Chapman and Hall: London, 1990.

136. Douhal, A.; Lahmani, F.; Zewail, A. H., Proton-transfer reaction dynamics. *Chemical physics* **1996,** *207* (2), 477-498.

137. Reece, S. Y.; Nocera, D. G., Proton-coupled electron transfer in biology: results from synergistic studies in natural and model systems. *Annual review of biochemistry* **2009,** *78*, 673-699.

138. Schowen, R. L., Harmony and dissonance in the concert of proton motions. *Angewandte Chemie International Edition* **1997,** *36* (13- 14), 1434-1438.

139. Kasha, M. J., *Chem. Soc., Faraday Trans 2* **1986,** *82* (2379).

140. Tuckerman, M. E.; Marx, D.; Klein, M. L.; Parrinello, M., On the quantum nature of the shared proton in hydrogen bonds. *Science* **1997,** *275* (5301), 817-820.

141. Agmon, N., Elementary steps in excited-state proton transfer. *The Journal of Physical Chemistry A* **2005,** *109* (1), 13-35.

142. Gervasio, F. L.; Procacci, P.; Cardini, G.; Guarna, A.; Giolitti, A.; Schettino, V., Interaction between Aromatic Residues. Molecular Dynamics and ab Initio Exploration of the Potential Energy Surface of the Tryptophan– Histidine Pair. *The Journal of Physical Chemistry B* **2000,** *104* (5), 1108-1114.

143. Chang, H.-C.; Ming Lee, K.; Jiang, J.-C.; Lin, M.-S.; Chen, J.-S.; Lin, I. J.; Hsien Lin, S., Charge-enhanced C–H–O interactions of a self-assembled triple helical spine probed by high-pressure. *The Journal of chemical physics* **2002,** *117* (4), 1723-1728.

144. Chang, H.-C.; Jiang, J.-C.; Lai, W.-W.; Lin, J.-S.; Chen, G.-C.; Tsai, W.-C.; Lin, S. H., High-Pressure Raman Studies on Aqueous Protonated Thiazole: Presence of Charge-Enhanced C– H⊙⊙⊙ O Hydrogen Bonds. *The Journal of Physical Chemistry B* **2005,** *109* (48), 23103-23107.

145. Komoto, Y.; Sakota, K.; Sekiya, H., Excited-state double-proton transfer in the (3-methyl-7-azaindole)–(7-azaindole) hetero-dimer in the gas phase. *Chemical physics letters* **2005,** *406* (1), 15-19.

146. Ishikawa, H.; Iwata, K.; Hamaguchi, H.-o., Picosecond dynamics of stepwise double proton-transfer reaction in the excited state of the 2-aminopyridine/acetic acid system. *The Journal of Physical Chemistry A* **2002,** *106* (10), 2305-2312.

147. Chai, S.; Zhao, G.-J.; Song, P.; Yang, S.-Q.; Liu, J.-Y.; Han, K.-L., Reconsideration of the excited-state double proton transfer (ESDPT) in 2-aminopyridine/acid systems: role of the intermolecular hydrogen bonding in excited states. *Physical Chemistry Chemical Physics* **2009,** *11* (21), 4385-4390.

148. Descalzo, A. B.; Rurack, K.; Weisshoff, H.; Martínez-Máñez, R.; Marcos, M. D.; Amorós, P.; Hoffmann, K.; Soto, J., Rational Design of a Chromo- and Fluorogenic Hybrid Chemosensor Material for the Detection of Long-Chain Carboxylates. *Journal of the American Chemical Society* **2005,** *127* (1), 184-200.

149. Musso, H.; Wager, P., Phenoxazine, V. Neue Synthesen für 7-Amino-phenoxazone-(2). *Chemische Berichte* **1961,** *94* (9), 2551-2561.

150. Stöber, W.; Fink, A.; Bohn, E., Controlled growth of monodisperse silica spheres in the micron size range. *Journal of Colloid and Interface Science* **1968,** *26* (1), 62-69.

151. Gans, P.; Sabatini, A.; Vacca, A., Investigation of equilibria in solution. Determination of equilibrium constants with the HYPERQUAD suite of programs. *Talanta* **1996,** *43* (10), 1739-1753.

152. Bell, J.; Climent, E.; Hecht, M.; Buurman, M.; Rurack, K., Combining a droplet-based microfluidic tubing system with gated indicator releasing nanoparticles for mercury trace detection. *ACS Sensors* **2016,** *1* (4), 334-338.

153. Rurack, K.; Spieles, M., Fluorescence quantum yields of a series of red and near-infrared dyes emitting at 600− 1000 nm. *Analytical Chemistry* **2011,** *83* (4), 1232-1242.

154. Carrasco, S.; Benito-Pena, E.; Walt, D. R.; Moreno-Bondi, M. C., Fiber-optic array using molecularly imprinted microspheres for antibiotic analysis. *Chemical Science* **2015,** *6* (5), 3139-3147.

155. Pantano, P.; Walt, D. R., Ordered nanowell arrays. *Chemistry of Materials* **1996,** *8* (12), 2832-2835.

156. Epstein, J. R.; Walt, D. R., Fluorescence-based fibre optic arrays: a universal platform for sensing. *Chemical Society Reviews* **2003,** *32* (4), 203-214.

157. Gale, P. A.; Busschaert, N.; Haynes, C. J.; Karagiannidis, L. E.; Kirby, I. L., Anion receptor chemistry: highlights from 2011 and 2012. *Chemical Society Reviews* **2014,** *43* (1), 205-241.

158. Bianchi, A.; Bowman-James, K.; García-Espana, E., *Supramolecular Chemistry of Anions*. Wiley-VCH: New York, 1997.

159. Leitner, A.; Sturm, M.; Lindner, W., Tools for analyzing the phosphoproteome and other phosphorylated biomolecules: a review. *Analytica chimica acta* **2011,** *703* (1), 19-30.

160. Mason, C. F., *Biology of Freshwater Pollution*. 2nd. ed. ed.; Longman: New York, 1991.

161. M Frawley Cass, S.; J Tepe, J., Identification of phosphoproteins and their impact as biomarkers in cancer therapeutics. *Current Signal Transduction Therapy* **2011,** *6* (1), 113-140.

162. Albelda, M. T.; Frías, J. C.; García-España, E.; Schneider, H.-J., Supramolecular complexation for environmental control. *Chemical Society Reviews* **2012,** *41* (10), 3859-3877.

163. Schmidtchen, F. P.; Berger, M., Artificial organic host molecules for anions. *Chemical reviews* **1997,** *97* (5), 1609-1646.

164. Baggiani, C.; Anfossi, L.; Giovannoli, C., MIP-based immunoassays: State of the Art, limitations and Perspectives. *Molecular Imprinting* **2013,** *1*, 41-54.

165. Manesiotis, P.; Hall, A. J.; Emgenbroich, M.; Quaglia, M.; Lorenzi, E. D.; Sellergren, B., An enantioselective imprinted receptor for Z-glutamate exhibiting a binding induced color change. *Chemical Communications* **2004,** (20), 2278-2279.

166. Hall, A. J.; Manesiotis, P.; Emgenbroich, M.; Quaglia, M.; De Lorenzi, E.; Sellergren, B., Urea Host Monomers for Stoichiometric Molecular Imprinting of Oxyanions§. *The Journal of Organic Chemistry* **2005,** *70* (5), 1732-1736.

167. Ghosh, A.; Verma, S.; Ganguly, B.; Ghosh, H. N.; Das, A., Influence of Urea N–H Acidity on Receptor–Anionic and Neutral Analyte Binding in a Ruthenium (II)–Polypyridyl-Based Colorimetric Sensor. *European Journal of Inorganic Chemistry* **2009,** *2009* (17), 2496-2507.

168. Boiocchi, M.; Del Boca, L.; Gómez, D. E.; Fabbrizzi, L.; Licchelli, M.; Monzani, E., Nature of urea-fluoride interaction: incipient and definitive proton transfer. *Journal of the American Chemical Society* **2004,** *126* (50), 16507-16514.

169. Wan, W.; Wagner, S.; Rurack, K., Fluorescent monomers: "bricks" that make a molecularly imprinted polymer "bright". *Analytical and Bioanalytical Chemistry* **2015,** *408* (7), 1753-1771.

170. Gawlitza, K.; Wan, W.; Wagner, S.; Rurack, K., Fluorescent Molecularly Imprinted Polymers. *Advanced Molecularly Imprinting Materials* **2016**, 89.

171. Hamase, K.; Iwashita, K.; Zaitsu, K., Enantio-Selective Derivatization of Amino Compounds in the Presence of a Molecular Imprint Polymer. *Analytical sciences* **1999,** *15* (5), 411-412.

172. Peng, H.; Zhang, Y.; Zhang, J.; Xie, Q.; Nie, L.; Yao, S., Development of a thickness shear mode acoustic sensor based on an electrosynthesized molecularly imprinted polymer using an underivatized amino acid as the template. *Analyst* **2001,** *126* (2), 189-194.

173. Shinde, S.; Bunschoten, A.; Kruijtzer, J. A.; Liskamp, R. M.; Sellergren, B., Imprinted polymers displaying high affinity for sulfated protein fragments. *Angewandte Chemie International Edition* **2012,** *51* (33), 8326-8329.

174. Emgenbroich, M.; Borrelli, C.; Shinde, S.; Lazraq, I.; Vilela, F.; Hall, A. J.; Oxelbark, J.; De Lorenzi, E.; Courtois, J.; Simanova, A., A Phosphotyrosine-Imprinted Polymer Receptor for the Recognition of Tyrosine Phosphorylated Peptides. *Chemistry-a European Journal* **2008,** *14* (31), 9516-9529.

175. Fery-Forgues, S.; Fayet, J.-P.; Lopez, A., Drastic changes in the fluorescence properties of NBD probes with the polarity of the medium:

involvement of a TICT state? *Journal of Photochemistry and Photobiology A: Chemistry* **1993,** *70* (3), 229-243.

176. Wagner, R.; Wan, W.; Biyikal, M.; Benito-PeÃ±a, E.; Moreno-Bondi, M. C.; Lazraq, I.; Rurack, K.; Sellergren, B. r., Synthesis, Spectroscopic, and Analyte-Responsive Behavior of a Polymerizable Naphthalimide-Based Carboxylate Probe and Molecularly Imprinted Polymers Prepared Thereof. *The Journal of Organic Chemistry 78* (4), 1377-1389.

177. Günter, W.; Thomas, G.; Rainer, S.; Thomas, S.; Christian, K., Molecular Imprinting for the Preparation of Enzyme-Analogous Polymers. In *Molecular and Ionic Recognition with Imprinted Polymers*, American Chemical Society: 1998; Vol. 703, pp 10-28.

178. Koshland, D., Application of a theory of enzyme specificity to protein synthesis. *Proceedings of the National Academy of Sciences* **1958,** *44* (2), 98-104.

179. Singh, S.; Bhushan, L.; Ladha, J.; Gupta, R.; Rao, A.; Sivaprasad, B., Weed management in dry-seeded rice (Oryza sativa) cultivated in the furrow-irrigated raised-bed planting system. *Crop Protection* **2006,** *25* (5), 487-495.

180. Leon, R. G.; Ferrell, J. A.; Brecke, B. J., Impact of exposure to 2, 4-D and dicamba on peanut injury and yield. *Weed Technology* **2014,** *28* (3), 465-470.

181. Vivian, R.; Reis, A.; Kálnay, P. A.; Vargas, L.; Ferreira, A. C. C.; Mariani, F., Weed management in soybean-Issues and practices. *Soybean-Pest Resistance* **2013**.

182. Wu, H.; Stanton, R.; Lemerle, D., Herbicidal control of Solanum elaeagnifolium Cav. in Australia. *Crop Protection* **2016,** *88*, 58-64.

183. Schulz, B.; Segobye, K., 2, 4-D transport and herbicide resistance in weeds. *Journal of experimental botany* **2016,** *67* (11), 3177-3179.

184. Santos, E.; Correia, N.; Silva, J. R. M.; Velini, E. D.; Passos, A.; Durigan, J. C., Herbicide detection in groundwater in Córrego Rico-SP watershed. *Planta Daninha* **2015,** *33* (1), 147-155.

185. Cessna, A. J.; McConkey, B. G.; Elliott, J. A., Herbicide transport in surface runoff from conventional and zero-tillage fields. *Journal of environmental quality* **2013,** *42* (3), 782-793.

186. Garabrant, D. H.; Philbert, M. A., Review of 2,4-dichlorophenoxyacetic acid (2,4-D) epidemiology and toxicology. *Critical Reviews in Toxicology* **2002,** *32* (4), 233-257.

187. Burns, C. J.; Swaen, G. M. H., Review of 2,4-dichlorophenoxyacetic acid (2,4-D) biomonitoring and epidemiology. *Critical Reviews in Toxicology* **2012,** *42* (9), 768-786.

188. Who, *Guidelines for drinking-water quality, Second edition, Vol. 1. Recommendations*. 1993; p x+188p-x+188p.

189. Haupt, K.; Dzgoev, A.; Mosbach, K., Assay System for the Herbicide 2,4-Dichlorophenoxyacetic Acid Using a Molecularly Imprinted Polymer as an Artificial Recognition Element. *Analytical Chemistry* **1998,** *70* (3), 628-631.

190. Nomura, Y.; Muguruma, H.; Yano, K.; Kugimiya, A.; McNiven, S.; Ikebukuro, K.; Karube, I., Selective recognition of 2,4-dichlorophenoxyacetic acid using a molecularly imprinted polymer. *Analytical Letters* **1998,** *31* (6), 973-980.

191. Legido-Quigley, C.; Oxelbark, J.; De Lorenzi, E.; Zurutuza-Elorza, A.; Cormack, P. A. G., Chromatographic characterisation, under highly aqueous conditions, of a molecularly imprinted polymer binding the herbicide 2,4-dichlorophenoxyacetic acid. *Analytica Chimica Acta* **2007,** *591* (1), 22-28.

192. Yun, Y.-H.; Shon, H.-K.; Yoon, S.-D., Preparation and characterization of molecularly imprinted polymers for the selective separation of 2,4-dichlorophenoxyacetic acid. *Journal of Materials Science* **2009,** *44* (22), 6206-6211.

193. Han, D.; Jia, W.; Liang, H., Selective removal of 2,4-dichlorophenoxyacetic acid from water by molecularly-imprinted amino-functionalized silica gel sorbent. *Journal of Environmental Sciences* **2010,** *22* (2), 237-241.

194. Yang, W.; Jiao, F.; Zhou, L.; Chen, X.; Jiang, X., Molecularly imprinted polymers coated on multi-walled carbon nanotubes through a simple indirect method for the determination of 2, 4-dichlorophenoxyacetic acid in environmental water. *Applied Surface Science* **2013,** *284*, 692-699.

195. Liu, Y.; He, Y.; Jin, Y.; Huang, Y.; Liu, G.; Zhao, R., Preparation of monodispersed macroporous core-shell molecularly imprinted particles and their

application in the determination of 2,4-dichlorophenoxyacetic acid. *Journal of Chromatography A* **2014,** *1323*, 11-17.

196. Xie, C.; Gao, S.; Guo, Q.; Xu, K., Electrochemical sensor for 2, 4-dichlorophenoxy acetic acid using molecularly imprinted polypyrrole membrane as recognition element. *Microchimica acta* **2010,** *169* (1-2), 145-152.

197. Singh, K. P.; Ahalawat, S.; Prajapati, R. K.; Kumar, S.; Singh, P.; Kumar, D. S., Electrochemical sensing for the detection of 2, 4-dichlorophenoxy acetic acid using molecularly imprinted polymer membrane. *Ionics* **2010,** *16* (6), 529-537.

198. Peng, D.; Li, X.; Zhang, L.; Gong, J., Novel visible-light-responsive photoelectrochemical sensor of 2, 4-dichlorophenoxyacetic acid using molecularly imprinted polymer/BiOI nanoflake arrays. *Electrochemistry Communications* **2014,** *47*, 9-12.

199. Anirudhan, T. S.; Alexander, S., Multiwalled carbon nanotube based molecular imprinted polymer for trace determination of 2, 4-dichlorophenoxyaceticacid in natural water samples using a potentiometric method. *Applied Surface Science* **2014,** *303*, 180-186.

200. Leung, M. K.-P.; Chow, C.-F.; Lam, M. H.-W., A sol–gel derived molecular imprinted luminescent PET sensing material for 2, 4-dichlorophenoxyacetic acid. *Journal of Materials Chemistry* **2001,** *11* (12), 2985-2991.

201. Wang, S.; Ge, L.; Li, L.; Yan, M.; Ge, S.; Yu, J., Molecularly imprinted polymer grafted paper-based multi-disk micro-disk plate for chemiluminescence detection of pesticide. *Biosensors and Bioelectronics* **2013,** *50*, 262-268.

202. Ton, X.-A.; Bui, B. T. S.; Resmini, M.; Bonomi, P.; Dika, I.; Soppera, O.; Haupt, K., A Versatile Fiber-Optic Fluorescence Sensor Based on Molecularly Imprinted Microstructures Polymerized in Situ. *Angewandte Chemie-International Edition* **2013,** *52* (32), 8317-8321.

203. Wang, X.; Yu, J.; Wu, X.; Fu, J.; Kang, Q.; Shen, D.; Li, J.; Chen, L., A molecular imprinting-based turn-on Ratiometric fluorescence sensor for highly selective and sensitive detection of 2, 4-dichlorophenoxyacetic acid (2, 4-D). *Biosensors and Bioelectronics* **2016,** *81*, 438-444.

204. Campos, C. D.; da Silva, J. A., Applications of autonomous microfluidic systems in environmental monitoring. *RSC Advances* **2013,** *3* (40), 18216-18227.

205. Boonpangrak, S.; Whitcombe, M. J.; Prachayasittikul, V.; Mosbach, K.; Ye, L., Preparation of molecularly imprinted polymers using nitroxide-mediated living radical polymerization. *Biosensors and Bioelectronics* **2006,** *22* (3), 349-354.

206. Sambe, H.; Hoshina, K.; Moaddel, R.; Wainer, I. W.; Haginaka, J., Uniformly-sized, molecularly imprinted polymers for nicotine by precipitation polymerization. *Journal of Chromatography A* **2006,** *1134* (1), 88-94.

207. Krupadam, R. J.; Korde, B. A.; Ashokkumar, M.; Kolev, S. D., Novel molecularly imprinted polymeric microspheres for preconcentration and preservation of polycyclic aromatic hydrocarbons from environmental samples. *Analytical and bioanalytical chemistry* **2014,** *406* (22), 5313-5321.

208. Takimoto, K.; Takano, E.; Kitayama, Y.; Takeuchi, T., Synthesis of monodispersed submillimeter-sized molecularly imprinted particles selective for human serum albumin using inverse suspension polymerization in water-in-oil emulsion prepared using microfluidics. *Langmuir* **2015,** *31* (17), 4981-4987.

209. Schirhagl, R.; Qian, J.; Dickert, F. L., Immunosensing with artificial antibodies in organic solvents or complex matrices. *Sensors and Actuators B: Chemical* **2012,** *173*, 585-590.

210. Hong, C.-C.; Lin, C.-C.; Hong, C.-L.; Lin, Z.-X.; Chung, M.-H.; Hsieh, P.-W., Handheld analyzer with on-chip molecularly-imprinted biosensors for electrical detection of propofol in plasma samples. *Biosensors and Bioelectronics* **2016,** *86*, 623-629.

211. Huang, S.-C.; Lee, G.-B.; Chien, F.-C.; Chen, S.-J.; Chen, W.-J.; Yang, M.-C., A microfluidic system with integrated molecular imprinting polymer films for surface plasmon resonance detection. *Journal of micromechanics and microengineering* **2006,** *16* (7), 1251.

212. Hong, C.-C.; Lin, C.-C.; Hong, C.-L.; Chang, P.-H., Enhanced anesthetic propofol biochips by modifying molecularly imprinted nanocavities of biosensors. *Biomedical microdevices* **2012,** *14* (3), 435-441.

213. Harz, S.; Schimmelpfennig, M.; Tse Sum Bui, B.; Marchyk, N.; Haupt, K.; Feller, K.-H., Fluorescence optical spectrally resolved sensor based on molecularly imprinted polymers and microfluidics. *Engineering in Life Sciences* **2011,** *11* (6), 559-565.

214. Liu, Y.; Wang, Y.; Liu, L.; He, Y.; He, Q.; Ji, Y., The detection method for small molecules coupled with a molecularly imprinted polymer/quantum dot chip using a home-built optical system. *Analytical and bioanalytical chemistry* **2016,** *408* (19), 5261-5268.

215. Li, B.; Zhang, Z.; Qi, J.; Zhou, N.; Qin, S.; Choo, J.; Chen, L., Quantum Dot-Based Molecularly Imprinted Polymers on Three-Dimensional Origami Paper Microfluidic Chip for Fluorescence Detection of Phycocyanin. *ACS Sensors* **2017,** *2* (2), 243-250.

216. Piletska, E. V.; Guerreiro, A. R.; Romero-Guerra, M.; Chianella, I.; Turner, A. P. F.; Piletsky, S. A., Design of molecular imprinted polymers compatible with aqueous environment. *Analytica Chimica Acta* **2008,** *607* (1), 54-60.

217. Teh, S.-Y.; Lin, R.; Hung, L.-H.; Lee, A. P., Droplet microfluidics. *Lab on a Chip* **2008,** *8* (2), 198-220.

218. Pfeiffer, S. A.; Nagl, S., Microfluidic platforms employing integrated fluorescent or luminescent chemical sensors: a review of methods, scope and applications. *Methods and Applications in Fluorescence* **2015,** *3* (3), 034003.

219. Hahn, Y.; Hong, D.; Kang, J.; Choi, S. 2016.

220. Trivedi, V.; Doshi, A.; Kurup, G.; Ereifej, E.; Vandevord, P.; Basu, A. S., A modular approach for the generation, storage, mixing, and detection of droplet libraries for high throughput screening. *Lab on a Chip* **2010,** *10* (18), 2433-2442.

221. Organization, W. H., Overcoming antimicrobial resistance. *Overcoming antimicrobial resistance.* **2000**.

222. Commission, E., *Official J. Eur. Union* **2010,** *37*, 1-72.

223. Commission, E., *Official J. Eur. Union* **2010,** *1*, 15.

224. Charm, S.; Chi, R., Microbial receptor assay for rapid detection and identification of seven families of antimicrobial drugs in milk: collaborative study. *Journal-Association of Official Analytical Chemists* **1987,** *71* (2), 304-316.

225. Riediker, S.; Diserens, J.-M.; Stadler, R. H., Analysis of β-lactam antibiotics in incurred raw milk by rapid test methods and liquid chromatography coupled with electrospray ionization tandem mass spectrometry. *Journal of agricultural and food chemistry* **2001,** *49* (9), 4171-4176.

226. Angelidis, A. S.; Farver, T. B.; Cullor, J. S., Evaluation of the Delvo-X-Press assay for detecting antibiotic residues in milk samples from individual cows. *Journal of food protection* **1999,** *62* (10), 1183-1190.

227. Wolfbeis, O. S., Fiber-optic chemical sensors and biosensors. *Analytical chemistry* **2008,** *80* (12), 4269-4283.

228. Wang, X.-D.; Wolfbeis, O. S., Fiber-optic chemical sensors and biosensors (2008–2012). *Analytical chemistry* **2012,** *85* (2), 487-508.

229. Wagner, S.; Bell, J.; Biyikal, M.; Gawlitza, K.; Rurack, K., Integrating fluorescent molecularly imprinted polymer (MIP) sensor particles with a modular microfluidic platform for nanomolar small-molecule detection directly in aqueous samples. *Biosensors and Bioelectronics* **2017**.

230. Walt, D. R., Fiber optic array biosensors. *BioTechniques* **2006,** *41* (5), 529, 531, 533 passim-529, 531, 533 passim.

231. Bourgeat-Lami, E.; Lang, J., Encapsulation of inorganic particles by dispersion polymerization in polar media: 1. Silica nanoparticles encapsulated by polystyrene. *Journal of colloid and interface science* **1998,** *197* (2), 293-308.

232. Aakeröy, C. B.; Hussain, I.; Desper, J., 2-Acetaminopyridine: A Highly Effective Cocrystallizing Agent. *Crystal Growth & Design* **2006,** *6* (2), 474-480.

233. Steiner, T., The whole palette of hydrogen bonds. *Angewandte Chemie International Edition* **2002,** *48*, 41.

234. Smith, G.; Kennard, C. H. L.; White, A. H., Herbicides. Part I. Crystal structure of 2,4-D (2,4-dichlorophenoxyacetic acid). *Journal of the Chemical Society, Perkin Transactions 2* **1976,** (7), 791-792.

235. Wang, X.; Liu, X.; Wang, X., Surface-relief-gratings based on molecularly imprinted polymer for 2, 4-dichlorophenoxyacetic acid detection. *Sensors and Actuators B: Chemical* **2015,** *220*, 873-879.

236. Prusty, A. K.; Bhand, S., A capacitive sensor for 2, 4-D determination in water based on 2, 4-D imprinted polypyrrole coated pencil electrode. *Materials Research Express* **2017,** *4* (3), 035306.

237. Long, G. L.; Winefordner, J. D., Limit of detection. A closer look at the IUPAC definition. *Analytical Chemistry* **1983,** *55* (7), 712A-724A.

8 Supplementary Information

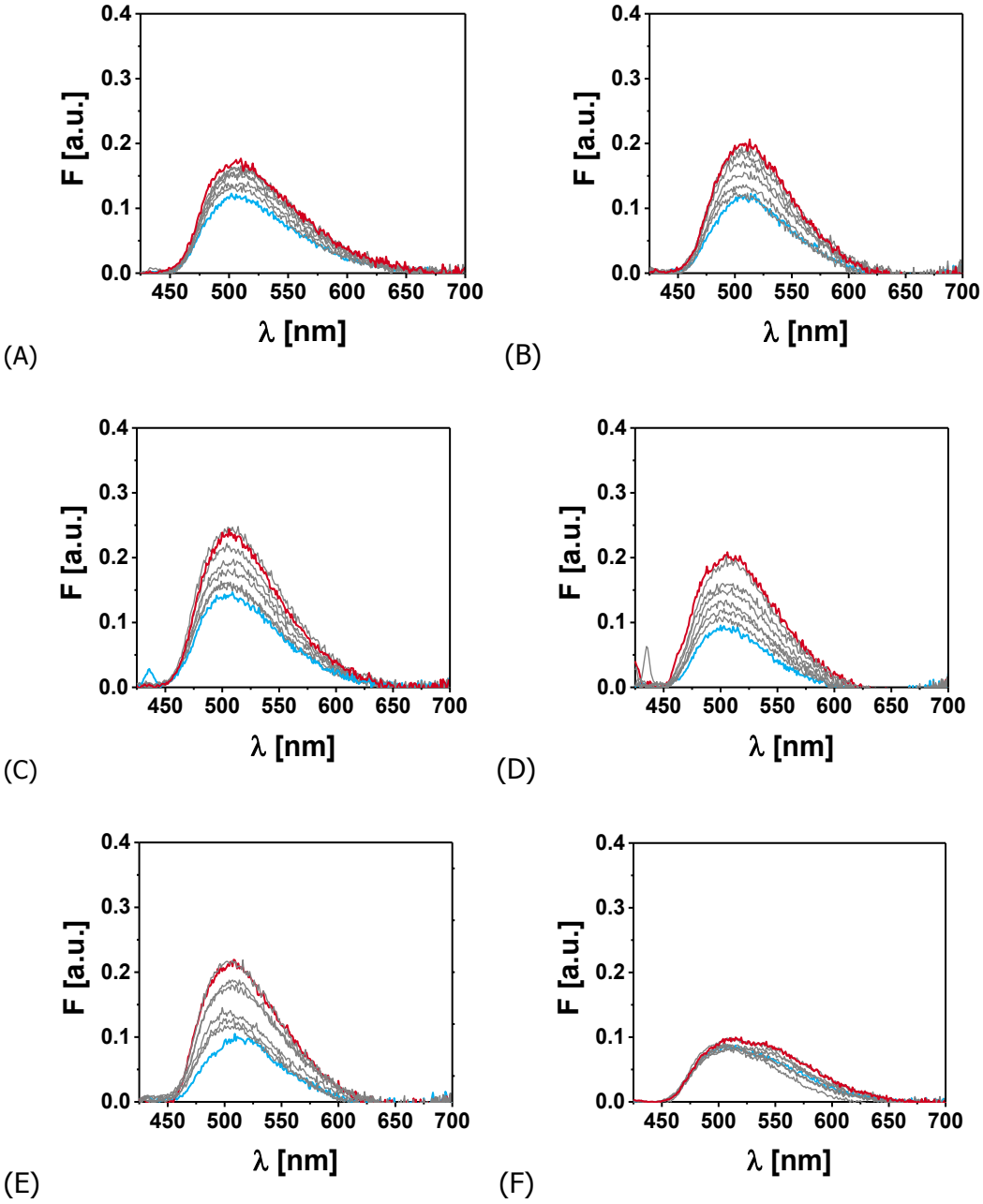

Fig. S84: Fluorescence spectra of 1 mg mL^{-1} MIP(**14**)-Z-D-Phe/TMA@SiO_2 particles particles in $CHCl_3$ in the presence of 1 mM Z-D-Phe/TMA (A), Z-D-Phe/TEA (B), Z-D-Phe/TBA (C), Z-D-Phe/THA (D) and Z-D-Phe/TOA (E) and NIP(**14**)-Z-D-@SiO_2 titrated with 1 mM Z-D-Phe/TMA (F), (increasing concentrations in grey, start point spectrum in blue and end point spectrum in red, steps of 0, 1.0, 2.5, 5.0, 9.9, 19.6, 33.8, 47.6 µM are shown).

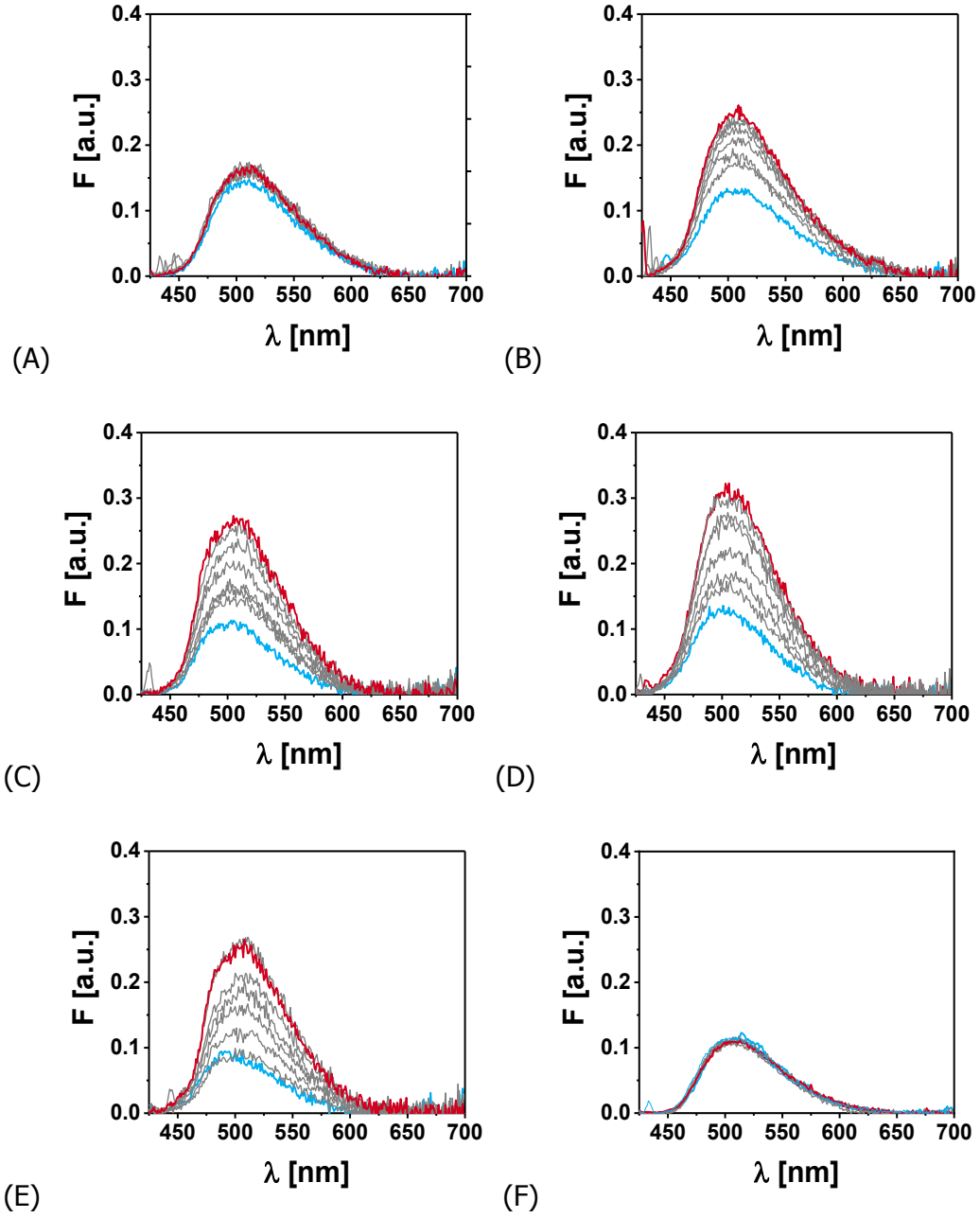

Fig. S85: Fluorescence spectra of 1 mg mL^{-1} MIP(**14**)-Z-D-Phe/TEA@SiO_2 particles in the presence of 1 mM Z-D-Phe/TMA (A), Z-D-Phe/TEA (B), Z-D-Phe/TBA (C), Z-D-Phe/THA (D) and Z-D-Phe/TOA (E) and NIP(**14**)-Z-D-@SiO_2 titrated with 1 mM Z-D-Phe/TEA (F), (increasing concentrations in grey, start point spectrum in blue and end point spectrum in red, steps of 0, 1.0, 2.5, 5.0, 9.9, 19.6, 33.8, 47.6 µM are shown).

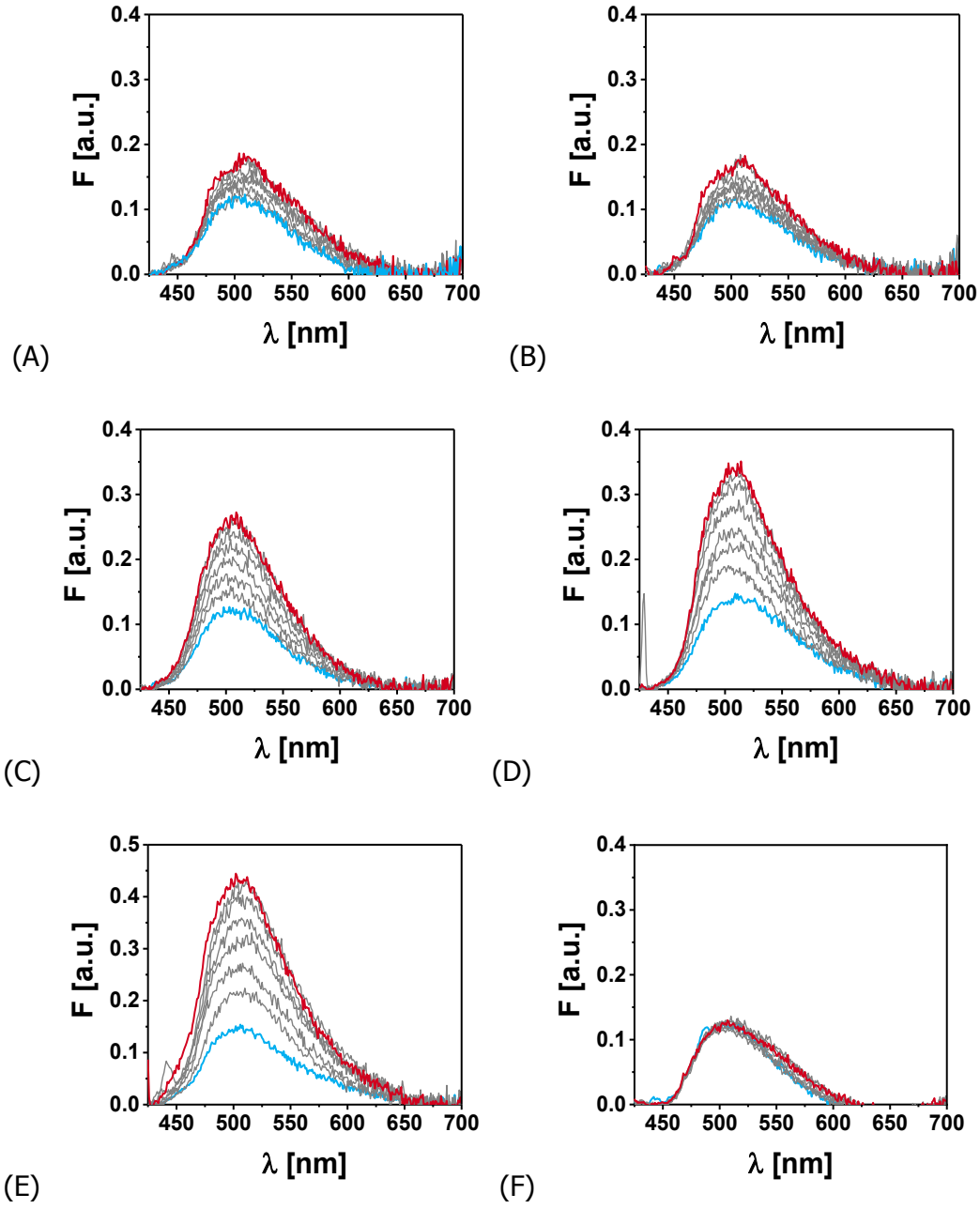

Fig. S86: Fluorescence spectra of 1 mg mL^{-1} MIP(**14**)-Z-D-Phe/TBA@SiO_2 particles in the presence of 1 mM Z-D-Phe/TMA (A), Z-D-Phe/TEA (B), Z-D-Phe/TBA (C), Z-D-Phe/THA (D) and Z-D-Phe/TOA (E) and NIP(**14**)-Z-D- @SiO_2 titrated with 1 mM Z-D-Phe/TBA (F), (increasing concentrations in grey, start point spectrum in blue and end point spectrum in red, steps of 0, 1.0, 2.5, 5.0, 9.9, 19.6, 33.8, 47.6 µM are shown).

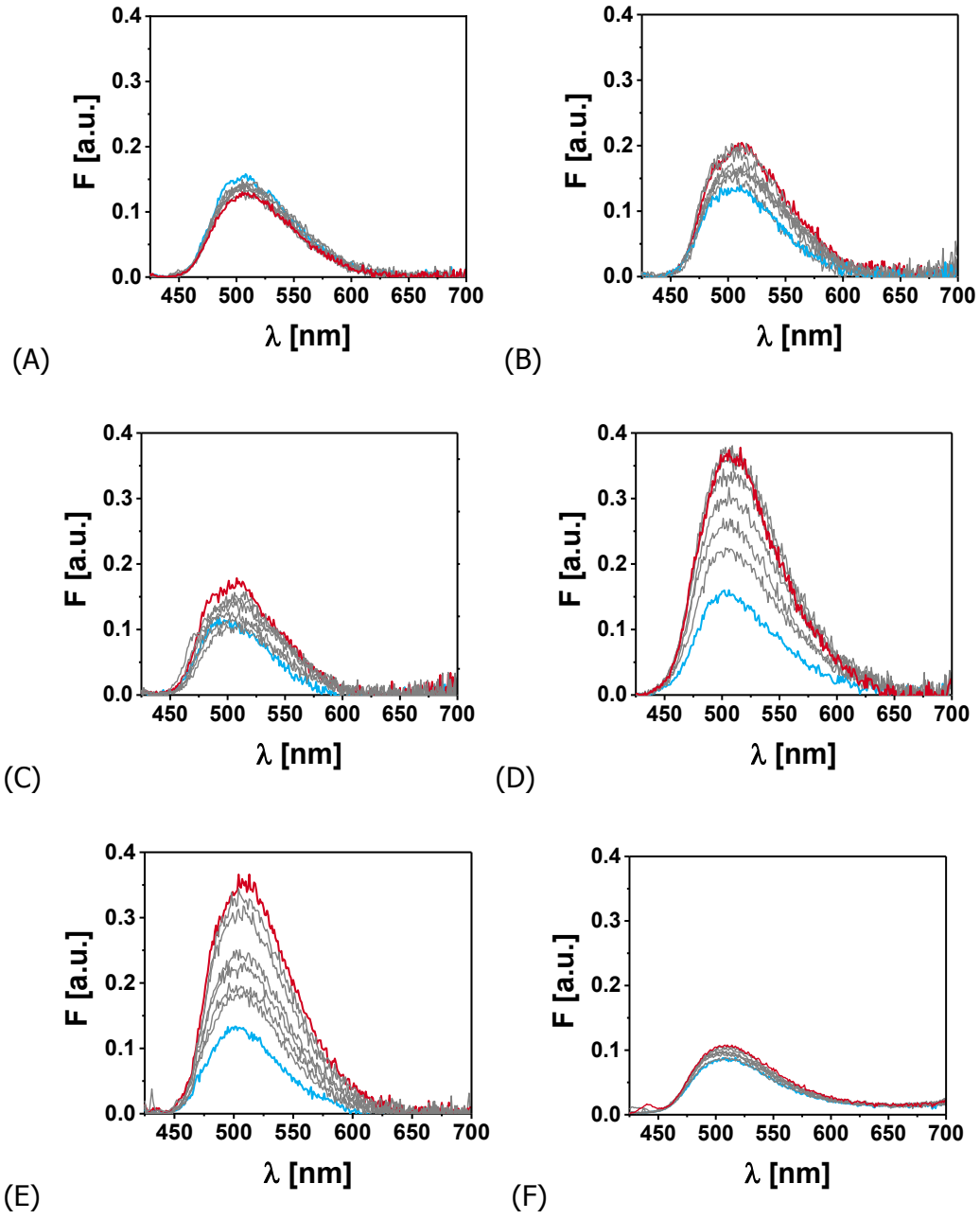

Fig. S87: Fluorescence spectra of 1 mg mL^{-1} MIP(**14**)-Z-D-Phe/THA@SiO_2 particles in the presence of 1 mM Z-D-Phe/TMA (A), Z-D-Phe/TEA (B), Z-D-Phe/TBA (C), Z-D-Phe/THA (D) and Z-D-Phe/TOA (E) and NIP(**14**)-Z-D- @SiO_2 titrated with 1 mM Z-D-Phe/THA (F), (increasing concentrations in grey, start point spectrum in blue and end point spectrum in red, steps of 0, 1.0, 2.5, 5.0, 9.9, 19.6, 33.8, 47.6 µM are shown).

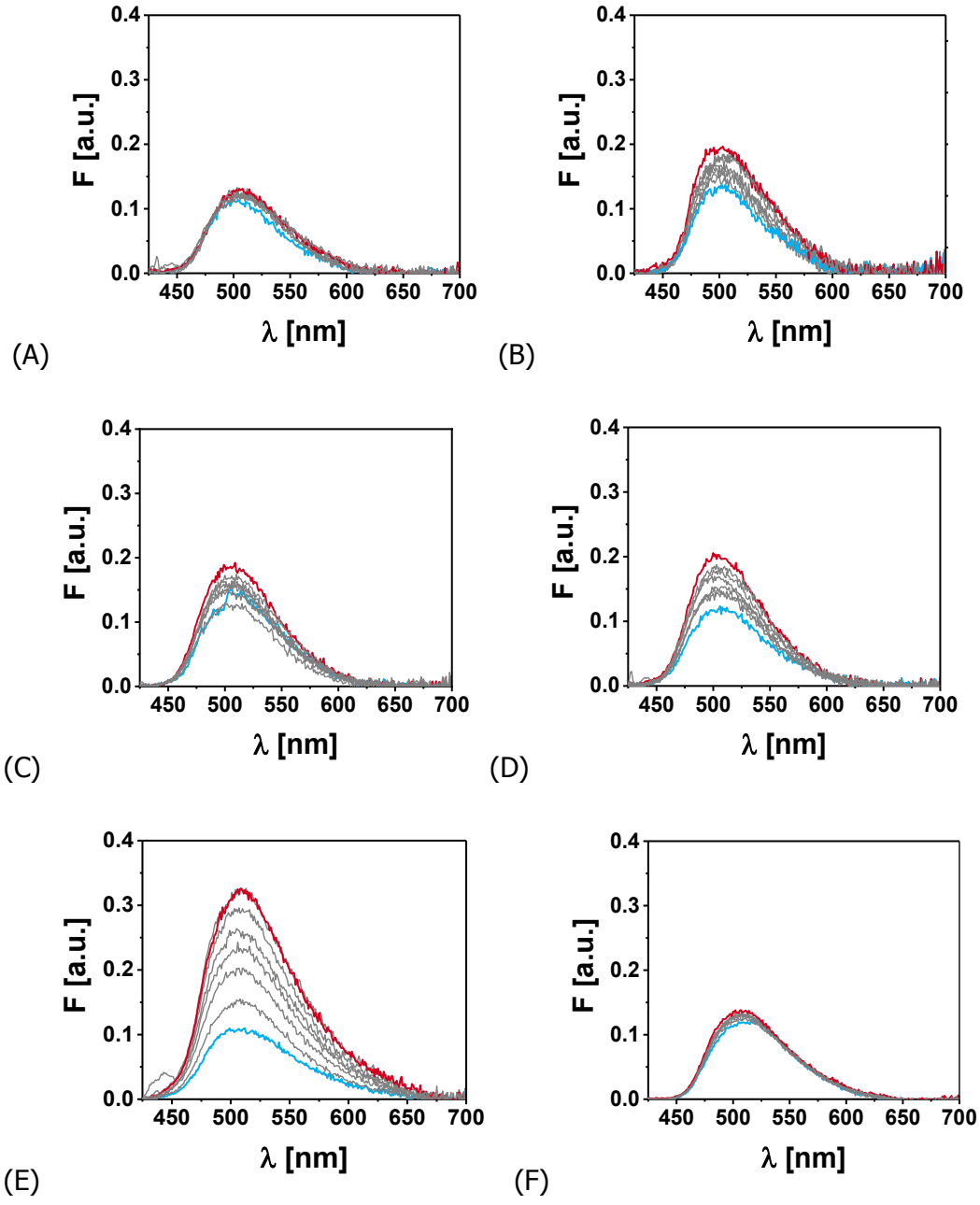

Fig. S88: Fluorescence spectra of 1 mg mL^{-1} MIP(**14**)-Z-D-Phe/TOA@SiO_2 particles in the presence of 1 mM Z-D-Phe/TMA (A), Z-D-Phe/TEA (B), Z-D-Phe/TBA (C), Z-D-Phe/THA (D) and Z-D-Phe/TOA (E) and NIP(**14**)-Z-D- @SiO_2 titrated with 1 mM Z-D-Phe/TOA (F), (increasing concentrations in grey, start point spectrum in blue and end point spectrum in red, steps of 0, 1.0, 2.5, 5.0, 9.9, 19.6, 33.8, 47.6 µM are shown).

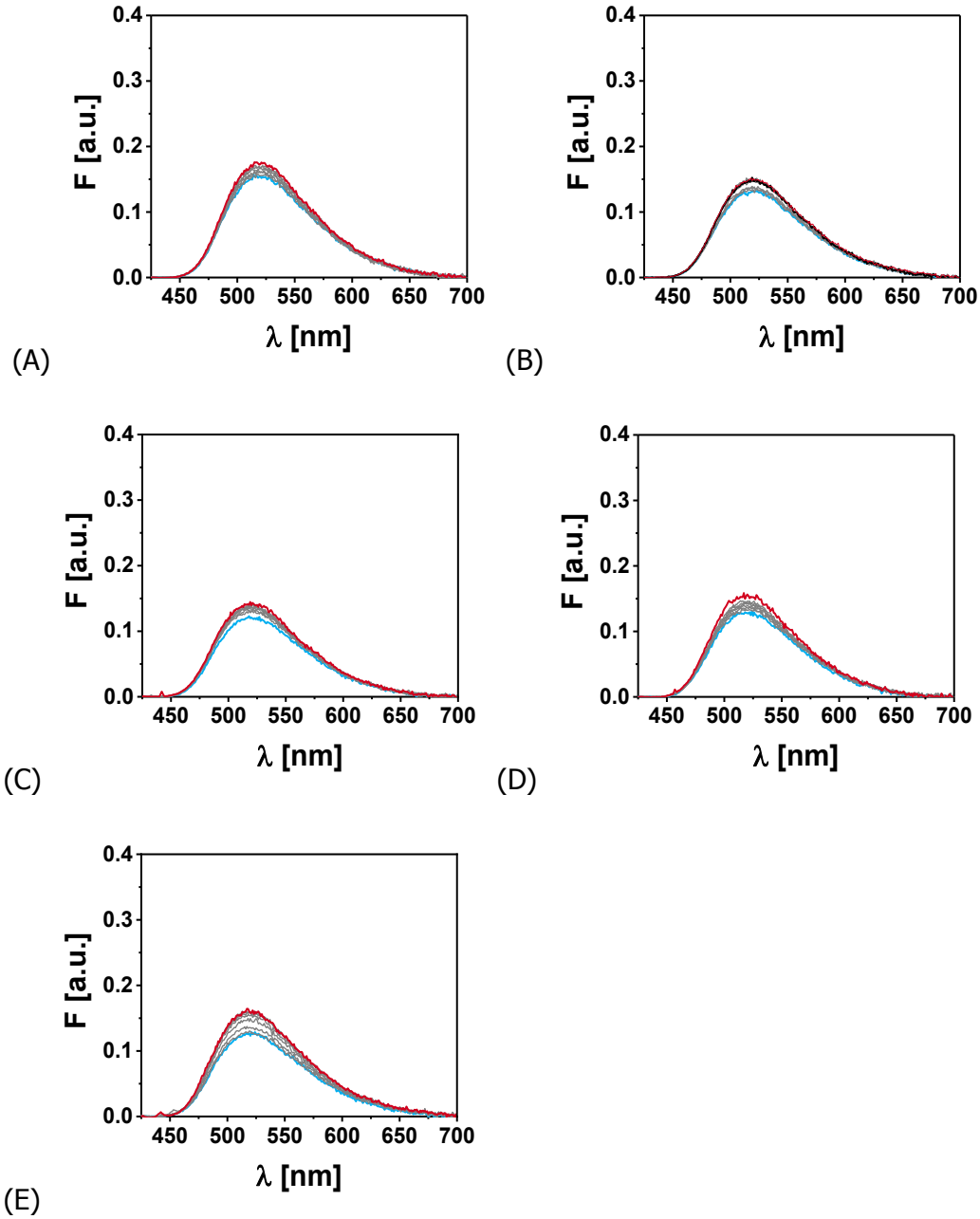

Fig. S89: Fluorescence spectra of 1 mg mL^{-1} MIP(**14**)-Z-D-Phe/TEA@SiO_2 particles in the presence of 1 mM Z-L-Phe/TMA (A), Z-L-Phe/TEA (B), Z-L-Phe/TBA (C), Z-L-Phe/THA (D) and Z-L-Phe/TOA (E), (increasing concentrations in grey, start point spectrum in blue and end point spectrum in red, steps of 0, 1.0, 2.5, 5.0, 9.9, 19.6, 33.8, 47.6 µM are shown).

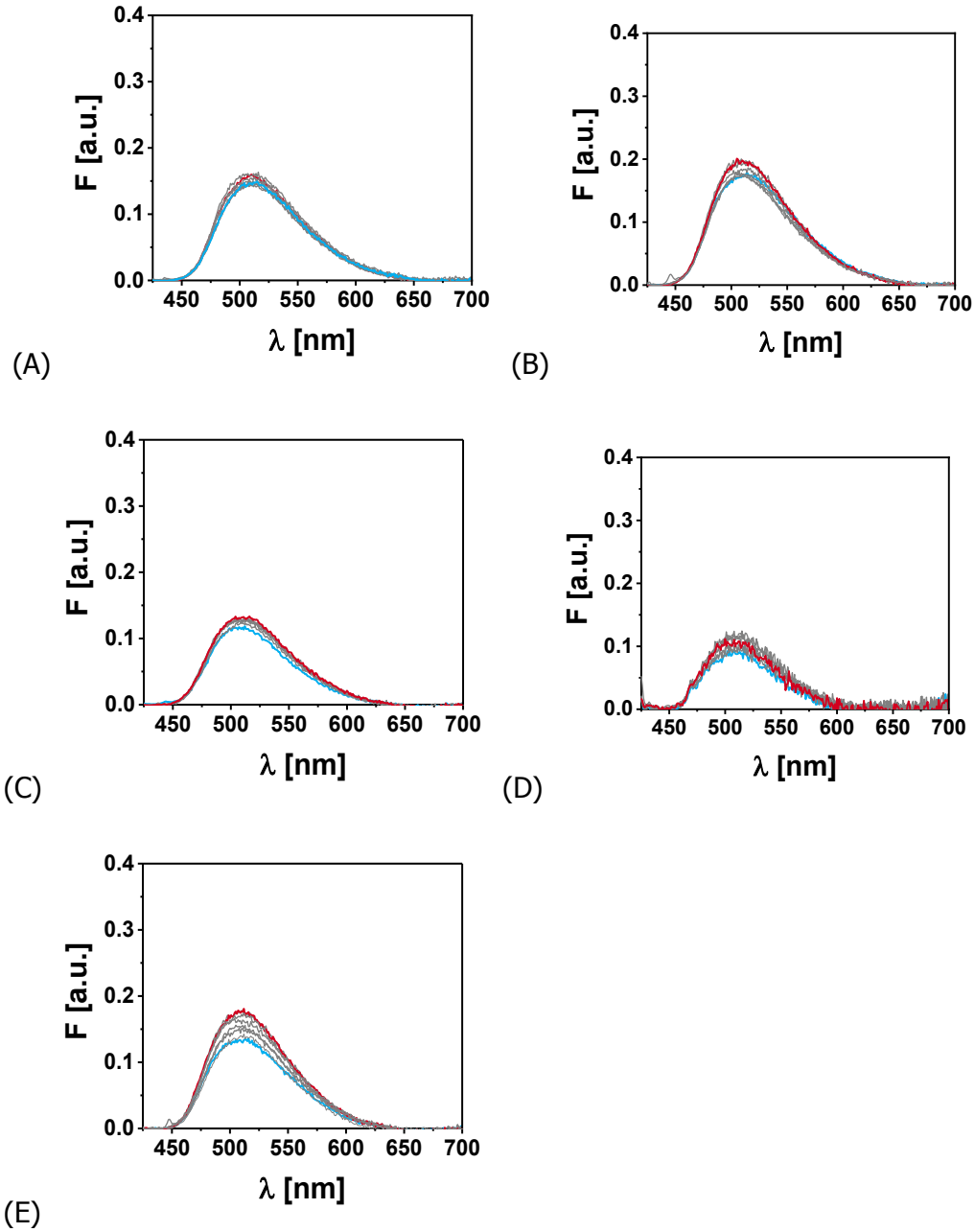

Fig. S90: Fluorescence spectra of 1 mg mL^{-1} MIP(**14**)-Z-D-Phe/THA@SiO_2 particles in the presence of 1 mM Z-L-Phe/TMA (A), Z-L-Phe/TEA (B), Z-L-Phe/TBA (C), Z-L-Phe/THA (D) and Z-L-Phe/TOA (E), (increasing concentrations in grey, start point spectrum in blue and end point spectrum in red, steps of 0, 1.0, 2.5, 5.0, 9.9, 19.6, 33.8, 47.6 µM are shown).

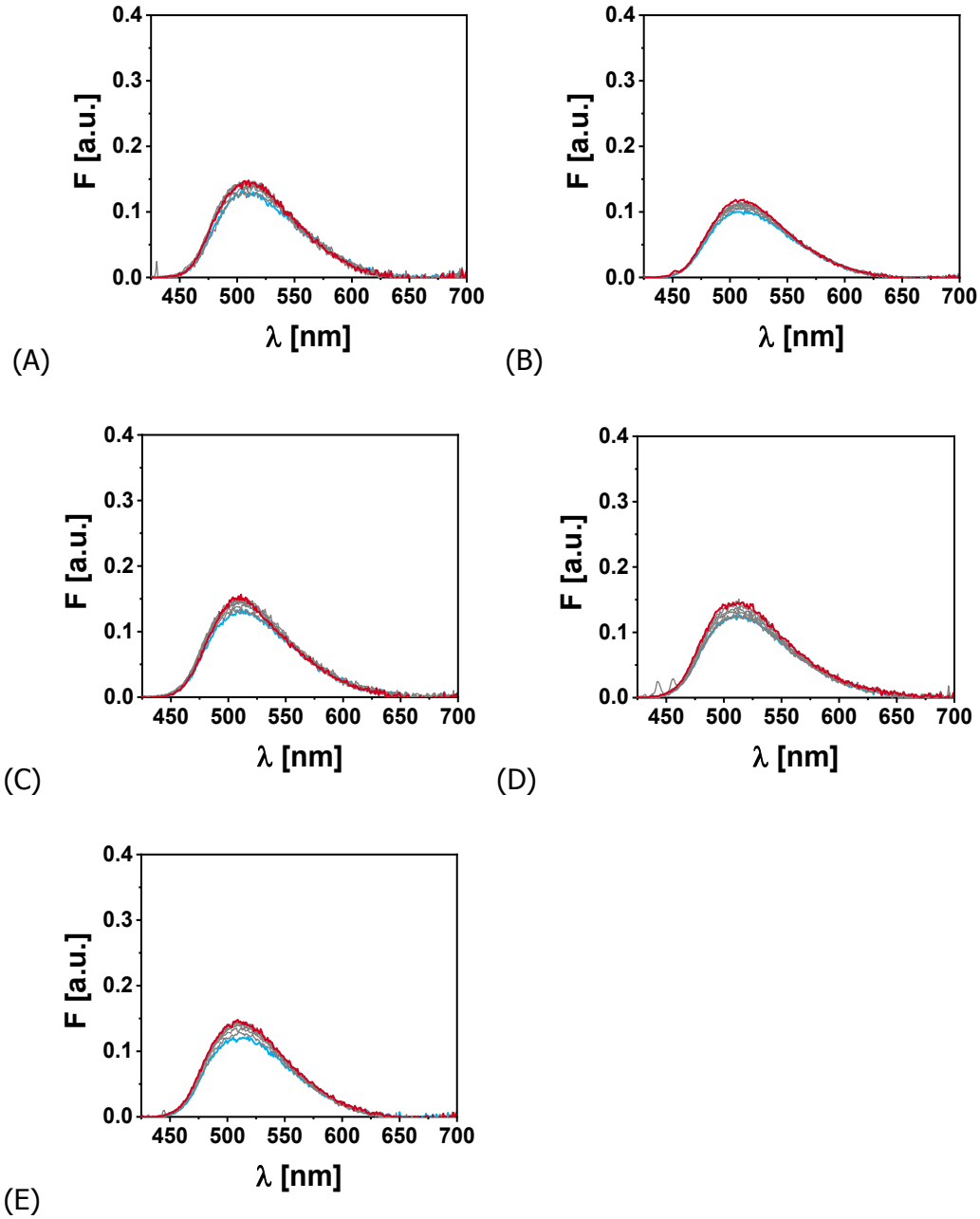

Fig. S91: Fluorescence spectra of 1 mg mL^{-1} MIP(**14**)-Z-D-Phe/TOA@SiO_2 particles in the presence of 1 mM Z-L-Phe/TMA (A), Z-L-Phe/TEA (B), Z-L-Phe/TBA (C), Z-L-Phe/THA (D) and Z-L-Phe/TOA (E), (increasing concentrations in grey, start point spectrum in blue and end point spectrum in red, steps of 0, 1.0, 2.5, 5.0, 9.9, 19.6, 33.8, 47.6 µM are shown).

Tab. S1. Overview of sensing performance of MIP systems for 2,4-D published so far (abbreviations: LOD = limit of detection; PBS = phosphate buffered saline; Tris = tris(hydroxymethyl)-aminomethan, used with HCl; AuNP-PPy = gold nanoparticle-polypyrrole; CNT = carbon nanotube; PVC = polyvinylchloride; µCP = micro-contact printed; QD = quantum dot)

Ref.	MIP matrix / format	Detection mode	Sample medium	Clean up[a]	LOD /nM	Assay time	In-field use[b]
[200]	Silica (sol gel) / crushed monoliths	Fluorescence (UV range)	Water (PBS pH 7, Triton)	[c]	45,000	>30 min	[d]
[197]	Polymer / film coated onto filter paper	Conductometry	Water (Tris pH 8)	[c]	1,000	Partly very low[e]	[d]
[196]	Polymer / film electrodeposited on electrode	Cyclic voltammetry	Water (PBS pH 6.9, N_2 purged), tap water	[c]	830[f]	15 min	[g]
[201]	Polymer / film coated onto filter paper	Chemiluminescence (indirect competitive assay with enzyme conjugate)	Water (PBS pH 7.4), tap water	[c]	0.001[f]	>10 min (multi step incl. washing and reagent handling)	[d]
[202]	Polymer / film coated onto optical fibre	Fluorescence (visible range)	MeOH:water 4:1	[c]	2.5	5–20 min incubation (plus rinsing and drying steps)	+
[198]	Polymer / AuNP-PPy MIP hybrid casted onto electrode	Photoelectrochemical	Water (Tris pH 7), soil	Ethanol extract of soil	0.2[f]	25 min incubation	[d]
[199]	Polymer / thin layer grafted onto CNT; objects embedded into PVC membrane	Potentiometry	Tap and ground water (Tris pH 5)	–	1.2	7 min	[d]
[235]	Polymer / µCP grating layer on glass slide	Refractive index (diffraction efficiency of surface relief grating)	MeOH:water 4:1	[c]	10,000	12 min (equilibration time only)	[d]
[203]	Silica (sol gel) / thin layer grafted onto QD	Fluorescence (visible range)	Water (PBS pH 7.5), tap and lake water	microfiltration	140[f]	5 min (response time only)	+
[236]	Polymer / film electrodeposited on electrode	Cyclic voltammetry	Water (PBS pH 7), tap water	Oxidation (pH = 12, 1.3V, 600s)	0.1	5 min	[h]
This work	Polymer / thin layer grafted onto SiO_2 particle	Fluorescence (visible range)	Lake and river water	–	20	2 min	+

a: When real samples were analyzed. b: Potential for in-the-field or on-line use. c: Model studies only. d: Only with major modifications. e: Response times partly very low as written by the authors. f: LOD calculated from 3σ of noise which is largely instrument-determined and known to generally result in too low values, see.[237] g: Purging step very impractical. h: Low selectivity

Tab. S2: Crystal data and structure refinement for **22** and **22**/2,4-D complex

Name	**22**	**22/2,4-D**
Empirical formula	C_{22} H_{23} B F_2 N_3 O_2	C_{23} H_{21} Cl_2 N_3 O_3
Formula weight	410.24	458.33
Temperature	150(2) K	154(2) K
Wavelength	0.71073 Å	0.71073 Å
Crystal system	Triclinic	Monoclinic
Space group	P-1	P2(1)/c
Unit cell dimensions	a = 9.5310(4) Å b = 11.8271(5) Å c = 13.8876(7) Å α= 70.7875(18)°. β= 84.9987(19)°. γ = 83.9194(18)°.	a = 21.1447(10) Å b = 10.9956(5) Å c = 9.2217(4) Å α= 90°. β= 92.6920(19)°. γ = 90°.
Volume	1467.68(11) $Å^3$	2141.67(17) $Å^3$
Z	4	4
Density (calculated)	1.857 Mg/m^3	1.421 Mg/m^3
Absorption coefficient	0.136 mm^{-1}	0.334 mm^{-1}
F(000)	860	952
Crystal size		0.32 x 0.28 x 0.18 mm^3
Theta range for data collection	2.58 to 29.63°.	2.67 to 28.73°.

Index ranges	-13<=h<=13, -16<=k<=16, -19<=l<=19	-28<=h<=28, -14<=k<=14, -12<=l<=11
Reflections collected	88116	27669
Independent reflections	8283 [R(int) = 0.0502]	5316 [R(int) = 0.0778]
Completeness to theta = 29.63 + 28.73°	99.8 %	95.8 %
Absorption correction		Semi-empirical from equivalents
Max. and min. transmission		0.2970 and 0.2028
Refinement method	Full-matrix least-squares on F^2	Full-matrix least-squares on F^2
Data / restraints / parameters	8283 / 0 / 355	5316 / 0 / 280
Goodness-of-fit on F^2	1.809	1.025
Final R indices [I>2sigma(I)]	R1 = 0.1140, wR2 = 0.4010	R1 = 0.0498, wR2 = 0.1275
R indices (all data)	R1 = 0.1426, wR2 = 0.4299	R1 = 0.0621, wR2 = 0.1366
Largest diff. peak and hole	1.848 and -0.643 e.$Å^{-3}$	0.668 and -0.656 e.$Å^{-3}$

Publications

Wagner, S; Zapata, C.; Wan, W.; Gawlitza, K.; Weber, M.;Rurack, K.; Role of Counterions in Molecularly Imprinted Polymers for Anionic Species. *Langmuir* **2018**.

Wagner, S.; Bell, J.; Biyikal, M.; Gawlitza, K.; Rurack, K., Integrating fluorescent molecularly imprinted polymer (MIP) sensor particles with a modular microfluidic platform for nanomolar small-molecule detection directly in aqueous samples. *Biosensors and Bioelectronics* **2018,** *99*, 244-250.

Gawlitza, K.; Wan, W.; Wagner, S.; Rurack, K., Fluorescent Molecularly Imprinted Polymers. *Advanced Molecularly Imprinting Materials* **2016**, 89.

Wan, W.; Wagner, S.; Rurack, K., Fluorescent monomers: "bricks" that make a molecularly imprinted polymer "bright". *Analytical and Bioanalytical Chemistry* **2015**, 408 (7), 1753-1771.

Declaration of authorship/ Selbstständigkeitserklärung

I hereby declare that this thesis is my own work and effort. All utilized sources, aids and appliances are declared in the text. Contributions of others are referenced appropriately.

Hiermit versichere ich, die vorliegende Dissertation selbstständig erarbeitet und verfasst zu haben. Alle verwendeten Quellen und Hilfsmittel werden im Text genannt. Fremdbeiträge sind eindeutig als solche gekennzeichnet.

Berlin, _____

Sabine Wagner